A multi-isotope (S-Sr-Nd) investigation of the Flatreef, Northern Limb, Bushveld Complex:

Petrogenetic implications and comparison with the Merensky Reef

Jarlen Jocelyn Keet

Thesis

Submitted in fulfilment of the requirements in respect of the Doctor of Philosophy degree in the Department of Geology, Faculty of Natural and Agricultural Sciences, University of the Free State.

Bloemfontein, 2022

DECLARATION

I, Jarlen Jocelyn Keet, declare that this thesis (inclusive of published articles) that I herewith submit for the Doctor of Philosophy degree at the University of the Free State, is my independent work, and that I have not previously submitted it for a qualification at another institution of higher education.

Jarlen J. Keet

28/11/22

ABSTRACT

Historically, research on the Bushveld Complex (BC) in the northern limb mainly focused on the near surface Platreef. The Platreef is well-known for being complicated and erratic due to significant degrees of country rock assimilation and contamination along strike. A correlation of the disrupted magmatic stratigraphy of the Platreef to the Upper Critical Zone of the western and eastern limbs has thus proven difficult. The discovery of the Flatreef, the down-dip, sub-horizontal extension of the Platreef, on the farms Turfspruit and Macalacaskop, opened new avenues for enquiry. The proportion of assimilated country rock within the Flatreef is significantly less than in the near surface Platreef, with a stratigraphy that is less disrupted and affected by footwall interaction than the Platreef, such that Bastard Reef and Merensky Reef correlates may be identified in the Flatreef stratigraphy.

In this study Sr, Nd and S isotopic compositions across the stratigraphic units of the Flatreef as intersected by drill hole UMT-393 on the farm Macalacaskop, and to a lesser extent, drill hole UMT-276 on the farm Turfspruit is reported. The initial $^{87}Sr/^{86}Sr$ ratio (Sr_i) (also indicated as $^{87}Sr/^{86}Sr_i$) results show a significant shift from about 0.706 to 0.707 in the immediate footwall, to values > 0.709 near the top of the Main Reef. This isotopic shift matches the isotopic shift described for the Merensky Reef of the eastern and western BC. The mineralized units of the Flatreef, namely the Main Reef and Upper Reef, have $\delta^{34}S$ values ranging between -0.2 to 1.5‰ (with the exception of three outliers), and 0.52% and 11.2‰ in UMT-393, respectively. The S-isotope data for UMT-276 are lighter with $\delta^{34}S$ values ranging between -0.96 and 2.24‰ for the Main Reef and 3.19‰ was recorded for an Upper Reef sample. These near-mantle $\delta^{34}S$ values fall within the range of about 0 to 3‰ reported for the Merensky Reef in the eastern and western BC. The initial epsilon Nd (ε_{Nd}^{i}) values for the Flatreef were found to range between –5.2 to -7.6, strongly overlapping with ε_{Nd}^{i} values of the Upper Critical Zone and the lower reaches of the Main Zone from the eastern (with ε_{Nd}^{i} values ranging between -4.8 and -8.5 for the Upper Critical Zone) and western limbs (with ε_{Nd}^{i} values ranging between -6.3 and -7.6 for the Upper Critical Zone, and -6.3 and -7.4 for the Main Zone) of the Bushveld Complex.

It is evident from our findings that the Flatreef was less affected by interactions with footwall rocks compared to the Platreef, with isotopic signatures overlapping significantly with those reported for the upper reaches of the Upper Critical Zone in the remainder of the BC. Our findings provide further support for the contention that the Flatreef is the stratigraphic equivalent of the Upper Critical Zone inclusive of the Merensky Reef and the Bastard Reef in the remainder of the BC.

The similar isotopic composition of the hanging wall and footwall units of the Flatreef suggests that these units may have been continuous and were separated by subsequent magma pulses of the remainder of the Flatreef. Due to significant overlap between the ε_{Nd}^{i} values of the Flatreef and local potential contaminants occurring at the base of the Northern Limb, it is proposed that the Sr-Nd isotopic composition of the magmas that gave rise to the Flatreef are most likely attributable to the interaction of mantle-derived magma with upper and lower crustal rocks of the Kaapvaal Craton within a sub-Bushveld staging chamber, with possible syn- to post-emplacement modification thereof as a result of interaction with locally available dolomitic footwall rocks. The reef horizons of the Flatreef may have been emplaced as sills fed from the proposed staging chamber, which would explain the similarities in lithology and geochemistry of the hanging wall and footwall units as mentioned above. This would imply that the Main Zone could not have been the source of PGEs within the Flatreef, and by extension, the Merensky Reef.

DEDICATION

To my nieces, nephew and cousins. I may be the first in the family, but I am not the last. We are not defined by where we come from… there is nothing you cannot do.

ACKNOWLEDGEMENTS

I would like to thank Prof Frederick Roelofse, not only for his committed supervision of this project, but also for his patience, all his support, suggestions and encouragement during the course of this study; it is highly appreciated. I would also like to thank Prof Christoph Gauert who helped conceive this project, thank you for your input and support from afar. This project would not have evolved to what it is today without the guidance of my supervisors.

This project was funded in part by the Inkaba /Iphakade funding, the nGAP grant (UID 119698) and NRF grants to my supervisors.

Ivanplats Ltd. is also thanked for access to the core yard for logging and sampling, especially to Dr Danie Grobler and the geologists who assisted during my visit. Dr. Grobler's expertise on the northern limb was of great assistance in this project.

Ms. Henriette Ueckermann is thanked for assisting with Laser Ablation Multi-Collector Inductively Coupled Plasma Mass Spectrometry (LA-ICP-MS) housed at the University of Johannesburg. Dr. Linda Iaccheri at the Wits Isotope Geoscience Laboratory is thanked for the preparation of samples for Nd-isotopic analysis. Mr. Mike Butler at iThemba Laboratories is thanked for S isotope analyses. Mr Marlin Patchappa from the EarthLab at the University of Witwatersrand is thanked for the geochemical analyses. Mr. Deon van Niekerk is thanked for assisting with the Jeol JXA 8230 Superprobe that is housed at Rhodes University. This instrument is sponsored by NRF/NEP grant 40113 (UID 74464).

My sincere thanks also go to the Geology Department's laboratory staff members at the University of the Free State. Mr. Jonas Choane and Mr. Pelele Lehloenya, thank you for preparing the fusion discs and pressed pellets; Mr. Daniel Radikgomo, thank you for preparing the thin sections and epoxies used in this study and for teaching me how to prepare my own; Mrs. Megan Welman-Purchase, thank you for calibrating the XRF and SEM instruments, and rerunning fusion discs countless times. Special thanks also to Mrs. Rina Immelman[†], Mrs. Charlene Van Der Vyver and Mr. Andries Felix for their administrative support throughout this project. I would also like to thank my colleagues at the department for their continuous support.

Lady-Bridget One (née Akuffo) and the Akuffo family, thank you so much for opening your home to me whenever I was in Johannesburg, whether it was for analyses, or visa application, everything you did for me is highly appreciated. Several other people have contributed to my academic journey and growth over the past years. It is difficult to acknowledge each and every

contribution; but to everyone who played a role in this project as well as my personal development, I am so grateful, thank you.

I would also like to thank my parents, my parents-in-law and my church family for all their support and encouragement throughout my academic journey.

To my husband, Danrich Keet, words are not enough to express my gratitude to you. You have supported me through every season, going above and beyond to ensure that I finish strong. Thank you, for everything. I would not have made it this far without you.

Most importantly, I would like to thank my Saviour, Jesus Christ, without whom none of this would have been possible.

TABLE OF CONTENTS

LIST OF FIGURES

CHAPTER 1

CHAPTER 2

CHAPTER 3

CHAPTER 4

CHAPTER 5

CHAPTER 6

CHAPTER 7

LIST OF TABLES

CHAPTER 4

CHAPTER 6

LIST OF APPENDICES

CHAPTER 1 :
INTRODUCTION

1.1 Study context

With the continuous advancement in environmentally-related technologies such as catalytic converters, hydrogen fuel cells, electronics, etc., the global demand for platinum group elements (PGE) is continuously growing in modern society (Mudd et al., 2018) (Fig. 1.1). Of the multiple applications that use PGE, the automotive industry has the highest demand for Pt, Pd and Rh (Fig. 1.1a, b and e) and the electronics industry the highest demand for Ru and Ir (Fig. 1.1c and d). The past decade has seen the demand for Pd overtaking that of Pt in the automotive industry (Fig 1.1 a, b and f) (Cowley, 2021). South Africa is one of the leading producers of PGE in the world (Fig. 1.2a), with vast deposits located in the Bushveld Complex (BC) (Fig. 1.2b) (Thormann et al., 2017). With an area of approximately 20000 km^2 and an average thickness of approximately 4 km north (Finn et al., 2015), and approximately 65000 km^2, and nearly 8 km thick south of the Thabazimbi-Murchison Lineament (TML) (Eales and Cawthorn, 1996; Cawthorn and Walraven, 1998), the Rustenburg Layered Suite of the BC is not only the largest layered igneous intrusion on Earth, but it is also the largest known PGE reserve (Cawthorn, 2010). Other metals such as V, Cr, Ni and Co are also enriched in this intrusion. The layered part of the complex outcrops as four distinct limbs, namely the eastern, western, far western and northern limb (Fig. 1.2b). The BC is formally divided into three main suites, namely the Rustenburg Layered Suite (RLS), consisting of mafic to ultramafic layered rocks; the Lebowa Granite Suite, a succession of granites; and the Rashoop Granophyre Suite, consisting of granophyres and granites (Eales and Cawthorn 1996, Kruger 2005). Three key stratigraphic units within the RLS are associated with PGE-Ni-Cu mineralization, namely, the Merensky Reef, the UG-2 Reef and the Platreef. Mining operations are therefore concentrated close to where these reefs outcrop (Fig. 1.2b). The recently discovered Flatreef, which is the main focus of this study, is located in the northern limb of the BC, and represents the down-dip, sub-horizontal extension of the Platreef, the latter which outcrops along much of the eastern margin of the northern limb, where it is in contact with Transvaal Supergroup sedimentary rocks and Archaean granite basement (van der Merwe 2008).

Significant interaction with floor rocks is thought to have contributed to the apparent erratic and complex nature of the Platreef. This complexity made it difficult to correlate the Platreef with the Merensky Reef in the remainder of the BC even though it is located at a similar stratigraphic position to the latter. The Flatreef was discovered in the course of a deep drilling programme conducted by Ivanplats in 2007 (Grobler et al. 2019). This discovery changed the

narrative regarding Platreef mineralization in the northern limb relative to the rest of the BC as previous studies in the northern limb focused on the relatively “shallow” Platreef that has been subjected to intense assimilation and contamination by footwall rock.

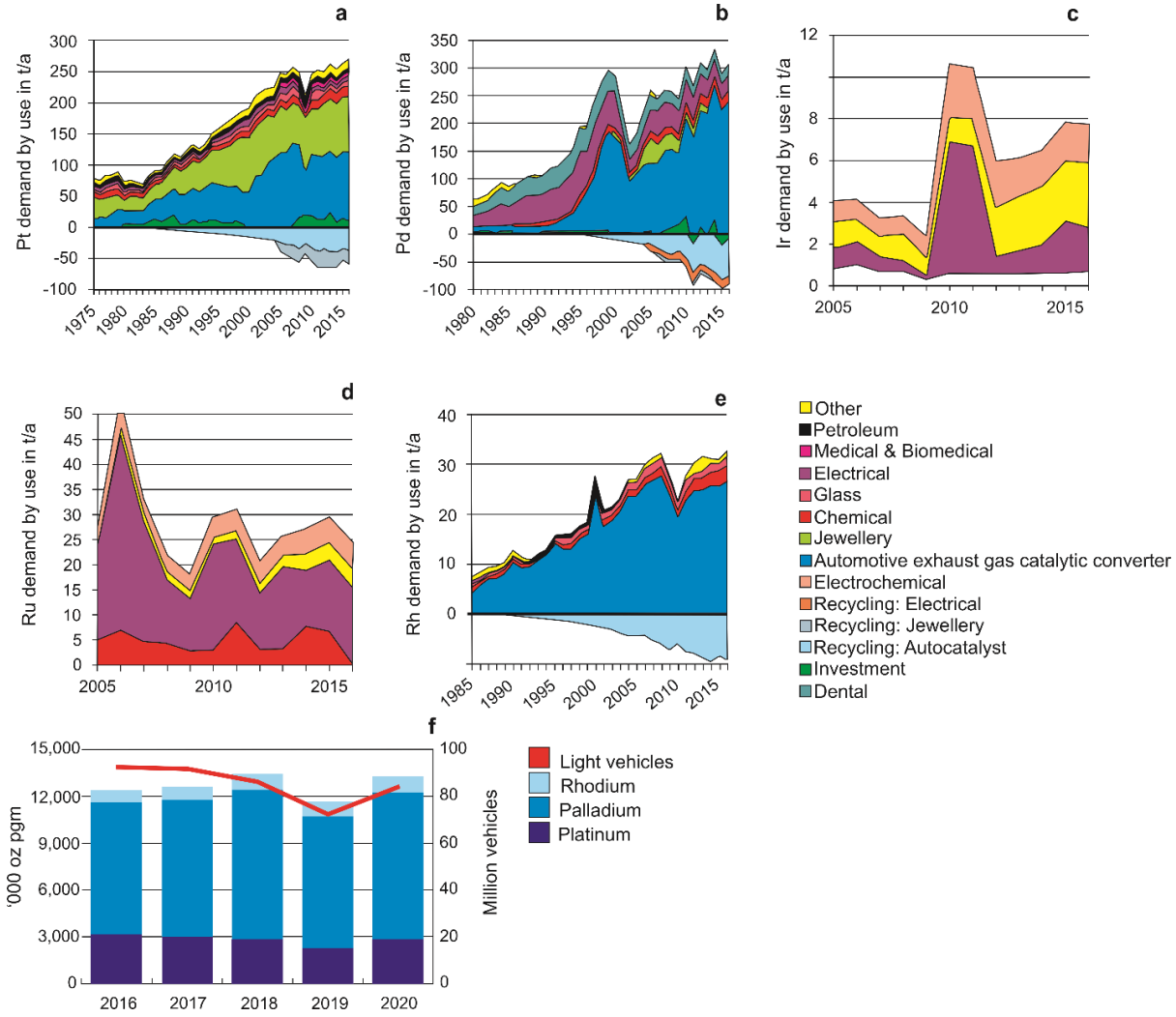

Figure 1.1 a-e Global demand for Pt, Pd, Ir, Ru and Rh, respectively, over selected years. Modified after Thormann et al. (2017). **f** Pt, Pd and Rh (referred to as ‘pgm’) demand from the auto catalyst industry and light vehicle output between 2016 and 2020. Modified after Cowley (2021).

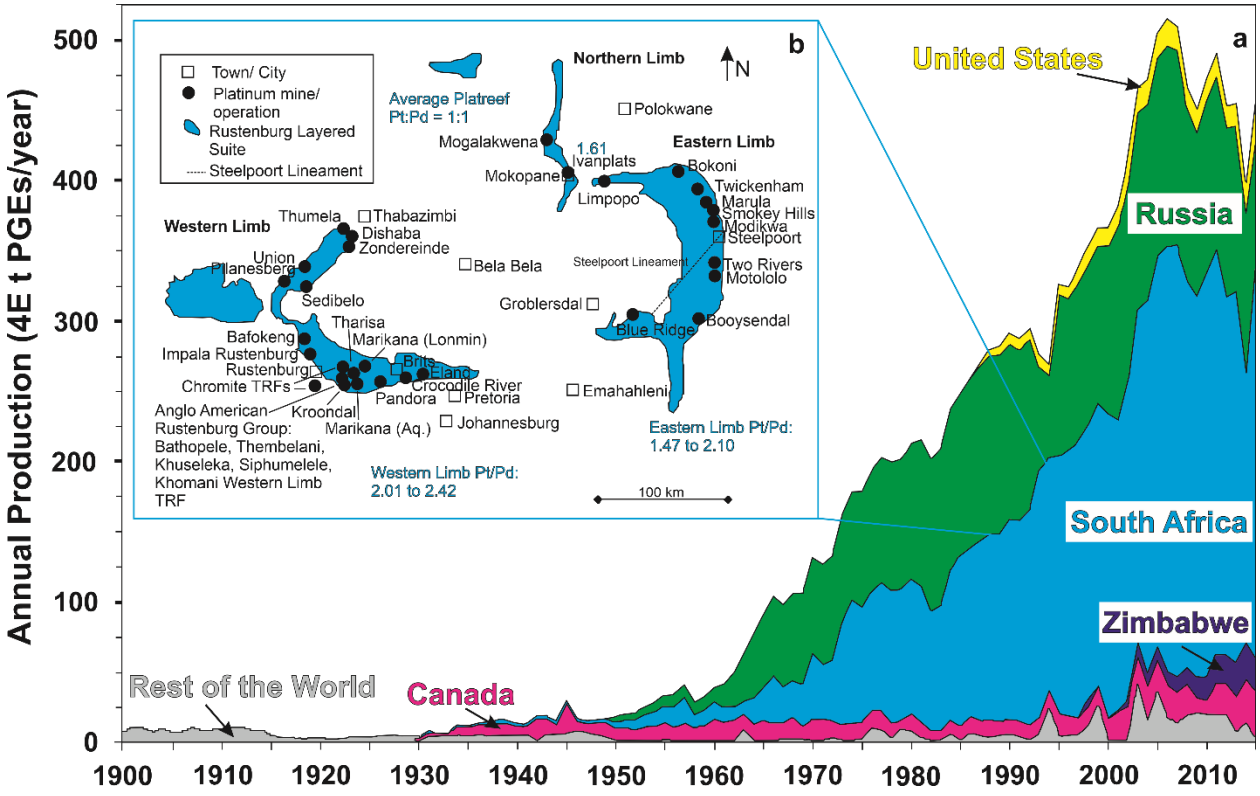

Figure 1.2 a Graph showing the global supply of PGE; modified after Mudd et al. 2018. **b** Inset, PGE mines and mine projects in the RLS of the BC, modified after Thormann et al. (2017). Pt/Pd ratios, as calculated by Grobler et al. (2019) for Merensky Reef and Platreef from several online resource statements, is included in blue text

1.2 Research aims and objectives

The growing economic importance of the Platreef in the northern limb of the BC is undeniable. Advances in mineral exploration of the Platreef in recent years have led to the northern limb being the focus of intensive research, where historically the focus was mostly on the western and eastern limbs of the BC. The discovery of the Flatreef, i.e., the down dip, sub-horizontal extension of the Platreef, allows for the study of a magmatic stratigraphy where the influence of local footwall interaction is negligible (Grobler et al. 2019). The aim of this study is to establish whether the Flatreef correlates with the Merensky and Bastard Cyclic Units, which constitutes the transitional zone between the Upper Critical Zone and Main Zone of the western and eastern BC, based on its isotopic signature.

The principal objectives are as follows:

- To establish the Sr-, S- and Nd-isotopic stratigraphy of the Flatreef.
- Comparing variations in the Sr-, S- and Nd-isotopic composition across the Flatreef with variations across the Merensky and Bastard reefs in order to establish whether the Flatreef may be considered a correlate of the Merensky and Bastard reefs as known from the eastern and western limbs of the BC.

- To constrain the petrogenesis of the Flatreef and to consider the implications thereof for the petrogenesis of the Merensky Reef.

1.3 Thesis Layout and Author Contributions

This is a publication-based thesis consisting of seven chapters, three of which are presented as journal-style published / submitted papers. Information such as the regional geology and specific explanations may be repeated in these chapters, however, each journal-style chapter focuses on one or more of the objectives listed above. This introductory chapter provides a broad overview of the global PGE demand and supply (with special reference to the BC) as well as the outline of this study.

Chapter 2: This chapter provides an introduction to the regional geology of the BC as well as the northern limb, summarizing key aspects of available literature regarding its stratigraphy, mineralization and emplacement.

Chapter 3: This chapter presents detailed descriptions of the Flatreef units intersected by boreholes UMT-393 and UMT-276.

Chapter 4: Article 1 titled “Strontium isotope variations in the Flatreef on Macalacaskop, northern limb, Bushveld Complex: Implications for the source of platinum-group elements in the Merensky Reef”. This article was published in *Mineralium Deposita* in 2021.

Authors: Jarlen J. Beukes[*], Frederick Roelofse, Christoph D. K. Gauert, Danie F. Grobler and Henriette Ueckermann ([*]Jarlen J. Keet (née Beukes))

This article investigates strontium isotopic variations in plagioclase across the Flatreef and how these relate to the Merensky Reef in the remainder of the BC.

Candidate’s contribution:

The candidate was responsible for logging, sample collection, analyses, interpretation of data, the writing of the paper as well as figure production.

The candidate contributed between 85 and 90% of the paper.

Frederick Roelofse and Christoph Gauert assisted with data interpretation and discussion during preparation of the manuscript.

Danie Grobler assisted in understanding the magmatic stratigraphy of the Flatreef.

Henriette Ueckermann assisted with LA-MC-ICP-MS analyses.

Chapter 5: Article 2 titled “A comparative study of sulfur isotope variations within the Flatreef and Merensky Reef of the Bushveld Complex, South Africa”. This article was published in *The Canadian Mineralogist* in 2021.

Authors: Jarlen J. Keet, Frederick Roelofse, Christoph D. K. Gauert, Danie F. Grobler and Mike Butler

This article provides whole-rock S isotope data collected across the Flatreef as intersected by boreholes UMT-276 and UMT-393, as well as across the Merensky Reef at Two River’s Platinum, eastern BC.

The candidate contributed between 75 and 85% of the paper.

The candidate was responsible for the logging, sample collection, preparation of samples for analyses, data interpretation and write-up of the paper.

The candidate was responsible for the production of all figures except for figures 4 and 5.

Frederick Roelofse and Christoph Gauert assisted with data interpretation and discussion during preparation of the manuscript.

Danie Grobler assisted in understanding the magmatic stratigraphy of the Flatreef.

Mike Butler conducted the S isotope analyses.

Chapter 6: Article 3 titled “Neodymium isotope variations in the Flatreef on Macalacaskop, northern limb, Bushveld Complex”. The present version of this article represents a revised version of the article originally submitted to *Mineralium Deposita* in early 2022. The revised article is currently under review with *Mineralium Deposita.*

Authors: Jarlen J. Keet, Frederick Roelofse, Christoph D. K. Gauert, Linda Iaccheri, Danie F. Grobler and Henriette Ueckermann

The candidate contributed between 75 and 80% of the paper.

The candidate was responsible for the logging, sample collection, preparation of samples for analyses, data interpretation and write-up of the paper.

The candidate was responsible for the production of all figures.

Frederick Roelofse and Christoph Gauert assisted with data interpretation and discussion during preparation of the manuscript.

Linda Iaccheri prepared the samples for Nd-isotopic analysis.

Danie Grobler assisted in understanding the magmatic stratigraphy of the Flatreef.

Henriette Ueckermann assisted with the Nd-isotopic determinations.

Chapter 7: This chapter brings together data sets and main ideas from the results chapters, i.e., journal style chapters and additional data, to achieve the aims set out in chapter 1 through a detailed discussion.

Note that spelling (American vs. British spelling) and / or stylistic variations may be encountered in chapters 4-6 due to the requirements of the journals to which the work was submitted.

1.4 Methodology

Data for this thesis were collected using a range of analytical techniques, a detailed account of which is provided in each article chapter.

CHAPTER 2 :
GEOLOGICAL BACKGROUND

2.1 The Bushveld Complex

The Bushveld Magmatic Province consists of the felsic volcanic Rooiberg Group, representative of the initial phase of Bushveld-related magmatism (Buchanan et al., 2002) and the following intrusive suites: a suite of early mafic Bushveld sills, the RLS (which many authors incorrectly call the Bushveld Complex), consisting of ultramafic-mafic layered rocks, the Rashoop Granophyre Suite and the Lebowa Granite Suite (Kruger, 2005) (Fig. 2.1). The BC, located in the north-eastern part of South Africa, was emplaced into the central portion of the Kalahari Craton, upon the Witwatersrand and Pietersburg blocks of the Kaapvaal Craton, at approximately 2.06 Ga (Zeh et al., 2015) (Fig 2.2). Major cratonic lineaments such as the TML are possible representatives of suture zones through which younger domains accreted during the development of the Kaapvaal Craton (Elington and Armstrong, 2004). The sedimentary lithologies of the Transvaal Supergroup surround the BC and these sediments are located within the Transvaal and Griqualand West basins, where they typically overlie Archaean basement (Bekker et al. 2001). The RLS south of the TML is estimated to have an areal extent of 65000 km^2 and a thickness of about 8 km (Eales and Cawthorn, 1996; Cawthorn and Walraven, 1998), making it the world's largest known layered igneous intrusion. Recent geophysical data on the BC north of the TML (Finn et al., 2015) increases the total areal extent of the BC to approximately 85000 km^2.

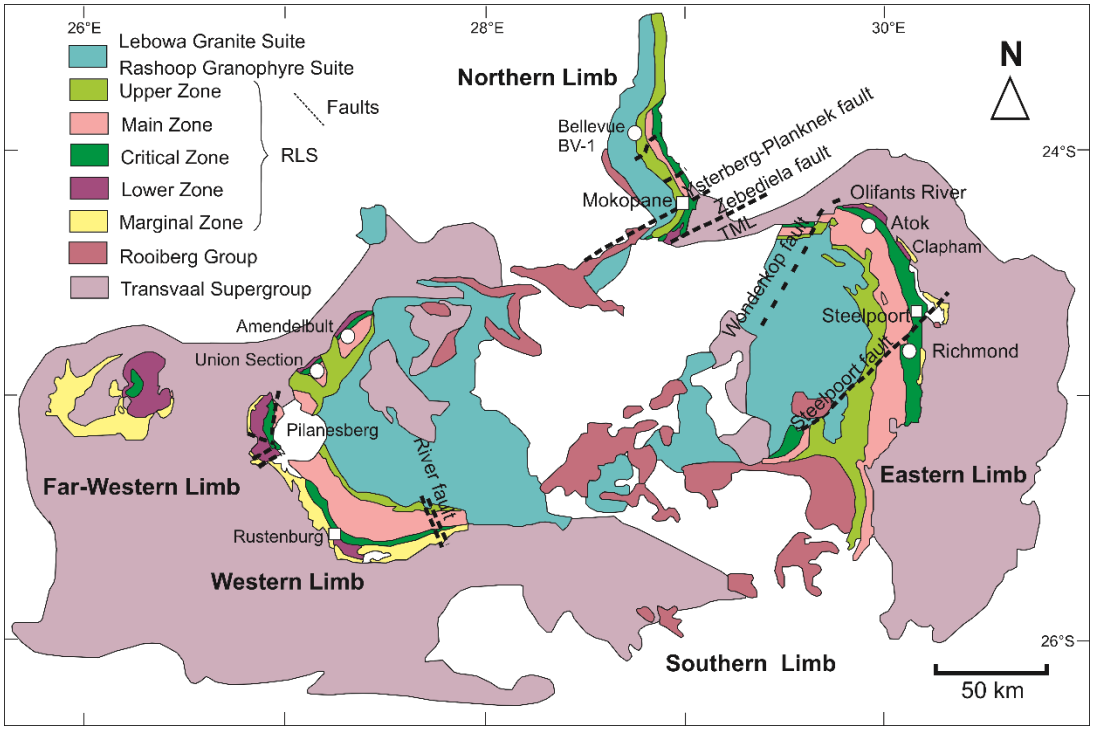

Figure 2.1 Simplified geological map of the BC indicating the different stratigraphic zones of the RLS. Modified after Eales and Cawthorn (1996); Yudovskaya et al. (2013). TML= Thabazimbi Murchison Lineament. The Lebowa Granite and Rashoop Granophyre Suites are combined in the legend.

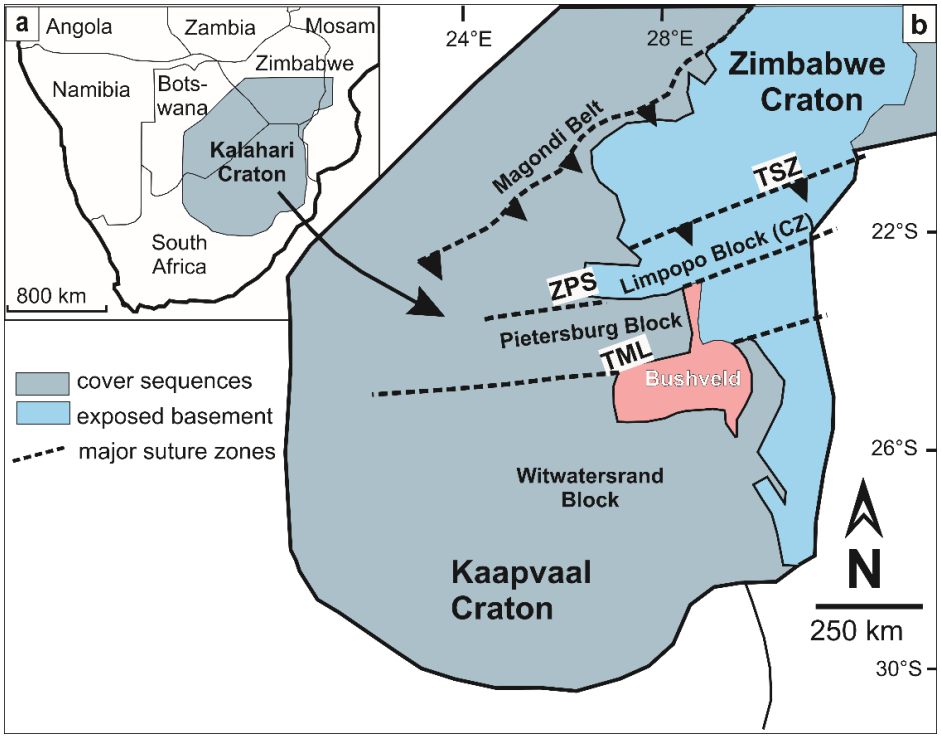

Figure 2.2 a Location of the Kalahari Craton in Southern Africa. **b** Major units and significant terrane boundaries (suture zones) of the Kalahari Craton, and location of the Bushveld Complex. Modified after Zeh et al. (2015). TSZ – Triangle shear zone; ZPS – Zoetfontein–Palala shear zone; TML – Thabazimbi–Murchison-Lineament

The RLS outcrops in four different geographical areas, namely, the eastern, the northern, the western and far western limbs (Eales and Cawthorn, 1996, Fig. 2.1). A fifth limb, known as the southern (Bethal) limb, is located under younger Karoo sedimentary cover. Only the northern limb is located north of the TML, with the remaining four limbs located to the south. The recently discovered ultramafic-mafic succession known as the Waterberg Project could potentially extend the northern limb's border further north (Huthmann et al., 2016, 2018; Kinnaird et al. 2017). Considering isostasy of the crust following the emplacement of the enormous BC, Cawthorn and Webb (2001) reinterpreted gravity data and suggested a connection at depth between the arcuate eastern and western limbs. This hypothesis is further supported by seismic and magnetic modelling (Webb et al., 2004; Cole et al., 2013). However, connectivity between the remainder of the limbs remains debatable (Cawthorn, 2015).

2.1.1 The Rustenburg Layered Suite

The RLS is a layered ultramafic-mafic package, approximately 9 km thick, subdivided vertically into distinct zones on the basis of variations in its mineralogy and petrology (Hall, 1932) or major shifts in isotopic composition (Kruger, 2005). These units are, from bottom to top: the Marginal (MZN), Lower (LZ), Critical (CZ), Main (MZ) and Upper (UZ) zones (Fig. 2.1). The RLS was emplaced along a regional unconformity between the Rooiberg Group volcanics and the Transvaal Supergroup sediments or Archaean basement granites and gneisses (von Gruenewaldt et al., 1985; Eales and Cawthorn, 1996; Bekker et al., 2001).

The zones of the RLS consist of a variety of rock types and different magmas were apparently responsible for their formation. Earlier studies (e.g., Davies et al. 1980; Sharpe, 1981; Cawthorn and Davies, 1983; Harmer and Sharpe, 1985) proposed that the RLS was produced by three distinct magma types. The first magma type, B1, which is MgO-rich, produced the Lower Zone and the lower Critical Zone. The second magma type is the Al_2O_3-rich B3 magma, which produced the rocks of the Main Zone, whereas the intermediate B2 magma is thought to have produced the rocks of the upper Critical Zone. However, more recent studies (e.g., Wilson, 2012) have argued that the exact number of magmas responsible for the formation of the LZ and underlying units was unclear. A wide variety of pre- and syn-BC mafic sills intruded the country rocks surrounding the BC (Sharpe and Hulbert, 1985; von Gruenewaldt et al., 1985) (Fig. 2.3). Whole-rock Sr isotope data recorded by Kruger (1994) were interpreted to suggest that the lower MZ, CZ and LZ formed during an open-system "Integration Stage" that was characterised by multiple injections of fresh mafic magma; whereas the upper MZ and UZ formed during a closed-system "Differentiation Stage", which was dominated by large-scale fractional crystallization and limited injections of new magma (Fig. 2.4).

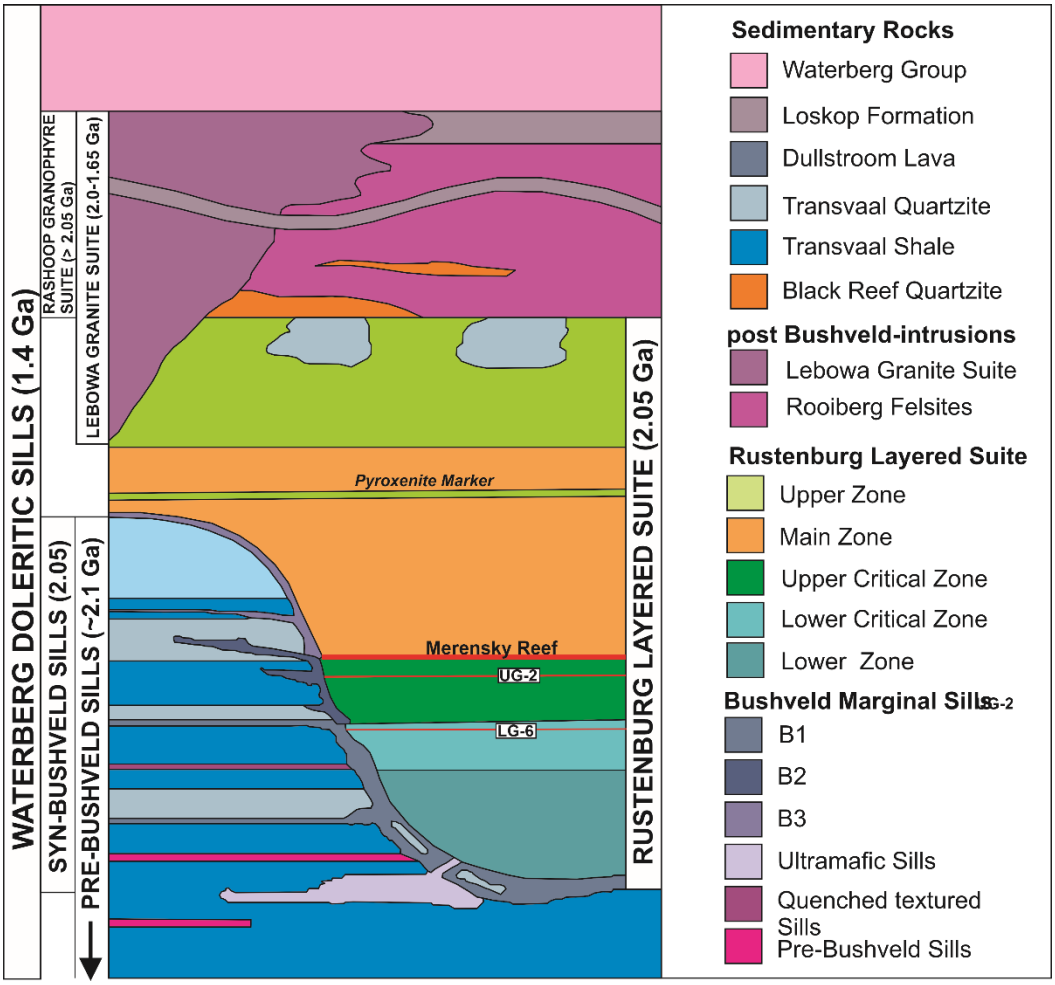

Figure 2.3 Schematic cross-section of the RLS and its marginal rocks. Modified after von Gruenewaldt et al. (1985).

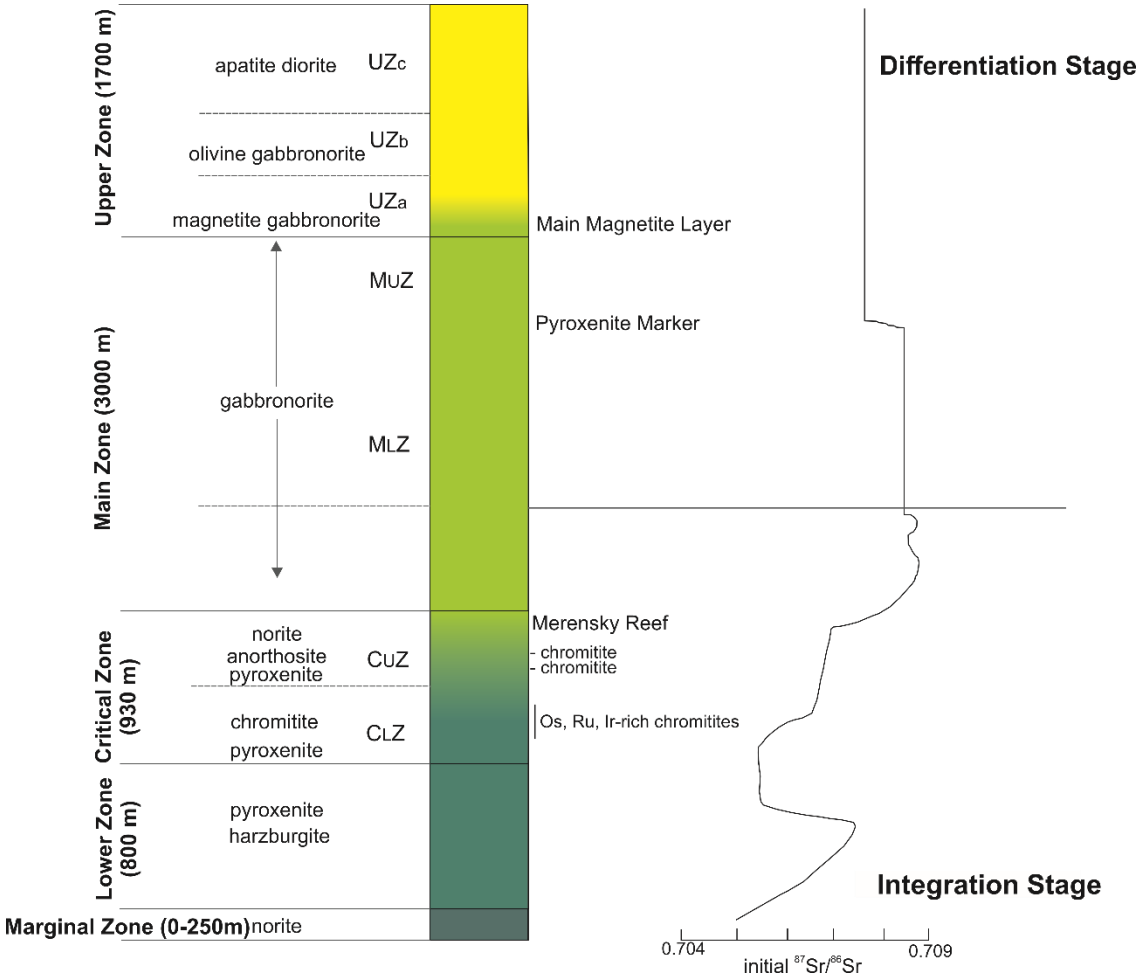

Figure 2.4 Generalised stratigraphy of the western and eastern limbs of the RLS. Major subdivisions, main rock types and thickness of each zone of the RLS are indicated. Positions of lower (LG), middle (MG) and upper group (UG) chromitites are shown. Variations in the initial $^{87}Sr/^{86}Sr$ ratio for whole-rocks and plagioclase (separates) as per Kruger (1994) are also shown. Modified after Eales and Cawthorn (1996) and Kruger (2005).

2.1.1.1 Marginal Zone (MZN)

Due to poor exposure and limited drilling, the provenance of this lowermost succession of the RLS remains poorly understood (Wilson, 2015). The MZN is the most enigmatic of the RLS zones (Cawthorn, 2015) and in some areas it is missing from the RLS succession (Wilson, 2012). Where present, it consists of variably fine-grained norite, pyroxenite and gabbronorite, with a thickness varying between 150 m and 800 m (Eales and Cawthorn, 1996). Due to the common occurrence of quartz and biotite associated with quartzitic and dolomitic xenoliths from the Transvaal Supergroup within the MZN rocks, Cawthorn et al. (2006) and Cawthorn (2007) proposed that the MZN is unlikely to represent the true chilled margins of the RLS, but more likely, contaminated magmas that rapidly crystallized before the emplacement of the voluminous layered intrusion. A previously unknown Basal Ultramafic Series (BUS) was reported in the eastern limb of the BC, occurring below the MZN (Wilson, 2015).

2.1.1.2 Lower Zone (LZ)

The LZ cumulate rocks are dominated by orthopyroxene and lesser olivine (Cawthorn, 2007). The rocks of the LZ include dunite, harzburgite and pyroxenite (Cameron, 1978). The LZ lacks consistency in thickness and lateral continuity throughout the BC. The floor topography largely controls the thickness of the LZ (Eales and Cawthorn, 1996). In the Olifants River Trough in the eastern limb, where the LZ is best exposed, the LZ is up to 1584 m thick and is subdivided into a Lower Pyroxenite subzone, a Harzburgite subzone, and an Upper Pyroxenite subzone (Cameron, 1978). Further to the south, in the Clapham area, the LZ is approximately 900 m thick (Wilson, 2015). In the western limb, the LZ is about 1000 m thick and is subdivided into two subzones. Relative to the lower subzone that is dominated by pyroxenite and olivine-bearing rocks, the upper subzone consists of less pyroxenite (Teigler and Eales, 1996). The distribution and thickness of the LZ in the northern limb is irregular. It occurs as seven isolated satellite bodies and as an apparent xenolithic inclusion along the eastern margin of the mafic intrusion (de Villiers 1970; van der Merwe 1976; van der Merwe, 2008). It is usually separated from the overlying mineralized mafic package by intervals of country rock (Yudovskaya et al. 2013). Economically important chromitite seams have been documented in the LZ in the northern limb but are not present in the LZ of the eastern and western limbs (Hulbert and von Gruenewaldt, 1982). Except for an approximately 90 cm thick noritic layer occurring midway in the LZ succession, which has been identified in both the western and eastern limbs, no cumulus plagioclase is present in the LZ (Lee and Tredoux, 1986; Teigler, 1990). Although similarity in rock types and the cyclical development of rock units is observed in the various LZ successions in the different limbs of the BC, Wilson (2015) concluded, upon assessing details of these LZ sequences, that no precise correlation exists.

2.1.1.3 Critical Zone (CZ)

The CZ, located stratigraphically above the LZ (Fig. 2.4), is economically significant as it hosts world class PGE deposits, most notably within the UG-2 Reef, Merensky Reef and Platreef (Naldrett et al. 2009). It is between 1300 m and 1800 m thick and is characterized by the appearance of cumulus chromite (Naldrett et al. 2009). Based on the first appearance of cumulus plagioclase, the CZ is subdivided into 2 subzones, namely, the Upper Critical Zone (UCZ) and the Lower Critical Zone (LCZ) (Cameron, 1980, 1982). The LCZ, which is approximately 800 m thick, consists mostly of pyroxenite with occasional olivine-bearing units and chromitite layers (Cawthorn, 2015). These chromitite layers are grouped into two packages, the Lower Group (LG1-LG7, numbered from the bottom upwards) and the Middle Group (MG1 and MG2) (Fig. 2.4). The boundary between the LCZ and UCZ occurs between the MG2 and MG3 chromitite layers (Eales and Cawthorn, 1996), where plagioclase becomes a cumulus phase.

The major chromitite layers of the UCZ are grouped into the Middle Group (MG3 and MG4) and Upper Group chromitites (UG1 and UG2) (Fig. 2.4). Disseminated chromite as well as several minor chromitite layers/stringers, such as the chromitite stringers bracketing the Merensky Reef pegmatoid, are also hosted by the UCZ (Maier et al. 2013). The UCZ may be subdivided into two parts. The succession of rocks in the lower part of the UCZ is mainly non-cyclical and comprises of anorthosite, norite and minor orthopyroxenite (Naldrett et al. 2009). The upper part, however, consists of cyclic units containing part or all of chromitite, harzburgite, pyroxenite, norite and anorthosite, generally in that order (Naldrett et al. 2009). It is in this subunit of the UCZ where the stratiform PGE mineralization of the UG-2 and Merensky Reef is located.

2.1.1.4 Main Zone (MZ)

The MZ is 2200 to 3100 m thick and overlies the CZ (Ashwal et al., 2005; Fig. 2.4). The exact boundary between the CZ and MZ is not distinct and is currently taken as the top of the Bastard Cyclic Unit, where it is capped by the Giant Mottled Anorthosite (Eales and Cawthorn, 1996). Others have suggested that the boundary should be placed within the Merensky Cyclic Unit due to the presence of a distinct excursion in Sr-isotopic values (Kruger 1992, 2005, Cawthorn 2015). The MZ mostly consists of norite, gabbro, gabbronorite and anorthosite (Mitchell, 1990). It lacks olivine (apart from in the northern limb) and chromian spinel, and is more homogeneous and unlayered compared to the CZ (Eales and Cawthorn, 1996). It was proposed by Kruger (2005) that the MZ be subdivided into a cyclic and heterogeneous Lower Main Zone and differentiated Upper Main Zone (Fig. 2.4). A significant layer, known as the Pyroxenite Marker, is located towards the top of the MZ (Eales and Cawthorn, 1996). It is characterized by a major reversal in mineral compositions and a distinct excursion towards lower $^{87}Sr/^{86}Sr$ isotope ratios (Sharpe, 1985, Fig. 2.4), and likely represents the level at which the last major influx of magma into the RLS occurred. The Pyroxenite Marker hosts minor PGE mineralization (Maier et al., 2001).

2.1.1.5 Upper Zone (UZ)

The UZ is stratigraphically located above the MZ and is the most laterally extensive zone of the RLS. The position of the base of the UZ is taken at the level where cumulus magnetite first appears within a mottled anorthosite layer (SACS 1980; Eales and Cawthorn, 1996). Others have suggested that the boundary between the MZ and overlying UZ should be placed at the level of the Pyroxenite Marker, concomitant with the observed shift in $^{87}Sr/^{86}Sr$ ratios (Kruger, 1990, 1994, 2005, Fig. 2.4). The well-layered UZ is approximately 2800 m thick and is composed of basal noritic rocks and subsequent gabbroic rocks inclusive of gabbronorite, anorthosite and magnetite gabbro (Molyneux, 1970; von Gruenewaldt, 1973). The number of magnetitite layers identified across the RLS differs (Maier et al. 2013). In the eastern and

western limbs up to 26 magnetitite layers have been recorded (Cawthorn and Molyneux, 1986; Tegner et al., 2006). These magnetitite layers usually have sharp lower contacts and gradational upper contacts (Eales and Cawthorn, 1996). The UZ is subdivided into 3 subzones based on cumulus mineralogy (SACS, 1980; Eales and Cawthorn, 1996; Maier et al. 2013). The rocks of subzone A consist of cumulus plagioclase, pyroxene and magnetite and subzones B and C additionally contains olivine and apatite, respectively (Cawthorn, 2015).

2.1.2 Mineralization in the Rustenburg Layered Suite of the western and eastern limbs

The presence of world-class PGE deposits in the RLS, particularly in its CZ, is one of the important reasons why it has been studied intensively over the past century. By virtue of their PGE concentrations and lateral traceability it comes as no surprise that most of the BC research focused on the Merensky Reef and UG-2 stratiform horizons relative to its other PGE-enriched layers. These layers include the Bastard and Pseudo reefs which usually overlies and underlies the Merensky Cyclic Unit, respectively (Viljoen and Schürmann, 1998). They are not laterally continuous and have non-economic PGE concentrations (Naldrett et al., 1986). The UG-2 represents the largest PGE resource in the world (Vermaak, 1985) with reported PGE grades exceeding 10 ppm (Kinnaird et al., 2002). With average PGE grades ranging between 5 and 10 ppm and Pd/Pt ratios of ~0.6 (Barnes and Maier, 2002; Cawthorn et al. 2005; Naldrett et al. 2009, Wilson and Chunnett, 2006; Osbahr et al., 2013), the Merensky reef represents the second largest PGE resource on Earth (Godel, 2015). The PGE mineralization in both the Merensky Reef and the UG-2 is associated with base metal sulfides which include pyrrhotite, pentlandite, chalcopyrite and minor pyrite (Osbahr et al., 2014). However, no consensus has yet been reached regarding the origin of the Merensky Reef and associated PGE mineralization. Two main schools of thought about the Merensky Reef exists, namely “Uppers” and “Downers” (Naldrett et al. 2009). The “Uppers” school argues that the source of metals in the Merensky Reef are from ascending fluids from underlying footwall cumulates which are enriched in PGE (e.g., Boudreau and McCallum, 1992; Boudreau, 2008; Mathez, 1995). These authors suggest that volatile-rich fluids, carrying dissolved sulfur and PGEs, mixed with the resident magma, causing sulfur saturation and associated deposition of PGMs. In contrast, “Downers” propose that PGEs were scavenged from an overlying magma column by a dense sulfide melt that percolated downwards (e.g., Naldrett, 1989; Naldrett et al., 2008; Cawthorn, 2005). Traditionally it was proposed that sulfur saturation was caused by magma mixing (e.g., Campbell et al. 1983; Naldrett et al., 1986; Naldrett and von Gruenewaldt, 1989; Li et al. 2001) or pressure changes rather than chemical processes in the magma chamber (Cawthorn, 2005). Alternatively, it has been proposed that stratiform PGE mineralization developed through in-situ crystallization (Latypov et al., 2015, 2017) or by

slumping of semi-consolidated cumulate slurries and associated hydrodynamic sorting (Maier et al., 2013).

2.1.2.1 The Merensky Reef

Wilson and Chunnett (2006) describe the term “Reef” as the mineralized zone located within medium- to coarse-grained plagioclase-pyroxenite with metal content that is considered economic to mine. “Merensky Reef” is a mining term (Lee, 1996) that can be defined as “a mineralized zone within or closely associated with ultramafic cumulates at the base of the Merensky (cyclic) unit” (Cawthorn et al., 2002). The Merensky Cyclic Unit (MCU), which contains the Merensky Reef at its base (Roberts et al., 2007), is found at the transitional zone between the UCZ and MZ, and is overlain by the petrographically similar, though sparsely mineralized Bastard Cyclic Unit (BCU) (Wilson and Chunnett, 2006). The MCU generally has a footwall consisting of anorthosite, norite or pyroxenite overlain by a basal chromitite layer (2 to > 4 cm thick); followed by pegmatoidal feldspathic pyroxenite or feldspathic harzburgite and dunite of varying thickness that is usually capped by a 2 to 10 cm thick upper chromitite layer overlain by an orthopyroxenite sequence (e.g., Naldrett et al., 2009, Viljoen 1999, Cawthorn and Boerst, 2006). The Merensky Reef dips with a slope ranging from 9˚ to 27˚ towards the center of the BC, however in some localized areas dips as steep as 65˚ have been recorded (Lee, 1996). Large-scale mining of the Merensky Reef started in 1929 near Rustenburg in the southern sector of the Western Limb (Viljoen, 2016)

The Merensky Reef was traditionally thought to occur at consistent stratigraphic levels and to be continuous over kilometers of strike length (Cawthorn et al. 2002). However, in actuality, the Merensky Reef varies in thickness, composition and the location of mineralization within it across the RLS of both the eastern and western BC (Viljoen, 2016, Fig. 2.5). The mines use the term, “facies”, to describe these lateral variations of the Merensky Reef. The Merensky Reef can generally be subdivided into a normal reef and potholed reef, where the normal reef displays the least degree of transgression and conformably overlies the footwall cumulates (Barnes and Maier, 2002, Fig. 2.5). The normal reef typically consists of a pegmatoidal feldspathic pyroxenite bracketed by two chromitite seams (Barnes and Maier, 2002). Up to four and as little as one chromitite seam may be present in the reef. “Potholes” refer to where the Merensky Reef abruptly transgresses the footwall (Lee, 1996). Potholed reefs overlie footwall cumulates unconformably, where potholes cut between 1 and 100 m deep into the footwall (Latypov, 2015). Potholed reefs are more dominant in the northwestern sector of the BC, and are located at a greater depth than the normal reef by up to 30 m (Barnes and Maier, 2002).

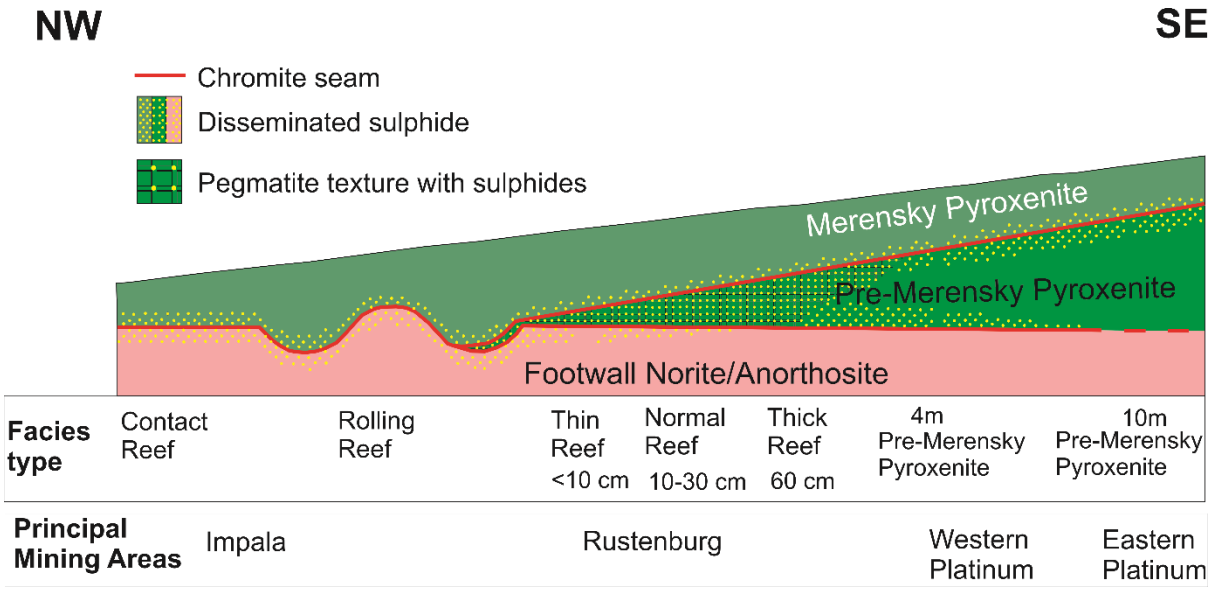

Figure 2.5 SE-NW schematic section illustrating the variations in Pre-Merensky and Merensky pyroxenites in the southern BC. The thick reef facies is found mostly in the east adjacent to the Pilanesberg intrusion in the extreme NW. Structural induced irregularities in the Merensky footwall influences the variation of the types of reef observed laterally. Modified after Naldrett et al. (2009).

2.1.2.2 The UG-2 Chromitite

The RLS hosts several chromitite layers that are enriched in PGEs relative to their host rocks, however, the highest PGE concentrations are recorded for the UG-2 chromitite horizon (Kinnaird et al. 2002). Although chromite is mined from selected chromitite layers from all 3 chromitite groups of the CZ (LG, MG and UG) (Viljoen, 2016), most of these chromitite layers are not thick enough or rich enough in PGEs to be economic for the mining of PGEs with the exception of the UG-2 chromitite. It is interesting to note that the Merensky Reef and Platreef are commonly characterised by their highest PGE grades being associated with the presence of one or more chromitite stringers (Viljoen, 2016). The UG-2 is found 40-140 m (Cawthorn, 1999) and up to 360 m (Barnes and Maier, 2002) below the Merensky Reef in the eastern and western limbs, respectively. The UG-2 unit consists of a 0.5-1.0 m thick chromitite typically underlain by a pegmatoidal feldspathic pyroxenite, and less commonly anorthosite (Lee, 1996). The occurrence of two to four minor chromitites in the hanging wall feldspathic pyroxenite has also been noted. The UG-2 chromitite is generally composed of 60-90% chromite with 10-35% orthopyroxene oikocrysts and interstitial plagioclase, has a Cr_2O_3 content of ~43.5%, and an average Cr/Fe ratio between 1.26 and 1.4 (Lee, 1996; Barnes and Maier, 2002; Viljoen, 2016). As with the Merensky Reef, potholes is a common feature of the UG-2 chromitite and have been observed in all mines mining this layer (Hahn and Ovendale, 1994). Base metal sulfides generally occur at low concentrations (Vermaak, 1985). Teigler and Eales (1993) suggested that PGE enrichment in chromitite layers may have taken place without bulk sulfur saturation contrary to what is suggested for the Merensky Reef where bulk

saturation may have been responsible for base metal sulfide crystallisation and associated PGE scavenging.

2.2 The Northern Limb of the RLS

The ENE-WSW trending Thabazimbi-Murchison Lineament (TML) separates the northern limb from the remainder of the RLS. The N-E striking Ysterberg-Planknek and Zebediela faults are the near-surface expressions of the TML (Fig. 2.1; Kinnaird and Nex, 2015; Grobler et al. 2019). The role of the TML in the emplacement of the BC is poorly understood, but it has been proposed that the TML may have acted as a dyke-like feeder for the magmas that gave rise to the RLS (Kinnaird et al. 2005). The thickness of the N-S trending northern limb outcrop varies over a strike length of 110 km. Its shape is evidently influenced by several underlying structural features (Fig. 2.6; van der Merwe, 1976). Recent geophysical modelling of the shallowly buried (commonly <1500 m) RLS intrusion north of the TML have shown it to have an areal extent of approximately 20000 km^2 (Finn et al. 2015).

The floor rocks of the northern limb vary along strike (Fig. 2.6; Sharman-Harris et al., 2005; Holwell and McDonald, 2006; van der Merwe, 2008; Kinnaird and Nex, 2015). To the south, between the farms Tweefontein and Townlands, the footwall rocks consist of shale, banded ironstone, calc-silicates, mudstone and siltstone of the Duitschland Formation. On the farms Tweefontein to Zwartfontein, the northern limb is underlain by dolostone of the Malmani Subgroup. Archaean granite underlies the northern limb to the north on the farms Overysel to Witrivier. A distinctive characteristic of the northern limb is the prominent transgression of the RLS northwards from the TML, through the Transvaal Supergroup (van der Merwe, 2008). This transgressive relationship of the mafic magma with floor rocks is significant as the degree of reaction and assimilation of the floor rocks is directly associated with the type of floor rock (van der Merwe, 2008).

The relationship between the RLS stratigraphy of the northern limb and the remainder of the BC is illustrated in Fig. 2.7. It is apparent that the mafic package in the northern limb differs somewhat from the conventional RLS stratigraphy in the western and eastern limbs. Some of the inconsistencies include: the presence of economic, well-developed chromitite layers in the LZ of the northern limb that are not present in the LZ, and mostly restricted to the CZ, of the western and eastern limbs (Hulbert and von Gruenewaldt, 1982; Eales and Cawthorn, 1996; Teigler and Eales, 1996); the apparent absence of the LCZ from the stratigraphy of the RLS in the northern limb (McDonald et al. 2005); the presence of an approximately 200 m thick sequence of troctolite and olivine gabbronorites in the MZ of the northern limb that is not reported for the MZ in the rest of the BC (van der Merwe 1976; Ashwal et al., 2005).

Ultramafic cumulates representing the LZ only crop out in the southernmost part of the northern limb, south of the town Mokopane. To the north of the town, they crop out as distinct satellite intrusions such as the Zwartfontein and Uitloop intrusions (Fig. 2.6; van der Merwe, 1976; Hulbert and von Gruenewaldt, 1985; Yudovskaya et al., 2013). A Ni-Cu-PGE mineralized, layered, mafic package termed the Grasvally norite-pyroxenite-anorthosite (GNPA) member stratigraphically overlies the LZ sequence south of the Ysterberg-Planknek Fault (Hulbert, 1983). The GNPA sequence is 400-800 m thick and consists of pyroxenites, norites, anorthosites, gabbronorites and PGE-rich chromitite layers (van der Merwe, 2008; Smith et al., 2014). The base metal sulfides and PGE reside in close association in both the upper and lower parts of the GNPA (Maier et al. 2008).

It was initially believed that the well-developed Pyroxenite Marker, which is a thin, continuous unit of orthopyroxenite (Cawthorn et al., 1991; Nex et al., 2002), occurring at the boundary between the lower and upper Main zones in the western and eastern limbs (Kruger, 2005), was not developed in the northern limb (Ashwal et al. 2005). A recent study, however, suggested that a layer equivalent to the Pyroxenite Marker is indeed present in the northern limb (Cawthorn, 2020). Although the MZ has proven to be largely barren of PGEs in the western and eastern BC due to inferred depletions in metal contents (Maier and Barnes, 1999), the upper MZ of the northern limb presents intriguing possibilities for PGE mineralized horizons such as the Troctolite Unit (Cheshire, 2011), PGE-sulfide mineralization at Moordrift (Maier and Barnes, 2010; Holwell et al., 2013), the Aurora project (Maier et al., 2008; McDonald et al., 2017) and the Waterberg Project (Kinnaird et al., 2012; Huthmann et al., 2016).

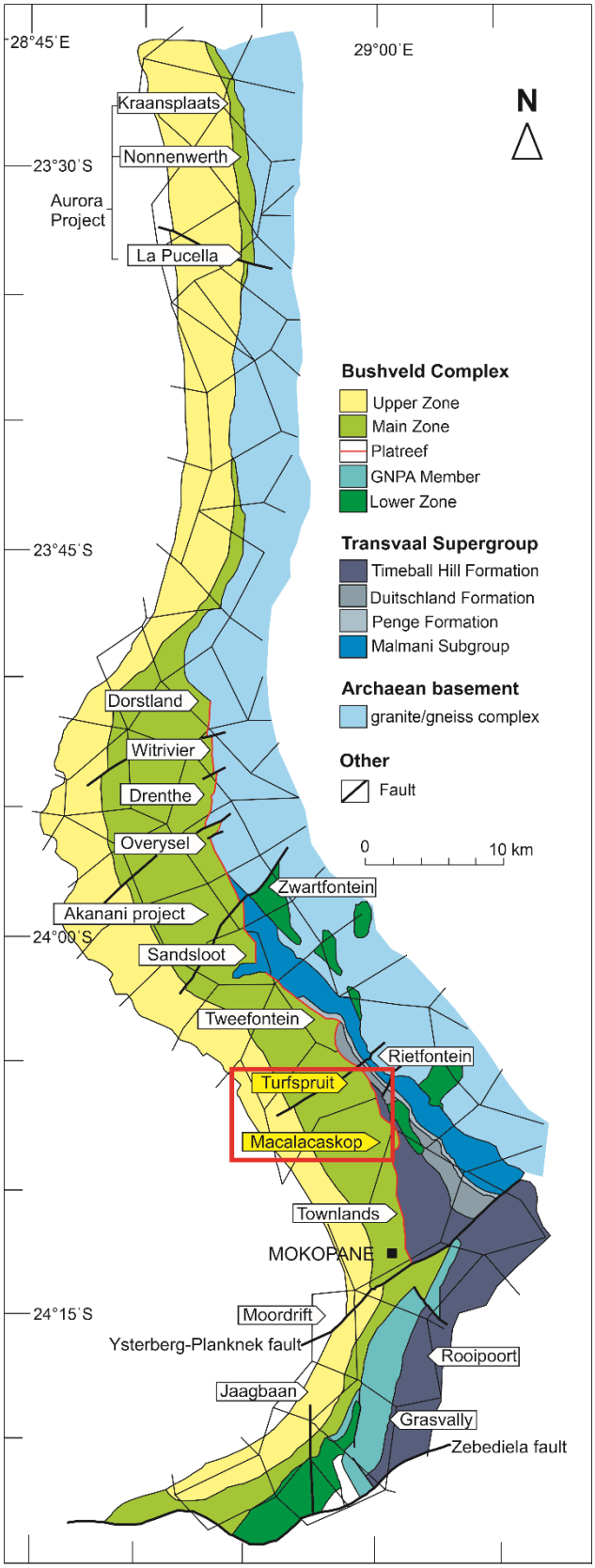

Figure 2.6 Geological map of the northern limb of the BC. After McDonald and Holwell (2011) based on van der Merwe (1976). The study area is indicated by the red rectangle.

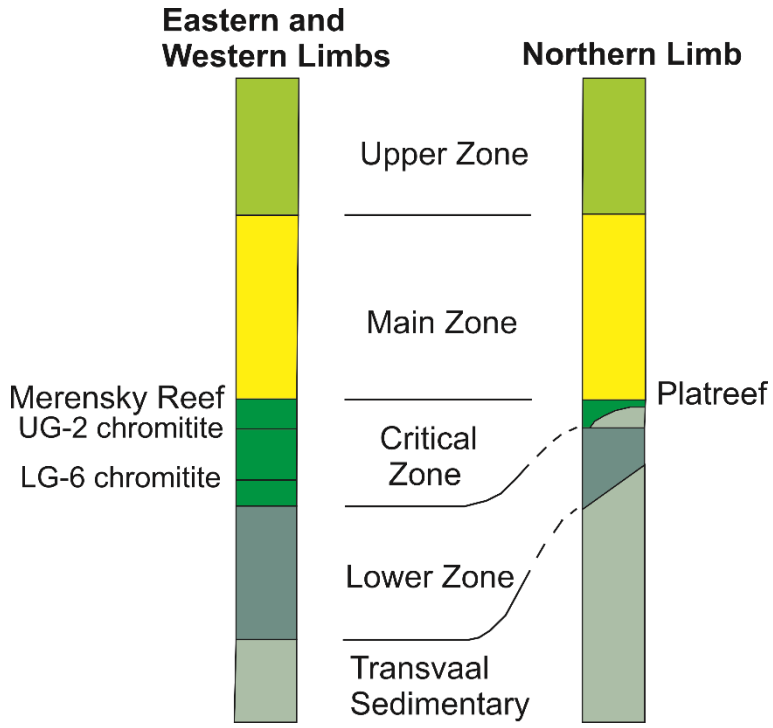

Figure 2.7 Schematic stratigraphic columns of the RLS, showing the putative correlation between stratigraphic units of the northern limb and eastern / western limbs. An inferred correlation is indicated between the Merensky Reef and Platreef. Modified after White (1994) and McDonald and Holwell (2011).

2.2.1 The Platreef

Kinnaird and McDonald (2005) define the Platreef as: “Mafic units enriched in Ni-Cu-PGE that occur between the Archaean granite-gneiss basement or the Transvaal Supergroup and the gabbros and gabbronorites of the Main zone, north of the Planknek Fault”. Located at the base of the mafic succession north of the Ysterberg-Planknek fault, the Platreef is the principal ore horizon in the northern limb and outcrops along a 30 km strike length before it is cut out by the overlying MZ (Fig. 2.6; Ashwal et al., 2005; van der Merwe, 2008; Kinnaird and Nex, 2015). It is broadly accepted that the entire mineralized Platreef sequence intruded as multiple distinctive pyroxenite sills (Kinnaird et al., 2005; Manyeruke et al., 2005; Maier et al., 2008). The thickness of the Platreef is mainly controlled by the topography of the floor rocks and has been reported to be between 10-400 m thick (Kinnaird, 2005). The Platreef is therefore substantially thicker than the < 2 m thick Merensky and UG-2 reefs that occur at approximately the same stratigraphic position in the eastern and western limbs of the RLS. The Platreef is generally dominated by orthopyroxenite, followed by norites, gabbros, anorthosites and sporadic serpentinized harzburgite and xenoliths of floor rocks (Gain and Mostert, 1982; Kinnaird et al., 2005). The presence of interlayered metasedimentary rocks in the Platreef package may increase its thickness (Kinnaird and Nex, 2015).

The transgressive relationship of the Platreef with the diverse floor rocks along strike in addition to magmatic, metasomatic and hydrothermal processes, contributed to the complex and erratic nature of the deposit as well the associated PGE mineralization in specific layers (e.g., Harris and Chaumba, 2001; Hutchinson and Kinnaird, 2005; Kinnaird, 2005; Manyeruke et al., 2005; Sharman-Harris et al., 2005; Holwell and McDonald, 2006, 2007; van der Merwe, 2008; McDonald et al. 2009). Contamination by floor rocks also resulted in the formation of hybrid lithologies, such as wehrlite and lherzolite, informally termed para-pyroxenites (McDonald and Holwell, 2011).

The distribution of base metal sulfide and PGE mineralization in the Platreef vary with depth and along strike (Kinnaird et al., 2005; McDonald and Holwell, 2011). PGE mineralization throughout the Platreef stratigraphy is largely related to the presence of base metal sulfides (mainly pyrrhotite, pentlandite, chalcopyrite and minor pyrite), bismuthides, tellurides, antimonides and arsenides (Gain and Mostert, 1982; Kinnaird et al., 2005; Hutchinson and Kinnaird, 2005; Hutchinson and McDonald, 2008). The Ni-Cu-PGE mineralization is not limited to the pyroxenitic units of the Platreef, but is also present in xenoliths, footwall rocks and occasionally in the base of the overlying MZ (Holwell et al., 2006; Kinnaird and Nex, 2015). At Overysel, sulfide mineralization is reported to penetrate into footwall gneiss (Holwell and McDonald, 2006). The Pt/Pd ratio of the Platreef is around unity compared to the remainder of the BC where the ratio is typically > 2 (Hutchinson and Kinnaird, 2005; McDonald and Holwell, 2011). The magmatic origin of PGE mineralization in the upper Platreef has been broadly confirmed (e.g., Holwell et al. 2007; Maier et al. 2008; Penniston-Dorland et al. 2008; Yudovskaya et al. 2017; Junge et al. 2019; Klemd et al. 2020), however, how it formed and how it relates to the rest of the BC is poorly understood.

Numerous studies have proposed various models to account for the mineralization of the Platreef (see McDonald and Holwell 2011, for an extensive review of these models). The “pudding basin” model as proposed by Naldrett et al. (2008, 2009), describes the BC as having been formed from multiple influxes of magma, where a new influx would cause over-pressurization in the magma chamber resulting in partially fractionated magma being expelled, similarly to the space between two similar-sized nested pudding basins being filled through a feeder located at the base of the lower basin. In relation to the Platreef and UCZ in the remainder of the BC, the authors suggest that the Platreef represents PGE-enriched UCZ magma that escaped up the margins of the limb at different stages of the UCZ development. Furthermore, multiple “pudding basins” are suggested to be present in the BC, one consisting of the eastern and western limbs, one consisting of the northern limb and one at the far western limb, all exposed at different erosion levels.

Buchanan et al. (1981) proposed a model of contact style mineralization where sulfides separated due to country rock contamination after emplacement of Platreef magma, i.e., in situ contamination. Subsequent studies on the contact style Platreef have proposed that sulfides and associated mineralization formed in a deep staging chamber (Holwell et al., 2007; McDonald and Holwell, 2007; McDonald et al., 2009). Sulfur saturation and subsequent collection of PGE by the sulfide melt thus occurred prior to intrusion (Holwell et al., 2007). Sharman et al. (2013) proposed that S was assimilated in a staging chamber bounded by Duitschland Formation of the Transvaal Supergroup. Based on the near mantle range of S isotope data of the upper part of the Platreef, Holwell et al. (2007) proposed that the sulfides and associated mineralization of the Platreef did not form by in-situ contamination. The assimilation of S from country rock is considered as an ore modifying process rather than an initiator of primary mineralization (McDonald and Holwell, 2011), consistent with the findings of Holwell et al. (2007) and Hutchinson and McDonald (2008) who showed that metal tenors of the sulfides are diluted by high proportions of country rock input.

2.2.2 The Flatreef

Until recently, mining of the Platreef in the northern limb has been carried out exclusively by the Mogalakwena mine, the world's largest PGE producing mine, with five open pit operations on the farms Overysel, Zwartfontein and Sandsloot. The deep drilling exploration programme undertaken by Ivanplats Ltd. in 2007, following initial drilling on the farms Turfspruit and Macalacaskop to delineate mineralization suitable for open pit extraction, led to the discovery of the Flatreef. The Flatreef, so called due to its sub-horizontal orientation, refers to the down-dip extension of the Platreef (Fig. 2.8). It is a thick, PGE-bearing mafic zone located at depths of about 750 to 850 m. Mining development of the Flatreef deposit represents the first attempt at underground mining of the "Platreef" in the northern limb.

The Flatreef differs from the steep, shallow Platreef in that its layering is undisturbed, less contaminated and more laterally continuous (Fig. 2.8; Grobler et al. 2019). Historically, several studies of the Platreef in the northern limb focused on the near surface, complex, highly contaminated Platreef (e.g., Kruger, 2005; Kinnaird, 2005; Kinnaird et al., 2005; Sharman-Harris et al., 2005; Hutchinson and Kinnaird, 2008; Pronost et al. 2008; Sharman et al., 2013). Some of the findings of these studies made it difficult to relate the Platreef stratigraphy to the remainder of the BC. The Platreef has been characterized as a contact-style mineralization PGE deposit as it is located at the base of the intrusion, is significantly thicker than reef-style deposits, have massive to disseminated ores and are enriched in base metal sulfides (Maier et al. 2008). It has, however, been shown that stratiform or reef-style mineralization is present

in the thick, undisturbed, upper section of the Platreef, i.e., Flatreef (*sensu stricto*; Yudovskaya et al. 2017).

A stratigraphic correlation between the Platreef in the northern limb and the Merensky Reef in the eastern and western limbs was originally proposed by Wagner (1929) and this idea formed the core of interpretations of subsequent studies (e.g., White 1994). However, the proposed link between the northern limb and the remainder of the BC has been challenged (McDonald et al. 2005). Recent lithostratigraphic and isotopic studies on the newly discovered Flatreef (Grobler et al., 2019; Beukes et al., 2021; Keet et al., 2021; Keir-Sage et al., 2021; Mayer et al., 2021) have shifted the “complicated” narrative of the Platreef.

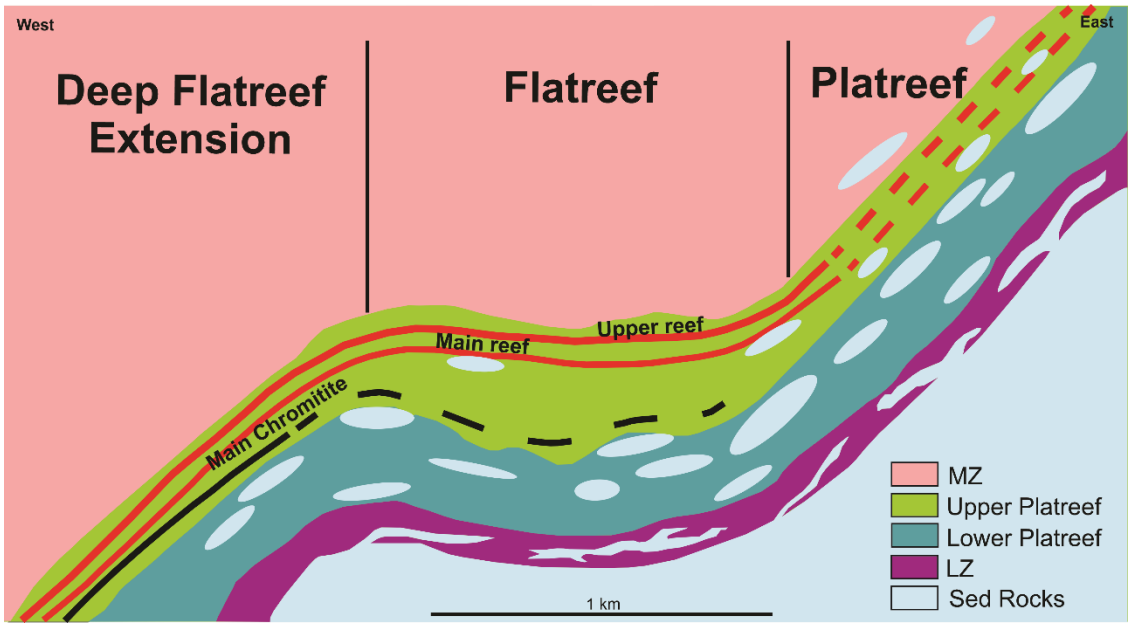

Figure 2.8 Schematic section representing the relationship between Platreef, Flatreef and the deep downdip extension of the Flatreef at Turfspruit, and the position of its main mineralised zones. Large sedimentary xenoliths are metamorphosed and assimilated by intruding Bushveld magma. Modified after Grobler et al. (2019).

CHAPTER 3 :
STRATIGRAPHY OF THE FLATREEF

In this chapter detailed stratigraphic descriptions are presented for the Flatreef units as intersected by boreholes UMT-393 and UMT-276. The igneous lithologies and presence of hybrid lithologies, such as parapyroxenites, as well as floor rock xenoliths is closely related to the interaction of the Platreef magmas with the local country rocks and underlying structures (McDonald and Holwell, 2011). The principal borehole selected for this research study is UMT-393, as it intersected a relatively thick Flatreef succession and evidently contains insignificant hybrid rocks and dolomitic / calc silicate xenoliths, indicating that the Flatreef intersected by this borehole likely underwent limited localized country rock contamination. The Flatreef mainly consists of anorthosite, norite, feldspathic pyroxenite, orthopyroxenite and harzburgite.

3.1. Drill Core UMT-393

Borehole UMT-393 is located on the farm Macalacaskop (243KR) which is adjacent to the town, Mokopane. The borehole is 1164 m deep, intersecting approximately 743 m of MZ rocks and an underlying 324 m thick mafic-ultramafic Flatreef (inclusive of the immediate footwall), which overlies ultramafic rocks of LZ affinity (Fig. 3.1 a). Several granitic veins are observed cross cutting the Flatreef stratigraphy as described by Kinnaird et al. (2005). The uppermost unit of the Flatreef is termed the hanging wall (HW) unit, which is further divided into the HW1, HW2 and HW3 units, from bottom to top. The HW3 unit represents the basal part of the MZ which comprises of mostly norite at its base, where it is in contact with HW2. Further from its basal contact, the HW3 unit consists mostly of medium-grained gabbronorite. This unit is visually more homogeneous compared to the underlying, layered Flatreef. The MZ norite of HW3 has a gradational contact with the underlying HW2 (Fig. 3.2a). The HW2 unit mainly consists of mottled anorthosite in sharp contact with an underlying succession of interlayered norite-pyroxenite-anorthosite, termed “norite cycles” (Kinnaird, 2005), of the HW1 (Fig.3.2b).

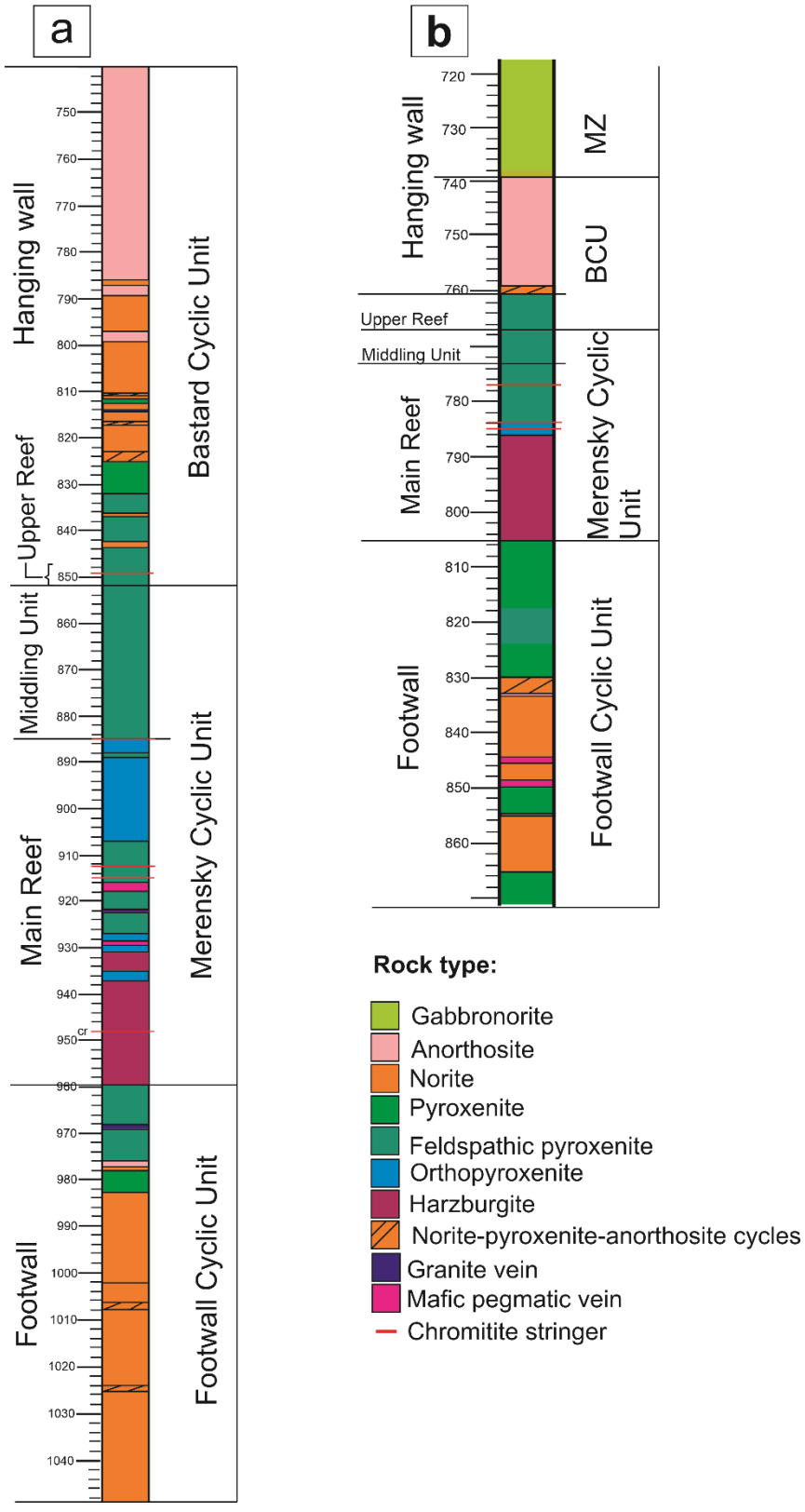

Figure 3.1 Stratigraphic log of Flatreef magmatic stratigraphy including rock types as intersected by drill holes **a** UMT-393 at Macalacaskop and **b** UMT-276 at Turfspruit. Drill hole UMT-393 comprises of relatively thicker stratigraphic unit and overlies LZ whereas UMT-276 directly overlies a sedimentary calc-silicate assimilation zone known as the Footwall Assimilation Zone (FAZ).

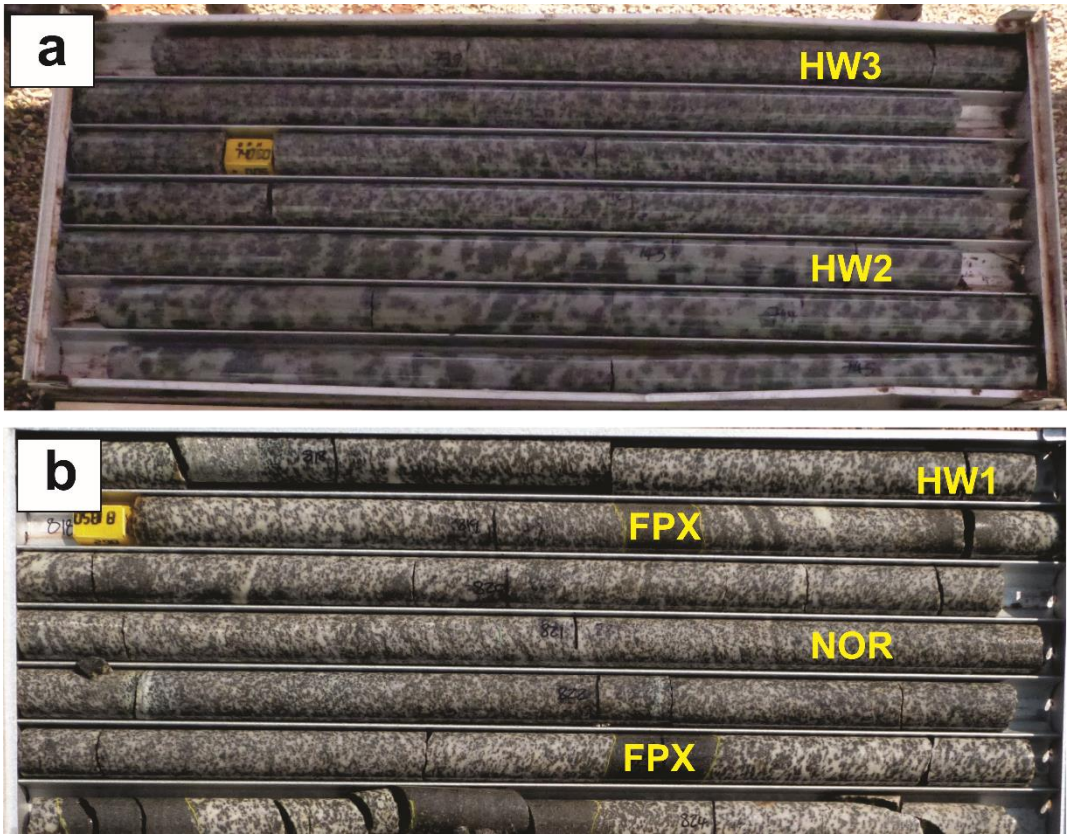

Figure 3.2 Drill core photographs of UMT-393. **a** MZ norite grades into mottled anorthosite of HW2 that marks the top of the Flatreef, **b** interlayered norite-pyroxenite at various thicknesses of the HW1. FPX = feldspathic pyroxenite, NOR = norite.

Below the HW unit, at a depth of about 846 m to 852 m, is a mineralized feldspathic pyroxenite horizon equated with the Bastard Reef in the remainder of the BC, which is in sharp contact with a basal chromitite stringer (Fig. 3.3 a and b; Grobler et al., 2019). Yudovskaya et al. (2017) termed this layer the “Upper Reef”. The Upper Reef has elevated PGE grade with a 3PGE grade of about 1.6 ppm. The HW together with the Upper Reef represents the stratigraphic equivalent of the Bastard Cyclic Unit in the western and eastern limbs of the BC (BCU; Fig. 3.1a).

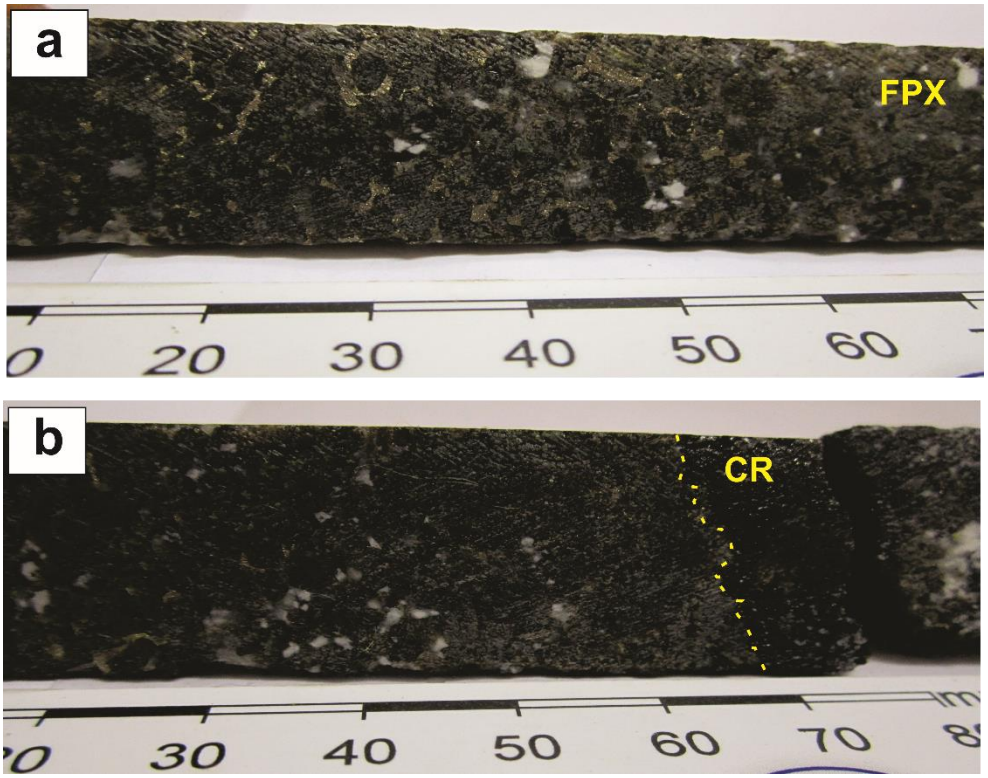

Figure 3.3 Drill core photographs of UMT-393 Bastard Reef pyroxenite indicating **a** net textured base metal sulfides present in close proximity to the chromitite stringer, **b** chromitite stringer with sharp undulating contact. Scale in mm. FPX=feldspathic pyroxenite, CR= chromitite stringer.

Underlying the BCU is an ~35 m thick Middling Unit (MD) consisting of unmineralized feldspathic pyroxenite (Fig. 3.4) and orthopyroxenite with a basal chromitite stringer of < 1 cm thick (Fig. 3.5b). The MD may also be characterised by interlayered pyroxenite-norite-anorthosite and feldspathic orthopyroxenite in other intersections of the Flatreef on the mine property (Grobler et al. 2019).

Figure 3.4 Drill core photograph of MD comprising of feldspathic pyroxenite (FPX) with a granitic vein (GRV) cross cutting the lithologies.

Below the MD, at a depth of about 885 m, is a mineralized package of orthopyroxenite, feldspathic pyroxenite, pegmatoidal orthopyroxenite, harzburgite and chromitite stringers. This unit has the highest PGE content in this Flatreef intersection (total Pt+Pd of up to 5 ppm). This unit is correlated with the Merensky Reef in the western and eastern limbs (Grobler et al. 2019). Yudovskaya et al. (2017) termed this unit the “Main Reef”. The term “Merensky Reef” is used for this mineralized package in this study, but is, however, referred to as the “Main Reef” henceforth and in some of the subsequent chapters for simplicity in comparison to the remainder of the BC. The MD and Main Reef is grouped into the Merensky Cyclic Unit (MCU) of the Flatreef (Fig. 3.1a). The upper part of the Main Reef (Fig. 3.5a), referred to as the M2, consists of orthopyroxenite and feldspathic pyroxenite and is associated with a well-developed thin (<1 cm) upper chromitite stringer (Fig. 3.5b) and a second, poorly developed, chromitite stringer near the base of the unit. The lower part of the Main Reef, referred to as the M1, is intersected at a depth of about 927 m. It is subdivided into an $M1_U$ consisting of pegmatoidal orthopyroxenite (Fig. 3.5c) and medium-grained orthopyroxenite, and an $M1_L$ consisting mainly of harzburgite (Fig. 3.5d). An internal chromitite stringer is observed near the base of the $M1_L$. Base metal sulfides occur disseminated throughout the Merensky Reef unit. Mafic pegmatitic veins occur closely associated with the Merensky Reef and are absent from the overlying units (Fig. 3.5e).

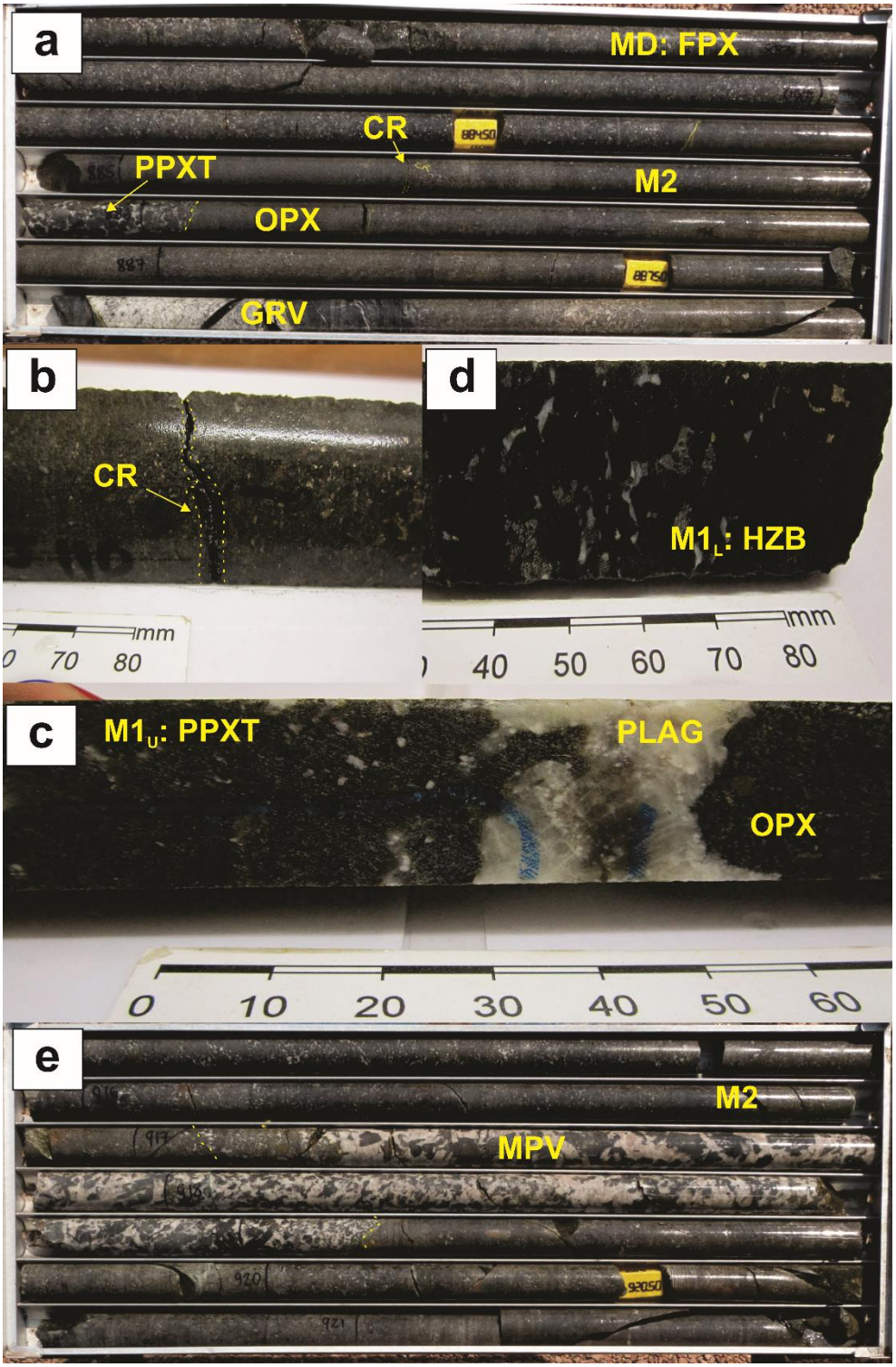

Figure 3.5 Drill core photograph of **a** the thin upper chromitite stringer at the contact between MD and upper Merensky Reef (M2). The presence of a pegmatoidal pyroxenite layer (PPXT) and a thick granitic vein (GRV) is also observed in the M2 orthopyroxenite (OPX). **b** A close-up image of the upper chromitite stringer in (**a**). Base metal sulfide concentrations increase in close proximity to the stringer. **c** Pegmatoidal pyroxenite (PPXT) of the $M1_U$. **d** Serpentinised harzburgite of the $M1_L$. **e** An approximately 2 m thick mafic pegmatoidal vein (MPV) cross cutting pyroxenite near the base of the M2.

The Main Reef overlies the 106 m thick Footwall Cyclic Unit (FCU). This unit varies considerably along strike and depth in the study area. Similarly to the HW1, interlayered norite-pyroxenite-anorthosite (norite cycles) is a common feature in the FCU (Fig. 3.6a). Certain packages of norite cycles are poorly developed and relatively more altered as hybrid lithologies are also present, commonly near the base of the unit (Fig. 3.6b). The FCU in UMT-393 is underlain by ultramafic lithologies of LZ affinity (Fig. 3.6c).

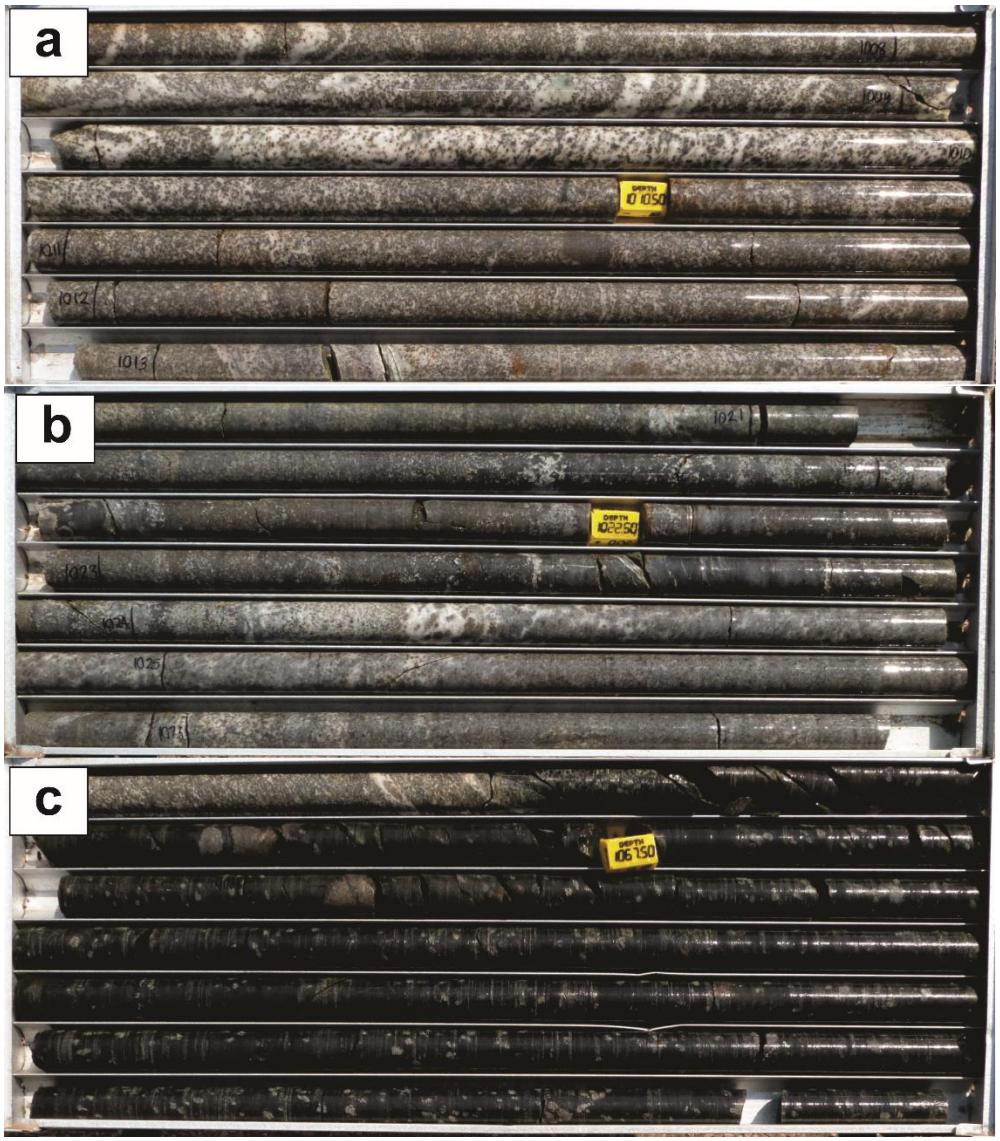

Figure 3.6 Drill core photographs of UMT-393 FCU at a depth of approximately 960 m **a** typical interlayered norite-pyroxenite-anorthosite present in the unit, **b** poorly developed norite cycles with altered hybrid lithologies, c harzburgite of LZ affinity that underlies the FCU.

3.2. Drill Core UMT-276

Drill core UMT-276 was drilled about 3 km north-west of UMT-393 on the adjacent farm, Tursfpruit. The Flatreef stratigraphy in UMT-276 is broadly similar to that of UMT-393 in that HW3 (basal part of the MZ), HW2, HW1, BCU, MCU and FCU are intersected and granitic veins of various thicknesses cross cut the lithologies. A significant difference between these two boreholes is that the Flatreef is significantly thinner in UMT-276. Furthermore, in UMT-276, a zone of sedimentary calc-silicate assimilation, referred to as the Footwall Assimilation Zone (FAZ), occurs below the Flatreef. The difference in the thickness of the Flatreef between UMT-393 and UMT-276 may be attributed to the control of floor rock topography, where thicker successions tend to develop in sub-basins (Kinnaird et al., 2005). In borehole UMT-276, the MZ gabbronorite is underlain by mottled anorthosite of the HW2 (Fig. 3.7a). Mineralized feldspathic pyroxenite of the Upper Reef of about 3 m thick is intersected at a depth of approximately 772 m. The MD consisting of feldspathic pyroxenite underlies the Bastard Reef and is capped by a chromitite stringer. The Main Reef is located below the MD at a depth of approximately 780 m and consists mainly of mineralized medium- to coarse-grained feldspathic pyroxenite of the M2, pegmatoidal orthopyroxenite of the $M1_U$ and medium- to coarse-grained feldspathic harzburgite of the $M1_L$ (Fig. 3.7b). Below the FCU at a depth of 865 m, lithologies are more altered and hybrid lithologies predominate (Fig. 3.7c).

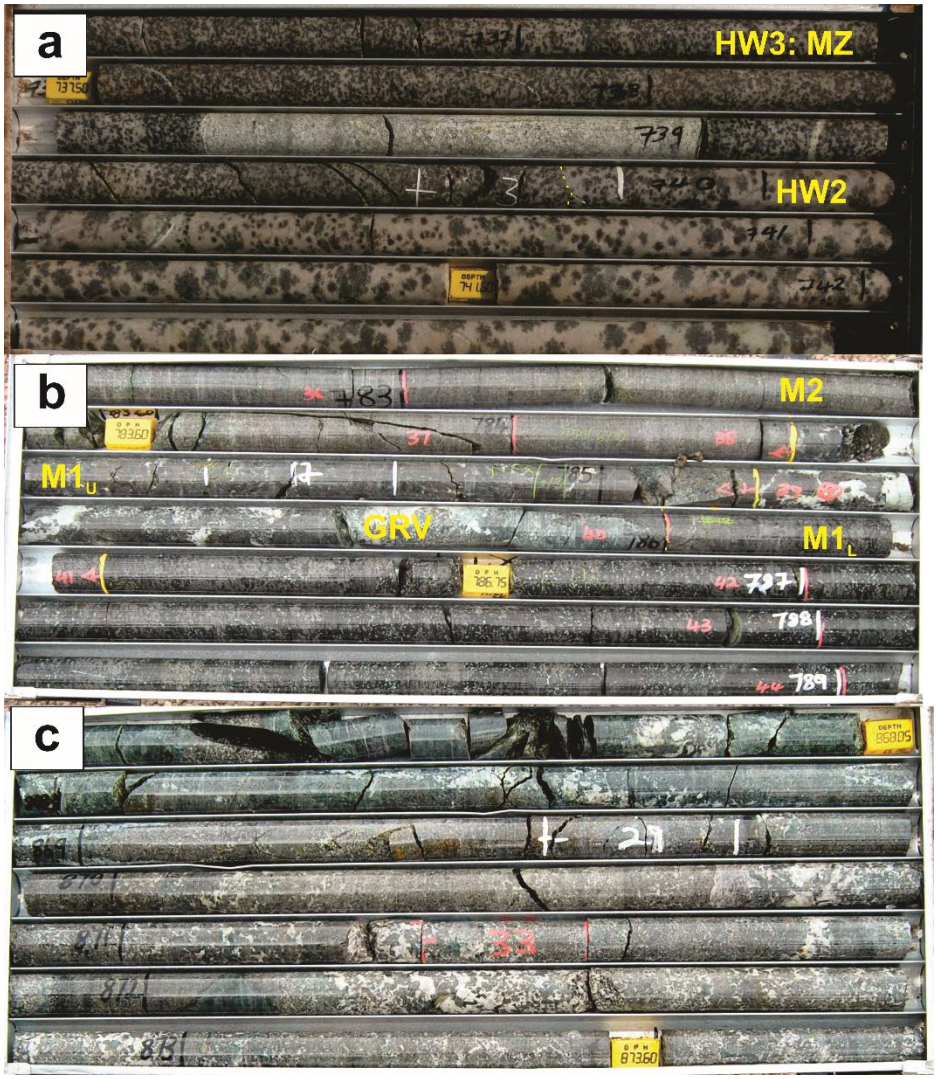

Figure 3.7 Drill core photographs of UMT-276 showing **a** sharp contact of overlying MZ gabbronorite and HW2 mottled anorthosite, **b** a relatively thin Merensky Reef package consisting of M2 feldspathic pyroxenite, $M1_U$ pegmatoidal pyroxenite and $M1_L$ feldspathic harzburgite. **c** altered and hybrid lithologies representing calc-silicate assimilation of the FAZ.

CHAPTER 4 :
ARTICLE 1

Strontium isotope variations in the Flatreef on Macalacaskop, northern limb, Bushveld Complex: Implications for the source of platinum-group elements in the Merensky Reef

4.1 Abstract

The Platreef of the Bushveld Complex is one of three key stratigraphic units, along with the Merensky and UG-2 reefs, in which platinum-group elements are concentrated. The correlation between the Platreef and the stratigraphy from the western and eastern limbs of the BC has been challenging due to the heterogeneous and variable nature of the Platreef along strike. However, the discovery of the Flatreef, interpreted as the down dip, sub-horizontal extension of the Platreef, on the farms Turfspruit and Macalacaskop, opened new avenues for enquiry that allow the study of a magmatic stratigraphy less affected by footwall interaction. In this study, we report on the Sr isotope composition of plagioclase through a ~ 280-m-thick intersection of the Flatreef and its foot- and hanging walls as intersected by borehole UMT-393 drilled on the farm Macalacaskop. Comparison of the Sr-isotopic composition and the anorthite content of plagioclase across this intersection with data from the Merensky and Bastard cyclic units elsewhere in the Bushveld Complex, supports the contention that the Flatreef is a correlative of the Upper Critical Zone – Main Zone transition, including the Merensky and Bastard cyclic units. The available data suggest that the sulfides of the Flatreef and its correlatives in the remainder of the Bushveld Complex originally formed in a deeper staging chamber. During continued magma ascent some of the sulfides were entrained and deposited in the Flatreef.

4.2 Introduction

The Bushveld Complex (BC) (Fig. 1, Maier et al. 2020) is not only the largest layered igneous intrusion on Earth but also hosts the largest resources of platinum group elements (PGE), chromium and vanadium. Although the complex is well studied, many questions remain unanswered and extensions to the known mineral resources are still being made on a regular basis. An assessment of 2015 total PGE resources versus 2010 data shows that the total PGE resources for the Platreef nearly doubled (Mudd et al. 2018). It is only in recent years, with advances in mineral exploration of the Platreef, that the northern limb of the BC has become the focus of more intensive research relative to the western and eastern limbs.

The study of whole rock Sr isotopic variations across the stratigraphy of the BC provided valuable insight into the origin of the PGE-rich Merensky Reef, in the western and eastern

limbs (Kruger and Marsh 1982; Sharpe 1985; Lee and Butcher 1990; Kruger 1994). These authors concluded that the Merensky Reef formed in response to mixing of compositionally and isotopically distinct magmas that gave rise to a distinct inflection in the Sr isotope composition close to the level of the Merensky Reef. It has subsequently been argued, based on plagioclase separates from the Merensky and Bastard cyclic units showing Sr isotope compositions characteristic of the Main Zone, and orthopyroxene separates showing Cr/MgO ratios characteristic of the Critical Zone, that the mixing of cumulus minerals rather than magmas was instrumental in the genesis of the Merensky Reef (Seabrook *et al.* 2005).

The first *in situ* Sr isotope study in the BC was performed by Chutas *et al.* (2012), who made use of the micro-drilling technique. The first *in situ* Sr isotope investigation of BC plagioclase using LA-MC-ICPMS was performed by Yang *et al.* (2013). Karykowski *et al.* (2017) analysed the *in situ* Sr isotope composition of plagioclase across the entire stratigraphy of the western BC. Collectively these studies documented the existence of disequilibrium between coexisting plagioclase and orthopyroxene as well as between the cores of plagioclase crystals within the Merensky and Bastard units of the Upper Critical Zone of the BC. The presence of intra- and intercrystalline isotopic disequilibrium in the BC and other layered intrusions (Seabrook *et al.* 2005, Yang *et al.* 2013, Roelofse *et al*. 2015, Wilson *et al*. 2017, Karykowski *et al.* 2017, Hagen-Peter *et al.* 2019) makes the use and interpretation of whole rock isotope data in isolation problematic.

The Sr-isotopic stratigraphy of the northern limb of the BC was first investigated by Mangwegape *et al.* (2016), who showed variations across the stratigraphy of the northern limb that were comparable to variations throughout the eastern and western limbs of the complex. Huthmann *et al.* (2017) reported *in situ* Sr-isotopic data for plagioclase of the Waterberg Project in the far Northern Limb. They suggested that the Waterberg mafic and ultramafic rocks are not connected to the rest of the BC. The Sr isotopic record of the northern limb, especially of its lower reaches, appears to have been significantly affected by footwall assimilation (van der Merwe 1976; Cawthorn *et al.* 1985; Barton *et al.* 1986), and it has been argued that the Sr isotopic composition of the Platreef is strongly influenced by the nature of the local footwall (Barton *et al.* 1986; Harris *et al.* 2001). For example, at Overysel, where the floor rocks are granitic, initial $^{87}Sr/^{86}Sr$ (Sr_i) in the Platreef ranges from 0.7104 to 0.7227 calculated at 2.05 Ga (Cawthorn *et al.* 1985). Barton *et al.* (1986) reported similar values for the Platreef at Overysel (0.7107 to 0.7226 calculated at 2.05 Ga), but strikingly different values (0.7054 to 0.7147) towards the south at Sandsloot, where the footwall is dolomitic. At Turfspruit, Kruger (2005a) reported initial Sr isotope ratios of 0.710-0.711 for the shallow Platreef. Overall, the Platreef exhibits significantly more radiogenic Sr isotope compositions

compared to the “typical” BC stratigraphy as reported by Lee and Butcher (1990), Kruger (1990), Kruger (1994) and Karykowski *et al.* (2017), for example.

The discovery of the Flatreef, a deep, sub-horizontal, down-dip extension of the Platreef, enabled us to study a supposedly less contaminated magmatic stratigraphy of the Platreef (Grobler *et al.* 2019). In this study, we report *in situ* Sr isotope data for plagioclase across the Flatreef stratigraphy, as sampled by borehole UMT-393 drilled on the farm Macalacaskop by Ivanplats (Pty) Ltd.

4.3 Regional geology

The Rustenburg Layered Suite (RLS), which forms the mafic-ultramafic portion of the BC, crystallized between ~2055 – 2057 Ma (Zeh *et al.* 2015; Scoates and Wall 2015). The northern limb of the BC, part of which forms the focus of this study, has a sinuous outcrop, striking N-S and dipping roughly WSW with a strike length of approximately 100 km and a width of 5 km (van der Merwe 1976) (Fig. 4.1). This outcrop stretches from the Melinda Fault in the north where it is overlain by Waterberg sediments, to the Zebediela Fault in the south, where it is overlain by Karoo sediments (Kinnaird *et al.* 2005). New geophysical data by Finn *et al*. (2015) show that the northern limb has a modelled area of ~160 km x ~125 km. The Thabazimbi-Murchison lineament (TML) structurally separates the northern limb from the western and eastern limbs (Yudovskaya *et al*. 2017).

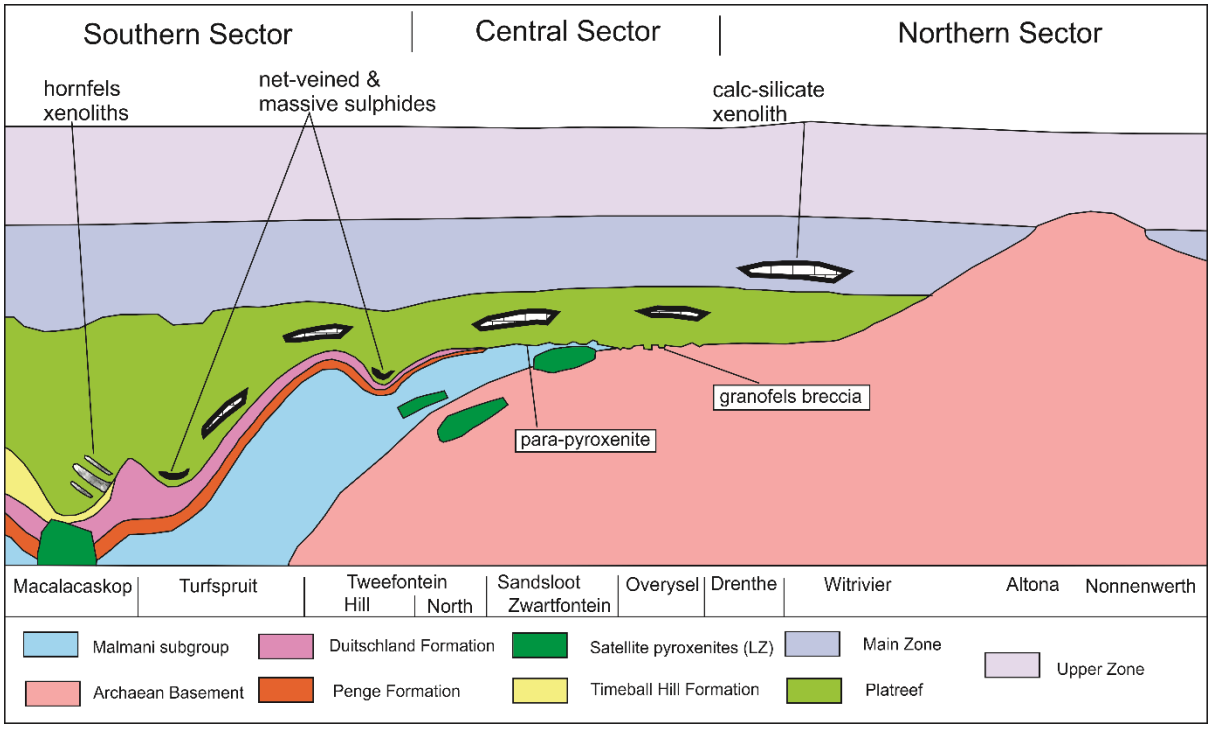

Figure 4.1 Schematic longitudinal section through the Platreef over the entire strike length modified after Kinnaird et al. (2005). Note that between Witrivier and Altona a significant strike length is not shown

4.3.1 Stratigraphy of the northern limb

The stratigraphy of the northern limb has been correlated with that of the western and eastern limbs since the start of exploration in the BC about a century ago (Wagner 1929; White 1994; Kinnaird *et al*. 2005; Naldrett *et al.* 2008; Yudovskaya *et al.* 2017; Grobler *et al.* 2019). The zonal subdivision as applied to the eastern and western limbs of the RLS is also used in the northern limb, despite the presence of localised yet distinctive stratigraphic differences (Ashwal *et al.* 2005; McDonald *et al.* 2005). Significant parts of the stratigraphy of the RLS appears to be missing from parts of the northern limb (McDonald and Holwell 2011) or are possibly not recognised. A detailed description of the stratigraphy of the northern limb is provided in the introductory paper to this thematic issue (Maier *et al.* 2020).

4.3.2 The Platreef and Flatreef at Turfspruit and Macalacaskop

The Platreef is the main host to the PGE mineralization in the northern limb. Due to the presence of topographic basement highs in the southern sector (see Fig. 4.1), the Platreef reaches up to 400 m in thickness at Macalacaskop, whereas at Turfspruit, the thickness is up to ~250 m (Kinnaird 2005). Due to the intrusion of the RLS into the Transvaal Supergroup, the Transvaal sediments underwent localised contact metamorphism. The contamination of Platreef magma by country rock assimilation and related hydrothermal activity resulted in the apparent complex and erratic nature of the layering. Correlation of the Platreef stratigraphy with the RLS in the eastern and western BC therefore remains controversial (McDonald *et al.* 2005; Maier *et al*. 2008; McDonald and Holwell 2011). Dolomitic and calcsilicate xenoliths occur frequently within the Platreef on Turfspruit, whereas on Macalacaskop, xenoliths of quartzite, hornfelsed banded ironstone, shale, mudstone and siltstone are present (Hutchinson and Kinnaird 2005; Kinnaird *et al.* 2005, Hutchinson and McDonald 2008; McDonald and Holwell 2011).

Prior to deep drilling in the southern sector of the northern limb by Ivanplats (Pty) Ltd., knowledge on the stratigraphy of the Platreef was mostly derived from drilling that intersected a relatively shallow Platreef along the eastern edge of the northern limb (Kinnaird *et al.* 2005; Kinnaird 2005). Originally, drilling by Ivanplats at Turfspruit and Macalacaskop was directed at outlining mineralization that would permit open pit mining down to a depth of ~400 m. However, in 2007, a deep drilling program was launched by the company to determine the feasibility of underground mining (Grobler *et al.,* 2019). This led to the discovery of the Flatreef, the down-dip, sub-horizontal extension of the Platreef found to the southwest of the limited outcrop at Turfspruit and Macalacaskop. The Flatreef is located at depths of approximately 750-850 m. The sub-horizontal dip of the Flatreef extends for approx. 1-2 km but returns to its

usual 40° westerly dip in the far western portions of Turfspruit (Grobler *et al.* 2019). The Flatreef is divided into the following stratigraphic units (as per Grobler *et al.* 2019), simplified in Fig. 4.2 a and b:

- Hanging wall unit 2 (HW2) – A laterally consistent mottled anorthosite with occasional ultramafic autoliths located below the MZ.
- Hanging wall unit 1 (HW1) – Transitional zone between MZ and the Flatreef consisting of sulfide poor interlayered pyroxenite, norite, mottled anorthosite and gabbro. The upper and lower contacts of pyroxenite layers/lenses are normally altered.
- Bastard Reef – A pyroxenite layer below HW1 that generally has mineralization particularly associated with a poorly developed basal chromite stringer. This unit was termed the “Upper Reef” by Yudovskaya *et al.* (2017).
- Middling unit – Underlying the Bastard Reef this unit consists of pyroxenite-norite-anorthosite cycles and weakly mineralized feldspathic orthopyroxenite.
- Merensky Reef – A sulfide rich orthopyroxenite bracketed by an erratically developed upper, and a continuous basal chromite stringer (M2). Underlying the mineralized orthopyroxenite are mineralized pegmatoidal orthopyroxenite ($M1_U$) and/or harzburgite ($M1_L$). Yudovskaya *et al*. (2017) grouped these lithologies into the Main Reef.
- Footwall Cyclic Unit (FCU) – This unit underlies the Merensky Reef and shows strong lithological variation along strike and depth. It is commonly characterized by “Norite Cycles” (Kinnaird *et al*. 2005) consisting of alternating pyroxenite-norite-anorthosite layers. Sedimentary xenoliths are abundant. Units in which the cyclic magmatic package has been modified and where magmatic contacts are missing, are referred to as the “Footwall Assimilation Zone”.

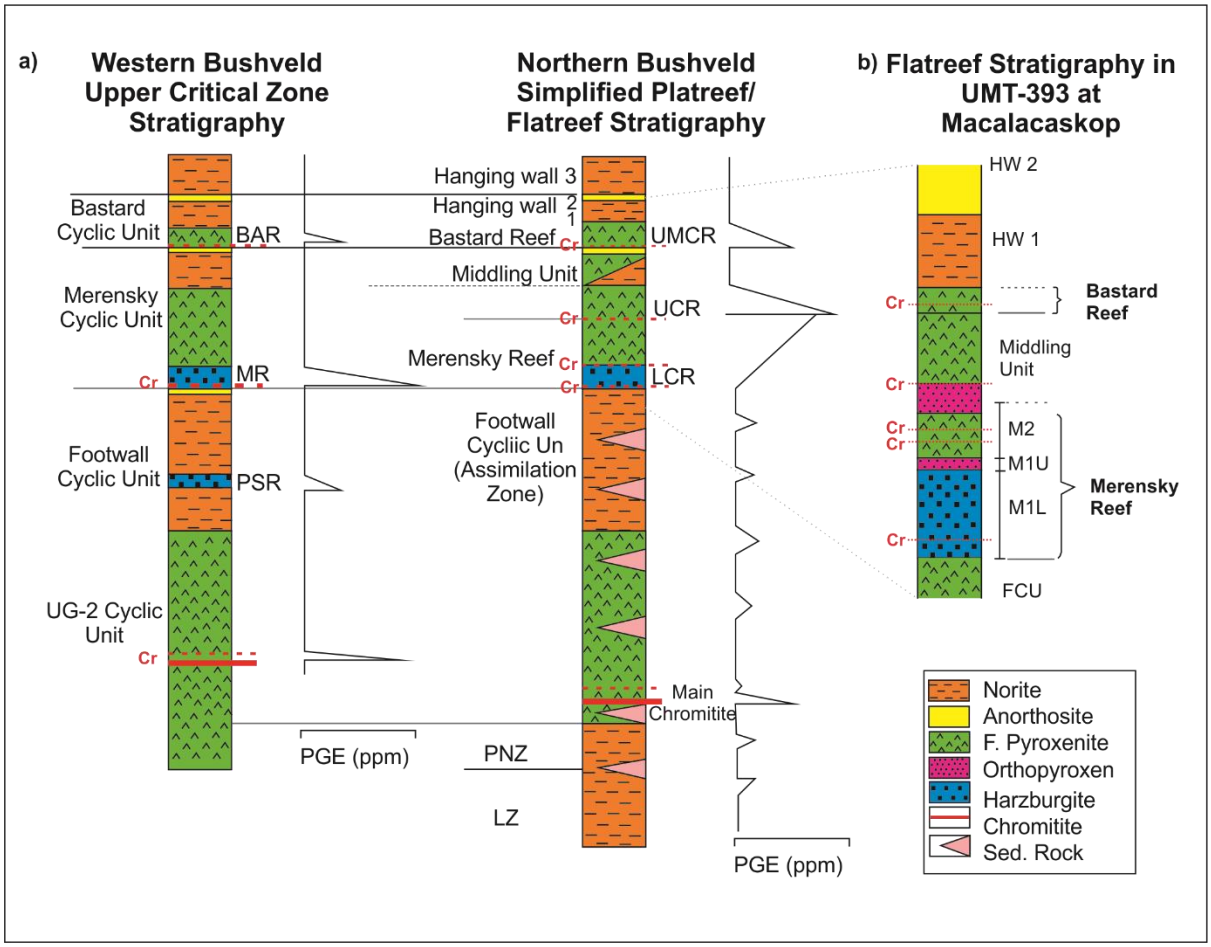

Figure 4.2 a Schematic illustration of a stratigraphic comparison between Platreef/Flatreef with the Upper Critical Zone (UCZ) in the western BC. **b** Stratigraphy of the Flatreef in borehole UMT-393, Macalacaskop. Modified after Grobler et al., 2019. Cr = chromite stringer

4.4 Sample locations and descriptions

Samples for *in situ* Sr isotope analysis were collected from drill core UMT-393 generated during drilling of a 1163.5 m deep hole at 24.122856°S 28.975577°E (see Fig. 4.2 in Maier *et al.* 2020, for the location of the borehole). We analysed samples from the hanging wall units (HW 1 and 2), Bastard Reef, Middling unit (MD), Merensky Reef and Footwall Cyclic Unit (FCU).

The FCU is characterised by poorly developed pyroxenite-norite-anorthosite interlayered lithologies. Nine samples have been analysed from the uppermost 70 m of the FCU. The samples comprise medium grained norite, medium to coarse grained feldspathic pyroxenite and mottled anorthosite. Base metal sulfides (BMS) are irregularly disseminated within the FCU. Orthopyroxene and plagioclase are the dominant minerals present. In the pyroxenite, plagioclase occurs interstitially to cumulus orthopyroxene (Fig. 4.3a), whereas in the anorthosite, orthopyroxene is interstitial to apparently cumulus plagioclase. Clinopyroxene is present as oikocrysts enclosing orthopyroxene and plagioclase chadacrysts or as exsolution

lamellae occurring within orthopyroxene. Reaction relationships are visible for clinopyroxene oikocrysts and included/resorbed orthopyroxene (Fig. 4.3b). Rounded plagioclase inclusions in orthopyroxene are mostly observed in norite samples (Fig. 4.3c). Deformed orthopyroxene (Fig. 4.3d), as exemplified by the presence of bent clinopyroxene exsolution lamellae, and spindle shaped plagioclase twins (Fig. 4.3a), are not common in the FCU but were observed in some samples.

The lower Merensky Reef (M1L) is ~30 m thick and consists of harzburgite (Fig. 4.2b) primarily containing olivine and orthopyroxene with minor plagioclase and approximately 5% BMS. The M1L shows the highest degree of alteration (mostly serpentinization) resulting in only remnants of olivine being observed (Fig. 4.3e). Undulose extinction of olivine is a dominant deformation feature in the olivine bearing lithologies of the M1L (Fig. 4.3f). Orthopyroxene in FCU pyroxenite close to M1L contact displays triple junctions (with apparent 120° angles) indicative of textural equilibration (Fig. 4.3g). A chromite stringer is present near the base of M1L (Fig. 4.3h). Chromite is more commonly found as disseminated inclusions within olivine (Fig. 4.3e) and orthopyroxene throughout this layer. M1L is overlain by M1U, consisting of a 5 m thick, medium grained, relatively unaltered orthopyroxenite with approximately 3% sulfides.

The upper Merensky Reef (M2, ~30 m thick) consists of mineralized orthopyroxenite and feldspathic pyroxenite (Figs. 4.2b and 4.5). The orthopyroxenite is medium-grained and generally displays equilibrium textures such as 120° triple junctions. Clinopyroxene is mainly present as oikocrysts enclosing orthopyroxene and plagioclase or as exsolution lamellae within orthopyroxene. Notably, exsolution lamellae of clinopyroxene are only found in the larger orthopyroxene crystals (Fig. 4.4a). Deformation textures such as bent exsolution lamellae and bent twin lamellae are observed in orthopyroxene and plagioclase, respectively (Fig. 4.4b). Chromite forms 2 thin layers, one near the base of M2 and the other at the top. This layer contains the highest Pt + Pd concentrations (5 ppm) in UMT-393 (Fig. 4.5). Base metal sulfides appear as i) inclusions within pyroxene crystals, ii) interstitial phases or iii) veins (as seen in orthopyroxenite at the base of the MD).

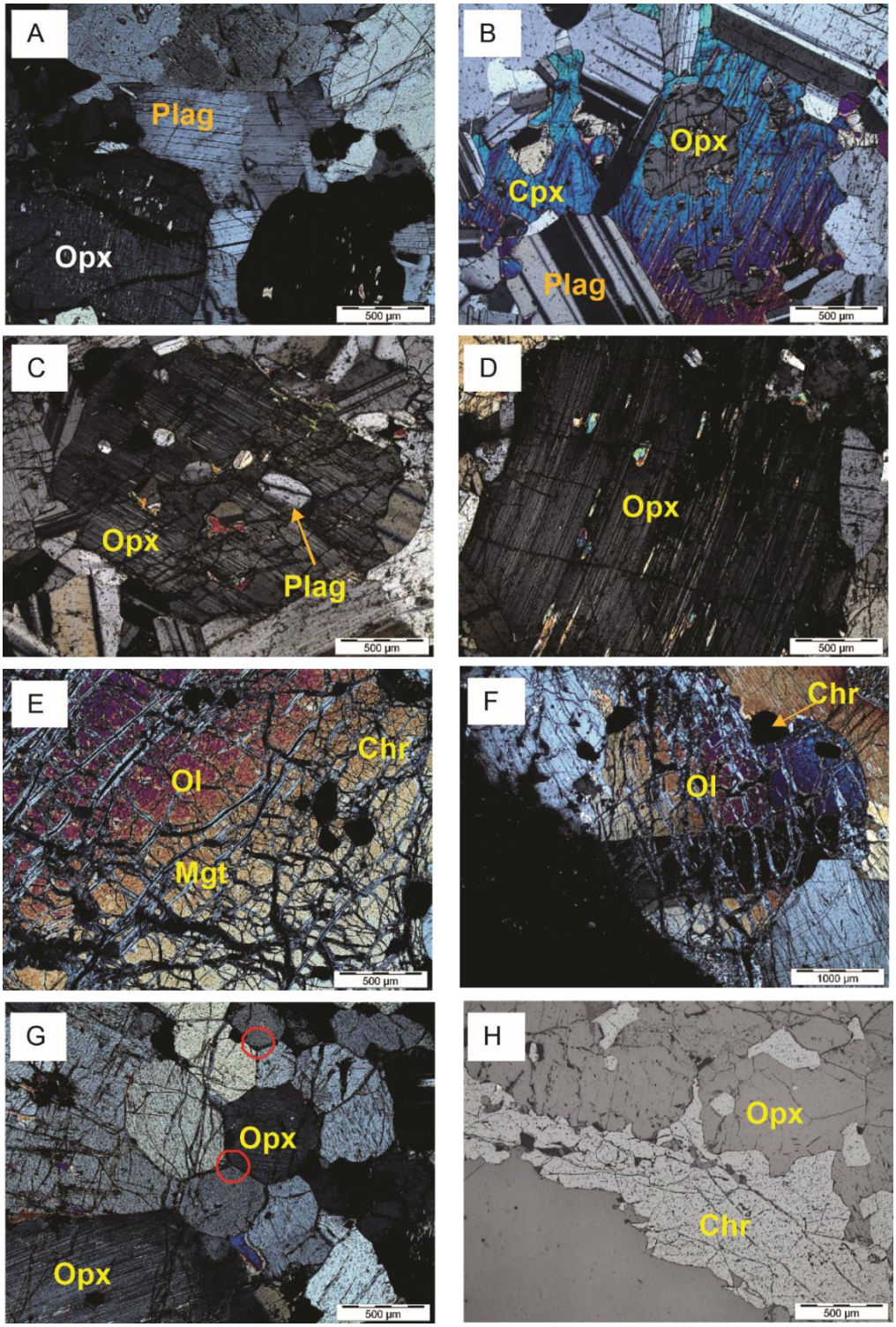

Figure 4.3 Photomicrographs showing typical petrological features of the FCU, $M1_L$ and M2 in cross-polarized, transmitted (**A-G**) and plane-polarized, reflected light (**H**). **A** Bent intercumulus plagioclase with cumulus orthopyroxene displaying exsolution lamellae in the FCU feldspathic pyroxenite; **B** Clinopyroxene oikocryst with reactionary relationships with included orthopyroxenes in norite of the FCU; **C** Orthopyroxene crystal with anhedral plagioclase inclusions in a FCU norite sample; **D** Bent orthopyroxene crystal from a poorly developed norite cycle in the FCU; **E** Serpentinised olivine accompanied by euhedral chromite and mesh textured magnetite in the Merensky Reef ($M1_L$); **F** Undulose extinction of serpentinized olivine in $M1_L$ harzburgite; **G** Equilibration textures in FCU pyroxenite adjacent to $M1_L$, note apparent 120˚ triple junctions indicated by red circles; **H** Chromite stringer found near the base of the Merensky Reef ($M1_L$).

The MD overlying the Merensky Reef is dominated by feldspathic pyroxenite containing minor amounts of BMS which are overgrown by alteration minerals such a mica and amphibole (Fig. 4.4c). The feldspathic pyroxenite is characterised by cumulus orthopyroxene and lesser intercumulus plagioclase. Above the MD occurs the sulfide-rich feldspathic pyroxenite of the Bastard Reef. Particularly elevated PGE concentrations are associated with the basal chromite layer of the Bastard Reef. Several orthopyroxene crystals within the pyroxenites of the Bastard Reef, MD and Merensky Reef, as well as olivine crystals found mostly in the harzburgite of the Merensky Reef, contain plagioclase inclusions. Similar features have been interpreted as resorbed remnants of crystals suspended in the resident magma prior to emplacement of unevolved magma (Maier *et al.*1994).

The hanging wall unit (HW1 and HW2) consists of interlayered pyroxenite, norite and mottled anorthosite. It is up to 83 m thick and is overlain by the MZ (HW3). Zoned plagioclase occurs sporadically in the anorthosite of HW2 near the base of the MZ (Fig. 4.4d) consistent with the findings of Roelofse and Ashwal (2012), who showed the presence of distinctly zoned plagioclase near the base of the MZ overlying the Platreef in the Moordkopje (MO-1) drill core. Feldspathic pyroxenite of HW1 and the MD commonly contains clusters of texturally equilibrated fine-grained orthopyroxene located between medium- to coarse-grained orthopyroxene (Fig. 4.4e). McDonald *et al.* (2017) described these clusters in the orthopyroxenites and websterites of the Aurora Project Cu-Ni-PGE magmatic sulfide deposit in the northern BC as possible autoliths. Norite samples from the HW consist of cumulus plagioclase and orthopyroxene in approximately equal proportions with minor interstitial clinopyroxene oikocrysts partially enclosing orthopyroxene and plagioclase (Fig. 4.4f). Clinopyroxene oikocrysts in the pyroxenites, however, enclose smaller anhedral plagioclase and pyroxene chadacrysts containing mineral inclusions (Fig. 4.4g). Hanging wall unit anorthosite consists predominantly of cumulus plagioclase with lesser amounts of orthopyroxene and clinopyroxene occurring as oikocrysts. Plagioclase present as inclusions within orthopyroxene tends to exhibit wider twin lamellae (Fig. 4.4h), compared to the plagioclase that is not enclosed within orthopyroxene.

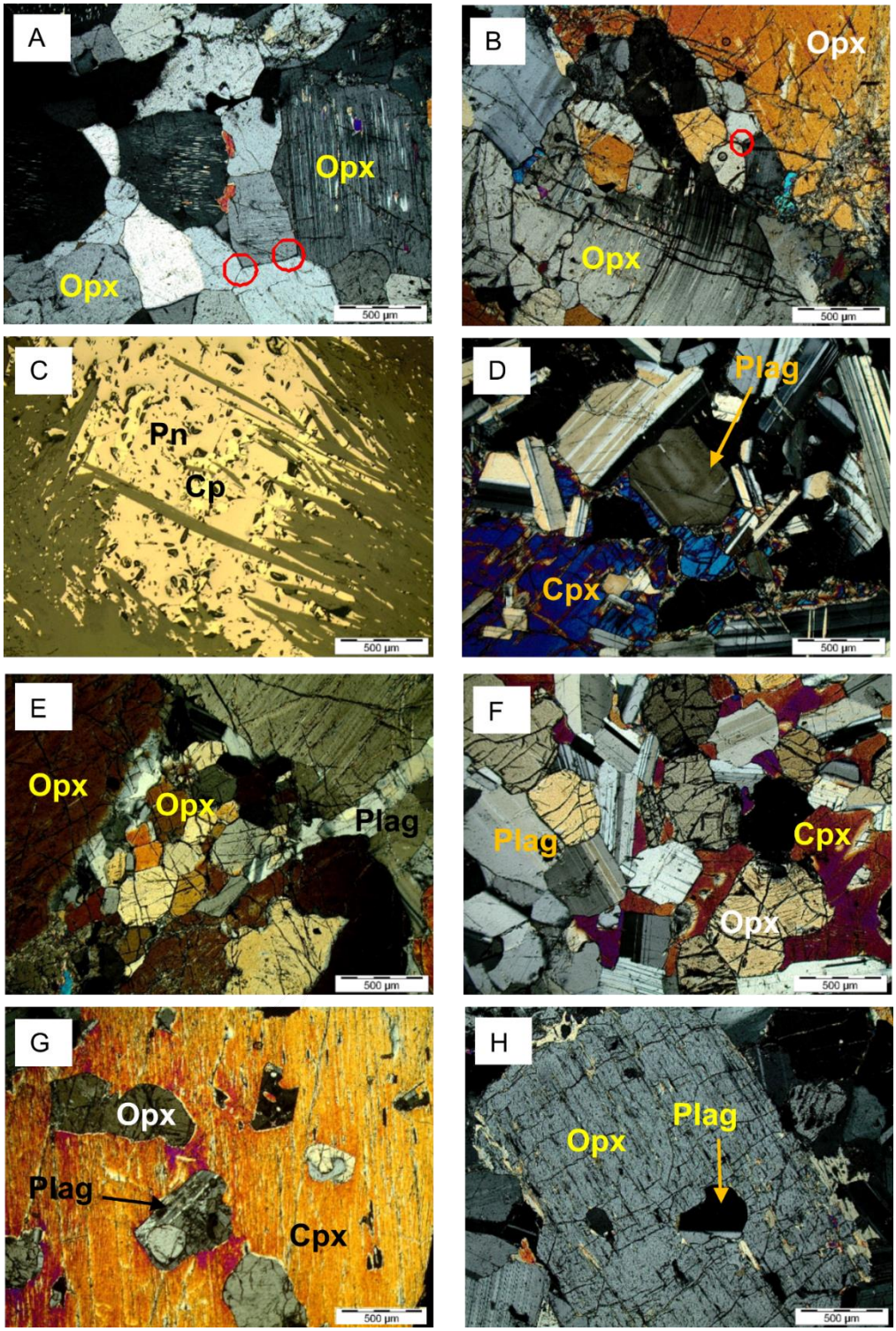

Figure 4.4 Photomicrographs of typical rock textures of the Flatreef under cross-polarized, transmitted (**A, B, D-H**) and plane-polarized, reflected light (**C**). **A** Orthopyroxenite comprised mainly of impinging orthopyroxene crystals in the Merensky Reef (M2); **B** Deformed orthopyroxene with exsolution lamellae in M2 feldspathic pyroxenite; **C** pentlandite (Pn) and chalcopyrite (Cp), overgrown by actinolite in the MD. **D** Clinopyroxene oikocryst with plagioclase chadacrysts in anorthosite from HW2. Note the zonation of plagioclase. **E** HW feldspathic pyroxenite with fine grained orthopyroxene interstitial to coarser orthopyroxene. **F** Norite with cumulus orthopyroxene and plagioclase from HW1; **G** Clinopyroxene oikocryst with plagioclase and orthopyroxene inclusions in a porphyritic textured pyroxenite in HW1; **H** Plagioclase inclusions exhibiting wide twin lamellae within an orthopyroxene from a HW norite sample.

4.5 Analytical Methods

A total of 55 polished mounts and 5 thin sections were prepared for Sr isotope analysis. *In situ* Sr isotope analyses of plagioclase crystals were performed by laser ablation multi-collector inductively coupled plasma mass spectrometry (LA-MC-ICPMS) at the Spectrum Analytical Facility of the University of Johannesburg. A minimum of three plagioclase crystals were analysed for every sample. The aim of this study was not to study isotopic disequilibrium within plagioclase, but to obtain Sr isotopic data that could be used to compare the Flatreef with the remainder of the BC. Spot analyses were mostly performed on plagioclase cores, although plagioclase rims were occasionally also analysed.

The instrumental setup consisted of a 193 nm ArF RESOlution SE excimer laser, linked to a Nu Plasma II MC-ICPMS equipped with 16 Faraday detectors and 5 ion counting detectors. Samples were ablated in He gas (gas flow of 0.28 L/min) within a Laurin Technic dual-volume cell. Plasma RF power was 1300W, coolant gas flow 13.0 L/min, auxiliary gas flow 0.88 L/min, and nebuliser gas flow 1.0 L/min. Prior to the commencement of daily measurements, the instrumentation was tuned for optimal signal intensity and stability, using an in-house glass standard of plagioclase composition. Tuning was also performed during the day as required.

For all measurements, backgrounds were measured on peak for 25 seconds before the start of the ablation and subtracted from the ablation signals. An integration time of 0.2 s was used. For thin sections, line measurements of lengths between 350 µm and 500 µm, depending on grain size, were performed at a speed of 0.008 mm/s. These line lengths resulted in ablation times of between 45 and 60 s for thin section measurements. For polished mounts, spot diameters of 100 µm were used. Ablation time for spot measurements was 70 s. For all measurements a repetition rate of 10 Hz was used, and the laser beam had a nominal energy of 4 mJ at 50% attenuation, delivering a laser density of about 3.3 J/cm^2.

Kr isobaric interferences on ^{84}Sr and ^{86}Sr were corrected by blank subtraction. The accepted ^{86}Sr/^{88}Sr ratio of 0.1194 (Steiger and Jäger, 1977) was used to correct mass bias. To assess analytical stability and accuracy the in-house plagioclase glass standard, containing high Sr and low Rb concentrations, was measured after every 10 to 20 samples, and the USGS reference glass standard BHVO2G was measured after every five samples (Table A-3, Appendix A). The ^{87}Rb contribution was calculated from the ^{85}Rb signal after mass bias correction, using the natural ^{87}Rb/^{85}Rb isotope ratio of 0.3858. The Sr mass bias correction factor was adjusted through analysis of the BHVO2G reference glass to effectively correct for Rb mass bias, to obtain the accepted ^{87}Sr/^{86}Sr value of 0.70347. An empirical correction was

applied to address laser-induced fractionation of Rb and Sr, determined so as to obtain the correct $^{87}Rb/^{86}Sr$ value of 0.0668 for reference glass BHVO2G (Elburg et al, 2005). For detailed information regarding detector setup and monitoring for potential interferences, refer to Huthmann *et al*. (2017).

During the course of this study the BHVO2G reference material returned an average $^{87}Sr/^{86}Sr$ ratio of 0.70339 ± 0.0002 (2 σ). Initial $^{87}Sr/^{86}Sr$ ratios (Sr_i) were calculated for an age of 2054.89 Ma (Zeh *et al.* 2015), using a decay constant of 1.393×10^{-11} (Nebel *et al.* 2011).

Plagioclase elemental compositions of 25 samples were determined at the Department of Geology, Rhodes University, using a JEOL JXA 8230 Superprobe, equipped with four wavelength-dispersive spectrometers. Analyses were performed at an acceleration voltage of 15 kV and a beam current of 20 nA. Counting times were 10 seconds on peak and 5 seconds on background for all elements excluding potassium where counting time was 30 seconds on peak and 15 seconds on background. Natural standards and ZAF correction matrices were used for quantification. The An contents of plagioclase reported are from the same samples Sr isotopic analyses were performed on, but the microprobe analyses were not performed on exactly the same spots used for LA-MC-ICPMS analyses.

4.6 Results

4.6.1 Sr isotope composition of plagioclase

A total of 262 Sr isotope measurements were performed on 60 samples of the Flatreef as intersected by borehole UMT-393. Table 4.1 contains the average in situ Sr isotopic compositions and anorthite contents of plagioclase for all analysed samples. A graphic representation of the results is shown in Fig. 4.5, with the full dataset, including data for individual spots analysed, given in Tables A-1 and A-2 in Appendix A.

The lowest Sr_i ratio in plagioclase is found in a norite sample from the FCU with values ranging between 0.7062 and 0.7066. This sample is from a stratigraphic depth of 1028.28m, which is the deepest sample analysed from the UMT-393 drill core. Similar Sr_i of plagioclase in a norite sample approximately 360m below the Merensky Reef, western BC, was reported by Karykowski *et al.* (2017) where Sr_i ranges from 0.7057 to 0.7065 (weighted average of 0.7061). In the Flatreef, plagioclase shows a trend of increasing Sr_i upwards throughout FCU, attaining a maximum Sr_i of 0.7073 below the contact with feldspathic pyroxenite of $M1_L$. An irregular upward increase in Sr_i continues throughout the Merensky Reef, culminating in the highest observed Sr_i of 0.7096 in orthopyroxenite at the top of M2. The lowermost sample from

the Merensky Reef has a Sr_i of 0.7071, with the Merensky Reef as a whole having an average plagioclase Sr_i of 0.7079. The average Sr_i of the Middling unit, Bastard Reef and Hanging wall units are ~0.7078, 0.7081 and 0.7076, respectively. Thus, the Sr_i of these units is lower than in the Merensky Reef, but higher than in the FCU. The middling unit shows pronounced inter- and intracrystalline isotope variation among plagioclase with Sr_i ranging from 0.7068 to 0.7095. In comparison, the Sr_i of plagioclase in a pyroxenite sample approximately 2 m above the Merensky Reef in the western BC (an equivalent to the Middling unit) ranges between 0.7063 to 0.7077 (Yang *et al.* 2013). Flatreef samples from the units overlying and underlying the Middling unit show relatively little variation in Sr_i. For example, the Bastard Reef in our profile shows a range in Sr_i from 0.7077 to 0.7083. In comparison, Yang *et al.* (2013) analysed two Bastard Reef samples from the western limb with Sr_i ranging between 0.7068 and 0.7082.

4.6.2 An content of plagioclase

Stratigraphic variation in anorthite content of plagioclase is shown in Fig. 4.5. The highest An% was found in the FCU, where anorthosite contains plagioclase with an average An% of 79 (An78-80) (Fig. 4.5). In the Merensky Reef, plagioclase is interstitial and its compositions are significantly more sodic. Interstitial plagioclase of the harzburgitic $M1_L$ has an average An content of 61 (An60-64), whereas the An% of interstitial plagioclase in orthopyroxenite of $M1_U$ varies between 57 and 66, with an average of 61. In comparison, interstitial plagioclase from a pyroxenite from the Merensky Cyclic Unit in the western limb displays An% ranging from 64 to 66 (Yang *et al.* 2013). In the Middling unit, interstitial plagioclase within feldspathic pyroxenites show a wide range of An contents, from 54-77 (An66 on average). In the feldspathic pyroxenites of the Bastard Reef An% of interstitial plagioclase ranges between 56 and 73 which is similar to that reported by Yang *et al.* (2013) for the western Bushveld Complex, i.e. 52 to 74. Interstitial plagioclase in feldspathic pyroxenite of HW1 has a compositional range of An69-73 (average An71). The An% in the cumulus plagioclase of HW anorthosite is lower, ranging between 63 and 73 (70 on average). In contrast, the An% of HW anorthosite in the western BC ranges between 72 and 75 (Yang *et al.* 2013).

Table 4-1 Average in situ Sr isotope compositions and anorthite contents of plagioclase crystals in the various rock types of the Flatreef. Initial $^{87}Sr/^{86}Sr$ calculated at 2054.89 Ma. The full isotopic dataset is given in Table A-1 (Appendix A).

Sample	Depth (m)	Litho	Strat	$^{87}Sr/^{86}Sr$	$^{87}Rb/^{86}Sr$	$^{87}Sr/^{86}Sr_i$	2SE	An	*n*
JDJ053	739.08	GN	MZ	0.70815	0.01100	0.70783	0.00016	70	7
JDJ054	742.37	SAN	HW2	0.70798	0.00530	0.70782	0.00020		6
JDJ056	748.30	MAN	HW2	0.70789	0.00993	0.70761	0.00019		3
JDJ059	760.37	MAN	HW2	0.70814	0.00497	0.70800	0.00019		3
JDJ061	765.98	MAN	HW2	0.70798	0.00852	0.70774	0.00020		3
JDJ063	772.93	MAN	HW2	0.70798	0.00445	0.70785	0.00020		3
JDJ064	775.52	MAN	HW2	0.70797	0.00459	0.70784	0.00017		4
JDJ065	779.37	MAN	HW2	0.70795	0.00861	0.70770	0.00022		6
JDJ069A	787.38	N	HW2	0.70809	0.02426	0.70738	0.00019		5
JDJ069B	787.69	MAN	HW2	0.70763	0.00598	0.70746	0.00020		6
JDJ070	787.85	MAN	HW2	0.70737	0.00451	0.70724	0.00027		3
JDJ071	789.30	SAN	HW2	0.70794	0.00374	0.70784	0.00023		3
JDJ072	789.74	N	HW1	0.70759	0.00191	0.70753	0.00019		7
JDJ073	793.45	N	HW1	0.70811	0.00319	0.70802	0.00024		3
JDJ074	797.00	N	HW1	0.70774	0.00560	0.70757	0.00020		7
JDJ076	802.43	N	HW1	0.70788	0.00180	0.70783	0.00025		3
JDJ077	807.60	N	HW1	0.70769	0.00413	0.70757	0.00023		3
JDJ078	810.60	N	HW1	0.70755	0.00391	0.70744	0.00020		4
JDJ079	811.06	N	HW1	0.70770	0.00150	0.70765	0.00025		3
JDJ080	811.49	N	HW1	0.70783	0.00474	0.70769	0.00022		3
JDJ082	816.02	N	HW1	0.70779	0.00643	0.70761	0.00020		4
JDJ083	819.00	N	HW1	0.70751	0.00127	0.70747	0.00021		3
JDJ085	822.78	N	HW1	0.70780	0.01674	0.70731	0.00020		4
JDJ086	824.42	PX	HW1	0.70757	0.00136	0.70753	0.00013	72	6
JDJ087	825.17	N	HW1	0.70766	0.00358	0.70756	0.00022		4
JDJ092	834.32	FPX	HW1	0.70793	0.00686	0.70774	0.00013	59	4
JDJ097	848.63	FPX	BAR	0.70821	0.00454	0.70808	0.00022		4
JDJ098	849.35	FPX-CR	BAR	0.70837	0.01255	0.70801	0.00018	57	4
JDJ099	851.88	FPX	BAR	0.70813	0.00180	0.70808	0.00020		3
JDJ104	868.63	FPX	MD1	0.70877	0.01189	0.70842	0.00021		4
JDJ105	871.20	FPX	MD1	0.70803	0.01522	0.70758	0.00020		4
JDJ107	877.07	FPX	MD1	0.70771	0.00555	0.70755	0.00026		4
JDJ109A	884.50	FPX	MD1	0.70775	0.00594	0.70758	0.00016	67	4
JDJ112A	888.80	PPXT	M2	0.70778	0.00215	0.70772	0.00027		3
JDJ112B	888.98	FPX	M2	0.70771	0.00791	0.70749	0.00024		3
JDJ117	906.86	OPX	M2	0.70964	0.00060	0.70962	0.00026		5
JDJ119	912.27	FPX	M2	0.70882	0.70882	0.70862	0.00014	71	4
JDJ120	915.35	FPX	M2	0.70737	0.00049	0.70736	0.00015	68	4
JDJ121	918.12	MPV	M2	0.70795	0.00518	0.70780	0.00017		3
JDJ123	922.84	FPX	M2	0.70743	0.00678	0.70723	0.00018		5
JDJ125A	926.97	FPX	$M1_U$	0.70750	0.00848	0.70726	0.00024		5
JDJ125B	927.32	PPXT	$M1_U$	0.70745	0.00726	0.70724	0.00017		6
JDJ126A	928.39	OPX	$M1_U$	0.70731	0.00489	0.70717	0.00015		4

Sample	Depth (m)	Litho	Strat	$^{87}Sr/^{86}Sr$	$^{87}Rb/^{86}Sr$	$^{87}Sr/^{86}Sr_i$	2SE	An	*n*
JDJ126B	928.47	OPX-CR	$M1_U$	0.70747	0.00596	0.70729	0.00016	59	6
JDJ127	930.83	OPX	$M1_U$	0.70740	0.00469	0.70726	0.00014	62	8
JDJ128	931.39	HA	$M1_L$	0.70718	0.00719	0.70697	0.00018		4
JDJ129	934.20	HA	$M1_L$	0.70742	0.01136	0.70709	0.00019		6
JDJ133	942.27	HA	$M1_L$	0.70746	0.01304	0.70708	0.00037		4
JDJ136	945.53	HA	$M1_L$	0.70722	0.00384	0.70711	0.00017		5
JDJ137	948.08	HA	$M1_L$	0.70733	0.00658	0.70714	0.00013	62	5
JDJ139	953.63	HA	$M1_L$	0.70713	0.00600	0.70696	0.00018		5
JDJ141	960.06	FPX	$M1_L$	0.70724	0.00383	0.70713	0.00017		3
JDJ143	962.00	FPX	FCU	0.70715	0.00438	0.70703	0.00013	62	4
JDJ147	975.63	FPX	FCU	0.70690	0.00399	0.70679	0.00015		6
JDJ152	981.20	FPX	FCU	0.70682	0.00722	0.70661	0.00020		3
JDJ154	983.20	N	FCU	0.70661	0.00357	0.70650	0.00017		4
JDJ157A	989.06	FPX	FCU	0.70682	0.01619	0.70635	0.00022		4
JDJ157B	989.35	MAN	FCU	0.70652	0.00443	0.70639	0.00022		3
JDJ158	989.44	N	FCU	0.70650	0.00321	0.70641	0.00023		3
JDJ163	1003.34	N	FCU	0.70670	0.00818	0.70646	0.00014	74	5
JDJ170	1028.28	N	FCU	0.70663	0.00813	0.70639	0.00016		5

SAN, MAN, N, FPX, OPX, MPV and HA indicate spotted anorthosite, mottled anorthosite, norite, feldspathic pyroxenite, orthopyroxenite, mafic pegmatoidal vein and harzburgite, respectively.
HW1, BAR, MD1, M1U, M1L and FCU indicate hanging wall 1, Bastard reef, Middling unit, M1 Upper, M1 Lower and the Footwall Cyclic Unit, respectively.

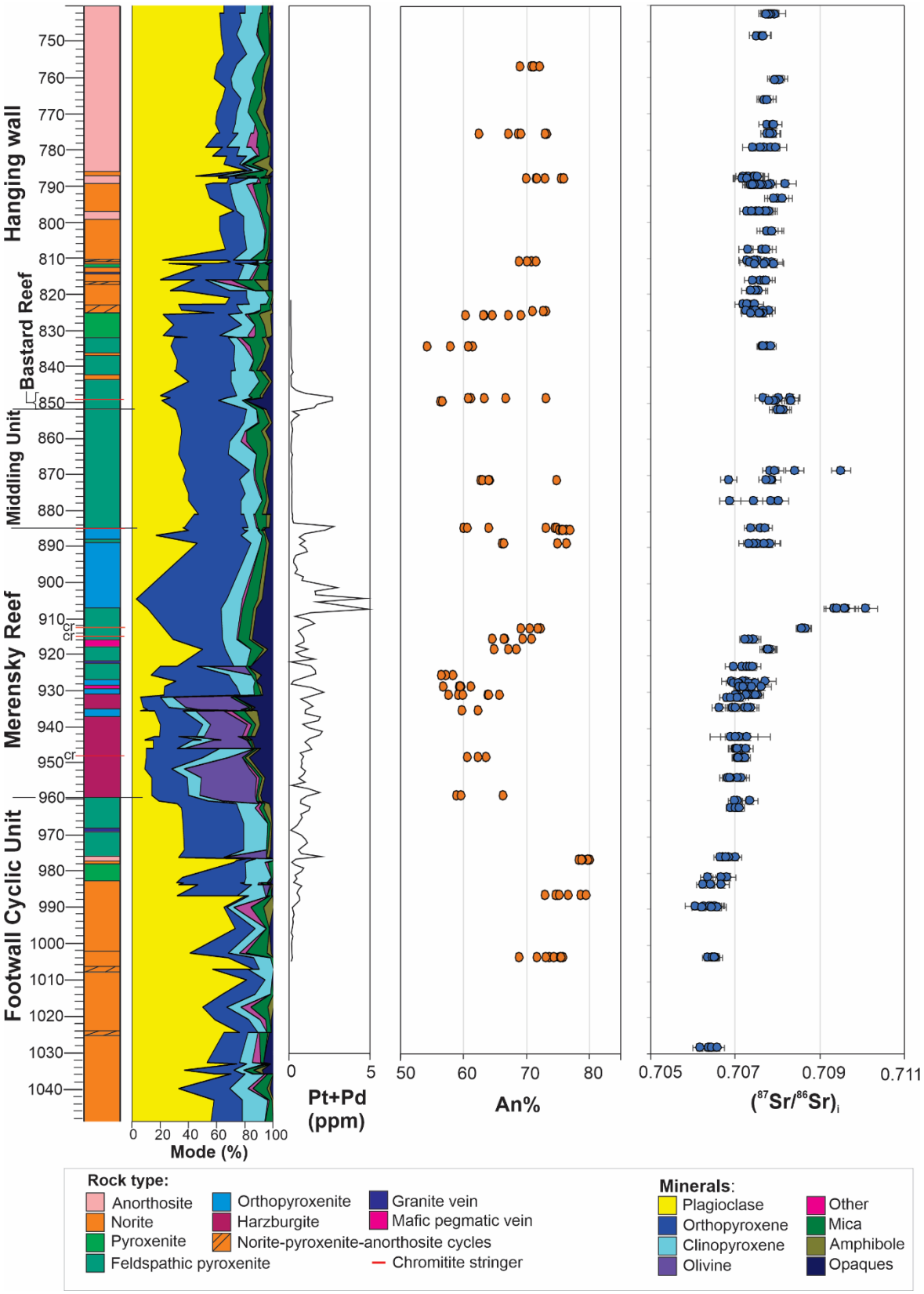

Figure 4.5 Variation in mineral modal proportions, Pt + Pd (from assay data, Ivanplats), plagioclase An content and initial $^{87}Sr/^{86}Sr$ of plagioclase with increase in stratigraphic height across the various lithologies of the Flatreef in borehole UMT-393.The 2SE of the $^{87}Sr/^{86}Sr_i$ is represented by the error bars.

4.7 Discussion

4.7.1 Correlation of the Flatreef with the UCZ – MZ transition interval in the remainder of the Bushveld Complex

The Sr isotopic variations of the western limb of the BC recorded by Kruger (1994) led to his identification of two stages in the development of the RLS. The Integration Stage encompasses the LZ to the lower MZ, whereas the Differentiation Stage comprises the remainder of the MZ and the Upper Zone. The pronounced variations in Sr_i within the Integration Stage were interpreted to be the result of multiple magma influxes. Kruger (1994) showed an irregular upward increase of whole-rock Sr_i throughout the UCZ from ~0.706 at its base to ~0.7063 immediately below the base of the Merensky Cyclic Unit (MCU), followed by a distinct inflection to a value of ~0.7075 at the top of the MCU. This is followed by a gradual upward increase in Sr_i throughout the Bastard Cyclic Unit (BCU), with values in the MZ typically being in excess of 0.708. Of particular interest for the present study, Yang *et al.* (2013) and Karykowski *et al.* (2017) reported similar trends for *in situ* Sr_i of plagioclase from the UCZ of the western BC. In an investigation of the Sr-isotopic stratigraphy of the Platreef at Turfspruit, Kruger (2005a) reported whole-rock initial Sr isotope ratios that were significantly more radiogenic (0.710-0.715; average 0.711) compared to the UCZ in the rest of the BC.

The compositions of plagioclase of the Flatreef in drill core UMT-393 straddle the boundary between the MZ and UCZ in binary plots of Sr_i vs An (Fig. 4.6). Yang *et al.* (2013) documented compositional disequilibrium between the core and rim domains of plagioclase in the Bastard and Merensky Reef in the western BC, with core domains being more radiogenic than rims. They interpreted this variation to have resulted from upward percolation of residual liquids derived from the LZ or LCZ, which have significantly lower Sr_i compared to the UCZ and MZ. In the Flatreef, particularly in the Middling unit, isotope disequilibrium is equally prominent, but in many samples, rims tend to be more radiogenic than core domains (e.g. in sample JDJ105 of the Middling unit Sri is 0.7068 and 0.7079 for core and rim respectively). These data variations may indicate a more radiogenic fluid overprinting plagioclase (Chutas *et al.* 2012), possibly derived from footwall carbonate devolatisation as suggested by Karykowski *et al.* (2017). Several samples from the hanging wall unit and the lower MZ show no intracrystalline isotopic variation as most of the analysed plagioclase grains have similar Sr_i in core and rim domains. These units are thus isotopically relatively homogeneous.

Interestingly, the large interstitial plagioclase of the pegmatoidal pyroxenite (sample JDJ125B) of $M1_U$ shows no evidence for significant *in situ* Sr isotopic variation, with a weighted average of 0.7073, similar to the plagioclase in adjacent feldspathic pyroxenite and orthopyroxenite which has an average Sr_i of 0.7072. These results are consistent with the findings of Yang *et*

al. (2013). They argued that growth of plagioclase crystals at the expense of smaller grains in the presence of an isotopically distinct fluid as suggested by Chutas *et al.* (2012), was not applicable in this case.

Plagioclase in the Footwall Cyclic Unit sampled from drill core UMT-393 has Sr_i ranging from 0.7064 in the lowermost sample to 0.7066 in a sample occurring ~20 m below the base of the Merensky Reef. This compares to values of 0.7061 to 0.7071 in the footwall of the Merensky Reef in the western Bushveld Complex (Yang *et al.* 2013). The combined Sr isotope data of this study thus indicate that the Merensky Reef coincides with a distinct change in Sr_i values from values of ~0.7064-0.7066 below the reef, to values typically in excess of 0.7075 within and above the reef (Fig. 4.5), analogous to the trend observed throughout the MCU and BCU in the western limb of the BC (Yang *et al.* 2013 and Karykowski *et al.* 2017).

Our findings are consistent with those of Mayer (2018) and Mayer et al. (2020, this issue) on a drill core from Turfspruit who reported broadly similar Sr isotopic variation as that found in the present study. Mayer et al. (2020, this issue) concluded that the Flatreef can be correlated with the UCZ in the Western Bushveld, as initially proposed by Grobler *et al.* (2019). On the farm Turfspruit, plagioclase An% increases upward throughout the FCU from a value of ~70 at 50 m below the base of the Merensky Reef, to ~76 in the immediate footwall to the Merensky Reef. In UMT-393, plagioclase at 45 m below the base of the Merensky Reef shows An% of 69-76 (average 74), increasing to 78-80 (average 79) at ~15 m below the base of the Merensky Reef. Mayer et al. (2020, this issue) reported median plagioclase An% of between 60 and 76 for the succession interpreted to represent the Merensky and Bastard reefs. In UMT-393, plagioclase An% varies between 54 and 77 (average 65) across the Merensky Reef to Bastard Reef interval.

This model is further supported by the mineral chemistry of plagioclase across the succession (Fig. 4.6) showing good overlap between the Flatreef with the UCZ and MZ. Yang *et al.* (2013) reported plagioclase An% varying from 68-78 in the Merensky footwall unit, 64-66 in the Merensky Reef, and 52-74 in the Bastard Reef of the western Bushveld Complex. These compositional ranges overlap with those of the FCU (74-79), Merensky Reef (56-77) and Bastard Reef (56-77) in the present work (Fig. 4.5).

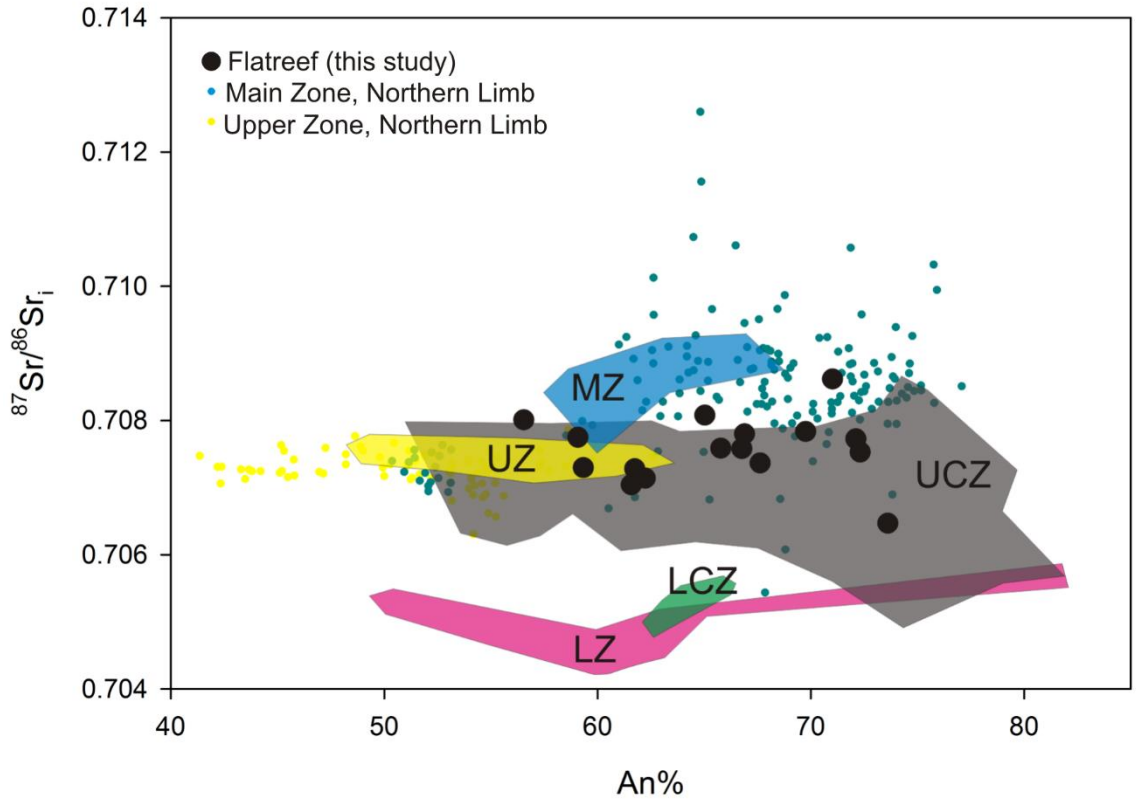

Figure 4.6 Variation of $^{87}Sr/^{86}Sr_i$ in plagioclase versus An% of plagioclase for rocks of the Flatreef on Macalacaskop. Labelled fields show data for the Western Limb from Karykowski et al. (2017) and Yang et al. (2013). Data for the Northern Limb come from Mangwegape et al. (2016). UZ = Upper Zone; MZ = Main Zone; UCZ = Upper Critical Zone; LCZ = Lower Critical Zone; LZ = Lower Zone.

4.7.2 Implications for the source of PGE mineralization in the Merensky Reef

The realisation that the Platreef most likely represents an up-dip sequence of the UCZ that has been significantly affected by contamination with footwall rock (Maier *et al.* 2008) has implications for the source of PGE mineralization within ore bodies such as the Merensky Reef.

Holwell *et al.* (2005) presented evidence to suggest that the intrusion of the MZ significantly post-dated crystallisation and subsequent deformation of the Platreef. Features to support such a contention include the truncation of the Platreef by MZ gabbronorites. Based on these observations, Holwell et al. (2005) conclude that the MZ could not have been the source of PGEs for the Platreef. Holwell and Jordaan (2006) came to a similar conclusion based on finger-like intrusions of MZ gabbronorite cutting through the Platreef at the Zwartfontein South pit.

If our interpretations suggesting a correlation between the Platreef and Flatreef with the UCZ in the remainder of the Bushveld Complex are correct, this would imply that the MZ cannot be

the source of PGE for the Merensky Reef throughout the Bushveld Complex. Our data are more consistent with the models of McDonald et al. (2005); McDonald and Holwell (2007), Sharman-Harris *et al.* (2005), Penniston-Dorland *et al*. (2008) and Sharman *et al.* (2013) whereby the sulfides formed through contamination of Bushveld magma in a staging chamber, followed by the entrainment of sulfides into the Bushveld magma chamber.

4.8 Conclusions

The variation in the Sr-isotope composition and An% of plagioclase across the Footwall Cyclic Unit, the Merensky Reef, Middling Unit, Bastard Reef and Hanging wall units of the Flatreef as exposed in borehole UMT-393 on the farm Macalacaskop, suggests the sequence to be a correlative of the UCZ – MZ transition interval in the remainder of the BC, inclusive of the Merensky Reef and Bastard Reef, as proposed by Grobler *et al.* (2019). The Platreef appears to be an up-dip extension of the Flatreef that has been significantly affected by footwall alteration. Because it has been shown that there was a significant hiatus separating the formation of the Platreef and the subsequent intrusion of MZ magmas, the MZ was likely not the source of PGEs for the Platreef or the Merensky Reef. Our data, and observations on the relationship between the Platreef and its hanging wall elsewhere in the northern limb, are consistent with models for the formation of the Flatreef / Platreef / Merensky Reef mineralization that comprise sulfide immiscibility in a staging chamber prior to emplacement.

4.9 Acknowledgements

This study was supported by the nGAP grant (UID 119698). The LA-MC-ICP-MS at the Spectrum Analytical Facilities, University of Johannesburg, was funded by NRF NEP grant # 93208. Deon Van Niekerk is thanked for his assistance with the use of the Jeol JXA 8230 Superprobe [instrument sponsored by NRF/NEP grant40113 (UID 74464)] housed at the Department of Geology, Rhodes University. Ivanplats is thanked for access to the samples analysed as part of this study. This work is based on research supported in part by the National Research Foundation of South Africa through grants 108995 and 109897 to FR. We are grateful for the constructive reviews by Bartosz Karykowski and an anonymous reviewer, as well as the associate editor, Wolfgang Maier, which helped to improve the manuscript significantly.

4.10 References

Ashwal LD, Webb SJ, Knoper MW (2005) Magmatic stratigraphy in the Bushveld Northern Lobe: continuous geophysical and mineralogical data from the 2950m Bellevue drill core. S. Afr. J. Geol. 108, 199-232

Barnes S-J, Maier WD (2002) Platinum-group element distributions in the Rustenburg Layered Suite of the Bushveld Complex, South Africa. (C. I. Edited by LJ Cabri, Ed.) In The Geology, Geochemistry, Mineralogy and Mineral Beneficiation of Platinum-Group Elements. 54:431-458

Barton JM, Cawthorn RG, White J (1986) The role of contamination in the evolution of the Platreef of the Bushveld Complex. Econ Geol 81:1096-1104

Cawthorn RG, Barton JM, Viljoen MJ (1985) Interaction of floor rocks with the Platreef on Overysel, Potgietersrus, Northern Transvaal. Econ Geol 80: 988-1006

Chutas NI, Bates E, Prevec SA, Coleman DS, Boudreau AE (2012) Sr and Pb isotopic disequilibrium between coexisting plagioclase and orthopyroxene in the Bushveld Complex, South Africa: microdrilling and progressive leaching evidence for sub-liquidus contamination within a crystal mush. Contrib Mineral Petrol 163: 653–668

Elburg MA, Vroon P, van der Wagt B and Tchalikian A (2005) Sr and Pb isotopic composition of five USGS glasses (BHVO-2G, BIR-1G, BCR-2G, TB-1G, NKT-1G). Chem Geol, 223:196-207.

Finn CA, Bedrosian PA, Cole JC, Khoza TD, Webb SJ (2015) Mapping the 3-D extent of the Northern Lobe of the Bushveld layered mafic intrusion from geophysical data. Precambrian Research 268: 279–294

Grobler DF, Brits JAN, Maier WD, Crossingham A (2019) Litho- and chemostratigraphy of the Flatreef PGE deposit, northern Bushveld Complex. Mineralium Deposita 54:3-28

Hagen-Peter G, Tegner C, Lesher CE (2019) Strontium isotope systematics for plagioclase of the Skaergaard intrusion (East Greenland): A window to crustal assimilation, differentiation, and magma dynamics. Geology 47 (4): 313-316.

Harris C, Chaumba JB (2001) Crustal contamination and fluid-rock interaction during the formation of the Platreef, northern limb of the Bushveld Complex, South Africa. J Petrol 42:1321-1347

Holwell DA, Armitage PEB, McDonald I (2005) Observations on the relationship between the Platreef and its hanging wall. Trans Inst Min Metall 114:B199-B207

Holwell DA, Jordaan A (2006) Three-dimensional mapping of the Platreef at the Zwartfontein South mine: Implications for the timing of magmatic events in the northern limb of the Bushveld Complex, South Africa. Trans Inst Min Metall 115:B41-B48

Hulbert LJ (1983) A petrological investigation of the Rustenburg Layered Suite and associated mineralisation south of Potgietersrus, South Africa. Unpublished DSc Dissertation, University of Pretoria, pp.511

Hulbert LJ, Von Gruenewaldt G (1982) Nickel Copper and platinum mineralisation in the Lower Zone of the Bushveld Complex, South of Potgietersrus. Econ Geol 77:1296-1306

Hutchinson D, Kinnaird JA (2005) Complex multistage genesis for the Ni-Cu-PGE mineralisation in the southern region of the Platreef, Bushveld Complex, South Africa. Appl Earth Sci (Trans. Inst. Min. Metall.B) 114:B209-224

Hutchinson D, McDonald I (2008) Laser ablation ICP-MS study of platinum-group elements in sulfides from the Platreef at Turfspruit, northern limb of the Bushveld Complex, South Africa. Mineralium Deposita 43:695–711

Huthmann FM, Kinnaird JA, Yudovskaya MA, Elburg, MA (2017) The Sr isotopic stratigraphy of the far northern Bushveld Complex. South African Journal of Geology 120: 499-510

Iljina MJ, Lee CA (2005) Chapter 4: PGE deposits in the marginal series of layered intrusions In: Exploration for platinum-group element deposits: Ottawa, Mineralogical Association of Canada Short Course Series, pp.75–96

Karykowski BT, Maier WD (2017) Microtextural characterisation of the Lower Zone in the western limb of the Bushveld Complex, South Africa: evidence for extensive melt migration within a sill complex. Contrib Mineral Petrol 172:60

Karykowski BT, Yang S-H, Maier W, Lahaye Y, Lissnberg CJ, O'Brien H (2017) In situ Sr Isotope Compositions of Plagioclase from a Complete Stratigraphic Profile of the Bushveld Complex, South Africa: Evidence for Extensive Magma Mixing and Percolation. J Petrol 58:2285–2308

Kinnaird JA (2005) Geochemical evidence for multiphase emplacement in the southern Platreef. Appl Earth Sci (Trans. Inst. Min. Metal. lB) 114:B225-242

Kinnaird JA, Hutchinson D, Schurmann L, Nex PAM, de Lange R (2005) Petrology and Mineralisation of the southern Platreef: northern limb of the Bushveld Complex, South Africa. Mineralium Deposita 40:576-597

Kinnaird JA, Nex PAM (2015) An Overview of the Platreef. In: Hammond NQ, Hatton C (eds) Platinum-group element (PGE) mineralisation and resources of the Bushveld Complex, Council for Geoscience, Pretoria, South Africa, pp.293–341

Kruger FJ (1990). The stratigraphy of the Bushveld Complex; a reappraisal and the relocation of the Main Zone boundaries. S Afr JGeol 93:76–381

Kruger FJ (1994) The Sr-isotopic stratigraphy of the western Bushveld Complex. S Afr J Geol 97:393-398

Kruger FJ (2005a) Filling the Bushveld Complex magma chamber: lateral expansion, roof and floor interaction, magmatic unconformities, and the formation of giant chromitite, PGE and Ti-V-magnetitite deposits. Mineralium Deposita 40:451–472

Kruger FJ (2005b). The Main Zone of the Bushveld Complex: Source of the Merensky Reef and the Platreef. 10th International Platinum Symposium Abstracts Volume, Oulu, Finland

Kruger FJ, Marsh JS (1982) Significance of $^{87}Sr/^{86}Sr$ ratios in the Merensky cyclic unit of the Bushveld Complex. Nature 298:53-55

Lee CA, Butcher AR (1990) Cyclicity in the Sr isotope stratigraphy through the Merensky reef and Bastard reef units, Atok section, eastern Bushveld Complex. Econ Geol 85:877–883

Maier WD, Eales HV (1994) Plagioclase inclusions in orthopyroxene and olivine of the UG2-Merensky Reef interval: regional trends in the western Bushveld Complex. S Afr J Geol 97:408-414

Maier WD, de Klerk L, Blaine J, Manyeruke T, Barnes S-J, Stevens MVA, Mavrogenes JA (2008) Petrogenesis of contact-style PGE mineralisation in the northern limb of the Bushveld Complex: comparison of data from the farms Rooipoort, Townlands, Drenthe and Nonnenwerth. Mineral Deposita 43:255–280

Maier WD, Yudovskaya M, Jugo P (2020) Mineral Deposita: this issue

Mangwegape M, Roelofse F, Mock T, Carlson RW (2016). The Sr-isotopic stratigraphy of the Northern Limb of the Bushveld Complex South Africa. J Afri Earth Sci 113:95-100

Mangwegape M (2016). Chemical and isotopic variations in plagioclase from the Upper and Main Zones, Northern Limb, Bushveld Complex. Unpublished MSc Thesis, University of the Free State, pp.196

Mayer C (2018) Strontium Isotope Stratigraphy of the Platreef at Turfspruit, Northern Limb, Bushveld Igneous Complex. Unpublished MSc Thesis, Laurentian University, pp.132

Mayer C, Jugo P, Leybourne M, Grobler D (2020) Strontium Isotope Stratigraphy through the Platreef at Turfspruit, Northern Limb of the Bushveld Igneous Complex: Evidence of correlation between the Platreef and the Merensky Reef. Mineralium Deposita: this issue

McDonald I, Holwell DA (2007) Did Lower zone magma conduits store PGE-rich sulfides that were later supplied to the Platreef? S Afr J Geol 110:611–616

McDonald I, Holwell DA (2011) Geology of the Northern Bushveld Complex and the Setting and Genesis of the Platreef Ni-Cu-PGE Deposit. Society of Economic Geologists. Rev Econ Geol 17:297-327

McDonald I, Holwell DA, Armitage PEB (2005) Geochemistry and mineralogy of the Platreef and "Critical Zone" of the northern lobe of the Bushveld Complex, South Africa: implications for Bushveld stratigraphy and the development of PGE mineralisation. Mineralium Deposita 40:526-549

McDonald I, Harmer RE, Holwell DA, Hughes HSR, Boyce AJ (2017) Cu-Ni-PGE mineralisation at the Aurora Project and potential for a new PGE province in the Northern Bushveld Main Zone. Ore Geol Rev 80:1135-1159

Mitchell AA (1990) The stratigraphy, petrography and mineralogy of the Main Zone of the North western Bushveld Complex. S Afr J Geol 93:818-831

Mudd GM, Jowitt SM, Werner T (2018) Global platinum group element resources, reserves and mining - Acritical assessment. Science of the Total Environment pp 614-625

Naldrett AJ, Kinnaird JA, Wilson AH, Chunnett G (2008) Links between the Platreef and the upper Critical Zone. 3rd Platreef Workshop Extended Abstract Volume, Mokopane, South Africa, 11th-13th July 2008

Nebel O, Scherer EE, Mezger K (2011) Evaluation of the ^{87}Rb decay constant by age comparison against the U–Pb system. Earth Planet Sci Lett 301:1–8.

Penniston-Dorland SC, Wing BA, Nex PAM, Kinnaird JA, Farquhar J, Brown M, Sharman ER (2008) Multiple sulfur isotopes reveal a primary magmatic origin for the Platreef PGE deposit, Bushveld Complex, South Africa. Geol36:979–982

Roelofse F, Ashwal LD (2012) The Lower Main Zone in the Northern Limb of the Bushveld Complex a >1.3km Thick Sequence of Intruded and Variably Contaminated Crystal Mushes. J Petrol 53:1449-1476

Roelofse F, Ashwal LD, Romer RL (2015) Multiple, isotopically heterogeneous plagioclase populations in the Bushveld Complex suggest mush intrusion. Chem. Erde – Geochem75:357–364

Scoates JS and Wall CJ (2015) Geochronology of layered intrusions. In: Charlier B, Namur O, Latypov R and Tegner C (eds) Layered Intrusions. Springer, pp. 3–74

Seabrook CL, Cawthorn RG, Kruger JF (2005) The Merensky reef, Bushveld Complex: Mixing of minerals not mixing of magmas. Econ Geol 100:1191-1206

Sharman-Harris E, Kinnaird JA, Harris C, and Horstmann UE (2005) A new look at sulfide mineralization of the northern limb, Bushveld Complex: A stable isotope study. Trans. Inst. Min. Metall 114:B252–B263

Sharman ER, Penniston-Dorland SC, Kinnaird JA, Nex PAM, Brown M, Wing BA (2013) Primary Origin of Marginal Ni-Cu-(PGE) Mineralization in Layered Intrusions: $\Delta^{33}S$ evidence from the Platreef, Bushveld, South Africa. Econ Geol 108:365–377

Sharpe MR (1985) Strontium isotope evidence for preserved density stratification in the main zone of the Bushveld Complex, South Africa. Nature 316:119-126

Smith JW, Holwell DA, McDonald I (2014) Precious and base metal geochemistry and mineralogy of the Grasvally Norite–Pyroxenite–Anorthosite (GNPA) member, northern Bushveld Complex, South Africa: implications for a multistage emplacement. Mineral Deposita 49:667–692

South African Committee for Stratigraphy (SACS). (1980). Stratigraphy of South Africa.Part1. In L. E. Kent, & (Comp) (Eds.), Lithostratigraphy of the Republic of South Africa, South West Africa/Namibia, and the Republics of Bophuthatswana, Transkei and Venda. (8 ed.)

Steiger RH, Jäger E (1977) Sub commission on geochronology: convention on the use of decay constants in geo- and cosmochronology. Earth Planet Sci Lett 36: 359–362

Teigler B, Eales HV (1996) The Lower and Critical Zones of the Western Limb of the Bushveld Complex as Intersected by the Nooitgedacht Boreholes. The Council for Geoscience and the Geological Survey of South Africa.

van der Merwe MJ (1976) The Layered Sequence of the Potgietersrus Limb of the Bushveld Complex. Econ Geol 71:1337-1351

van der Merwe MJ (2008) The geology and structure of the Rustenburg Layered Suite in the Potgietersrus/Mokopane area of the Bushveld Complex South Africa. Mineralium Deposita 43:405–419

Wagner P (1929) The Platinum Deposits and Mines of South Africa, Struick, London

White JA (1994) The Potgietersrus Prospect – Geology and exploration history XVth CMMI Congress, South Africa. South Afr Inst Min Metall 3:173-181

Wilson AH (2015) The Earliest Stages of Emplacement of the Eastern Bushveld Complex: Development of the Lower Zone, Marginal Zone and Basal Ultramafic Sequence. J Petrol 56(2):347–388

Wilson AH, Zeh A, Gerdes A (2017) In Situ Sr isotopes in Plagioclase and Trace Element Systematics in the Lowest Part of the Eastern Bushveld Complex: Dynamic Processes in an Evolving Magma Chamber. J Petrol 58(2):327–360

Yang S.-H, Maier WD, Lahaye Y, O'Brien H (2013) Strontium isotope disequilibrium of plagioclase in the Upper Critical Zone of the Bushveld Complex: evidence for mixing of crystal slurries. Contrib Mineral Petrol 166:59–974

Yudovskaya MA, Kinnaird JA, Sobolev AV, Kuzmin DV, McDonald I, Wilson AH (2013) Petrogenesis of the lower zone olivine-rich cumulates beneath the Platreef and their correlation with recognized occurrences in the Bushveld Complex. Econ Geol 108:1923–1952

Yudovskaya MA, Kinnaird JA, Grobler DF, Costin G, Abramova VD, Dunnet T, Barnes S-J (2017) Zonation of Merensky style platinum mineralization in Turfspruit thick reef facies (northern limb of the Bushveld Complex). Econ Geol 112(6):1333–1365

Zeh A, Ovtcharova M, Wilson AH, Schaltegger U (2015) The Bushveld Complex was emplaced and cooled in less than one million years – results of zirconology, and geotectonic implications. Earth Planet Sci Lett 418:103–114

CHAPTER 5 :
ARTICLE 2

A COMPARATIVE STUDY OF SULFUR ISOTOPE VARIATIONS WITHIN THE FLATREEF AND MERENSKY REEF OF THE BUSHVELD COMPLEX, SOUTH AFRICA

5.1 Abstract

The Flatreef, a down-dip, sub-horizontal extension of the Platreef, which underlie the farms Turfspruit and Macalacaskop, represents the future of platinum mining in South Africa. The stratigraphic connection between the Platreef, located at the base of the northern limb of the Bushveld Complex, and the Merensky Reef in the western and eastern limbs of the complex, was disputed for many years due to the heterogeneous nature of the Platreef along strike. However, the discovery of the Flatreef led to a new perspective on the Platreef as the former allowed for the study of a magmatic stratigraphy less affected by footwall interaction. Here, we report whole-rock S isotope (δ^{34}S) compositions across the stratigraphic units of the Flatreef and its footwall and hanging wall as intersected by boreholes UMT-276 and UMT-393, as well as stratigraphic units of the Merensky Reef at Two Rivers Platinum mine (TRP) in the eastern limb. The units of the Flatreef containing platinum group element (PGE) mineralization, namely the Main reef and Upper reef, have δ^{34}S values that overlap with the range recorded for the Merensky Reef in the western and eastern limbs. In UMT-393, Main reef δ^{34}S values range between -0.2 and 1.5‰ (with the exception of 3 outliers, 9.7‰, 11.1‰ and 7.9‰), and 0.52% and 11.2‰ for two Upper reef samples. However, in UMT-276, Main reef δ^{34}S values range between -0.96 and 2.24‰ and 3.19‰ was recorded for an Upper reef sample. The S isotope compositions recorded for Merensky reef pyroxenite at TRP are relatively higher with δ^{34}S values ranging between 1.24 and 4.83%. The top unit of the Flatreef, which is a transition zone below the Main zone, as well as the Footwall Cyclic Unit have heavier S isotope compositions with δ^{34}S values ranging between 6 and 17‰ for the former and 0.7 and 18.6‰ for the latter. At TRP, the hanging wall anorthosite has a δ^{34}S value of 2.9‰ in contrast to the 5.7‰ measured for the footwall anorthosite and 3.27‰ for the footwall feldspathic pyroxenite. The consistent near mantle S isotope signature and accompanying metal enrichment in the Main reef of the Flatreef may be explained by extensive interaction of sulfide minerals in a LZ conduit/pre-Platreef staging chamber with large volumes of uncontaminated magma. The δ^{34}S values of the Merensky Reef at TRP are slightly higher compared to that of the Main reef on Turfspruit and Macalacaskop possibly due to interaction with underlying carbonate rocks.

5.2 Introduction

It has long been known that the Platreef in the northern limb of the Bushveld Complex (BC) (Fig. 5.1) has been subject to extensive crustal contamination relative to the Merensky Reef in the eastern and western limbs of the BC due to its proximity to footwall country rocks (Buchanan et al. 1981; Buchanan and Rouse 1984; Schiffries and Rye, 1989; Harris and Chaumba 2001; Kruger 2005a; Manyeruke et al. 2005; Sharman-Harris et al. 2005). Although numerous studies have been carried out on the Platreef (e.g., Kinnaird and McDonald 2005, Kinnaird et al. 2005, Manyeruke et al. 2005, McDonald et al. 2005, McDonald and Holwell 2007, Hutchinson and McDonald 2008, Maier et al. 2008, Yudovskaya et al. 2017a, Grobler et al. 2019), a consensus on whether mineralization in the Platreef correlates with that of the Merensky Reef has not yet been established. The Merensky Reef, as well as the PGE-rich UG2 layer, are associated with reef-style mineralization and the Platreef with contact-style mineralization (Maier et al. 2008). A possible relationship between the Merensky Reef and the Platreef was proposed by Naldrett et al. (2012), who suggested that the Platreef may be the marginal structure through which excess magma responsible for the Merensky Reef escaped. The recent discovery of the Flatreef, a down-dip, sub-horizontal extension of the Platreef at Turfspruit, shows that reef-style mineralization is also present in the upper parts of the Platreef (Yudovskaya et al. 2017a, Grobler et al. 2019).

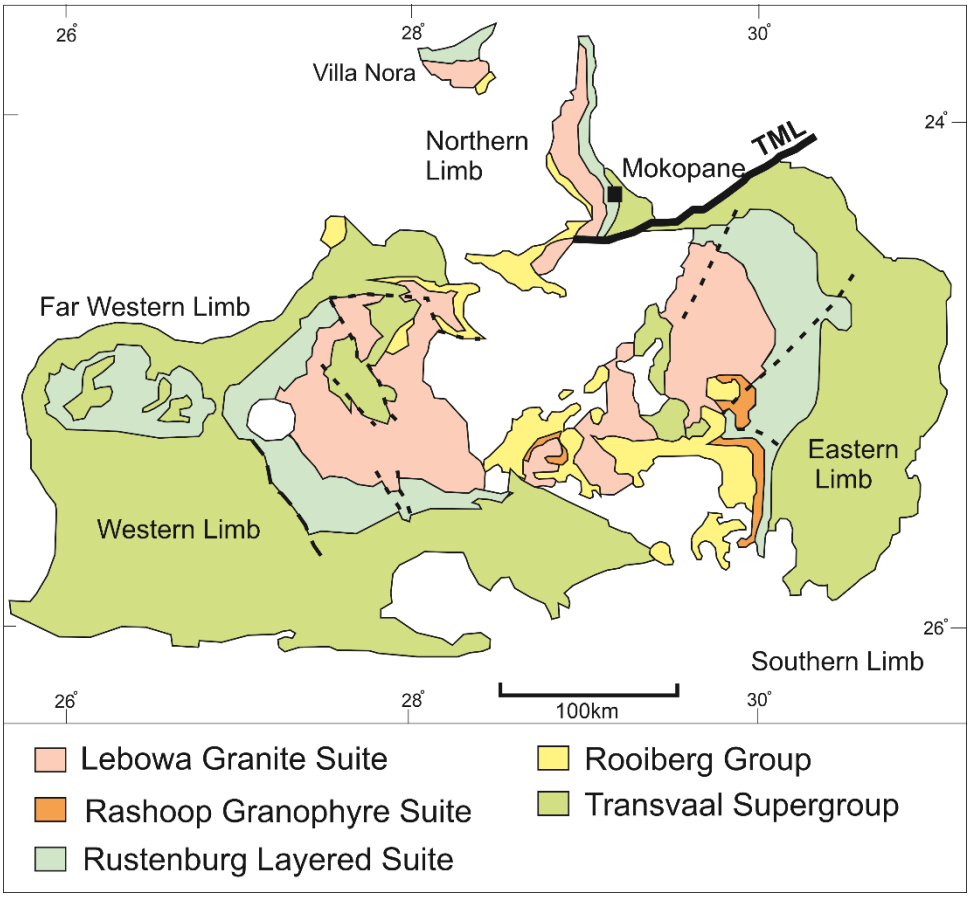

Figure 5.1 Simplified map showing the geology of the Bushveld Complex. Modified after Eales and Cawthorn (1996). TML Thabazimbi-Murchison Lineament

Sulfur isotope measurements are useful geochemical tools for assessing the source of magmatic Cu-Ni-PGE deposits (Ripley and Li, 2003). The S isotope composition of country rock must be distinct from that of mantle-derived S to successfully determine the source of S for magmatic Cu-Ni-PGE deposits using S isotope values (Ripley and Li, 2003). Sakai et al. (1984) reported δ^{34}S values from mantle-derived mid-oceanic ridge basalt glass, believed to reflect their mantle source, ranging between -0.3 to 0.8‰. Recent studies by Labidi et al. (2012, 2014, and 2015) have reported mantle δ^{34}S values compared to Vienna-Canyon Diablo Troilite, (VCDT) to be relatively more negative, ranging between around -2‰ and 0‰.

The BC is surrounded by 2.67-2.07 Ga Transvaal Supergroup country rocks (Bekker et al. 2001) and is locally also in contact with Archaean basement. The BC transgressively overlies Transvaal Supergroup and Archaean basement floor rocks in the northern limb, whereas in the eastern and western limbs it intruded into the Magaliesberg quartzite. The Transvaal Supergroup has average primary δ^{34}S values outside the mantle range. For example, the δ^{34}S values for footwall calc-silicate rocks in the southern sector of the northern limb range between

14.7‰ to 28.7‰ and in the northern and central sectors calc-silicate rocks have δ^{34}S between 0.7‰ and 12‰ (Sharman et al. 2013, Keir-Sage et al. 2021).

Previous studies in the western and eastern BC have reported δ^{34}S values of 2.7 ± 0.3‰, 1.7 ± 0.6‰ and 1.4 ± 0.1‰ for the UG2 chromitite, Merensky Reef and Main Zone gabbronorite, respectively (Penniston-Dorland, 2012). In the central sector of the eastern limb, δ^{34}S values from the Upper Critical Zone range between 1.42 and 3.10‰ with a single Merensky Reef sample having a value of 1.68‰ (Magalhães et al. 2018). At Nonnenwerth in the far north of the Northern Limb, for example, where the footwall consists of Archaean granite, δ^{34}S ranges between 0‰ to 2‰, which was interpreted as evidence of a mantle origin (Manyeruke et al. 2005). At Tweefontein in the central sector of the northern limb δ^{34}S from Platreef sulfide minerals range between 6.3 and 9.2‰ (Buchanan et al. 1981). Further south, Platreef rocks at Turfspruit and Macalacaskop have δ^{34}S values from ~3 to ~5‰ (Sharman-Harris et al. 2005) and at Townlands values range between 2.6 and 9.1‰ (Manyeruke et al. 2005). All of these values are suggestive of the influence of chemical sediment-derived sulfur. The Platreef in the southern sector therefore has heavier S isotope signature relative to the northern sector in line with changing footwall compositions. It is worth noting that earlier S isotope work was carried out on the shallow, highly contaminated and erratically mineralized Platreef where stratigraphic control on samples taken was difficult. Comparison and interpretation of results were therefore challenging.

A recent geochemical study by Keir-Sage et al. (2021) on the Flatreef at Turfspruit shows that δ^{34}S values of the mineralized Main reef (Fig. 5.2) range between 1.5 and 3.8‰, which was interpreted as an indication of minimal contamination by local footwall. Similarly, previous studies by Holwell et al. (2007), Penniston-Dorland et al. (2008) & Yudovskaya et al. (2017b) have reported δ^{34}S compositions at the top part of the Platreef ranging between 0 and 2‰, which appear to be unrelated to the variation of footwall rocks. These δ^{34}S isotope compositions are comparable to those of the Merensky Reef. Although several S isotope studies have been carried out on Platreef rocks in the northern limb, relatively less time has been focused on the recently discovered Flatreef. The immediate footwall lithologies of the Flatreef are not consistent on the farms Turfspruit and Macalacaskop. At the former, the Flatreef is underlain by the Footwall Assimilation Zone (FAZ) consisting of altered magmatic rocks, whereas at the latter locality, it is underlain by the Lower Zone. This inconsistency implies that the extent of crustal assimilation and contamination of the lithological units of the Flatreef will be expected to vary laterally. Furthermore, a relatively large S isotope database is available for the Merensky Reef in the western limb, however, little to no data are available

for the Merensky Reef in the southern sector of the eastern limb. In order to augment these discrepancies, we report whole-rock $\delta^{34}S$ compositions of whole-rocks of the Flatreef as sampled by boreholes UMT-276 and UMT-393 on the farms Turfspruit and Macalacaskop (Figs. 5.3A, 5.4 & 5.5), and of samples from the Merensky Reef in the eastern BC south of the Steelpoort fault, obtained from the Two Rivers Platinum mine (TRP) (Fig. 5.3B). Our main focus is to further test the connection between the Flatreef / Platreef and the Merensky Reef (Grobler et al. 2019, Beukes et al. 2021, Mayer et al. 2021, and Keir-Sage et al. 2021) by comparing our findings to published findings on the Merensky Reef and our own data collected at TRP, eastern BC.

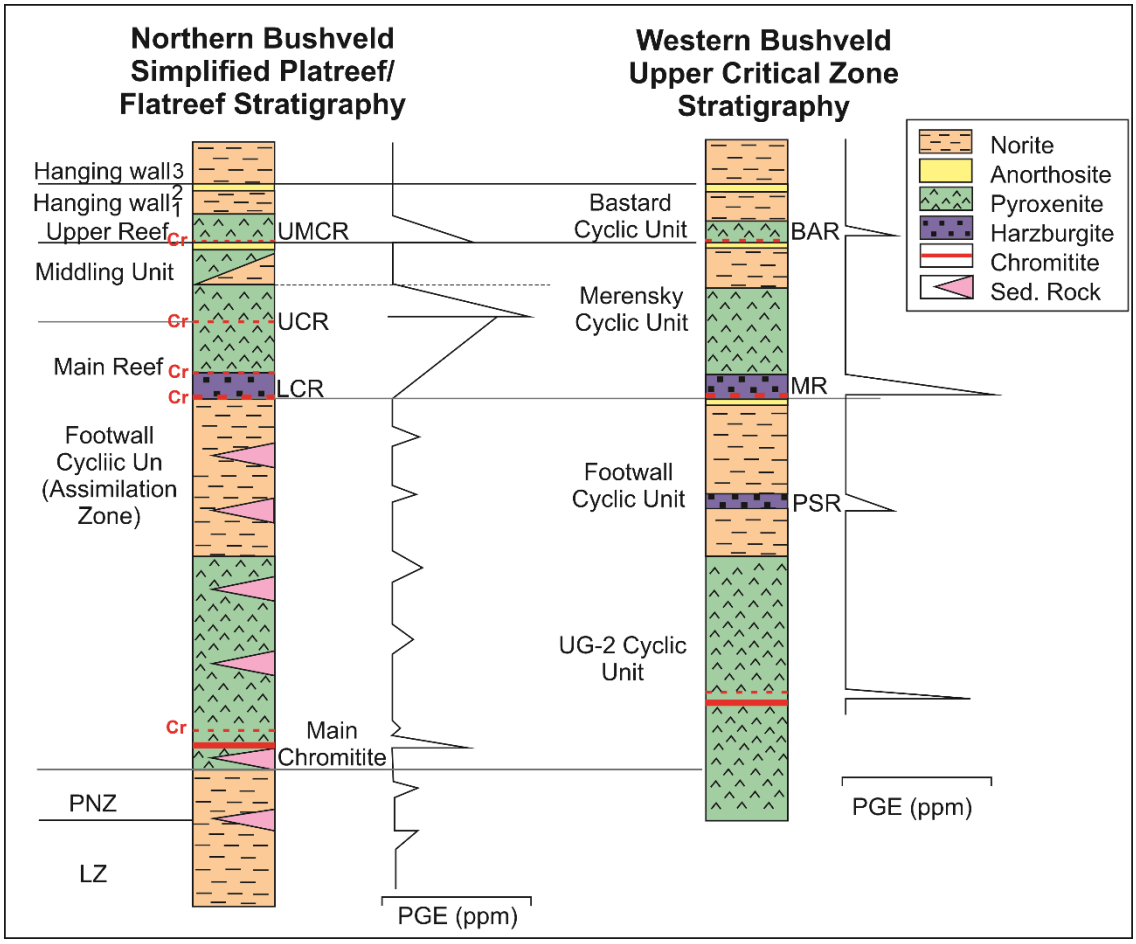

Figure 5.2 Schematic diagram of a stratigraphic comparison between Platreef/Flatreef and Upper Critical Zone (UCZ) in the western BC. UMCR, UCR, LCR, PNZ, LZ, BAR, MR, and PSR indicate the uppermost chromite seam, upper chromite seam, lower chromite seam, Pyroxenite-Norite Zone, Lower Zone, Bastard Reef, Merensky Reef, and Pseudo Reef, respectively.

5.3 Regional Geology

The Bushveld Complex (BC) has been the subject of numerous studies over the last century as the largest layered intrusion on Earth and, more importantly, as the world's largest known source of platinum group elements (PGEs) (Cawthorn 1999). Stratigraphically, the BC is divided into the following igneous suites, as formalized by SACS (1980): the Rashoop Granophyre Suite, the Rustenburg Layered Suite (RLS) and the Lebowa Granite Suite. The

complex is exposed in four main limbs, the eastern, western, far western and northern limbs (Eales and Cawthorn 1996). Historically, the Merensky Reef, the UG2 and the Platreef were exploited as the main PGE-bearing horizons occurring within the RLS. The RLS was emplaced at 2.054 Ga (Scoates and Friedman, 2008) possibly within a timeframe of less than 1 m.y. (Zeh et al. 2015). The RLS is informally divided into five zones, viz. the Upper, Main, Critical, Lower and Marginal zones.

5.3.1 Stratigraphy of the Northern Limb

5.3.1.1 Marginal Zone (MZN)

The MZN consists of centimeters to tens of meters of noritic and doleritic rocks (van der Merwe 1976). These rocks occur sporadically on the farms Macalacaskop and Turfspruit, in the southern sector of the northern limb (Kinnaird et al. 2005).

5.3.1.2 Lower Zone (LZ)

In the northern limb, the LZ has been intruded, transgressed and metamorphosed by the Critical Zone, a feature that is indicative of a major hiatus between the emplacement of the two intervals (van der Merwe, 1976). The LZ occurs either as isolated satellite bodies or as thick peridotite and pyroxenite sequences (Kinnaird and Nex 2015). From the study of drill cores on the Turfspruit and Sandsloot farms in the northern limb, Yudovskaya et al. (2013) found LZ ultramafic sequences at the base of the Platreef, separated from the Platreef by country rocks and thin intrusions of norite of the MZN, which are represented by assimilation textures. These LZ sequences are thicker and have olivine and orthopyroxene compositions that are more primitive than those occurring within the LZ of the western and eastern limbs and are believed to have formed prior to the formation of the Platreef (Teigler and Eales 1996; Yudovskaya et al. 2013; Wilson 2015; Karykowski and Maier 2017). Prior to this discovery, it was thought that the LZ was only present in seven satellite bodies in the Grasvally area to the south of Mokopane (van der Merwe, 2008). On Turfspruit and Macalacaskop, thick, serpentinised, fine- to medium-grained peridotite belonging to the LZ has been identified both at the base of the succession and in satellite intrusions (Kinnaird et al. 2005). Harzburgite, serpentinite and accompanying layers of chromitite on Townlands are also assigned to the LZ (Hulbert and Von Gruenewaldt 1982). The LZ lithologies (pyroxenite, harzburgite and dunite) of the northern limb are texturally distinct from the Platreef and can be up to 800 m thick (Yudovskaya et al. 2013).

5.3.1.3 The Platreef and Critical Zone (CZ)

The mineralized succession of the BC in the northern limb was first termed the “Platreef” by van der Merwe (1976), referring particularly to the porphyritic and pegmatoidal pyroxenite, which he suggested formed the base of the MZ. The Platreef has been defined as an irregularly mineralized PGE-Cu-Ni deposit characterised by pyroxenite located between the Transvaal metasedimentary footwall or Archaean basement and the MZ gabbronorite that overlie it (Kinnaird et al. 2005). The Platreef was interpreted to have formed as a result of the interaction of MZ magmas with the floor rocks (Kruger 2005). However, investigations on the relationship between the MZ and the Platreef indicated that prior to the intrusion of the MZ, the Platreef had already solidified (Holwell et al. 2005; Holwell and Jordaan 2006). The location of the Platreef between the MZ and LZ places it in a position that is normally stratigraphically occupied by the Lower Critical Zone (LCZ) and Upper Critical Zone (UCZ). The UCZ hosts the stratiform, platinum-bearing Merensky and UG2 reefs in the eastern and western limbs of the BC. In contrast to the Merensky Reef in the eastern and western limbs, the Platreef was regarded as a “contact-style” PGE deposit (Iljina and Lee, 2005). This type of mineralization extends over a strike length of 110 km from the Zebediela Fault south of Mokopane to north of the Melinda Fault (Kinnaird et al. 2005). However, recent studies of the Flatreef at Turfspruit show that reef-style or stratiform mineralization is also present in the upper parts of the Platreef (Yudovskaya et al. 2017a, Beukes et al. 2021, Keir-Sage et al. 2021, and Mayer et al. 2021). Until recently, significant occurrences of chromitite, as found in the CZ of the eastern and western limbs, appeared to be absent from the northern limb. The LCZ was therefore regarded as being entirely absent from the northern limb (McDonald and Holwell 2011). However, the work of Yudovskaya et al. (2013) and Grobler et al. (2019) has shown previously unknown, thick ultramafic intrusive rocks below the Platreef that were correlated with the LZ and LCZ.

The Platreef is divided into three sectors, namely the northern, central and southern sectors (van der Merwe 2008, Kinnaird and Nex, 2015), each characterized by different footwall lithologies (Fig. 5.2A). The northern sector, which is found on the Overysel, Drenthe and Witrivier farms, has an Archaean granite footwall. The central sector stretches from Zwartfontein farm to Tweefontein farm where the footwall consists of Malmani dolomite. The southern sector stretches from the farm Tweefontein to the farm Townlands, where the footwall consists of shale, banded ironstone, calc-silicate rocks, mudstone and siltstone of the Duitschland Formation. The variation in mineralization of the Platreef at these different locations is influenced by its interaction with the basal sediments of the Transvaal Supergroup.

5.3.1.4 Main Zone (MZ)

The MZ reaches a thickness of up to 2.2 km in the northern limb (van der Merwe 1976), significantly less than in the western and eastern limbs of the complex, where the MZ attains a thickness of up to 3.1 km (Mitchell, 1990; Ashwal et al., 2005). In the southern sector of the northern limb, the MZ is characterized by gabbronorite, gabbro and anorthosite dipping at 20° to 26° to the west and northwest (van der Merwe, 2008). In the northern limb at about 1 km above the base of the MZ, a 110-m-thick troctolite zone is developed (van der Merwe, 1976). This zone is not known from the eastern and western limbs. Numerous authors (e.g., Kruger 2005b; Ashwal et al. 2005; Roelofse and Ashwal 2012; Mangwegape et al. 2016) however, have investigated a potential connection between this troctolite zone and the Pyroxenite Marker in the western and eastern BC.

5.3.1.5 Upper Zone (UZ)

The UZ overlies the MZ in the southern sector and Archaean granite in the northern sector of the northern limb. Van der Merwe (1976) recognized 20 magnetitite layers in the UZ of the northern limb. A later study by Ashwal et al. (2005) on the Bellevue borehole (BV-1), identified the presence of 32 magnetitite layers throughout the UZ. The UZ has been divided into sub-zones based on the presence or absence of certain cumulus minerals (SACS 1980). At the base of the UZ in borehole BV-1, in sub-zone A, the rocks contain magnetite, plagioclase, low-Ca pyroxene and clinopyroxene. Sub-zone B overlies sub-zone A and is marked by the appearance of olivine as a minor cumulus phase. Lastly, sub-zone C is found at the top of the UZ where apatite appears as a minor cumulus phase. Outcrop of the UZ in the northern limb is poor and largely confined to the farm Townlands.

5.3.2 The Flatreef at Turfspruit and Macalacaskop

The “Flatreef”, a term given to describe the down-dip, sub-horizontal extension of the Platreef, is the main host of Ni-Cu-PGE mineralization on the Turfspruit and Macalacaskop farms, north of Mokopane (Fig. 5.3A). The discovery of the Flatreef was made by Ivanhoe Mines during a deep drilling programme that was initially carried out to outline mineralization that would allow for open pit mining. The stratigraphic units of the Flatreef were first presented by Grobler et al. (2012) as the “Turfspruit Cyclic Unit”. The mineralized stratiform units of the Flatreef were later termed “Upper reef” and “Main reef” by Yudovskaya et al. (2017a) (Fig. 5.2). Lower Critical Zone and Lower Zone have been identified at the base of the Flatreef (Grobler et al. 2019). Recent Sr-isotopic investigations have shown that the Flatreef is a correlative of the UCZ-MZ transition, which includes the Merensky Cyclic Unit (MCU) and Bastard Cyclic Unit (BCU) in the eastern and western BC (Beukes et al. 2021, Mayer et al. 2021). For simplicity,

we will be using the terms Main reef and Upper reef when referring to the mineralized Merensky Reef and Bastard Reef correlates of the Flatreef, respectively.

The Flatreef is comprised, from the base upwards, of a Footwall Cyclic Unit (FCU), the Main Reef (a correlate of the Merensky Reef), a middling unit, the Upper Reef (a correlate of the Bastard Reef) and a hanging wall unit 1 (HW1) (Fig. 5.2). The FCU occurs in close proximity to the footwall rocks and its lithologies vary greatly within the study area (Grobler et al. 2019). It consists of interlayered pyroxenite-norite-anorthosite sequences, referred to as “Norite Cycles” by Kinnaird et al. (2005). The Main reef (i.e., Merensky Reef) is divided into an upper (M1) and lower portion (M2). M1, overlying the FCU, is further subdivided into a sulfide-rich harzburgite (M1L) and a mineralized pegmatoidal orthopyroxenite ($M1_U$) overlying the M1L. M2 is composed of mineralized orthopyroxenite and feldspathic pyroxenite. The Main reef is bounded by a sporadic basal chromite stringer near the FCU contact and continuous chromite stringers within or at the top of the reef. The middling unit overlying the Main reef consists of interlayered pyroxenite-norite-anorthosite sequences and feldspathic orthopyroxenite. This unit is relatively poor in PGEs. The Upper reef (i.e., Bastard Reef) is a mineralized pyroxenite showing a poorly developed chromitite stringer at the contact with the underlying middling unit. The topmost unit of the Flatreef, HW1, underlies the MZ and consists mainly of a series of pyroxenite, norite, mottled anorthosite and gabbro cycles.

The floor rocks on Macalacaskop vary from Timeball Hill Formation quartzite in the south to shale in the north, whereas on Turfspruit, the floor consists of sulfidic shale and limestone of the Duitschland Formation (Kinnaird et al., 2005). On Turfspruit, the LZ consists mainly of interlayered harzburgite, dunite, and pyroxenite and is separated from the Platreef by country rocks (Yudovskaya et al. 2017a). However, as shown by Grobler et al. (2019) and Fig. 5.5, the Flatreef is not always separated from the LZ by country rock. In certain parts on Turfspruit the LCZ directly overlies the LZ.

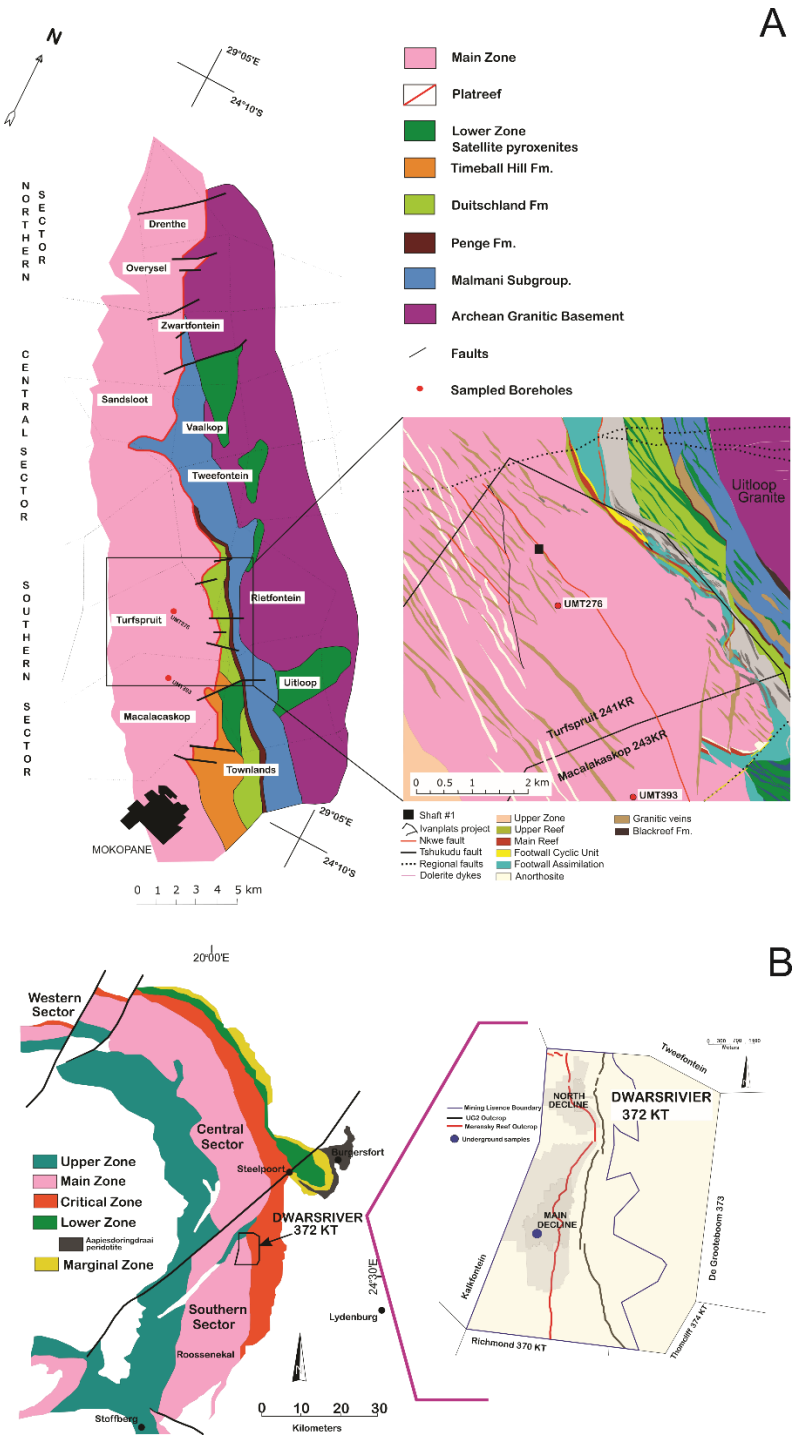

Figure 5.3 A Geology of the Northern Lobe of the Bushveld Complex showing the locations of boreholes UMT-276 and UMT-393 on the farms Turfspruit and Macalacaskop. (After van der Merwe, 1976, as modified by Ashwal et al., 2005). A detailed geology of the study area is given on the right as modified after Maier et al. 2021. **B** Geology of the Eastern Lobe of the Bushveld Complex showing the location of the study area at Dwarsriver 372KT (modified after Cameron & Abendroth, 1957; Sharpe & Chadwick, 1982; Clarke et al., 2005; Beukes et al., 2016). Key features such as the Merensky Reef outcrop and the main decline of the Two Rivers Platinum mine from which underground samples were taken, are shown on the right.

5.3.3 The Merensky Reef at Dwarsriver

The Merensky and UG2 reefs sub-crop on the farm Dwarsriver 372KT, located approximately 60 km northwest of the town of Lydenburg (Fig. 5.3B). Currently only the UG2 is mined by TRP. The eastern limb is comprised of a western, central and southern sector (Scoon, 2002). The TRP mining area is situated in the southern sector, about 7 km south of the Steelpoort fault. This lineament is identified as a potential feeder zone (Cawthorn et al. 2002), such that the succession in the central sector north of the Steelpoort fault differs from that of the southern sector south of the fault.

The Merensky Reef at TRP is characterized by a pyroxenite that is bounded by upper and basal chromite stringers (Rose et al. 2011). The Merensky Reef at TRP is divided into four facies based on variations in thickness and PGE distribution (Cowell 2003): Reef facies 1 (pyroxenite with PGE mineralization associated with the upper and basal stringers), Reef facies 2 (~2.7 m thick pyroxenite with PGE mineralization occurring uniformly, not restricted to the presence of chromite stringers), Reef facies 3 (4.58 m thick on average, three PGE mineralization peaks recognized where two are located at the upper and basal chromite stringers and the third within the Merensky Reef pyroxenite) and Reef facies 4 (maximum thickness of 1 m, only the basal chromite stringer is present with associated PGE mineralization). Reef facies 2 is the most widespread within the mining area. The Merensky Reef is sandwiched between a spotted anorthosite hanging wall and a spotted to mottled anorthosite footwall. An erratic occurrence of “brown sugar norite” (BSN), a fine to medium grained mela-gabbronorite, disrupts the normal layering of the MCU at TRP (Beukes et al. 2016).

5.4 Samples and analytical methods

A total of 59 whole-rock samples were collected from boreholes UMT-276 and UMT-393 (on the farms Turfspruit and Macalacaskop, respectively) and 13 whole-rock samples from TRP for S isotope determinations. The Flatreef samples were representative of all stratigraphic units of the Flatreef. Inclusive of the HW1 and FCU, the Flatreef has a thickness of about 126 m and 324 m in UMT-276 and UMT-393, respectively. The lithologies present in both boreholes are similar but the thicknesses vary. In both boreholes the highest Pt+Pd concentrations are found in the M2 unit. In UMT-276, the highest Pt+Pd value of 9 ppm was recorded in the top chromite stringer. In UMT-393, the highest value of 5 ppm occurs ~22 m below the top chromite stringer. Petrographic descriptions of the different lithologies are given in Beukes et al. (2021) and estimated modal mineralogy is presented in Tables B1 and B2 (Appendix B). The base metal sulfides in the Flatreef stratigraphical units range from fine,

disseminated to blebby in texture. The dominant sulfides are pyrrhotite, pentlandite and chalcopyrite. These sulfides are present as a primary magmatic phase (mostly as inclusions in pyroxene minerals and chromite) and late stage phase (associated with secondary minerals such as biotite). At TRP a total of 20 samples were collected underground of which 13 were prepared for S isotope analysis. These samples are from the MCU and include BSN lenses. Petrographic descriptions of these samples are given in Beukes et al. (2016) and estimated modal mineralogy is given in Figure B3 (Appendix B). Major element concentrations for a total of 59 Flatreef samples were determined by XRF on fused discs at the Geology Department, University of the Free State. Fusion discs were prepared from milled sample material. A Rigaku Primus IV WDXRF spectrometer with a maximum of 60kV in accelerator voltage was used. The spectrometer is linked to the SuperQ Version 4 analytical Software.

For S isotope determinations, pulverized rock samples along with an excess of V_2O_5 were weighed into tin capsules. The $^{34}S/^{32}S$ value was measured using a Thermo Scientific DELTA V Advantage isotope ratio mass spectrometer coupled to a Flash Elemental Analyzer (EA) by a ConFloIV interface at iThemba LABS, Johannesburg, South Africa. The results are reported in standard $\delta^{34}S$ notation in per mil (‰) relative to the VCDT standard. The analytical error of 0.62‰ was determined using the standard deviation of standards run at the beginning and end of each run (Table B4 – Appendix B).

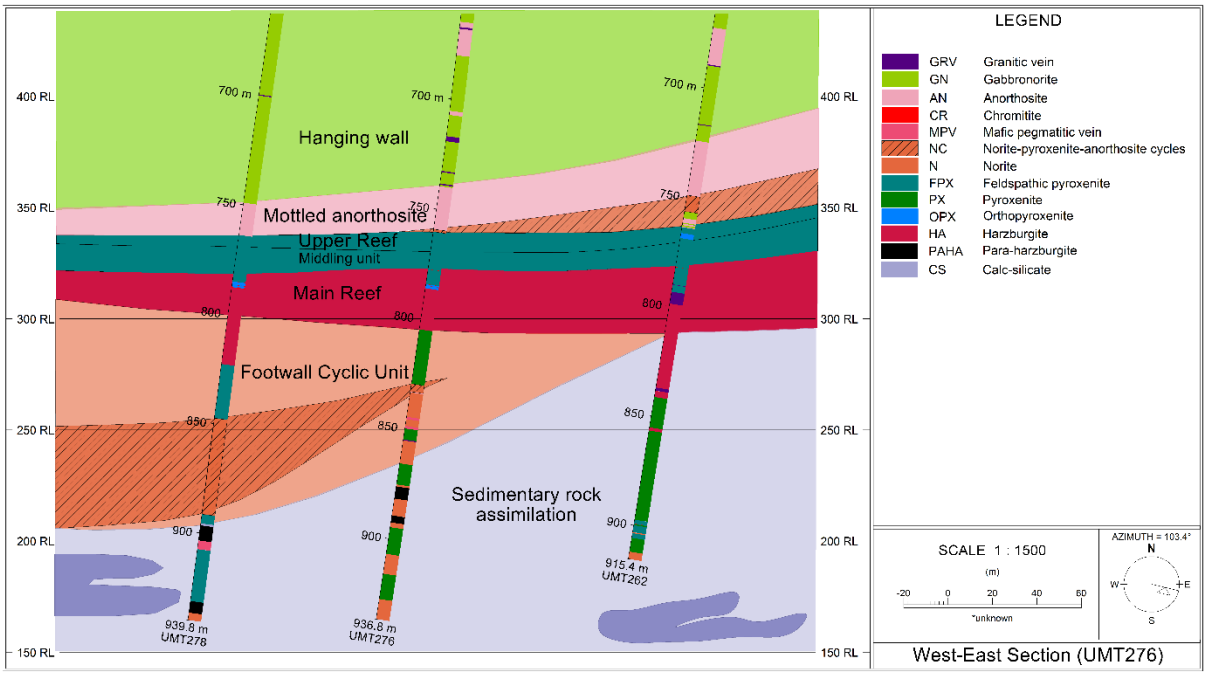

Figure 5.4 Dip section showing borehole UMT-276. Note that the footwall comprises of a zone of sedimentary rock assimilation

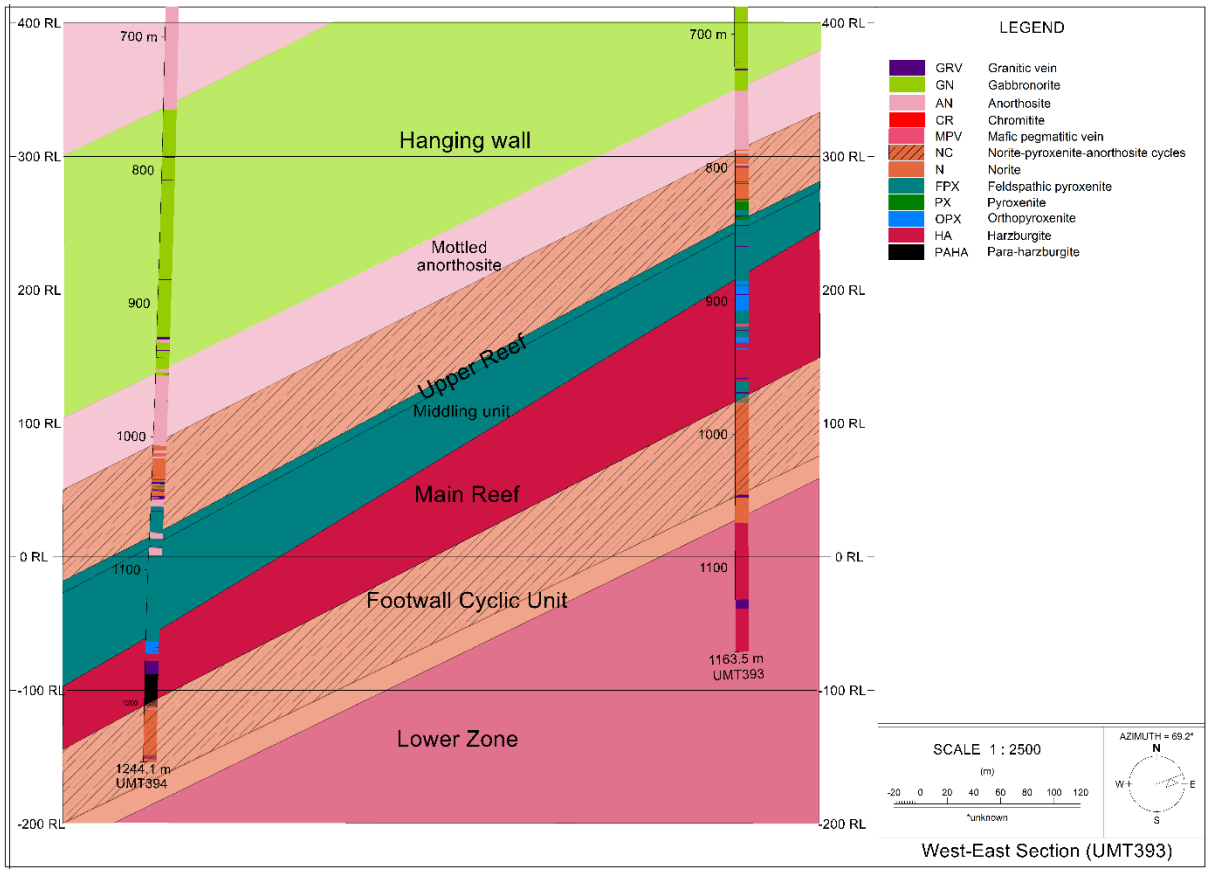

Figure 5.5 Dip section showing borehole UMT-393. Note that the FCU is underlain by the LZ.

5.5 Results

Major element data for the Flatreef and TRP Merensky Reef is given in Tables B5 to B7 (Appendix B). In the HW and MZ, which are relatively plagioclase-rich, CaO/Al_2O_3 values range between 0.5 and 1 at UMT-393 (Fig. 5.6a) and between 0.5 and 0.6 (with an outlier of 2.7 at 759.60m, feldspathic pyroxenite) in UMT-276 (Fig. 5.7a). An increase in CaO/Al_2O_3 values is observed for the mafic units of the Flatreef. In UMT-276, the CaO/Al_2O_3 increases to an average of 1 in the Upper reef and Middling unit. A gradual increase in CaO/Al_2O_3 values from the base of the Main reef at 805 m to the contact with plagioclase-rich units of the HW at 760 m is noticed at UMT-276. A similar trend is found for UMT-393. In the FCU of the UMT-393 which is dominated by plagioclase-rich lithologies CaO/Al_2O_3 values are lower (<1) than that of the overlying mafic units. In the pyroxenite and BSN samples of the Merensky at TRP, CaO/Al_2O_3 ranges between 0.6 and 0.9 (Fig. 5.8a). Lower CaO/Al_2O_3 values are observed for the HW and FW anorthosite (0.5 for each). The bottom part of the Main reef, (i.e. M1L) which consists mainly of harzburgite is highly serpentinised. Loss on ignition (LOI) values up to 5.87 wt. % and 9.37 wt. % are reported for this unit in UMT-393 and UMT-276, respectively (Figs. 5.6b and 5.7b). In the remainder of the Flatreef units where alteration is relatively lower, LOI

values are below 1 wt. %. The lowermost sample of the FCU in UMT-276, which is in close proximity to the underlying calc-silicate rock of the FAZ, has an LOI of 3.22 wt. % consistent with a high CaO/Al_2O_3 of 1.46. The LOI values for the Merensky Reef at TRP are ≤ 1 wt. % with the exception of sample JJB10 (LOI = 1.26 wt. %) (Fig. 5.8b).

Assay data from Ivanplats are presented in Tables B8 and B9 (Appendix B). The S content ranges between 0.02 and 1.31 wt. % in UMT-393 and 0.01 and 2.15% in UMT-276 (Figs. 5.6e and 5.7e). In both boreholes the lower wt. % S is reported for the hanging wall units. Peaks in S values throughout the Flatreef stratigraphy can be correlated with peaks in PGE concentration (Figs. 5.6e, d and 5.7e, d).

The stratigraphic units of the Flatreef display varied isotopic signatures (Figs. 5.6e and 5.7e, Tables B10 and B11, Appendix B). Both positive and negative $\delta^{34}S$ values are observed. The HW, which is characterized by cyclic pyroxenite, norite, anorthosite and gabbro, has a rather consistent, heavy $\delta^{34}S$ signature in UMT-393 (12 to 17‰) (Fig. 5.6e). A gradual increase in $\delta^{34}S$ with height is seen in this unit. However, near the contact with the overlying MZ, an opposite trend is observed. Two samples from the Upper reef in this borehole have contrasting $\delta^{34}S$ of -0.52‰ (sample JDJ097) and 11.26‰ (sample JDJ099). Both samples are feldspathic pyroxenite in close proximity to the chromitite stringer, however, JDJ097 found above the chromitite stringer is relatively more enriched in sulfide minerals. The Middling unit has isotopically lighter, homogeneous S compositions with $\delta^{34}S$ ranging between 4.6‰ and 5.9‰. The Main reef has near mantle $\delta^{34}S$ values ranging between -0.2‰ and 1.5‰ with the exception of samples JDJ-125, -126 and -141B with $\delta^{34}S$ of 9.7‰, 11.1‰ and 7.9‰, respectively. The latter sample is from the M1L near the contact with the underlying FCU and the former two occur in close proximity to the M2-$M1_U$ contact. The S isotopic composition of samples in the FCU vary quite considerably. The FCU hosts samples with the heaviest $\delta^{34}S$ (15.6 to 18.6‰) for this borehole, but also hosts rocks with magmatic S-isotopic signatures ($\delta^{34}S$ values between -0.17 to 2.7‰).

The S isotopic composition of samples from borehole UMT-276 is relatively light compared to that of UMT-393 (Fig. 5.7e). Heavy S isotope values are found in the MZ and HW with $\delta^{34}S$ values of 7.4‰, 10.8‰ and 6‰, respectively. The Main reef shows $\delta^{34}S$ values with an average of -0.4‰, which is lower than that reported for the upper part of the Platreef on Turfspruit (1.1‰ on average) by Sharman-Harris et al. (2005). The FCU in UMT-276 yielded $\delta^{34}S$ values between 0.7 and 13.7‰. Similar to the FCU in UMT-393, this unit has a heterogeneous S isotopic signature. Analysis of a mafic pegmatoidal vein located in the FCU

yielded a δ^{34}S value of 8.5‰. Yudovskaya et al. (2017b) reported δ^{34}S values of LZ ultramafic rocks on Turfspruit ranging between 9 to 14.2‰. A gradual increase in δ^{34}S is observed for the LZ ultramafic samples with an increase in depth (Fig. 5.6f). The δ^{34}S values for feldspathic pyroxenite of the Merensky Reef at TRP range between 1.2 and 4.8‰ with an average of 3‰ (Table B12, Appendix B). The BSN has an average δ^{34}S of 3.9‰. The anorthosite sample from the hanging wall has a δ^{34}S value of 2.9‰ in contrast to the 5.7‰ measured for the anorthosite sample from the footwall. The footwall feldspathic pyroxenite sample has a δ^{34}S of 3.27‰. An increase in S isotope composition with depth for a mining face at TRP is observed (Fig. 5.8c).

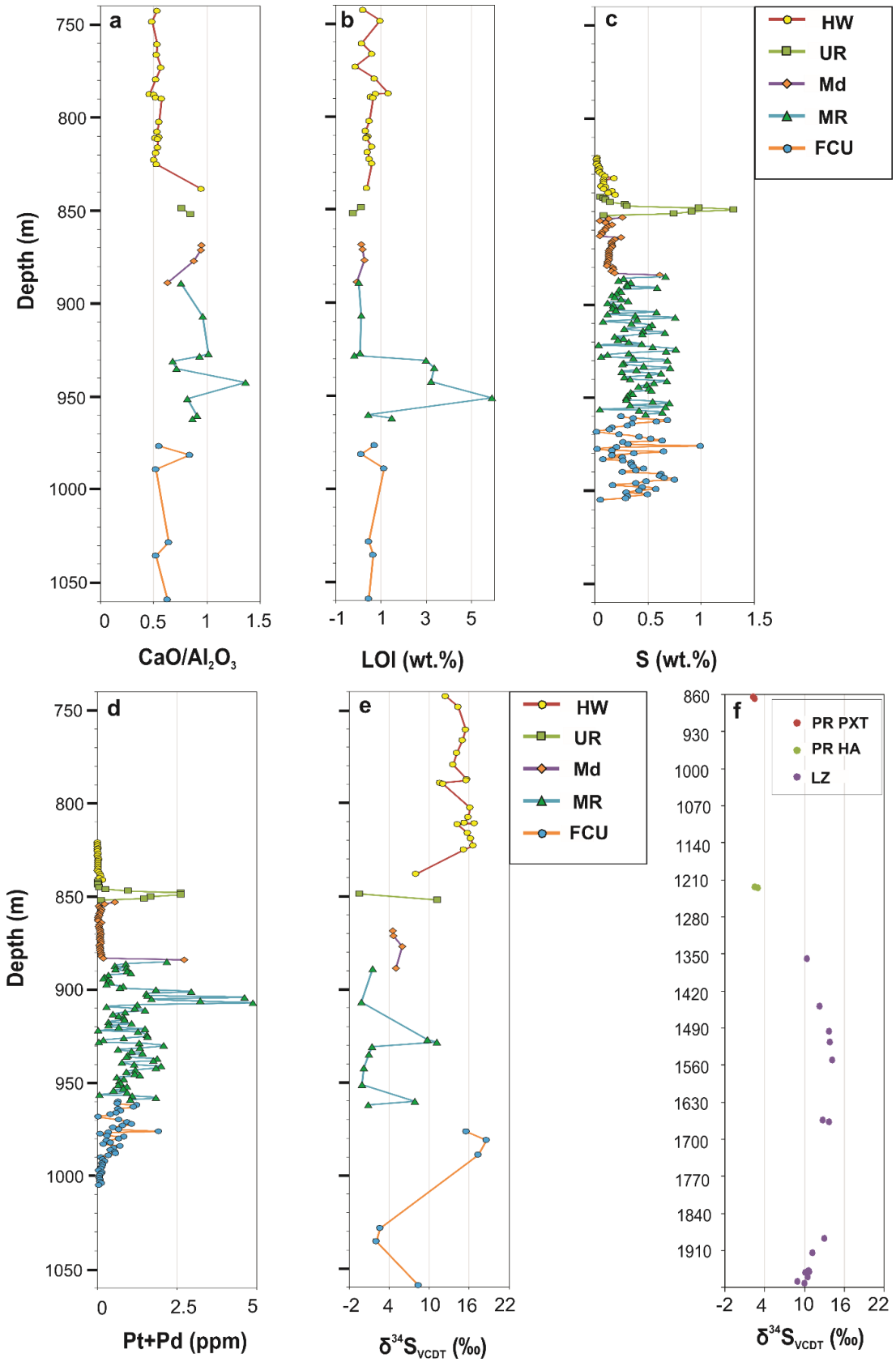

Figure 5.6 Variations in **a** CaO/Al_2O_3; **b** loss on ignition (LOI); **c** S wt. % (Ivanplats Assay data); **d** Pt +Pd in ppm (Ivanplats Assay data); **e** $\delta^{34}S$; with depth in borehole UMT393. **f** Variation of S isotope composition in the pyroxenite reef (PR PXT) and harzburgite reef (PR HA) of the Platreef, and the ultramafic rocks of the LZ with depth in UMT-006 after Yudovskaya et al. 2017.

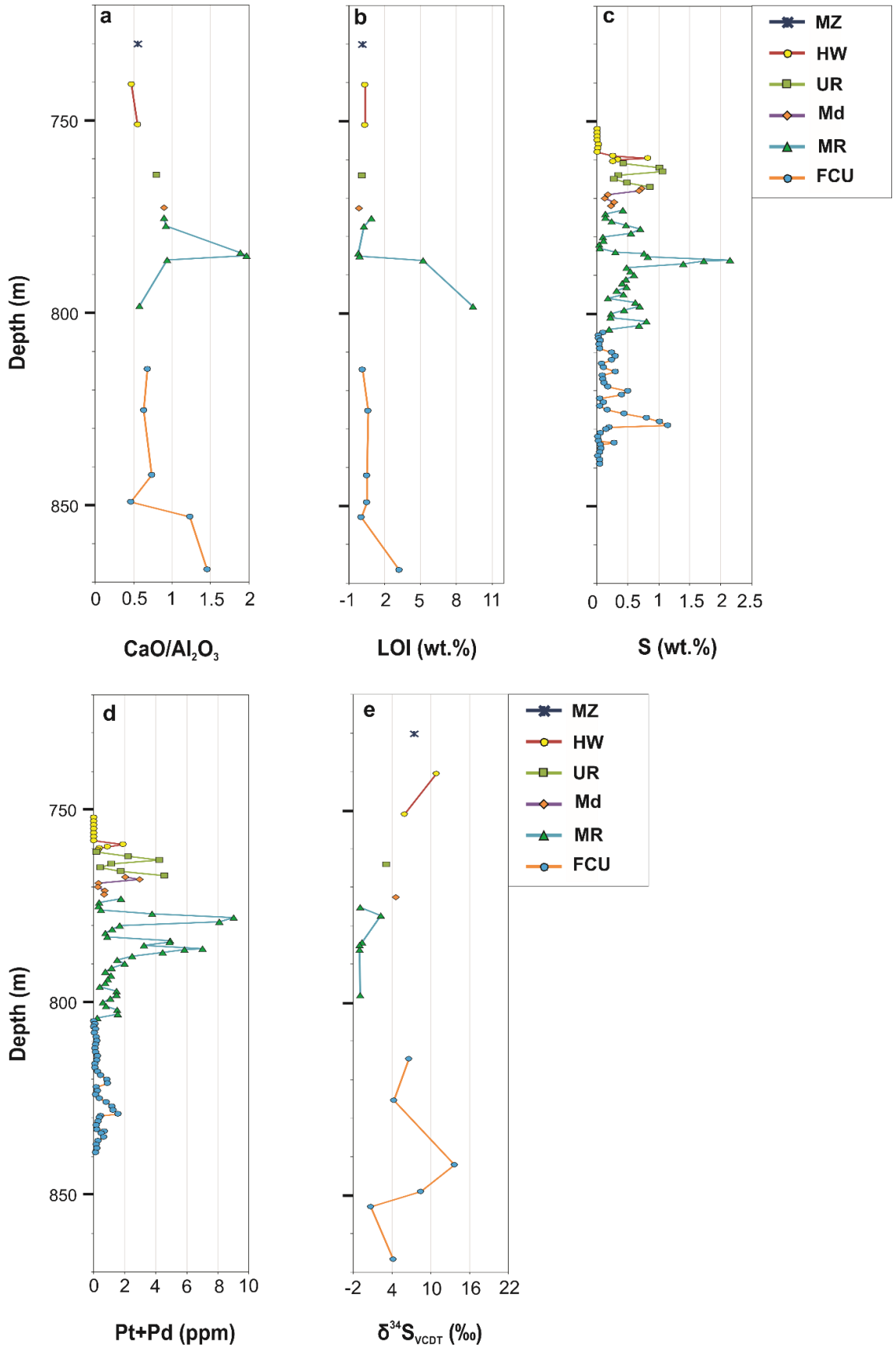

Figure 5.7 Variations in **a** CaO/Al_2O_3; **b** loss on ignition (LOI); **c** S wt. % (Ivanplats Assay data); **d** Pt +Pd in ppm (Ivanplats Assay data); **e** $\delta^{34}S$; with depth in borehole UMT276.

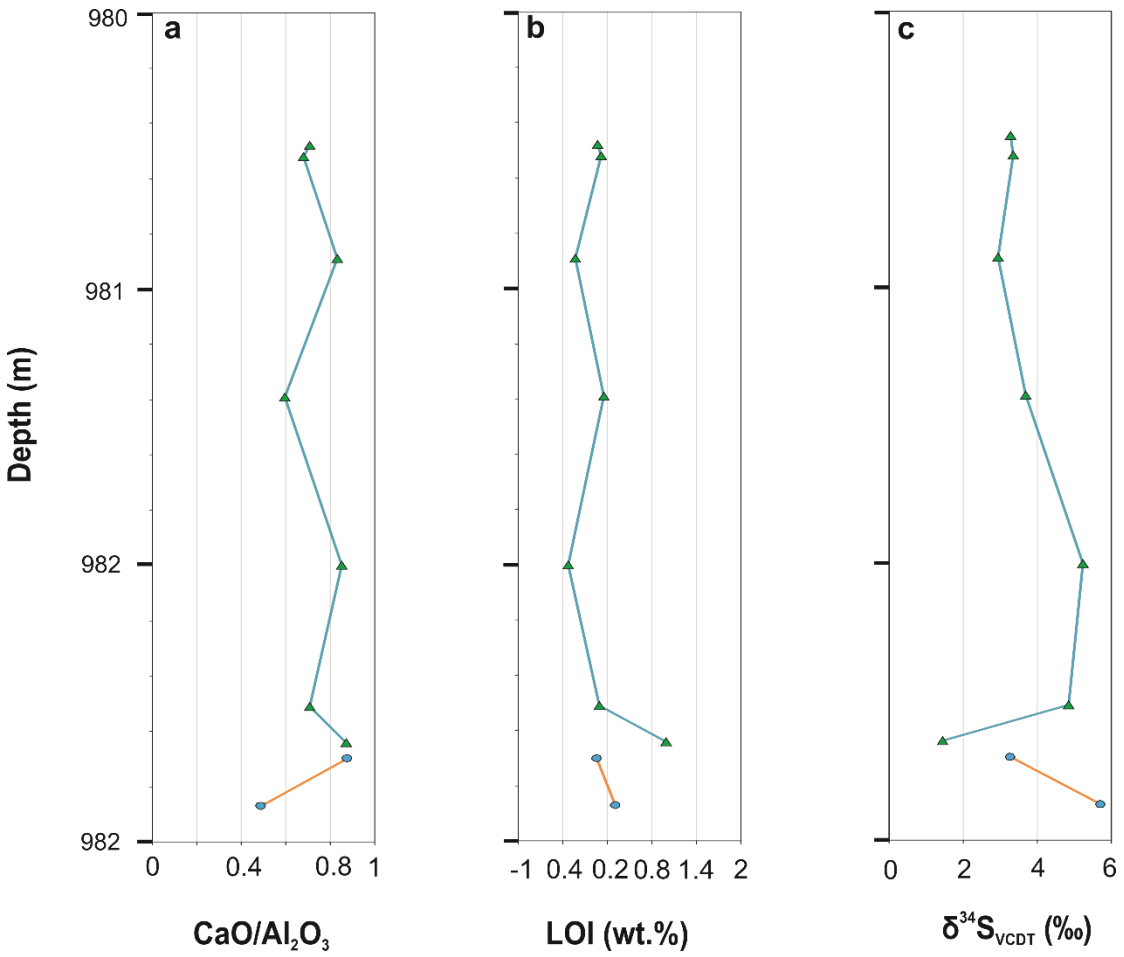

Figure 5.8 Variation of **a** CaO/Al_2O_3; **b** loss on ignition (LOI) and **c** $\delta^{34}S$ with stratigraphic height at a mining face at TRP, eastern BC.

5.6 Discussion

The Platreef is thought to have experienced two stages of crustal contamination, the first having occurred prior to the emplacement of Platreef magma, and the second as the result of the interaction of the magma with footwall rocks (Ihlenfeld & Keays 2011). It was proposed by McDonald & Holwell (2011) that the assimilation of S in the Platreef served as an ore-modifying process and not a mineralization trigger, therefore diluting a preexisting PGE-rich sulfide melt (Sharman et al. 2013). This cannot be confirmed by our study as our results are only based on whole-rock analyses and not in-situ determinations. Several factors such as alteration, sulfate minerals and late phase pyrite may influence the whole-rock powders. Giuliani et al. (2016) have shown that partial S loss during serpentinization combined with isotopic fractionation can cause an increase in the $^{34}S/^{32}S$ ratios in whole-rock samples. Heavy S isotope signatures may therefore be ascribed to this process of S removal during serpentinization and not the assimilation of heavy S isotopes from an external source. Sulfate

minerals present in rocks are potential sources for elevated δ^{34}S values. The S isotope investigation was therefore complemented with petrographic and whole-rock geochemical data to provide additional constraints on the δ^{34}S composition of the samples.

5.6.1 Sulfur isotope variation

Previous studies on the northern limb have shown that the PGE-bearing top portion of the Platreef is characterized by δ^{34}S values within the range of 0±2‰ (Holwell et al. 2007, Penniston-Dorland et al. 2008, Sharman et al. 2013). The Main and Upper reefs on Turfspruit and Macalacaskop are the stratigraphic equivalents of these upper portions of Platreef. In UMT-393, δ^{34}S values of the Main reef fall within the range -0.2 to 1.5‰. However, three outliers with higher δ^{34}S values were observed for this unit (Fig. 5.6e). It is of importance that these elevated δ^{34}S values were observed near the contacts with subsequent units. These higher values could be interpreted as the result of assimilation of sedimentary S from footwall or dolomitic/siliceous xenoliths. Alternatively, the δ^{34}S outlier in the $M1_L$ could also be attributed to S loss associated with serpentinization as this sample is slightly serpentinized. However, overlying harzburgite samples which were subject to greater serpentinization do not display heavy S isotope values. This process was therefore not prominent in this unit. In comparing the Main reef at UMT-276 and UMT-393, it would be expected that the latter, where the Main reef is approximately 75 m thick and further away from the FAZ, would have been less affected by footwall assimilation and contamination. In UMT-276 the Main reef is approximately 29 m thick and has δ^{34}S ranging from -1.1 to 2.2‰. The δ^{34}S values reported for the Main reef samples from UMT-276 are more negative and therefore isotopically lighter than those of UMT-393 and UMT-094 where Keir-Sage et al. (2021) reported Main reef δ^{34}S values between 1.5 and 3.8‰. These lighter δ^{34}S values, with the exception of sample JDJ015 (δ^{34}S = 2.24‰) in the Main reef of UMT-276, fall within the mantle S range proposed by Labidi et al. (2012). The degree of contamination with heavy S for the Main reef in this borehole intersection was therefore relatively less.

The HW and FCU of the Flatreef in this study have S isotopic signatures heavier than that of the Main reef, middling unit and Upper reef. The immediate footwall lithologies of the Flatreef as intersected by boreholes UMT-276 and -393 differ (Figs. 5.4 & 5.5) where the former is underlain by the FAZ, comprising modified magmatic rocks (including calc-silicate rocks) formed through the assimilation of Transvaal sedimentary rocks, and the latter is underlain by the LZ. A common feature in the FCU of both boreholes is the gradual increase in δ^{34}S values with depth. These results match the earlier findings of Sharman-Harris et al. (2005) who suggested that this trend towards heavier sulfur isotope compositions was the result of

progressively higher degrees of sedimentary S assimilation towards the floor. The FCU may therefore have assimilated the surrounding rock. The FCU is also heterogeneous in that even though it displays the heaviest S isotope compositions encountered in this study, it enigmatically also contains rocks with δ^{34}S values between -0.1 and 2.7‰. The FAZ at UMT-094, located on the western portion of Turfspruit, has δ^{34}S values between 1.8 and 8.9‰ (7.3‰ on average) and underlying calc-silicate rocks and dolostone have δ^{34}S up to 12‰ (Keir-Sage et al. 2021).

5.6.2 Model for Flatreef formation

Relative to the S isotope signature of the Main reef, higher δ^{34}S values were recorded for the immediate footwall and hanging wall. This heavy S isotope signature of the footwall and hanging wall lithologies could possibly be explained by the extensive interaction and subsequent assimilation/contamination of the magma with floor rocks. One of the issues emerging from this finding is why the hanging wall has heavy δ^{34}S values when it is located further away from the contact with floor rocks and its underlying units, inclusive of the Main reef, have lighter S isotope signatures. We propose that the hanging wall lithologies may have originally been continuous with the footwall lithologies as both units consists mainly of norite cycles (i.e., interlayered pyroxenite, norite, mottled anorthosite and gabbro). It is plausible that the remainder of the Flatreef, i.e., Main reef, Middling unit and Upper reef, intruded as different pulses separating the hanging wall and footwall.

It may be the case therefore that the consistent, relatively weakly contaminated S isotopic signature in the PGE-enriched Main reef was unaffected by the local footwall rocks (Keir-Sage et al. 2021). We propose that the magma that gave rise to the Flatreef/Merensky Reef was saturated in magmatic sulfide prior to its emplacement in the RLS stratigraphy. These sulfide minerals may have collected in LZ magma conduits/pre-Platreef staging chambers and then expelled as crystal-sulfide mush by an early pulse of MZ magma, as explained by McDonald and Holwell (2007, 2011). Sulfide collected in the conduit traps may have extensively interacted with large volumes of uncontaminated magmas resulting in near magmatic S isotopic compositions and high metal tenors. The sulfur isotope compositions and metal tenors of sulfide minerals may be modified by exchange reactions (Ripley & Li 2003). If the primary sulfide minerals have not been modified, their S isotope signature would remain magmatic. The S isotope exchange may also be accompanied by chalcophile element exchange such as the exchange of Fe for Cu, Ni, or PGE (Ripley & Li 2003), which results in metal enrichment of the sulfide liquid. This may explain the Pt+Pd peaks and the accompanying low δ^{34}S values in the Main reef of both boreholes (Fig. 5.6A, B, C&D).

One of the main contaminants of the Flatreef is dolostone from the underlying Malmani Subgroup (Grobler et al. 2019, Keir-Sage et al. 2021). Because the assimilation of dolostone would result in an increase in CaO only and not Al_2O_3, the CaO/Al_2O_3 ratio serves as an effective geochemical tool to trace carbonate assimilation within the Flatreef (Keir-Sage et al. 2021). Furthermore, the CaO/Al_2O_3 value of whole-rock may be used as an indicator of assimilation of calc-silicates by magmatic rocks as pure plagioclase has a ratio of 0.6 and orthopyroxene minor concentrations of CaO and Al_2O_3 (Kinnaird 2005). A mixture of these two minerals would therefore have a similar ratio to that of pure plagioclase and any significant deviation from 0.6 would thus imply the presence of clinopyroxene potentially as the result of interaction with dolomite (Kinnaird 2005). The CaO/Al_2O_3 values for the different lithologies of the Flatreef are relatively higher for the mineralized mafic units (i.e., namely Main reef, Middling unit and Upper reef) than the feldspar-rich mafic units of the HW and FCU. The bottom part of the Main reef has the highest CaO/Al_2O_3 and LOI wt. % which is evidence of contamination. Keir-Sage et al. (2021) recorded CaO/Al_2O_3 values ranging from between 1 and greater than 10 for footwall calc-silicate rocks and dolostone. The contamination signature of CaO/Al_2O_3 values in the footwall and FAZ does not extend into the FCU in our study.

5.6.3 S isotope variation of the Merensky Reef at TRP

The $\delta^{34}S$ values within the Merensky Reef at TRP range between 1.2 and 4.8‰ (3.24‰ on average). The $\delta^{34}S$ for the Merensky Reef in the western BC is on average 1.7‰ (values range between 1.1 and 2.6‰) and two Merensky Reef samples from the eastern BC returned $\delta^{34}S$ values of 1.9‰ (Penniston-Dorland et al. 2012) and 1.68‰ (Magalhães et al. 2018). In the central sector of the eastern limb, UCZ rocks (excluding the UG2 chromitite) have $\delta^{34}S$ values ranging between 1.42 and 1.68‰ (Magalhães et al. 2018), which is lower than what is reported for the samples from TRP. Mass-independently fractionated sulfur isotopes, which involves $\Delta^{33}S$ measurements, is an effective isotopic tracer (Penniston-Dorland et al. 2008). Magalhães et al. (2018) observed inconsistent variations of $\Delta^{33}S$ with Sr and Nd isotopes at the same stratigraphic levels, which indicated that distinct magma pulses incorporated assimilated S from different sources. The high $\delta^{34}S$ values of the Merensky Reef at TRP may be interpreted as a result of the localized assimilation of BSN. The BSN has a contaminated S isotope signature with $\delta^{34}S$ values ranging between 3 and 5.2‰. It is also important to note that north of TRP the CZ directly overlies Transvaal sedimentary rocks where the degassing of carbonates and water release by metamorphism has caused reef disturbances (Gauert et al. 2013, Scoon et al. 2017). The S isotopes of the Merensky Reef would therefore have a

heavier isotope signature, which is slightly more positive than the mantle derived δ^{34}S values because it is partially derived from underlying carbonate lithologies.

5.6.4 Comparison of S isotope composition in the Flatreef and Merensky Reef at TRP

Our results provide further evidence that the Main reef is the stratigraphic equivalent of the Merensky Reef in the remainder of the BC (Grobler et al. 2019). Our findings show that the S isotopic signatures of the Main reef in boreholes UMT276 and UMT393 (with the exception of the 3 outliers which may be attributed to contamination by footwall or dolomitic/siliceous xenoliths) and TRP Merensky Reef are similar. In figures 5.9 a and b, where the compositional data of UMT094 (Keir-Sage et al. 2021) is compared to our study, an overlap of data is observed. Although the S isotopic signatures are similar, δ^{34}S values recorded for the Merensky Reef at TRP are heavier than in the Main reef of UMT-276 and -393. Relative to the Main reef in UMT393 and TRP Merensky Reef, δ^{34}S values for the Main reef in UMT-276 are the lightest. It is evident that these units have undergone different degrees of heavy S contamination, the latter having been least contaminated. Similar to the Flatreef, samples from the immediate footwall and hanging wall rocks of the Merensky Reef at TRP do not display near magmatic δ^{34}S values. However, these S isotope values are lower than the elevated ones observed at the Flatreef. Our findings show that even though the hanging wall and footwall units of the Flatreef have heavily contaminated S isotope signatures, the PGE reefs, namely the Upper reef and Main reef, display lighter δ^{34}S values that overlap, and are slightly lower than that of the Merensky Reef at TRP and in the eastern BC.

In earlier studies of S isotope variation in the BC (Holwell et al. 2007, for example) mantle was reported to have δ^{34}S values of 0 ± 2‰. A study by Labidi et al. (2012) and the recent studies that followed, shows that the mantle S composition is more negative (around -2‰ to 0‰) in contrast to the positive values previously reported. The heavier δ^{34}S values reported in this study for the Flatreef and Merensky Reef at TRP are indicative of some degree of contamination by heavy S isotopes possibly in a crustal staging chamber as proposed by Sharman et al. 2005, Penniston-Dorland et al. 2008 and Sharman-Harris et al. 2013.

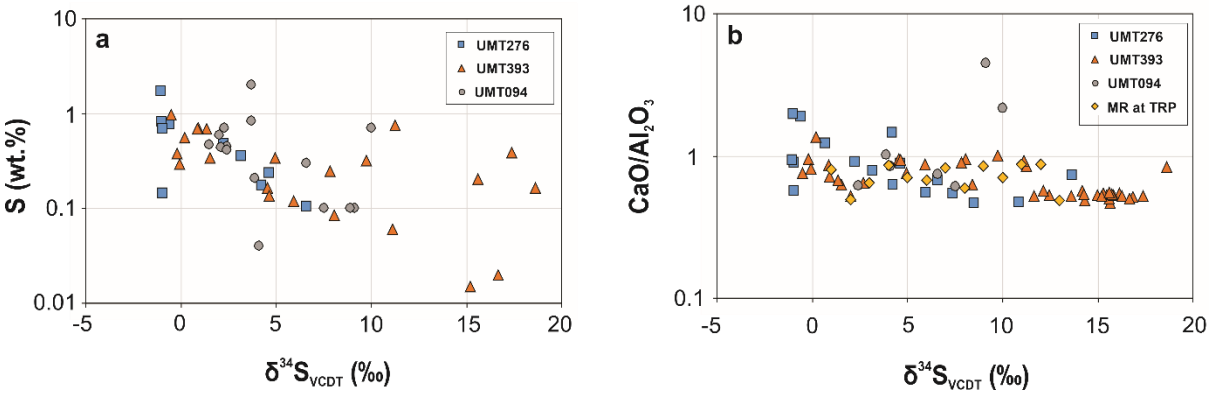

Figure 5.9 Comparison of compositional data of UMT393, UMT276, UMT094 (Keir-Sage et al., 2021) and MR at TRP (EBC). **a** S vs. $\delta^{34}S$ and **b** CaO/Al_2O_3 vs $\delta^{34}S$.

5.7 Conclusion

The S isotope data obtained from drill-core UMT-276 and UMT-393, show that the Main reef of the Flatreef is characterized by a S isotope signature, similar to that of the Merensky Reef in the eastern and western BC. The relatively uniform $\delta^{34}S$ values and accompanying metal enrichment of the Main reef may be the result of extensive interaction of sulfides in LZ conduits with large volumes of uncontaminated magma. The heaviest S isotope signatures are observed in the HW and FCU and can most probably be attributed to assimilation of footwall rocks/xenoliths where the geochemical evidence of the crustal assimilation is preserved. The hangingwall and footwall lithologies may have originally been continuous and later separated from each other by magma pulses of the remainder of the Flatreef. Surprisingly, $\delta^{34}S$ values from the Merensky Reef at TRP is slightly heavier than that reported for the eastern and western BC as well as the Main reef at Turfspruit and Macalacaskop, northern limb. Contamination by the assimilation of S from surrounding BSN/footwall rock as well as the degassing of underlying carbonates are the most plausible explanation for these elevated S isotope ratios.

5.8 Acknowledgements

The following institutions, companies and persons are thanked: The Environmental Isotope Laboratory at iThemba LABS for S isotope analysis; Ivanplats for access to the samples analyzed as part of this study; Albie Brits for cross section figures; Two Rivers Platinum Mine for access to Merensky Reef samples; the Geology Department at the University of the Free State for sample preparation and XRF analysis. We also thank Nivea Magalhaes and one anonymous reviewer for their constructive reviews.

5.9 References

Ashwal, L.D., Webb, S.J., & Knoper, M.W. (2005) Magmatic stratigraphy in the Bushveld Northern Lobe: continuous geophysical and mineralogical data from the 2950m Bellevue drill core. South African Journal of Geology. 108, 199-232

Bekker, A., Kaufman, A.J., Karhu, J.A., Beukes, N.J., Swart, Q.D., Coetzee, L.L., & Eriksson, K.A. (2001) Chemostratigraphy of the Paleoproterozoic Duitschland formation, South Africa: implications for coupled climate change and carbon cycling. American Journal of Science. 301, 261–285.

Beukes, J.J., Gauert, C.D.K., & Giebel, R.J. (2016) Cryptic mineral variation and PGE distribution in the Merensky Reef and its discontinuous melagabbronoritic hanging wall (Brown Sugar Norite – BSN) at Two Rivers Platinum mine, Eastern Bushveld Complex, South Africa. South African Journal of Geology 119(1), 243–272

Beukes, J. J., Roelofse, F., Gauert, C.D. K., Grobler, D. F., & Ueckermann, H. (2021) Strontium isotope variations in the Flatreef on Macalacaskop, northern limb, Bushveld Complex: implications for the source of platinum-group elements in the Merensky Reef. Mineralium Deposita. 56, 45-57.

Buchanan, D.L., Nolan, J., Suddaby, P., Rouse, J.E., Viljoen, M.J., & Davenport, M.J., & Davenport, J.W.J. (1981) The genesis of sulfide mineralization in a portion the Potgietersrus Limb of the Bushveld Complex. Economic Geology. 76, 568–579.

Buchanan, D. L. & Rouse J. E. (1984) Role of contamination in the precipitation of sulphides in the Platreef of the Bushveld Complex. In Sulphide Deposits in Mafic and Ultramafic Rocks (D.L. Buchanan & M.J. Jones, eds.). IMM, London, 141–146.

Cawthorn, R. G. (1999). The platinum and palladium resources of the Bushveld Complex. South African Journal of Science. 95, 481–489.

Cowell, M., (2003) Two Rivers Platinum Mine Trial Mining Report. Unpublished Company Report, 80pp.

Eales, H.V., & Cawthorn, R.G. (1996) The Bushveld Complex. In Layered intrusions (R.G. Cawthorn ed.). Elsevier, Oxford, (181–229)

Giuliani,A., Fiorentini, M.L., Martin, L.A.J., Farquhar, J., Phillips, D., Griffin, W.L., LaFlamme, C. (2016) Sulfur isotope composition of metasomatised mantle xenoliths from the Bultfontein kimberlite (Kimberley, South Africa): Contribution from subducted sediments and the effect of sulfide alteration on S isotope systematics Earth Planet. Sci. Lett., 445 (2016), 114-124

Grobler, D.F., & Nielsen S.A. (2012) Upper critical zone (Merensky Reef –UG2) correlates within the Platreef, Turfspruit 241KR, Northern Limb, Bushveld Igneous Complex: internal report, Platreef Resources Pty Ltd. 27 February 2012, 31 p

Grobler, D.F., Brits, J.A.N., Maier W.D., & Crossingham A. (2019) Litho- and chemostratigraphy of the Flatreef PGE deposit, northern Bushveld Complex. Mineralium Deposita. 5, 3-28

Harris, C. & Chaumba, J.B. (2001) Crustal contamination and fluid-rock interaction during the formation of the Platreef, northern limb of the Bushveld Complex, South Africa. Journal of Petrology. 42, 1321–1347

Hutchinson, D., & McDonald I. (2008) Laser ablation ICP-MS study of platinum-group elements in sulfides from the Platreef at Turfspruit, northern limb of the Bushveld Complex, South Africa. Mineralium Deposita. 43, 695–711

Holwell, D. A., & Jordaan, A. (2006). Three-dimensional mapping of the Platreef at the Zwartfontein South mine: Implications for the timing of magmatic events in the northern limb of the Bushveld Complex, South Africa. Transactions of the Institutions of Mining and Metallurgy, Section B: Applied Earth Science, Section B: Applied Earth Science. 115, 41–48.

Holwell, D. A., & McDonald, I. (2007) Distribution of platinum-group elements in the Platreef at Overysel, northern Bushveld Complex: A combined PGM and LA-ICP-MS study. Contributions to Mineralogy and Petrology. 154, 171–190.

Holwell, D.A., Armitage, P. E. B., & McDonald, I. (2005) Observations on the relationship between the Platreef and its hangingwall. Transactions of the Institutions of Mining and Metallurgy, Section B: Applied Earth Science. 114, 199–208.

Holwell, D.A., Boyce, A.J., McDonald, I. (2007) Sulfur isotope variations within the Platreef Ni-Cu-PGE deposit: genetic implications for the origin of sulfide mineralization. Economic Geology.102, 1091–1110

Ihlenfeld, C., & Keays, R.R., (2011) Crustal contamination and PGE mineralization in the Platreef, Bushveld Complex, South Africa: Evidence for multiple contamination events and transport of magmatic sulfides. Mineralium Deposita. 46, 813–832.

Iljina, M.J., &Lee, C.A. (2005) PGE deposits in the marginal series of layered intrusions. In Exploration for platinum-group element deposits. Ottawa, Mineralogical Association of Canada Short Course Series, pp. 75–96

Karykowski, B.T., & Maier, W.D. (2017) Microtextural characterisation of the Lower Zone in the western limb of the Bushveld Complex, South Africa: evidence for extensive melt migration within a sill complex. Contributions to Mineralogy and Petrology. 172, 1-18

Keir-Sage, E., Leybourne, M.I., Jugo, P.J., Grobler, D.F.& Mayer, C.C. (2021) Assessing the extent of local assimilation within the Flatreef, northern limb of the Bushveld Igneous Complex, using sulfur isotopes and trace element geochemistry. Mineralium Deposita. 56, 91-102.

Kinnaird, J.A., &Nex, P.A.M. (2015) An Overview of the Platreef. In: Hammond NQ, Hatton C (eds) Platinum-group element (PGE) mineralisation and resources of the Bushveld Complex, Council for Geoscience, Pretoria, South Africa, pp.293–341

Kinnaird, J.A., & McDonald, I., (2005) An introduction to mineralisation in the northern limb of the Bushveld Complex: Transactions of the Institution of Mining and Metallurgy. 114, 194–198.

Kinnaird, J.A., Hutchinson, D., Schurmann L., Nex, P.A.M., de Lange, R. (2005) Petrology and Mineralisation of the southern Platreef: northern limb of the Bushveld Complex, South Africa. Mineralium Deposita. 40, 576-597

Kruger, F. J. (2005a). Filling the Bushveld Complex magma chamber: Lateral expansion, roof and floor interaction, magmatic unconformities, and the formation of giant chromitite, PGE and Ti-V-magnetitite deposits. Mineralium Deposita.40, 451–472.

Kruger, F.J. (2005b). The Main Zone of the Bushveld Complex: Source of the Merensky Reef and the Platreef. 10th International Platinum Symposium Abstracts Volume, Oulu, Finland

Labidi, J., Cartigny, P., Birck, J.L., Assayag, N., Bourrand, J.J., 2012. Determination of multiple sulfur isotopes in glasses: a reappraisal of the MORB d^{34}S. Chem. Geol.334, 189–198.

Labidi, J., Cartigny, P., Hamelin, C., Moreira, M., Dosso, L., 2014. Sulfur isotope budget (^{32}S, ^{33}S, ^{34}S and ^{36}S) in Pacific–Antarctic ridge basalts: a record of mantle source heterogeneity and hydrothermal sulfide assimilation. Geochim. Cosmochim. Acta133, 47–67.

Labidi, J., Cartigny, P., Jackson, M.G., 2015. Multiple sulfur isotope composition of oxidized Samoan melts and the implications of a sulfur isotope 'mantle array' in chemical geodynamics. Earth Planet. Sci. Lett.417, 28–39.

Magalhães, N., Penniston-Dorland, S., Farquhar, J., & Mathez, E.A. (2018) Variable sulfur isotope composition of sulfides provide evidence for multiple sources of contamination in the Rustenburg Layered Suite, Bushveld Complex. Earth and Planetary Science Letters. 492:163–173.

Maier, W.D., de Klerk, L., Blaine, J., Manyeruke, T., Barnes, S-J, Stevens, M.V.A., & Mavrogenes, J.A. (2008) Petrogenesis of contact-style PGE mineralisation in the northern limb of the Bushveld Complex: comparison of data from the farms Rooipoort, Townlands, Drenthe and Nonnenwerth. Mineralium Deposita. 43:255–280

Mangwegape, M., Roelofse, F., Mock, T., & Carlson, R.W. (2016). The Sr-isotopic stratigraphy of the Northern Limb of the Bushveld Complex South Africa. Journal of African Earth Science. 113, 5-100

Manyeruke, T.D., Maier, W.D., & Barnes S-J (2005) Major and Trace Element Geochemistry of the Platreef on the farm Townlands, northern Bushveld Complex. South African Journal of Geology. 108, 381–396

Mayer, C.C., Jugo, P.J., Leybourne, M.I., Grobler, D.F., & Voinot, A. (2021) Strontium isotope stratigraphy through the Flatreef PGE-Ni-Cu mineralization at Turfspruit, northern limb of the Bushveld Igneous Complex: evidence of correlation with the Merensky Unit of the eastern and western limbs. Mineralium Deposita. 56, 59-72

McDonald, I., Holwell, D.A., & Armitage, P.E.B. (2005) Geochemistry and mineralogy of the Platreef and “Critical Zone” of the northern lobe of the Bushveld Complex, South Africa: implications for Bushveld stratigraphy and the development of PGE mineralisation. Mineral Deposita. 40, 526–549

McDonald, I., & Holwell, D.A. (2007) Did lower zone magma conduits store PGE-rich sulfides that were later supplied to the Platreef? South African Journal of Geology. 110, 611–616

McDonald, I., & Holwell, D.A. (2011) Geology of the Northern Bushveld Complex and the Setting and Genesis of the Platreef Ni-Cu-PGE Deposit. Society of Economic Geologists. Reviews in Economic Geology. 17, 297-327

Mitchell, A.A. (1990) The stratigraphy, petrography and mineralogy of the Main Zone of the Northwestern Bushveld Complex. South African Journal of Geology. 93, 818-831

Naldrett, A.J., Wilson, A., Kinnaird, J., Yudovskaya, M., & Chunnett, G. (2012) The origin of chromitites and related PGE mineralization in the Bushveld Complex: New mineralogical and petrological constraints. Mineralium Deposita.47, 209–232

Penniston-Dorland, S.C., Wing, B.A., Nex, P.A.M., Kinnaird, J.A., Farquhar, J., Brown, M., & Sharman, E., (2008). Multiple sulfur isotopes reveal a primary magmatic origin for the Platreef PGE deposit, Bushveld Complex, South Africa. Geology. 36, 979–982

Penniston-Dorland, S.C., Mathez, E.A., Wing, B., Farquhar, J., & Kinnaird, J.A., (2012) Multiple sulfur isotope evidence for surface-derived sulfur in the Bushveld Complex. Earth and Planetary Science Letters, v.337–338, 236–242.

Ripley, E.M., & Li, C., (2003) Sulfur isotope exchange and metal enrichment in the formation of magmatic Cu–Ni–(PGE) deposits. Economic Geology. 98, 635–641.

Roelofse, F., & Ashwal, L.D. (2012) The Lower Main Zone in the Northern Limb of the Bushveld Complex a >1.3km Thick Sequence of Intruded and Variably Contaminated Crystal Mushes. Journal of Petrology. 53, 1449-1476.

Rose, D., Viljoen, F., Knoper, M. & Rajesh, H., (2011) Detailed Assessment of Platinum-Group Minerals Associated with Chromitite Stringers in the Merensky Reef of the Eastern Bushveld Complex, South Africa. The Canadian Mineralogist. 49, 1385-1396.

Sakai, H., Des Marais, D.J., Ueda, A., and Moore, J.G. (1984), Concentrations and isotope ratios of carbon, nitrogen, and sulfur in ocean-floor basalts: Geochimica et Cosmochimica Acta. 48, 2433–2441.

Scoon, R.N. (2002) A new occurrence of Merensky Reef on the flanks of the Zaaikloof dome, northeastern Bushveld Complex: Relationship between diapirism and magma replenishment. Economic Geology. 97, 1037-1049

Scoon, R. N., Costin, G., & Gräbe, P. J. (2017). Geology and Origin of the Vanadiferous Fe-Ti Oxide-rich Kennedy's Vale Discordant Body, Eastern Limb of the Bushveld Complex, South Africa. South African Journal of Geology, 120, 251–270

Schiffries, C.M. & Rye, D.M. (1989) Stable isotopic systematics of the Bushveld Complex: I. Constraints of magmatic processes in layered intrusions. American Journal of Science. 289, 841–873.

Scoates, J. S., & Friedman, R. M. (2008) Precise age of the platiniferous Merensky reef, Bushveld Complex, South Africa, by the U-Pb zircon chemical abrasion ID-TIMS technique. Economic Geology. 103, 465–471.

Sharman-Harris, E.R., Kinnaird, J.A., Harris, C., & Horstmann, U.E. (2005) A new look at sulphide mineralisation of the northern limb, Bushveld Complex: a stable isotope study. Transactions of the Institution of Mining and Metallurgy, Section B. 114, 252-263.

Sharman, E.R., Penniston-Dorland, S.C., Kinnaird, J.A., Nex, P.A.M., Brown, M., & Wing, B.A. (2013) Primary Origin of Marginal Ni-Cu-(PGE) Mineralization in Layered Intrusions: $\Delta^{33}S$ evidence from the Platreef, Bushveld, South Africa. Economic Geology. 108, 365–377.

Teigler, B., & Eales H.V. (1996) The Lower and Critical Zones of the Western Limb of the Bushveld Complex as Intersected by the Nooitgedacht Boreholes. The Council for Geoscience and the Geological Survey of South Africa.

van der Merwe, M.J. (1976) The Layered Sequence of the Potgietersrus Limb of the Bushveld Complex. Economic Geology. 71, 1337-1351.

van der Merwe, M.J. (2008) The geology and structure of the Rustenburg Layered Suite in the Potgietersrus/Mokopane area of the Bushveld Complex South Africa. Mineralium Deposita. 43, 405–419.

Wilson, A.H. (2015) The Earliest Stages of Emplacement of the Eastern Bushveld Complex: Development of the Lower Zone, Marginal Zone and Basal Ultramafic Sequence. Journal of Petrology. 56, 347–388.

Yudovskaya, M.A., Kinnaird, J.A., Sobolev, A.V., Kuzmin, D.V., McDonald, I., & Wilson, A.H. (2013) Petrogenesis of the lower zone olivine-rich cumulates beneath the Platreef and their correlation with recognized occurrences in the Bushveld Complex. Economic Geology. 108, 1923–1952.

Yudovskaya, M.A., Kinnaird, J.A., Grobler, D.F., Costin, G., Abramova, V.D., Dunnet, T., & Barnes, S-J (2017a) Zonation of Merensky style platinum mineralization in Turfspruit thick reef facies (northern limb of the Bushveld Complex). Economic Geology. 112, 1333–1365.

Yudovskaya, M.A., Belousova, E., Kinnaird, J.A., Dubinina, E., Grobler, D.F., & Pearson, N. (2017b) Re-Os and S isotope evidence for the origin of Platreef mineralization (Bushveld Complex). Geochimica et Cosmochimica. 112, 1333–1365.

Zeh, A., Ovtcharova, M., Wilson, A.H., & Schaltegger, U. (2015) The Bushveld Complex was emplaced and cooled in less than one million years – results of zirconology, and geotectonic implications. Earth and Planetary Science Letters. 418,103–114.

CHAPTER 6 :
ARTICLE 3

Neodymium isotope variations in the Flatreef on Macalacaskop, northern limb, Bushveld Complex

6.1 Abstract

The origin of the recently discovered Flatreef remains debated due to the pronounced interaction of the magmatic rocks with sedimentary floor rocks, resulting in a complex intrusive stratigraphy. In this study, we report new Nd isotopic compositions of Flatreef lithologies as intersected by borehole UMT-393 on the farm Macalacaskop in order to better our understanding of the magmatic history of the ore deposit and to further test the putative correlation between the Flatreef / Platreef and the Upper Critical Zone of the remainder of the Bushveld Complex. The initial epsilon Nd (ε_{Ndi}) values for the Flatreef were found to range between –5.2 to -7.6, overlapping with ε_{Ndi} values of the Upper Critical Zone from the eastern (ranging between -4.8 and -8.5) and the Upper Critical Zone and Main Zone from the western limb (ranging between -6.3 and -7.6 for the former, and -6.3 and -7.4 for the latter) of the Bushveld Complex. The Flatreef ε_{Ndi} values also overlap with those of the Platreef, however, due to the varying footwall lithologies of the Platreef along strike, Platreef rocks display a wider variation in isotopic composition. Our findings support the proposed correlation of the Flatreef with the Upper Critical Zone – Main Zone transition interval in the remainder of the Bushveld Complex, which includes the Merensky and Bastard reefs. Due to significant overlap between the ε_{Ndi} values of the Flatreef and local potential contaminants occurring at the base of the Northern Limb, we propose that the Sr-Nd isotopic composition of the magmas that gave rise to the Flatreef are most likely attributable to the interaction of mantle-derived magma with upper and lower crustal rocks of the Kaapvaal Craton within a sub-Bushveld staging chamber, with possible syn- to post-emplacement modification as a result of interaction with locally available dolomitic footwall rocks

6.2 Introduction

The Bushveld Complex (BC) (Fig. 6.1a) is regarded as the most valuable mineral province on Earth (Naldrett, 2009). Covering an area of approximately 90 000 km^2 (Eales and Cawthorn 1996, Finn et al. 2015), it hosts the world's largest deposits of platinum group elements (PGE), chromium and vanadium. The Platreef has been suggested to be the equivalent of the Upper Critical Zone in the northern limb of the BC (Grobler et al. 2019). Relative to the Merensky Reef and UG-2 Reef in the western and eastern limbs of the BC, the Platreef in the northern limb has historically attracted less attention from researchers. The Platreef is defined as:

“Mafic units enriched in Ni-Cu-PGE that occur between the Archaean granite-gneiss basement or the Transvaal Supergroup and the gabbros and gabbronorites of the Main zone, north of the Planknek Fault” (Kinnaird and McDonald, 2005, p. B196). Although it is generally accepted that the stratiform mineralization of the upper Platreef is magmatic in origin (Holwell et al. 2007; Maier et al. 2008; Penniston-Dorland et al. 2008; Yudovskaya et al. 2017; Junge et al. 2019; Klemd et al. 2020), no consensus has been established regarding how the Platreef formed and how it relates to the rest of the BC. Some authors have proposed that the Platreef was emplaced as a sill or multiple sills (Kinnaird 2005; Manyeruke et al. 2005). In contrast, Kruger (2005) suggested that the Platreef formed in response to the intrusion of Main Zone magma that interacted with local floor rocks and subsequently flowed south into the western and eastern limbs, where it gave rise to the Merensky Reef. Naldrett et al. (2008) proposed a “nested pudding bowls” model where the Platreef formed from PGE-enriched Upper Critical Zone magmas that escaped up the margins between two nested basins.

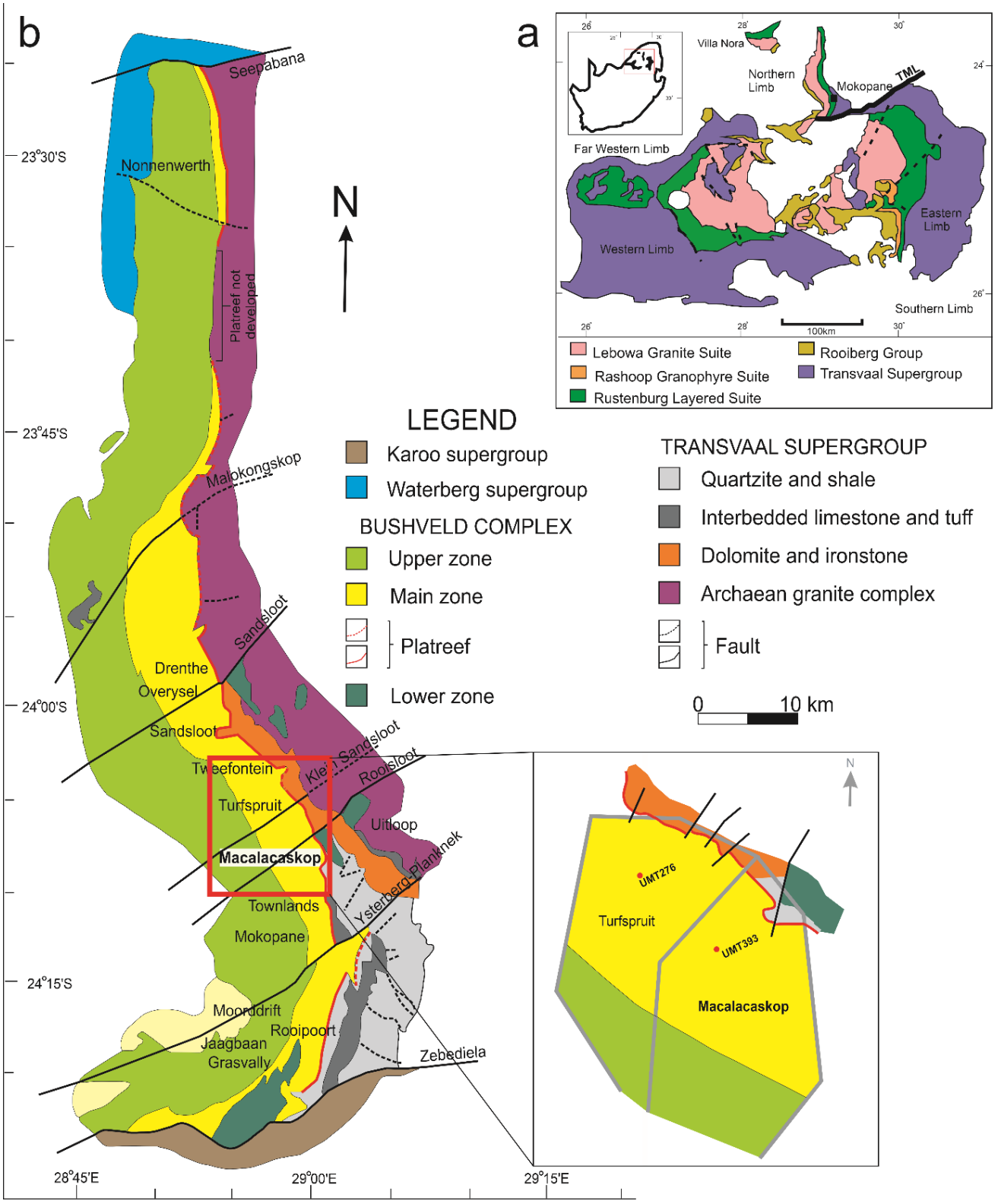

Figure 6.1 a Regional map of the Bushveld Complex displaying the different limbs and simplified geology modified after Eales & Cawthorn (1996) and Yudovskaya and Kinnaird (2010). TML = Thabazimbi-Murchison Lineament. **b** Simplified geological map of the Bushveld Complex showing the locations of boreholes UMT-276 and UMT-393 on the farms Turfspruit and Macalacaskop. (After van der Merwe 1976, as modified by Ashwal et al., 2005)

Isotopic studies have strongly influenced the narrative regarding models for emplacement and petrogenesis of the BC. Early whole-rock Sr-isotopic studies include those of Hamilton (1977), Kruger and Marsh (1982), Sharpe (1985), Lee and Butcher (1990) and Kruger (1994), who attributed variations in initial Sr-isotopic composition across the stratigraphy to the repeated intrusion of compositionally distinct magmas. Maier et al. (2000) presented the first whole-rock Nd isotopic data for the Bushveld layered sequence (formally known as the "Rustenburg Layered Suite"). The data were interpreted to reflect the interaction of mantle-derived melt with upper and lower crustal end-members. Harris et al. (2005) attributed $\delta^{18}O$ values higher than the mantle range to crustal contamination of parental magmas to the Bushveld Complex within a deep 'staging chamber'. Extensive crustal contamination of the Bushveld magmas is also supported by S isotope datasets (Buchanan et al. 1981; Buchanan and Rouse 1984). Various isotope investigations carried out on the Platreef specifically confirm that crustal contamination, in many instances of a localised nature, played a significant role in its formation. These isotopic studies include: O isotopes by Harris et al. 2001, 2005; Os isotopes by Reisberg et al. 2011; Nd isotopes by Pronost et al. 2008, Maier et al. 2008; S isotopes by Buchanan et al. 1981, Manyeruke et al. 2005, Sharman-Harris et al. 2005; Sr isotopes by Cawthorn et al. 1985, Barton et al. 1986, Kruger 2005.

The relatively recent discovery of the Flatreef in the northern limb of the BC has led to a better understanding of the provenance and emplacement of the Platreef. The Flatreef, is a sub-horizontal, high grade Ni-Cu-PGE orebody, forming a down-dip extension of the Platreef, the latter occurring up-dip to the Flatreef (Grobler et al. 2019). The Flatreef was intersected by Ivanplats (Pty) Ltd during a deep drilling campaign in 2007. Its stratigraphy is less disturbed and less contaminated than that of the Platreef as the Flatreef does not occur in direct contact with country rocks but commonly overlies thick ultramafic units correlated with the Lower Zone and Lower Critical Zone (Grobler et al. 2019). Beukes et al. (2021) and Mayer et al. (2021) reported the first in-situ Sr isotopic data of plagioclase in profiles of the Flatreef as intersected on the farms Macalacaskop and Turfspruit, respectively. Their data are consistent with the Flatreef being a correlate of the Upper Critical Zone – Main Zone transition, as proposed by Grobler et al. (2019). Recent S isotope studies on the Flatreef have shown that the $\delta^{34}S$ values of the main mineralized interval overlap with that of the Merensky Reef in the remainder of the BC (Keir-Sage et al. 2021; Keet et al. 2021). Relatively high $\delta^{34}S$ values in the lower part of the Flatreef were attributed to crustal assimilation of footwall lithologies. Abernethy (2020), however, reported ε_{Ndi} values for the Flatreef ranging between -7.2 and -9.2, which are lower than those of the Upper Critical Zone in the Western Bushveld Complex (Maier et al. 2000).

Neodymium isotope ratios are not strongly influenced by syn- or post-magmatic alteration, because Sm-Nd are relatively less mobile in fluids and have comparable geochemical

behaviour (Rollinson, 1993). The complementary Rb-Sr and Sm-Nd isotope systems can be effective tracers of crustal contamination. Compared to Rb-Sr studies, few Nd isotopic studies have been conducted on Bushveld rocks, restricted to the western limb (Maier et al. 2000; Prevec et al. 2005), eastern limb (Raines 2014; Boudreau et al. 2022) and northern limb (Pronost et al. 2008; Roelofse & Ashwal 2012; Mwenze 2019; Scoon et al. 2020; Abernethy 2020). In this contribution we present whole-rock Nd-isotopic data on 14 samples across the Flatreef as intersected by drillhole UMT-393 on the farm Macalacaskop. The aim is to further assess the putative correlation between the Flatreef and the Upper Critical Zone (inclusive of the Merensky Reef) as known from the rest of the Bushveld Complex.

6.3 The Rustenburg Layered Suite of the northern limb

The BC was emplaced into Transvaal Supergroup sedimentary rocks at ca. 2.055 Ga (Zeh et al. 2015; Scoates et al. 2021) and is formally divided into three plutonic igneous suites, *viz*. the Rashoop Granophyre Suite, the Lebowa Granite Suite and the mafic-ultramafic Rustenburg Layered Suite (SACS – South African Committee on Stratigraphy 1980) (Fig. 6.1a).

The RLS crops out in four limbs, *viz.* the eastern, western, far western and northern limbs and is generally subdivided into 5 stratigraphic zones: the Upper Zone, Main Zone, Critical Zone, Lower Zone and Marginal Zone (Cawthorn, 2015). The northern limb extends for about 110 km from the Zebediela Fault south of Mokopane to the Melinda Fault in the north (Kinnaird et al. 2005) (Fig. 6.1b).

The stratigraphy of the RLS in the northern limb has been documented by Kinnaird et al. (2005), Ashwal et al. (2005), Yudovskaya et al. (2013), Grobler et al. (2019), Maier et al. (2021a.) and many others, and will therefore only be briefly summarized here.

6.3.1 Marginal Zone (MZN)

The MZN is located at the base of the RLS and comprises of noritic to doleritic rocks with thicknesses ranging between centimetres to tens of meters (van der Merwe 1976). Rocks forming the lowermost parts of the Platreef were previously incorrectly identified as belonging to the LZ (Maier et al. 2021a).

6.3.2 Lower Zone (LZ)

On the farm Turfspruit the LZ is thicker than 700 m and its lithologies comprise mainly pyroxenite, dunite and harzburgite (Grobler et al. 2019), whereas on the farm Grasvally it is up to 1500 m thick comprising of harzburgite, pyroxenite and chromitite layers (Hulbert and von Gruenewaldt 1982). The presence of these chromitite layers constitute major differences to the LZ in the rest of the BC.

6.3.3 Critical Zone (CZ)

In the eastern and western limbs of the BC, the CZ is subdivided into 2 zones, the Lower Critical Zone (LCZ) and Upper Critical Zone (UCZ). The LCZ consists predominantly of pyroxenite with minor olivine-bearing units and chromitite layers (Cawthorn, 2015). The LCZ was initially believed to be absent from the northern limb (McDonald and Holwell 2011). However, packages of thick ultramafic rocks discovered below the Platreef have subsequently been correlated with the LZ and LCZ (Yudovskaya et al. 2013; Grobler et al. 2019). The Platreef is located at a similar stratigraphic position as the UCZ in the remainder of the BC i.e. occurring below the Main Zone.

6.3.3.1 Platreef

The term 'Platreef' was coined by van der Merwe (1976) in keeping with the term 'Platinum Horizon', used by Wagner (1929), to describe the PGE mineralized basal part of the RLS occurring along the base of much of the northern limb. The Platreef mainly consists of pyroxenite, gabbronorite, norite, peridotite, serpentinite and a variety of hybrid lithological units, termed parapyroxenite, which formed as a result of significant country rock interaction (McDonald and Holwell 2011). Kinnaird and McDonald (2005) defined the Platreef as Ni-Cu-PGE enriched mafic units positioned between underlying Transvaal Supergroup metasediments or Archaean basement granite and overlying Main Zone gabbronorite of the northern limb. However, Maier et al. (2021a) identified various problems with this definition as well as definitions suggested by other workers (Gain and Mostert 1982; Maier et al. 2008). The authors proposed the use of the term 'Platreef Unit' (Scoon et al. 2020) and defined it as "… a complex sequence composed of coalescing magmatic units, some of which representing sills, with enclosed metasedimentary inlayers that represents a contaminated analogue of the chromite-bearing Upper Critical Zone of the western and eastern Bushveld and is overlain by chromite-free Main Zone rocks". The term "Platreef" is suggested to be used for the irregularly PGE-mineralized parts or ore body.

The Platreef is generally divided into northern, central and southern sectors on the basis of varying footwall compositions (Merensky 1925; Kinnaird et al. 2005). The southern sector extends from the farms Townlands to Tweefontein where footwall lithologies include shale, banded ironstone, calc-silicate rocks, mudstone and siltstone of the Duitschland Formation. The farms Zwartfontein, Sandsloot, Vaalkop and Tweefontein comprise the central sector and are characterised mainly by dolomitic footwall rocks of the Malmani Subgroup. The northern and far northern sectors extend from Overysel to the Waterberg project and are underlain by granite gneiss. (Kinnaird and Nex 2015). Several large xenoliths and rafts of country rock (up to 1.5 km long and 100 m thick) are present in the Platreef (Kinnaird et al. 2005) (Fig. 6.2).

These xenoliths generally have compositions similar to those of the immediate footwall country rocks (Holwell et al. 2007). Where xenolith compositions differ to that of the underlying footwall, it has been suggested that they were transported northwards during emplacement (Holwell et al. 2007).

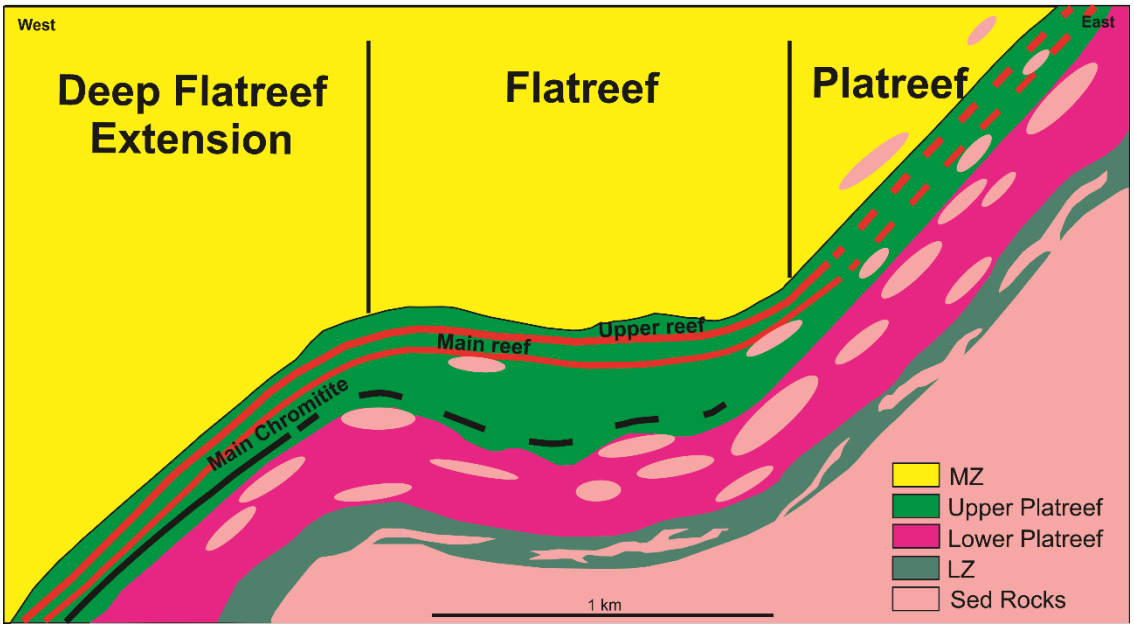

Figure 6.2 Schematic representation of the association between Platreef, Flatreef and the deep Flatreef extension at Turfspruit. Large sedimentary xenoliths are metamorphosed and assimilated by intruding Bushveld magma. Modified after Grobler et al. (2019).

Relative to the sulfide-poor mineralization of the Merensky Reef and UG-2, the Platreef is thicker and more sulfide-rich (Yudovskaya and Kinnaird 2010). This has stirred debate about the correlation of the Platreef with the UCZ in the remainder of the BC. Some studies (van der Merwe 1976; Kruger 2005) proposed that the interaction of Main Zone magmas with the country rock resulted in the formation of the Platreef along the footwall contact. However, other studies, such as that of White (1994), suggested that the Platreef may be correlated with the UCZ. New data on the Platreef, including work conducted on the recently discovered Flatreef, support the stratigraphic equivalence between the Platreef / Flatreef and the Upper Critical Zone inclusive of the Merensky Reef (Grobler et al. 2019; Beukes et al. 2021; Keet et al. 2021; Keir-Sage et al. 2021; Maier et al. 2021b; Mayer et al. 2021).

6.3.3.2 Flatreef

The Flatreef is defined as the down-dip extension of the Platreef where laterally continuous, sub-horizontal, PGE mineralized magmatic cyclic units are developed beneath the base of the Main Zone of the northern limb (Grobler et al. 2019). The Flatreef magmatic stratigraphy

underlies the farms Turfspruit and Macalacaskop north of Mokopane and is less contaminated and disturbed relative to the shallow Platreef up-dip (Grobler et al. 2019).

Grobler et al. (2019) sub-divided the Flatreef into different stratigraphic units, namely, the hangingwall unit (HW2 and HW1, which represents the transition zone between the Flatreef and Main Zone), the Bastard Reef, Middling unit, Merensky Reef and the Footwall Cyclic Unit (FCU). In the present work, the mineralized Merensky Reef and Bastard Reef of the Flatreef will be referred to as the Main Reef and Upper Reef, respectively, in keeping with Yudovskaya et al. (2017). The HW2 unit is the topmost unit of the Flatreef, which consists of mottled anorthosite with an average thickness of 4.2 m. The unit hosts sporadic ultramafic autoliths. The HW1 unit consists of mela- and leucogabbronorite cycles less than 20 m thick. In some drillhole intersections weakly mineralized interlayered pyroxenite, norite, mottled anorthosite and gabbro are present in the hangingwall unit. The Upper Reef, which is correlated to the Bastard Reef in the western and eastern limbs of the BC, is a pyroxenite between 5 and 10 m thick, with mineralization generally associated with its poorly developed bottom chromitite stringer. Below the Upper Reef is a pyroxenite-norite-anorthosite cyclic unit or feldspathic orthopyroxenite which forms the Middling unit (Md), varying in thickness from a few meters up to 100 m. This unit overlies the Main Reef, a mineralized mafic-ultramafic unit, subdivided into an upper- (M2) and lower portion (M1), which is correlated to the Merensky Reef. The M2 consists of sulfide-rich orthopyroxenite approximately 2 to 10 m thick, bound by an irregular top-, and a more continuous basal chromitite stringer. It is underlain by the M1, which consists of pegmatoidal orthopyroxenite (M1U) and/or pegmatoidal harzburgite (M1L). The FCU underlies the Main Reef and differs along strike in the study area. It consists dominantly of pyroxenite-norite-anorthosite cyclic units. The presence of country rock xenoliths is common towards the bottom of the Flatreef in close proximity to the floor rocks of the Transvaal Supergroup.

6.3.4 Main Zone (MZ)

The MZ in the northern limb has a maximum thickness of 2200 m and consists mainly of gabbronorite and norite (van der Merwe 1976). A prominent ultramafic marker layer occurring towards the top of the Main Zone in the Western Bushveld Complex (WBC) and Eastern Bushveld Complex (EBC), termed the Pyroxenite Marker, is poorly developed or absent in the northern lobe (Ashwal et al. 2005; Cawthorn 2020). The occurrence of finger-like MZ gabbronorite intrusions into the Platreef at Zwartfontein South pit indicates that emplacement of the MZ postdates formation of the Platreef (Holwell and Jordaan 2006).

6.3.5 Upper Zone (UZ)

In the northern limb the UZ is ~1100 m-thick, consisting of gabbro, magnetite gabbro, anorthosite, magnetitite and olivine diorite (van der Merwe 1976). A total of 32 magnetitite layers were identified in the UZ from the BV-1 drill core (Ashwal et al. 2005). The Main Magnetite Layer occurring near the base of the UZ represents the largest vanadium resource on Earth (Cawthorn and Molyneux 1986).

6.4 Location of samples analysed

Samples of this study were derived from drill core UMT-393 on the farm Macalacaskop (24.122856°S 28.975577°E), and include samples from the HW, Upper Reef, Md unit, Main Reef (M2 and M1) and FCU (Fig. 6.3). Borehole UMT-393 is 1163.50 m deep, and intersected 742.63 m of MZ gabbronorite followed by the Flatreef. At Macalacaskop, the footwall consists of quartzite and hornfelsed shale of the Timeball Hill Formation, whereas on the adjacent farm, Turfspruit, the footwall consists of sulfidic shale and limestone of the Duitschland Formation. In the Platreef south of Sandsloot, Transvaal Supergroup metasediments separate the Platreef from the underlying LZ (Yudovskaya et al. 2017). In the UMT-393 intersection at Macalacaskop, the FCU is directly underlain by LZ lithologies (Fig. 6.4). Here, the FCU consists of interlayered pyroxenite-norite-anorthosite with a total thickness of approximately 98 m. The distribution of base metal sulfides (BMS) in this unit is irregular. Contacts between the interlayered lithologies range from sharp, to undulating to gradational. Minor hybrid lithological layers are observed in particularly poorly developed cyclic units towards the base of the FCU. Three samples from the uppermost 27 m of the FCU were analysed as part of the present study. These samples consist of medium-grained feldspathic pyroxenite and norite.

The overlying Main Reef, from which 6 samples were analysed, has a total thickness of about 74 m. The basal portion of the Main Reef (M1L) is dominated by harzburgite and is characterised by intensive serpentinization. A thin chromitite stringer is present at a depth of 934 m, close to the basal contact with the underlying FCU. In the M1L, disseminated sulfides and chromite are commonly encountered. The M1U is about 5 m thick and consists mainly of mineralized, medium-grained orthopyroxenite. A poorly-developed chromitite stringer is observed near the top contact with the overlying unit at a depth of 928.39 m. The M2 which is the upper portion of the Main Reef consists of mineralized orthopyroxenite and feldspathic pyroxenite, commonly medium-grained with pegmatoidal patches. The M2 exhibits the highest total Pt + Pd concentrations with a maximum of 5 ppm (Beukes et al. 2021).

The Md unit is located above the Main Reef and consists of feldspathic pyroxenite containing less BMS than the adjacent units. The Upper Reef, on the contrary, consists of sulfide-rich feldspathic pyroxenite. It is characterised by an increase in PGE concentrations associated

with a basal chromitite stringer present at a depth of 849 m. The hangingwall unit (HW1 and HW2), which is the uppermost unit of the Flatreef, hosts lithologies that are somewhat similar to those of the FCU, namely, interlayered pyroxenite-norite-anorthosite. Keet et al. (2021) suggested that the hanging wall lithologies may initially have been continuous with the footwall lithologies and were separated by the intrusion of different pulses of the remainder of the Flatreef. The hanging wall, however, contains little to no hybrid lithologies.

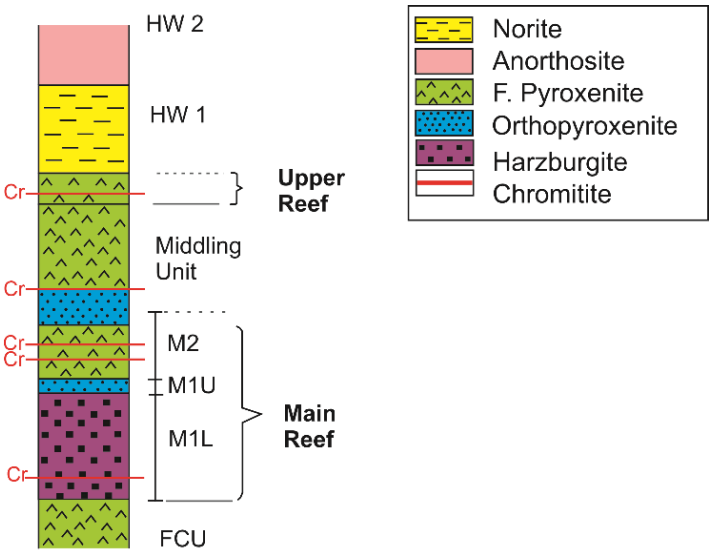

Figure 6.3 Simplified stratigraphic column of the Flatreef in borehole UMT-393, Macalacaskop. Modified after Beukes et al. (2021). Cr = chromitite stringer

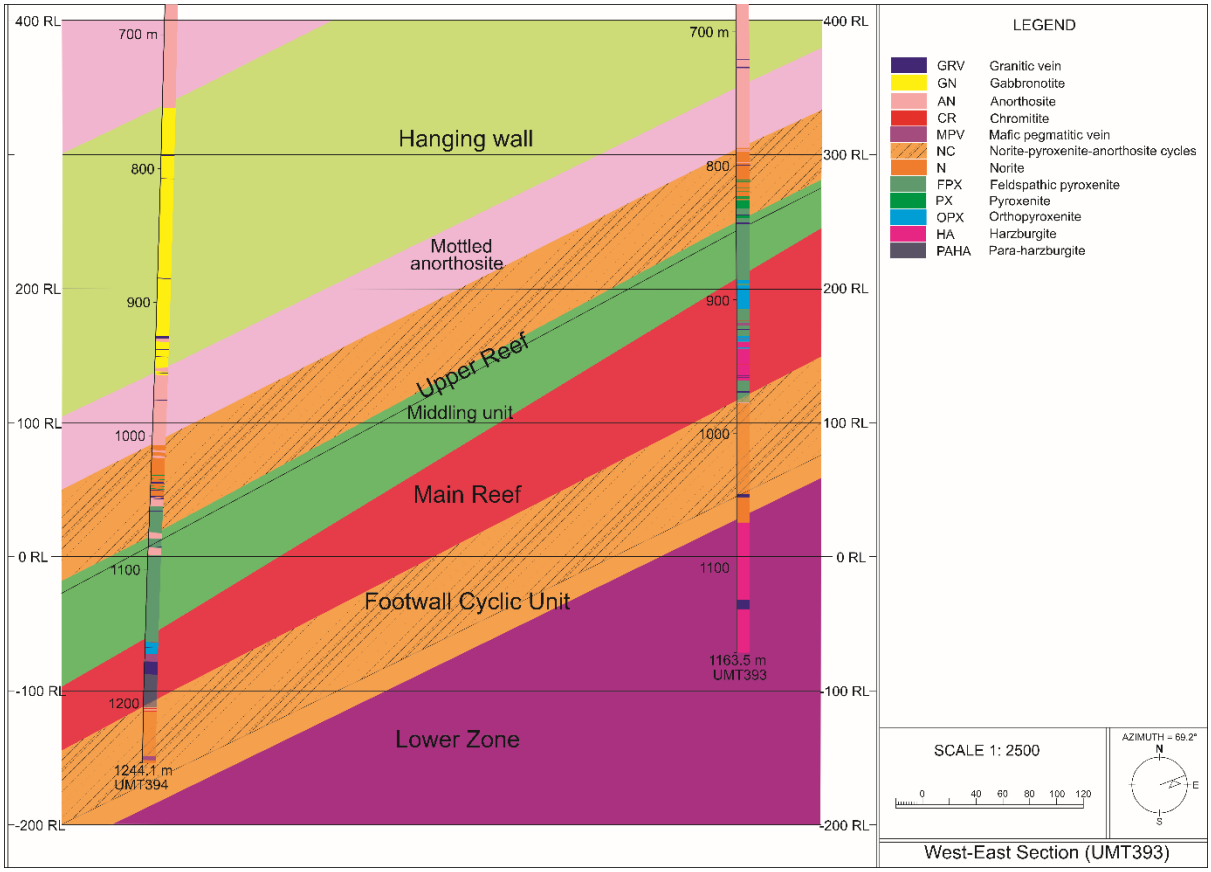

Figure 6.4 Dip section showing the various stratigraphic units of the Flatreef overlying LZ as intersected by borehole UMT-393. Modified after Keet et al. (2021)

6.5 Analytical methods

Powders of the samples were prepared by crushing and milling using a carbon steel jaw-crusher and swing mill, respectively, at the Department of Geology, University of the Free State. Trace element concentrations were determined at the Earth Lab of the University of the Witwatersrand on a Thermo Scientific iCAP RQ Inductively Coupled Plasma Mass Spectrometer (ICP-MS). The samples (50 mg) were weighed and digested in a mixture of HF-HNO_3 either via a microwave digester or using the open beaker/hotplate method depending on sample digestibility. The digested samples were subsequently diluted to 50 ml with 5 % HNO_3 containing Re and Rh (100 ppb) and In and Bi (50 ppb) as internal standards, the concentrations of which were monitored throughout analysis. The certified reference materials BCR-2 and BHVO-2 (Raczek et al. 2001) were analysed alongside the samples.

For Sm-Nd isotopic analysis, the samples were prepared at the Wits Isotope Geoscience Laboratory (WIGL) of the University of the Witwatersrand. Approximately 300 mg of sample powder was spiked with ^{149}Sm – ^{150}Nd enriched tracer and dissolved in an HF-HNO_3 mixture. Ion-exchange chemistry entailed a two-stage separation. Firstly, the bulk LREE were

separated from the matrix using PFA columns with a 2 ml resin bed of BioRad AG 50W-X8, 200-400 mesh. After resin equilibration, the samples were loaded into the column in 1 ml 1.5M HCl. The matrix was eluted in 1.5M HCl, whereas the LREE were eluted adding 6M HCl. Subsequently, Nd and Sm were separated on PFA columns using 1 ml LNSpec resin bed as cation exchange medium, and the samples were loaded into the column in 0.3ml 0.2M HCl.

Isotopic measurements were performed on a low resolution mode on a Nu Instruments Plasma II MC-ICP-MS (Nu Instrument, Wrexham) housed at the Analytical Facility of the University of Johannesburg. This MC-ICPMS instrument is equipped with 16 Faraday detectors and 5 ion counters. At the start of each measurement session, the instrument was optimised for sensitivity and stability. Samples and standards were introduced in a 2% HNO_3 solution using wet plasma, with a self-aspirating 200 µl/min Glass Expansion MicroMist U-series nebuliser. The nebuliser was coupled with a Peltier cooled quartz Glass Expansion Twister Spray Chamber, at 7°C. An intensity of 1V was generally obtained for ^{146}Nd on a 500ppb JNdi-1 standard solution. Nd analyses consisted of one block of 60 cycles, each with a 10-second integration time, and Sm analyses of one block of 20 cycles with an integration time of 10 seconds each. Using these parameters, an internal precision of < ±0.001% (1SE) on fractionation-corrected $^{143}Nd/^{144}Nd$ ratios were obtained.

Backgrounds for all extracts were measured at a magnet offset of half a mass unit away from the measurement position for 30 seconds directly before commencement of the measurement and subtracted from the signal. Automatic peak centring was performed prior to each measurement. Washout between samples was carried out with a 2% HNO_3 solution, monitoring the signals on mass 150 for Nd (the spike isotope), and mass 149 for Sm extracts to decrease back to background, which was usually achieved in less than 5 minutes. A full cycle of zero measurements, sample analysis, and washout, was completed in about 15 minutes for Nd measurements.

Data reduction was performed offline using a customized Microsoft Excel spreadsheet. Instrumental mass bias was determined based on the $^{146}Nd/^{145}Nd$ values of the spiked Nd extract, using $^{146}Nd/^{145}Nd=2.0719425$, which is equivalent to $^{146}Nd/^{144}Nd=0.7219$ (Vance and Thirlwall, 2002). This was used to calculate a mass bias exponent according to the exponential law. Interference corrections and spike subtractions were then performed to obtain $^{143}Nd/^{144}Nd$ for the sample. Nd concentrations were determined from the corrected mixture $^{150}Nd/^{144}Nd$ ratio. The Sm mass bias exponent was calculated based on the $^{152}Sm/^{147}Sm$ ratio (using the true value of 1.78307) of the spiked Sm extract, to enable the Sm concentration to be calculated from the corrected mixture $^{149}Sm/^{147}Sm$ ratio.

Analysis of the JNdi standard produced a running average of $^{143}Nd/^{144}Nd$ = 0.512110 ± 0.000018 (n=36) compared to the accepted values published by Tanaka et al. (2000), $^{143}Nd/^{144}Nd$ = 0.512115 ± 0.000007. Initial Nd isotopic ratios ($^{143}Nd/^{144}Nd_i$), were calculated for an age of 2.06 Ga, using a decay constant of 6.54 x $10^{-12}y^{-1}$ (Lugmair and Marti 1978). The ε_{Nd}^{i} values were calculated using the present-day composition of CHUR, $^{143}Nd/^{144}Nd$ = 0.512630 and $^{147}Sm/^{144}Nd$ = 0.1960 (Bouvier et al. 2008).

6.6 Results

Whole-rock trace elements are reported in Table C1 (Appendix C), with selected data presented in Table 6.1. Chondrite-normalized rare earth element patterns of the Flatreef lithologies are similar to those of the UCZ of the Western Bushveld Complex (WBC) as presented by Maier et al. (2013) (Fig. 6.5). These units appear to be slightly more enriched in LREE compared to HREE. The highest La_N is observed for the HW norite. The REE patterns of the feldspathic pyroxenite of the Flatreef are generally similar with the exception of the HW and M2 sample (the latter hosting a chromitite stringer) where negative Eu anomalies are observed. A similar trend is observed for M1L harzburgite. The Eu anomaly (Eu/Eu*) values for these samples are 0.64, 0.62 and 0.76, respectively (Table 6.1). The remainder of the analysed samples display varyingly positive Eu/Eu* values with an average of 1.37 with strong positive Eu/Eu* values observed for HW norite (1.41) and FCU norite (2.65). The Flatreef samples show a lower LREE enrichment (Ce/Sm_N = 1.89) relative to that of the UCZ of the WBC (Ce/Sm_N= 2.89, Maier et al. 2013). The Tb/Yb_N has an average value of 1 indicating almost no fractionation of HREE.

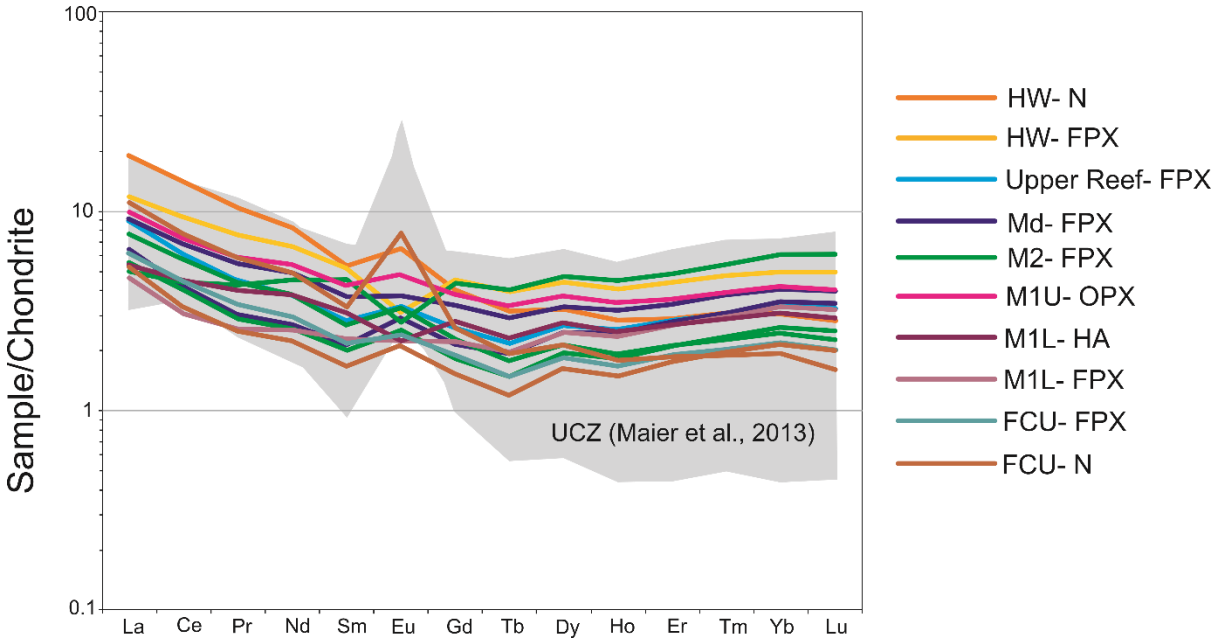

Figure 6.5 Chondrite-normalized REE plot of the Flatreef samples analysed in this study. The area in grey represents data of the UCZ (excluding UG-2) as reported by Maier et al. (2013). Normalizing values are taken from Anders and Grevesse (1989). HW, UR, Md, $M1_U$, $M1_L$, and FCU indicate hanging wall, Upper Reef, Middling unit, M1 Upper, M1 Lower and the Footwall Cyclic unit, respectively. N, FPX, OPX and HA indicate norite, feldspathic pyroxenite, orthopyroxenite and harzburgite, respectively.

Table 6-1 Selected trace elements and REE (ppm).

Sample	Depth (m)	Rock Type	Strat	V	Cr	Ni	Rb	Sr	Y	Zr	Th	La	Ce	Yb	Eu/Eu*	$(Ce/Sm)_N$	$(Tb/Yb)_N$
JDJ076	802.43	N	HW	84	967	227	6	196	4	17	0.78	4.42	8.46	0.50	1.41	2.64	1.03
JDJ086	824.42	FPX	HW	134	1956	447	6	53	6	18	0.72	2.78	5.64	0.81	0.64	1.82	0.80
JDJ097	848.63	FPX	UR	127	4182	1905	3	59	4	6	0.16	2.12	3.66	0.55	1.22	2.15	0.65
JDJ107	877.07	FPX	Md	124	2091	702	2	58	5	5	0.10	2.14	4.12	0.66	1.05	1.83	0.72
JDJ109A	884.50	FPX	Md	114	2001	2843	7	56	4	5	0.08	1.51	2.54	0.57	1.37	1.98	0.55
JDJ112B	888.98	FPX	M2	103	2310	1049	6	90	3	8	0.32	1.81	3.44	0.40	1.33	2.14	0.72
JDJ119	912.27	FPX	M2	188	3633	1160	2	24	6	6	0.06	1.17	2.65	0.98	0.62	0.97	0.66
JDJ120	915.35	FPX	M2	109	3676	1629	5	78	3	4	0.08	1.29	2.42	0.43	1.33	2.00	0.57
JDJ126	928.39	OPX	$M1_U$	122	3039	585	4	85	5	7	0.10	2.33	4.40	0.68	1.20	1.73	0.79
JDJ133	942.27	HA	$M1_L$	95	3611	2304	5	26	4	7	0.14	1.27	2.72	0.50	0.76	1.45	0.75
JDJ141A	960.06	FPX	$M1_L$	98	3611	767	2	46	3	5	0.05	1.08	1.84	0.54	0.99	1.34	0.59
JDJ152	981.20	FPX	FCU	112	2239	490	2	83	3	6	0.20	1.44	2.67	0.36	1.17	2.03	0.68
JDJ154A	983.20	N	FCU	115	2271	475	2	73	2	5	0.12	1.23	2.00	0.34	1.32	2.00	0.56
JDJ163	1003.34	N	FCU	107	854	133	3	248	3	9	0.25	2.58	4.64	0.31	2.65	2.32	1.00

*N, FPX, OPX and HA indicate norite, feldspathic pyroxenite, orthopyroxenite and harzburgite, respectively.

*HW, UR, Md, $M1_U$, $M1_L$, and FCU indicate hanging wall, Upper Reef, Middling unit, M1 Upper, M1 Lower and the Footwall Cyclic unit, respectively.

Nd- and Sr-isotope data are presented in Table 6.2 and Fig. 6.6. The ε_{Nd}^{i} and $^{87}Sr/^{86}Sr_{i}$ values were calculated for an age of 2.06 Ga. The ε_{Nd}^{i} values of the Flatreef units vary between -7.6 and -5.2. The ε_{Nd}^{i} broadly decreases with increase in stratigraphic height (Fig. 6.6a). The lowermost analysed sample of the FCU has an ε_{Nd}^{i} value of -6.3 followed by -5.4 towards the top. The lower Main Reef has slightly lower ε_{Nd}^{i} with values ranging between -7.3 and -6.7, whereas the upper Main Reef (M2) has ε_{Nd}^{i} of between -7.0 and -6.0. The lowest value is located in the Md unit and overlying Upper Reef feldspathic pyroxenite, exhibiting ε_{Nd}^{i} values of -7.6 and -7.5, respectively. The highest value was recorded for the HW norite with an ε_{Nd}^{i} value of -5.2. Variations in the average $^{87}Sr/^{86}Sr_{i}$ ratio for analysed samples across the Flatreef are presented in Fig. 6.6b. A general increase in $^{87}Sr/^{86}Sr_{i}$ with increase in stratigraphic height is observed, with a pronounced increase in the upper portion of the Main Reef. The Nd and Sr isotope compositions are therefore inversely proportional as shown by the weak negative correlation between ε_{Nd}^{i} and $^{87}Sr/^{86}Sr_{i}$ in Fig. 6.7a. These data overlap with UCZ anorthosite/norite/pyroxenite and MZ gabbronorite data of the WBC (Fig. 6.7a). Similarly, Th/La ratios plotted against $^{87}Sr/^{86}Sr_{i}$ and ε_{Nd}^{i}, respectively (Figs. 6.7b and c) overlap with WBC data, displaying a weak negative correlation in Fig. 6.7b, and no clear correlation is distinguishable in Fig. 6.7c.

Table 6-2 ε_{Ndi} and $^{87}Sr/^{86}Sr_i$ data calculated for an age of 2.06 Ga. Sr isotope values are averages of $^{87}Sr/^{86}Sr_i$ reported by Beukes et al. (2021).

Sample	Depth (m)	Rock type	Unit	Nd (ppm)	Sm (ppm)	$^{147}Sm/^{144}Nd$	$^{143}Nd/^{144}Nd$ (Measured)	ε_{Ndi}	2SE	$^{87}Sr/^{86}Sr_i$	2σ
JDJ076	802.43	N	HW	4.07	0.84	0.1241	0.511388	-5.24	0.55	0.70783	0.00012
JDJ086	824.42	FPX	HW	3.23	0.81	0.1521	0.511717	-6.21	0.53	0.70753	0.00038
JDJ097	848.63	FPX	UR	1.89	0.47	0.1488	0.511605	-7.53	0.54	0.70808	0.00059
JDJ107	877.07	FPX	Md	2.33	0.58	0.1497	0.511631	-7.26	0.53	0.70755	0.00102
JDJ109A	884.50	FPX	Md	1.36	0.36	0.1589	0.511740	-7.58	0.58	0.70758	0.00029
JDJ112B	888.98	FPX	M2	1.84	0.43	0.1411	0.511564	-6.32	0.54	0.70749	0.00038
JDJ119	912.27	FPX	M2	2.25	0.73	0.1954	0.512267	-6.96	0.55	0.70862	0.00007
JDJ120	915.35	FPX	M2	1.27	0.32	0.1526	0.511735	-6.00	0.61	0.70736	0.00018
JDJ126	928.39	OPX	$M1_U$	2.66	0.69	0.1567	0.511731	-7.18	0.52	0.70717	0.00009
JDJ133	942.27	HA	$M1_L$	1.95	0.52	0.1609	0.511815	-6.65	0.57	0.70708	0.00032
JDJ141A	960.06	FPX	$M1_L$	1.20	0.35	0.1765	0.511993	-7.30	0.62	0.70713	0.00038
JDJ152	981.20	FPX	FCU	1.54	0.37	0.1441	0.511653	-5.36	0.57	0.70661	0.00048
JDJ154A	983.20	N	FCU	1.14	0.28	0.1510	0.511736	-5.56	0.58	0.70650	0.00042
JDJ163	1003.34	N	FCU	2.46	0.54	0.1337	0.511466	-6.26	0.57	0.70646	0.00014

*N, FPX, OPX and HA indicate norite, feldspathic pyroxenite, orthopyroxenite and harzburgite, respectively.

*HW, UR, Md, $M1_U$, $M1_L$, and FCU indicate hanging wall, Upper Reef, Middling unit, M1 Upper, M1 Lower and the Footwall Cyclic unit, respectively.

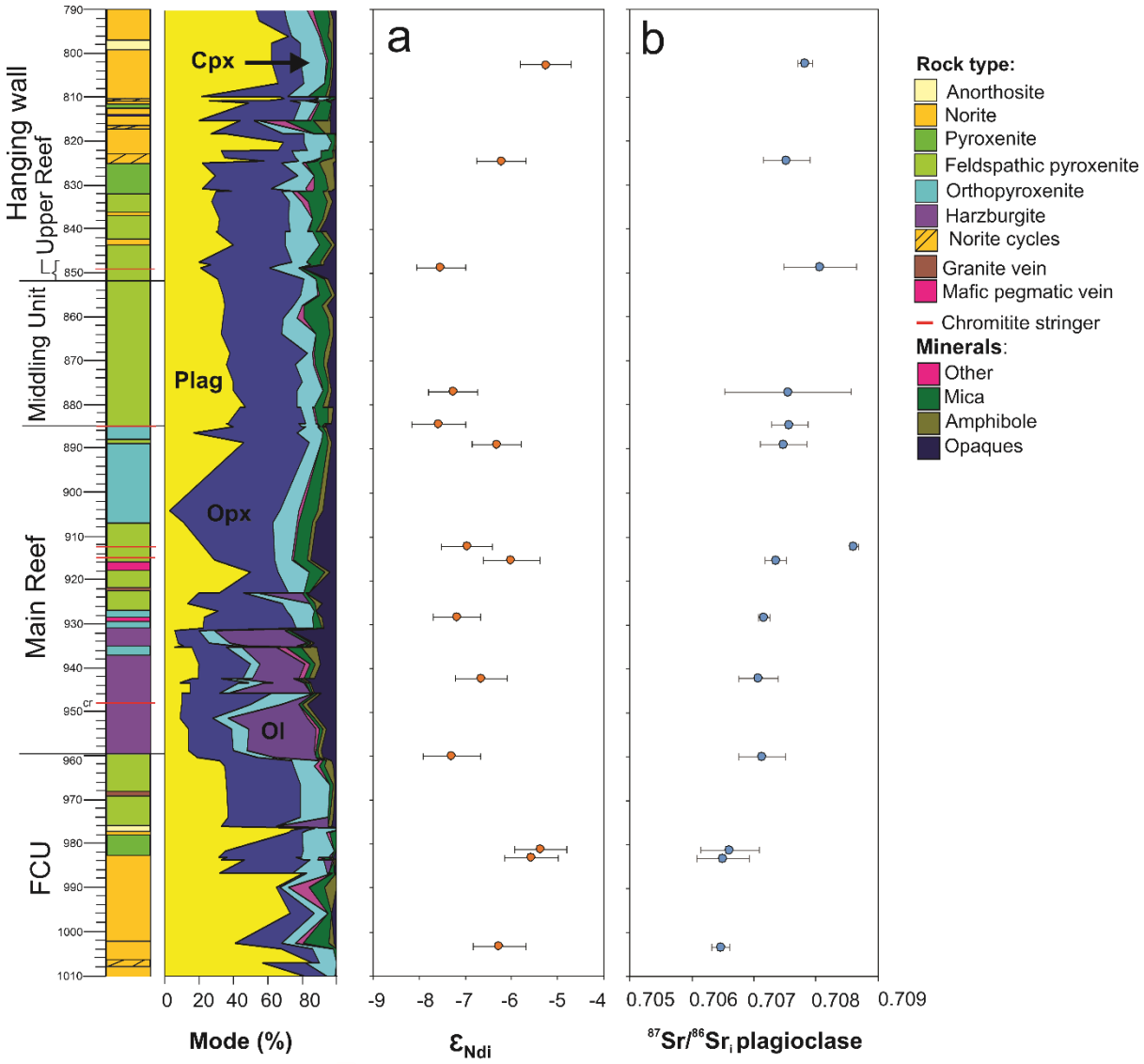

Figure 6.6 Variation in mineral modes, **a** ε_{Ndi} (2.06 Ga), and **b** $^{87}Sr/^{86}Sr_i$ (2.06 Ga) with increase in stratigraphic height across Flatreef stratigraphy as intersected by borehole UMT-393. Error bars represent 2SE and 2σ for ε_{Ndi} and $^{87}Sr/^{86}Sr_i$, respectively

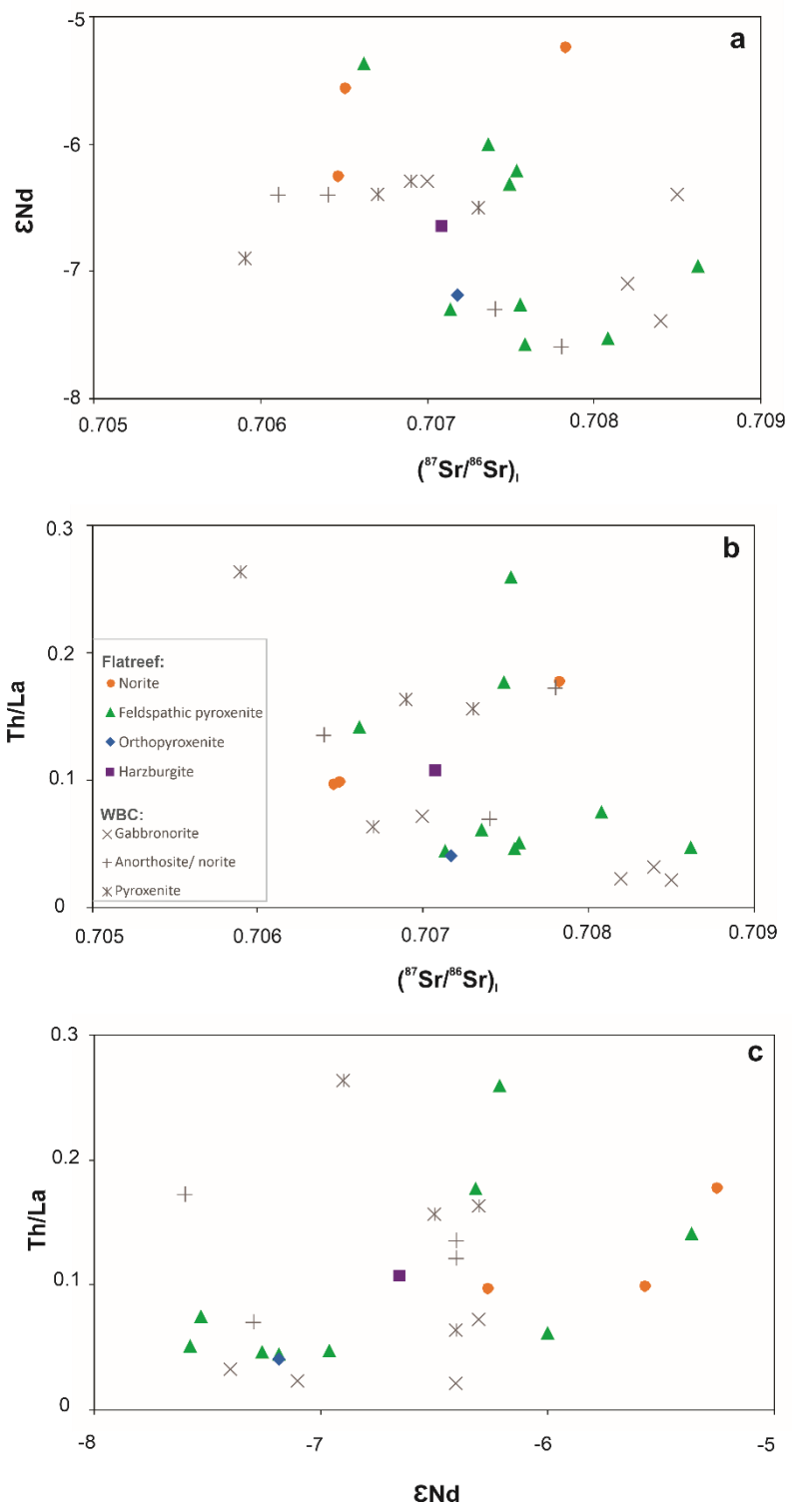

Figure 6.7 Binary variation diagrams of **a** ε_{Ndi} vs $^{87}Sr/^{86}Sr_i$, **b** Th/La vs $^{87}Sr/^{86}Sr_i$, and **c** Th/La vs ε_{Ndi} in Flatreef rocks. WBC data from Maier et al. (2000) are included for comparison (grey symbols). Epsilon Nd and initial Sr values calculated for an age of 2.06 Ga

6.7 Discussion

6.7.1 Comparison between Platreef/Flatreef and RLS of the remainder of the BC

Previous studies have shown a range of Nd isotopic values from across the BC (Fig 6.8). For the UCZ of the western limb, ε_{Ndi} values vary between -6.3 and -7.6, and for the MZ between -6.3 and -7.4 (Maier et al., 2000). The ε_{Ndi} values reported for the Merensky Reef interval at Winnaarshoek range from -8.5 to -4.5 (Raines 2014). Boudreau et al. (2022) analysed two MZ samples from the Apel anorthosite sequence in the eastern limb, an anorthosite and gabbronorite, having ε_{Ndi} of -8.3 and -6.3, respectively. Previous Sr and Nd isotopic work on the MZ of the northern limb showed ε_{Ndi} ranging between -8.6 and -6.6 and $^{87}Sr/^{86}Sr_i$ ranging between 0.708 and 0.715 (Roelofse and Ashwal 2012; Mwenze 2019; Abernethy 2020; Scoon et al. 2020).

The Platreef rocks display a wide variety of isotopic compositions (Fig. 6.8). Pronost et al. (2008) reported ε_{Ndi} values for Platreef rocks in the northern limb at the farms Sandsloot (where floor rock comprises dolomite from the Transvaal Supergroup) and Overysel (underlain by Archaean granite footwall rocks) ranging from -7.0 to -7.3 and -8.8 to -7.1, respectively. $^{87}Sr/^{86}Sr_i$ varies between 0.711 and 0.718 at Sandsloot, and 0.701 and 0.728 at Overysel. However, a broader variation in isotopic composition was reported by Mwenze (2019) for Sandsloot (ε_{Ndi} -22.9 to -2.9, $^{87}Sr/^{86}Sr_i$ 0.708 to 0.710), Overysel (ε_{Ndi} -10.8 to -4.9, $^{87}Sr/^{86}Sr_i$ 0.708 to 0.742) and Tweefontein, which is underlain by Transvaal Supergroup BIF and shale (ε_{Ndi} -14.3 to -5.1, $^{87}Sr/^{86}Sr_i$ 0.707 to 0.760). At Akanani (Zwartfontein farm adjacent to Sandsloot), where Platreef rocks are underlain by Transvaal dolomite floor rocks, ε_{Ndi} varies between -13.7 and 1.3, and $^{87}Sr/^{86}Sr_i$ between 0.709 and 0.712 (Scoon et al. 2020). Although ε_{Ndi} values reported in this study fall within the same range as that of the Platreef rocks (Fig. 6.8c), differences are observed in Nd-isotopic composition of the mineralized units. For example, the ε_{Ndi} values of the Main Mineralized Reef (MMR) at Akanani are distinctly lower (ε_{Ndi} average of -11.4) than those for the Main Reef of the present study (ε_{Ndi} average of -6.7). It is possible that the parental magma associated with the MMR was more severely contaminated with crust. Alternatively, it has been proposed that the MMR magma may be derived from metasomatised sub-continental lithospheric mantle (Scoon et al. 2020; Wasch et al. 2009).

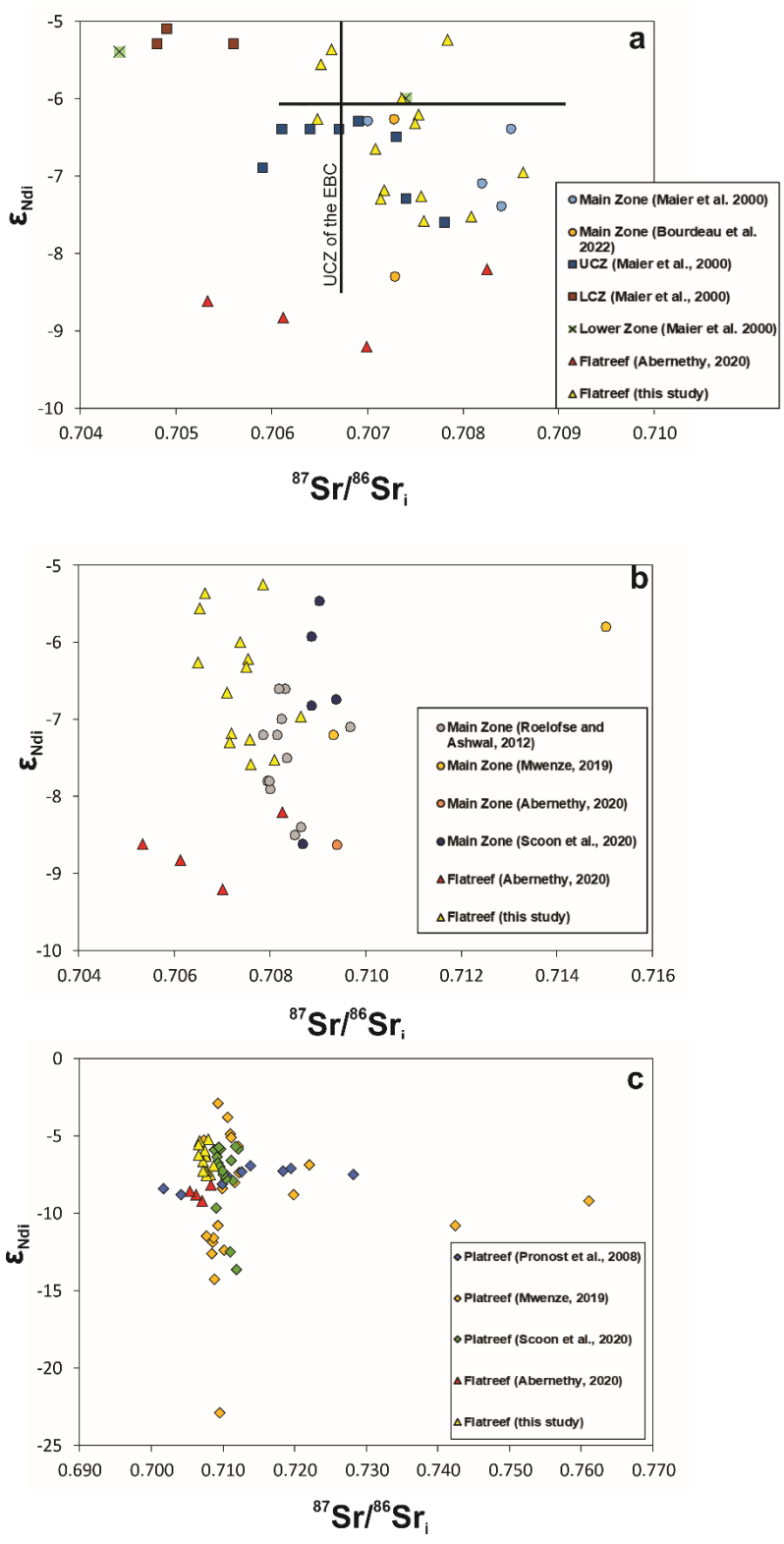

Figure 6.8 Plot of ε_{Ndi} vs $^{87}Sr/^{86}Sr_i$ for the **a** Flatreef (Abernethy 2020; this study), samples of the RLS of the western limb (Maier et al., 2000) and eastern limb (EBC, Lee and Butcher, 1990; Raines, 2014; Bourdeau et al., 2022) of the Bushveld Complex; **b** Flatreef samples of this study and adjacent farm, Turfspruit (Abernethy 2020) and Main Zone samples (Roelofse and Ashwal, 2012; Mwenze, 2019; Abernethy, 2020; Scoon et al., 2020) of the northern limb; **c** Flatreef samples (this study; Abernethy, 2020) and Platreef samples (Pronost et al., 2008; Mwenze, 2019; Scoon et al., 2020) of the northern limb.

Other Sr isotopic studies on the Platreef have returned $^{87}Sr/^{86}Sr_i$ values ranging from 0.711 to 0.723 and 0.705 to 0.715 at Overysel and Sandsloot respectively (Barton et al. 1986), and 0.710 to 0.711 at Turfspruit (Kruger 2005).

Beukes et al. (2021), Mayer et al. (2021) and the present study show that the Sr and Nd isotope compositions of the Flatreef rocks strongly overlap with that of the Merensky Reef and Bastard Reef in the remainder of the BC. Our findings show that ε_{Ndi} values across the Flatreef stratigraphy vary between -5.2 and -7.6, significantly overlapping with both the UCZ and MZ rocks of the eastern and western limbs of the BC (Raines 2014; Boudreau et al. 2022; Maier et al. 2000) (Fig. 6.8a). A recent study by Abernethy (2020) reported ε_{Ndi} values for the Flatreef on Turfspruit, ranging from -7.2 to -9.2. These values are significantly lower than what is recorded for the Flatreef in the current study as well as on the data from the UCZ and MZ (Maier et al. 2000; Raines 2014; Boudreau et al. 2022) in the remainder of the BC. The relatively low values of ε_{Ndi} from Turfspruit may indicate increased contamination; Abernethy proposed between 23% and 55% with higher estimates for the lower Flatreef. The contaminants used in the mixing models were footwall calcareous sediments (Abernethy, 2020), granite (Johannesburg Dome, Barton et al. 1999; banded gneiss from Overysel, Pronost et al. 2008; granite end member, Telus et al. 2012) and shale (data sourced from various literature; Hunter and Hamilton, 1978; Beukes et al. 1990; Jahn and Condie, 1995 and Li et al. 2010). Sr and Nd isotopes display inverse covariation, hence relative to $^{87}Sr/^{86}Sr_{i,}$ a weak inverse trend is observed when ε_{Ndi} is plotted against stratigraphic height (Fig. 6.6). The ε_{Ndi} decreases through the Main Reef, MD and Upper Reef. Beukes et al. (2021) and Mayer et al. (2021) showed an increase in Sr at the base of the main mineralized interval of the Flatreef from 0.707 to >0.709 at Macalacaskop and 0.706 to 0.709 at Turfspruit.

6.7.2 Sr-Nd isotopic constraints on the petrogenesis of the Flatreef

The identification of an isotopic shift at the base of the main mineralized interval of the Flatreef, similar to the isotope shift described for the EBC and WBC (Kruger 1994; Karykowski et al. 2017), is consistent with the suggestion of Grobler et al. (2019), that the Flatreef sequence is a correlate of the Merensky and Bastard Units in the remainder of the BC. Whole-rock $\delta^{34}S$ data across the Flatreef show that the Main Reef has a consistent near-mantle S isotopic signature similar to that of the Merensky Reef in the remainder of the BC, further supporting the contention that the Flatreef is a correlate of the UCZ-MZ transition interval (Keet et al. 2021; Keir-Sage et al. 2021). The Nd isotope data reported here are also consistent with these isotope findings.

Although the significantly more radiogenic Sr isotope composition of Platreef rocks may be attributed to local floor rock contamination, it is evident that the Nd isotopic composition of the Flatreef cannot be accounted for by the mixing of mantle-derived melt with Transvaal Supergroup rocks (Fig. 6.9). The Nd isotope data from this study overlap with that of the Rooiberg Group (Buchanan et al. 2004), Transvaal Supergroup sediments (Jahn and Condie 1995; Pronost et al. 2008; Abernethy 2020), Johannesburg Dome tonalite and granite (Barton et al. 1999), Ancient Gneiss Complex (Barton et al. 1980; Carlson et al. 1983), Archaean granite gneiss (Pronost et al. 2008) and Turfloop Batholith (Henderson et al. 2000). One of the mixing models presented in Figure 6.10 shows that in order to reproduce the observed Sr-Nd isotopic compositions for the Flatreef would necessitate a mantle-derived melt being contaminated with >>80% of Transvaal devolatilized carbonate footwall. Thermal and bulk-rock compositional constraints firmly exclude this as a possible petrogenetic model for the Flatreef.

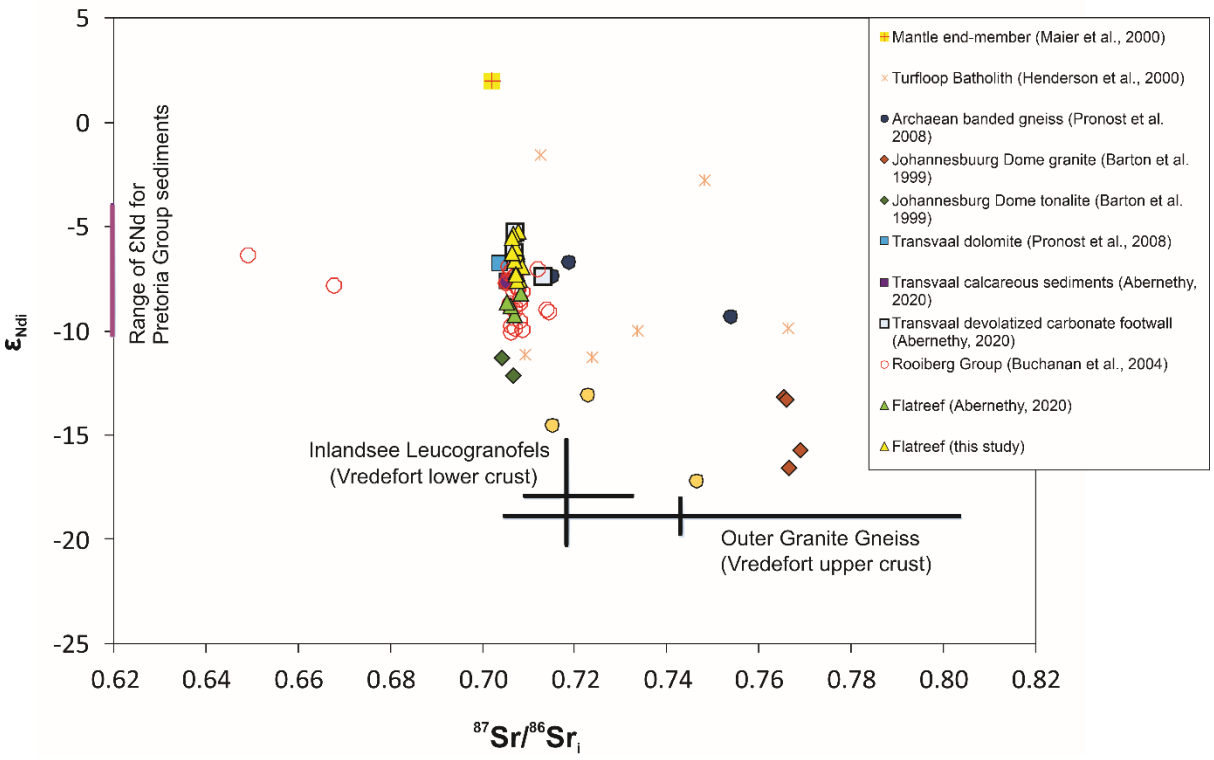

Figure 6.9 Plot of ε_{Ndi} vs $^{87}Sr/^{86}Sr_i$ calculated at 2.06 Ga of whole-rock data for the Transvaal Supergroup, Turfloop Batholith, Archaean granite gneiss, the Johannesburg Dome , the Rooiberg Group, the Vredefort Dome OGG and ILG, the Flatreef and a mantle melt end member (ε_{Ndi} =2, $^{87}Sr/^{86}Sr_i$= 0.702, Maier et al., 2000); modified after Roelofse and Ashwal (2012). It is clear that the isotopic composition of the Flatreef cannot be explained through the interaction of a mantle-derived melt and locally available contaminants as exposed along the base of the Platreef.

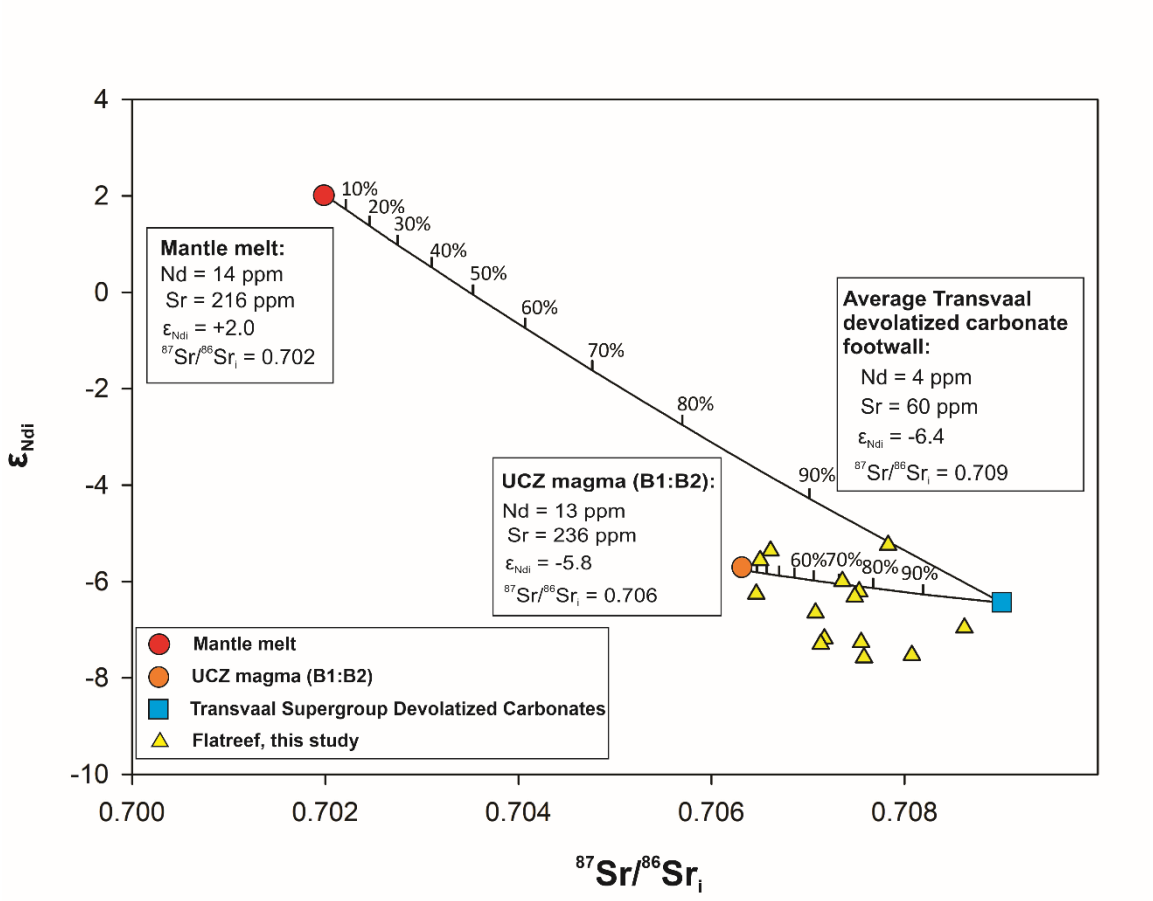

Figure 6.10 Isotopic mixing models for mixtures between mantle-derived melt (ε_{Ndi} =2.0, $^{87}Sr/^{86}Sr_i$=0.702, Maier at al. 2000; Nd =14 ppm, Sr =216 ppm, Roelofse and Ashwal 2012) and a 60:40 B1:B2 mixture (ε_{Ndi} =-5.8; $^{87}Sr/^{86}Sr_i$=0.706; Nd =13 ppm; Sr =236 ppm; Curl, 2001) respectively, and devolatized Transvaal Supergroup carbonates (ε_{Ndi} =-6.4; $^{87}Sr/^{86}Sr_i$=0.709; Nd =4 ppm; Sr =60 ppm; Abernethy, 2020).

Our preferred model to explain the Sr-Nd isotopic composition of the Flatreef is in keeping with Roelofse & Ashwal (2012), who showed that the isotopic composition of rocks of the RLS can be explained through the interaction of mantle-derived magma with upper and lower crustal lithologies derived from the Kaapvaal Craton within a sub-Bushveld staging chamber. As is clear from Figure 6.10, the Flatreef has Nd-isotopic compositions very similar to a 60:40 B1:B2 mixture proposed by Barnes and Maier (2002) to be parental to the Merensky Reef of the WBC, but the Flatreef exhibits consistently more radiogenic Sr-isotopic compositions compared to this mixture, with data points falling along a mixing array between a 60:40 B1:B2 mixture and Transvaal devolatilized carbonate footwall. We suggest that the Sr-isotopic composition of the Flatreef may have been modified by localised syn- to post-emplacement interaction between UCZ magma and dolomitic footwall rocks of the Transvaal Supergroup.

The HW and FCU lithologies have similar ε_{Ndi} values (average of -5.7), both being higher than that of the lithologies in the remainder of the Flatreef. This supports the proposal by Keet et

al. (2021), that the main mineralized Flatreef units intruded into the originally continuous package of the HW and FCU lithologies.

6.8 Conclusions

The ε_{Ndi} values determined in this study display significant overlap with UCZ-MZ data of the WBC and EBC. Our findings are consistent with recent isotope studies on the Flatreef which provide further support for the proposed correlation of the Flatreef stratigraphy with that of the uppermost UCZ, including the mineralized Merensky Reef and Bastard Reef (Grobler et al. 2019). The highest ε_{Ndi} values of the Flatreef are observed in the hanging wall and footwall units which could suggest that that these units were originally continuous but were subsequently separated by magma pulses of the mineralized units of the Flatreef. The Nd isotopic composition of the Flatreef cannot be accounted for by the interaction between mantle-derived magma and local contaminants occurring as footwall rocks along the eastern margin of the Northern Limb. Instead, the magma(s) that gave rise to the Flatreef were likely derived from a sub-Bushveld staging chamber in which mantle-derived melts interacted with lower and upper crustal rocks of the Kaapvaal Craton (cf. Roelofse & Ashwal 2012). However, the Flatreef exhibits Sr-isotopic compositions that are consistently more radiogenic than those expected for the mixture of magmas (60:40 B1:B2) that gave rise to the UCZ, a feature that may point to syn- to post-emplacement modification of the isotopic composition of the parental magma through interaction with locally available dolomitic rocks of the Transvaal Supergroup.

6.9 Acknowledgements

This study was supported by an nGAP grant (UID 119698) to J.J.K. The authors would like to thank Ivanplats for access to the samples analysed as part of this study, and Marlin Patchappa (EarthLab – University of the Witwatersrand) for geochemical analyses. Thorough reviews by Steve Prevec and an anonymous reviewer allowed us to significantly improve the manuscript.

6.10 References

Ashwal LD, Webb SJ, Knoper MW (2005) Magmatic stratigraphy in the Bushveld Northern Lobe: continuous geophysical and mineralogical data from the 2950m Bellevue drill core. S Afr J Geol 108, 199-232

Abernethy K (2020) Assimilation of Dolomite by Bushveld Magmas in the Flatreef; Implications for the Origin of Ni-Cu-PGE Mineralization and the Precambrian Atmosphere. PhD thesis, Cardiff University, Cardiff.

Anders E, Grevesse N (1989) Abundances of the elements: Meteoritic and solar. Geochimica et Cosmochimica Acta 53:197-214

Barnes S-J, Maier WD (2002) Platinum-group element distributions in the Rustenburg Layered Suite of the Bushveld Complex, South Africa. In: Cabri LJ (ed) The Geology, Geochemistry, Mineralogy and Mineral Beneficiation of Platinum-Group Elements. Canadian Institute of Mining, Metallurgy and Petroleum, Special Volume 54 pp 431-458

Barnes SJ, Maier WD, Curl EA (2010) Composition of the Marginal Rocks and Sills of the Rustenburg Layered Suite, Bushveld Complex, South Africa: Implications for the Formation of the Platinum-Group Element Deposits. Econ Geol, 105:1491-1511

Barton JM, Hunter DR, Jackson MPA, Wilson AC (1980) Rb-Sr age and source of the Bimodal Suite of the Ancient Gneiss Complex, Swaziland. Nature 283:756-758

Barton JM, Cawthorn RG, White J (1986) The role of contamination in the evolution of the Platreef of the Bushveld Complex. Econ Geol 81:1096-1104

Barton JM, Barton ES, Kröner A (1999) Age and isotopic evidence for the origin of the Archaean granitoid intrusives of the Johannesburg Dome, South Africa. J Afr Earth Sci 28:693-702

Beukes NJ, Klein C, Kaufman AJ, Hayes JM (1990) Carbonate Petrography, Kerogen Distribution, and Carbon and Oxygen Isotope Variations in an Early Proterozoic Transition from the Limestone to Iron-Formation Deposition, Transvaal Supergroup, South Africa. Econ Geol 85:663-690

Beukes JJ, Roelofse F, Gauert CDK, Grobler DF, Ueckermann H (2021) Strontium isotope variations in the Flatreef on Macalacaskop, northern limb, Bushveld Complex: implications for the source of platinum-group elements in the Merensky Reef. Mineralium Deposita 56:45-57

Bourdeau JE, Hayes B, Zhang SE, Logue A, Bybee GM (2021) Origin and significance of noritic blocks in layered anorthosites in the Bushveld Complex, South Africa. Contrib Mineral Petrol 177:1-26

Bouvier A, Vervoort JD, Patchett PJ (2008) The Lu-Hf and Sm-Nd isotopic composition of CHUR: Constraints from unequilibrated chondrites and implications for the bulk composition of terrestrial planets. Earth Planet Sci Lett 2073:48-57

Buchanan DL, Nolan J, Suddaby P, Rouse JE, Viljoen MJ, Davenport JWJ (1981) The genesis of sulfide mineralization in a portion the Potgietersrus Limb of the Bushveld Complex. Econ Geol 76:568–579

Buchanan DL, Rouse JE (1984) Role of contamination in the precipitation of sulphides in the Platreef of the Bushveld Complex. In: Buchanan DL, Jones MJ (eds) Sulphide Deposits in Mafic and Ultramafic Rocks. IMM, London, pp 141–146

Buchanan PC, Reimold WU, Koeberl C, Kruger FJ (2004). Rb-Sr and Sm-Nd isotopic compositions of the Rooiberg Group, South Africa: early Bushveld-related volcanism. Lithos 29: 373-388

Carlson RW, Hunter DR, Barker F (1983) Sm-Nd age and isotopic systematics of the bimodal suite, ancient gneiss complex, Swaziland. Nature 305:701-704

Cawthorn RG, Barton JM, Viljoen MJ (1985) Interaction of floor rocks with the Platreef on Overysel, Potgietersrus, Northern Transvaal. Econ Geol 80: 988-1006

Cawthorn RG, Molyneux TG (1986) Vanadiferous magnetite deposits of the Bushveld Complex. In: Anhaeusser CR, Maske S (eds) Mineral deposits of Southern Africa. Geol Soc S Afr Johannesburg 2:1251-1266

Cawthorn RG (2015) The Bushveld Complex, South Africa. In B. Charlier, O. Namur, R. Latypov and C. Tegner (eds.), Layered Intrusions, Springer Netherlands, pp. 517-587

Cawthorn RG (2020) Massive pyroxene compositional oscillations on a meter scale in the Pyroxenite Marker, northern limb, Bushveld Complex, South Africa. Lithos 356-357 105392

Finn CA, Bedrosian PA, Cole JC, Khoza TD, Webb SJ (2015) Mapping the 3-D extent of the Northern Lobe of the Bushveld layered mafic intrusion from geophysical data. Precambrian Research 268:279–294

Gain SB, Mostert AB (1982) The geological setting of the platinoid and base metal sulfide mineralization in the Platreef of the Bushveld Complex in Drenthe, north of Potgietersrus. Econ Geol 77:1395–1404

Grobler DF, Nielsen SA (2012) Upper critical zone (Merensky Reef –UG2) correlates within the Platreef, Turfspruit 241KR, Northern Limb, Bushveld Igneous Complex: internal report, Platreef Resources Pty Ltd. 27 February 2012, 31

Grobler DF, Brits JAN, Maier WD, Crossingham A (2019) Litho- and chemostratigraphy of the Flatreef PGE deposit, northern Bushveld Complex. Mineralium Deposita 54:3-28

Hamilton PJ (1977) Sr isotope and trace element studies of the Great Dyke and Bushveld mafic phase and their relation to early Proterozoic magma genesis in southern Africa. J Petrol 18:24-52

Harris C, Chaumba JB (2001) Crustal contamination and fluid-rock interaction during the formation of the Platreef, northern limb of the Bushveld Complex, South Africa. J Petrol 42:1321-1347

Harris C, Pronost J, Ashwal LD, Cawthorn RG (2005) Oxygen and Hydrogen Isotope Stratigraphy of the Rustenburg Layered Suite, Bushveld Complex: Constraints on Crustal Contamination. J Petrol 46:579-601

Hart RJ, Welke HJ, Nicolaysen, LO (1981) Geochronology of the deep profile through Archean basement at Vredefort, with implications for early crustal evolution. Journal of Geophysical Research 86:B10663-10680

Hart RJ, Andreoli MAG, Tredoux M, DeWit MJ (1990) Geochemistry across an exposed section of the Archaean crust at Vredefort, South Africa: with implications for mid-crustal discontinuities. Chem Geol 82:21-50

Henderson D, Long L, Barton Jr J (2000) Isotopic ages and chemical and isotopic composition of the Archaean Turfloop Batholith, Pietersburg granite—greenstone terrane, Kaapvaal Craton, South Africa. S Afr J Geol, 103: 38-46

Holwell DA, Jordaan A (2006) Three-dimensional mapping of the Platreef at the Zwartfontein South mine: Implications for the timing of magmatic events in the northern limb of the Bushveld Complex, South Africa. Trans Inst Min Metall 115:B41-B48

Holwell DA, Boyce AJ, McDonald I (2007) Sulfur isotope variations within the Platreef Ni-Cu-PGE deposit: genetic implications for the origin of sulphide mineralization. Econ Geol 102:1001-1110

Hulbert LJ, Von Gruenewaldt G (1982) Nickel Copper and platinum mineralisation in the Lower Zone of the Bushveld Complex, South of Potgietersrus. Econ Geol 77:1296-1306

Hunter DR, Hamilton PJ (1978) The Bushveld Complex, in Tarling, D. H., ed., Evolution of the Earth's Crust: London, Academic Press.

Jahn B, Condie KC (1995) Evolution of the Kaapvaal craton as viewed from geochemical and Sm-Nd isotopic analyses of intracratonic pelites. Geochimica et Cosmochimica Acta 59:2239-2258

Junge M ,Oberthür T, Kraemer D, Melcher F, Piña R, Derrey IT, Manyeruke T, Strauss H (2019) Distribution of platinum-group elements in pristine and near-surface oxidized Platreef ore and the variation along strike, northern Bushveld Complex, South Africa. Mineralium Deposita. 54: 885–912

Karykowski BT, Yang S-H, Maier WD, Lahaye Y, Lissenberg C, O'Brien H (2017) In situ Sr isotope compositions of plagioclase from a complete stratigraphic profile of the Bushveld Complex, South Africa: evidence for extensive magma mixing and percolation. J Petrol 58:2285–2308

Keet JJ, Roelofse F, Gauert CDK, Grobler D, Butler M (2021) A comparative study of sulfur isotope variations within the Flatreef and Merensky Reef of the Bushveld Complex, South Africa. The Canadian Mineralogist 59:1363-1380

Keir-Sage E, Leybourne MI, Jugo PJ, Grobler DF, Mayer CC (2021) Assessing the extent of local assimilation within the Flatreef, northern limb of the Bushveld Igneous Complex, using sulfur isotopes and trace element geochemistry. Mineralium Deposita 56:91-102

Kinnaird JA (2005) Geochemical evidence for multiphase emplacement in the southern Platreef. Appl Earth Sci (Trans. Inst. Min. Metal. lB) 114:B225-242

Kinnaird JA, McDonald I (2005) An introduction to mineralisation in the northern limb of the Bushveld Complex. Appl Earth Sci 114:194–198

Kinnaird JA, Hutchinson D, Schurmann L, Nex PAM, de Lange R (2005) Petrology and Mineralisation of the southern Platreef: northern limb of the Bushveld Complex, South Africa. Mineralium Deposita 40:576-597

Kinnaird JA, Nex PAM (2015) An Overview of the Platreef. In: Hammond NQ, Hatton C (eds) Platinum-group element (PGE) mineralisation and resources of the Bushveld Complex, Council for Geoscience, Pretoria, South Africa, pp.293–341

Klemd R, Beinlich A, Kern M, Junge M, Martin L, Regelous M, Schouwstra R (2020) Magmatic PGE Sulphide Mineralization in Clinopyroxenite from the Platreef, Bushveld Complex, South Africa. Minerals 10(6):570

Kruger FJ, Marsh JS (1982) Significance of $^{87}Sr/^{86}Sr$ ratios in the Merensky cyclic unit of the Bushveld Complex. Nature 298:53-55

Kruger FJ (1994) The Sr-isotopic stratigraphy of the western Bushveld Complex. S Afr J Geol 97:393-398

Kruger FJ (2005) Filling the Bushveld Complex magma chamber: lateral expansion, roof and floor interaction, magmatic unconformities, and the formation of giant chromitite, PGE and Ti-V-magnetitite deposits. Mineralium Deposita 40:451–472

Lee CA, Butcher AR (1990) Cyclicity in the Sr isotope stratigraphy through the Merensky reef and Bastard reef units, Atok section, eastern Bushveld Complex. Econ Geol 85:877–883

Li WY, Teng FZ, Ke S, Rudnick RL, Gao S, Wu FY, Chappell BW (2010) Heterogeneous magnesium isotopic composition of the upper continental crust. Geochimica et Cosmochimica Acta 74:6867-6884

Lugmair GW, Marti K (1978) Lunar initial $^{143}Nd/^{144}Nd$: differential evolution line of the lunar crust and mantle. Earth Planet Sci Lett 39:349–357.

Maier WD, Arndt NT, Curl EA (2000) Progressive crustal contamination of the Bushveld Complex: evidence from Nd isotopic analyses of the cumulate rocks. Contrib Mineral Petrol 140:316-327

Maier WD, de Klerk L, Blaine J, Manyeruke T, Barnes S J, Stevens MVA, Mavrogenes JA (2008) Petrogenesis of contact-style PGE mineralization in the northern lobe of the Bushveld Complex: comparison of data from the farms Rooipoort, Townlands, Drenthe and Nonnenwerth. Mineralium Deposita 43:255-280

Maier WD, Barnes S-J, Groves DI (2013) The Bushveld Complex, South Africa: formation of platinum-palladium, chrome- and vanadium-rich layers via hydrodynamic sorting of a mobilized cumulate slurry in a large, relatively slowly cooling, subsiding magma chamber. Mineralium Deposita 48:1-56

Maier WD, Jugo P, Yudovskaya M (2021a) Introduction paper to thematic issue on the Flatreef PGE deposit, northern Bushveld Complex. Mineral Deposita 56:1-10

Maier WD, Abernethy KEL, Grobler DF, Moorhead G (2021b) Formation of the Flatreef deposit, northern Bushveld, by hydrodynamic and hydromagmatic processes. Mineralium Deposita 56:11-30

Mangwegape M, Roelofse F, Mock T, Carlson RW (2016) The Sr isotopic stratigraphy of the Northern Limb of the Bushveld Complex South Africa. J Afri Earth Sci 113:95–100

Manyeruke, T.D., Maier, W.D., & Barnes S-J (2005) Major and Trace Element Geochemistry of the Platreef on the farm Townlands, northern Bushveld Complex. S Afr Geol 108:381–396

Mayer CC, Jugo PJ, Leybourne MI, Grobler DF, Voinot A (2021) Strontium isotope stratigraphy through the Flatreef PGE-Ni-Cu mineralization at Turfspruit, northern limb of the Bushveld Igneous Complex: evidence of correlation with the Merensky Unit of the eastern and western limbs. Mineralium Deposita 56: 59-72

McDonald I, Holwell DA, Armitage PEB (2005) Geochemistry and mineralogy of the Platreef and "Critical Zone" of the northern lobe of the Bushveld Complex, South Africa: implications

for Bushveld stratigraphy and the development of PGE mineralisation. Mineralium Deposita 40:526-549

McDonald I, Holwell DA (2011) Geology of the Northern Bushveld Complex and the Setting and Genesis of the Platreef Ni-Cu-PGE Deposit. Society of Economic Geologists. Rev Econ Geol 17:297-327

Mwenze T (2019) The implications of Sr and Nd isotope data on the genesis of the Platreef and associated BMS and PGE mineralisation, Bushveld Igneous Complex, South Africa. PhD thesis, University of the Western Cape, 148pp

Naldrett T, Kinnaird J, Wilson A, Chunnett G (2008) Concentration of PGE in the Earth's crust with special reference to the Bushveld Complex. Earth Science Frontiers 15:264-297

Naldrett AJ (2009) Fundamentals of magmatic sulfide deposits. In: Li C, Ripley EM (eds) New developments in magmatic Ni–Cu and PGE deposits. Geol Publ House, 1–26

Penniston-Dorland SC, Wing BA, Nex PAM, Kinnaird JA, Farquhar J, Brown M, Sharman ER (2008) Multiple sulfur isotopes reveal a primary magmatic origin for the Platreef PGE deposit, Bushveld Complex, South Africa. Geol 36:979–982

Prevec, SA (2019) The Bushveld Complex, South Africa: New Insights and Paradigms. Geoscience Canada 45:117-135

Prevec SA, Ashwal LD, Mkaza MS (2005) Mineral disequilibrium in the Merensky Reef, western Bushveld Complex, South Africa: new Sm-Nd isotopic evidence. Contrib Mineral Petrol 149:306-315

Pronost J, Harris C, Pin C (2008) Relationship between footwall composition, crustal contamination, and fluid-rock interaction in the Platreef, Bushveld Complex, South Africa. Mineralium Deposita 43:825-848

Raczek I, Stoll B, Hofmann AW, Jochum KP (2001) High precision trace element data for the USGS reference materials BCR-1, BCR-2, BHVO-2, AGV-1, AGV-2, DTS-1, DTS-2, GSP-1and GSP-2 by ID-TIMS and MIC-SSMS. The Journal for Geostandards and Geoanalysis 25:77-86

Raines, MD (2014) An assessment of equilibrium in the Merensky Reef: A textural, geochemical and Nd isotope study of coexisting plagioclase and orthopyroxene from Winnaarshoek in the eastern Bushveld Complex, RSA. MSc dissertation, Rhodes University, 159pp

Reimold WU, Hauser N, Hansen BT, Thirlwall M, Hoffmann M (2017) The impact pseudotachylitic breccia controversy: Insights from first isotope analysis of Vredefort impact-generated melt rocks. Geochimica et Cosmochimica Acta, 214: 266-281

Reisberg L, Tredoux M, Harris C, Coftier A, Chaumba J (2011) Re and Os distribution and Os isotope composition of the Platreef at the Sandsloot-Mogolakwena mine, Bushveld complex, South Africa. Chem Geol 281:352-363.

Roelofse F, Ashwal LD (2012) The Lower Main Zone in the Northern Limb of the Bushveld Complex - a > 1.3 km Thick Sequence of Intruded and Variably Contaminated Crystal Mushes. J of Petrol 53:1449-1476

Rollinson HR (1993) Using geochemical data: evaluation, presentation, interpretation: Harlow, England, Routledge.

Scoates JS, Wall CJ, Friedman RM, Weis D, Mathez EA, Van Tongeren JA (2021) Dating the Bushveld Complex: timing of crystallization, duration of magmatism, and cooling of the world's largest layered intrusion and related rocks. J Petrol 62:1-39

Scoon RN, Costin G, Mitchell A, Moine B (2020) Non-sequential injection of PGE-rich ultramafic sills in the Platreef unit at Akanani, northern limb of the Bushveld Complex: evidence from Sr and Nd isotopic systematics. J Petrol. https://doi.org/10.1093/petrology/egaa032

Sharman-Harris ER, Kinnaird JA, Harris C, Horstmann UE (2005) A new look at sulphide mineralisation of the northern limb, Bushveld Complex: a stable isotope study. Trans Inst Min Metal Section 114:B252-263

Sharpe MR (1985) Strontium isotope evidence for preserved density stratification in the main zone of the Bushveld Complex, South Africa. Nature 316:119-126

South African Committee for Stratigraphy (SACS) (1980) Stratigraphy of South Africa.Part1. In: Kent LE (Compiler) (ed.) Lithostratigraphy of the Republic of South Africa, South West Africa/Namibia, and the Republics of Bophuthatswana, Transkei and Venda. (8 ed.)

Tanaka T, Togashi S, Kamioka H, Amakawa H, Kagami H, Hamamoto T, Yuhara M, Orihashi Y, Yoneda S, Shimizu H et al (2000) JNdi-1: a neodymium isotopic reference in consistency with LaJolla neodymium. Chem Geol 168:279–281

Telus M, Dauphas N, Moynier F, Tissot FLH, Teng FZ, Nabelek PI, Craddock PR, Groat LA (2012) Iron, zinc, magnesium and uranium isotopic fractionation during continental crust differentiation: The tale from migmatites, granitoids, and pegmatites. Geochimica et Cosmochimica Acta 97:247-265

Teng FZ (2017) Magnesium Isotope Geochemistry: Reviews in Mineralogy and Geochemistry, 82: 219-287

Vance D and Thirlwall M (2002) An assessment of mass discrimination in MC-ICPMS using Nd isotopes. Chem Geol 185:227-240

van der Merwe MJ (1976) The Layered Sequence of the Potgietersrus Limb of the Bushveld Complex. Econ Geol 71:1337-1351

Wagner P (1929) The Platinum Deposits and Mines of South Africa, Struick, London

Wasch LJ, Van der Zwan FM, Nebel O, Morel MLA, Hellebrand EWG, Pearson DG, Davies GR (2009) An alternative model for silica enrichment in the Kaapvaal subcontinental lithospheric mantle. Geochimica et Cosmochimica Acta 73:6894–6917

White JA (1994) The Potgietersrus Prospect – Geology and exploration history XVth CMMI Congress, South Africa. South Afr Inst Min Metall 3:173-181

Yudovskaya MA, Kinnaird JA (2010) Chromite in the Platreef (Bushveld Complex, South Africa): occurrence and evolution of its chemical composition. Mineralium Deposita, 45:369-391

Yudovskaya MA, Kinnaird JA, Sobolev AV, Kuzmin DV, McDonald I, Wilson AH (2013) Petrogenesis of the lower zone olivine-rich cumulates beneath the Platreef and their correlation with recognized occurrences in the Bushveld Complex. Econ Geol 108:1923–1952

Yudovskaya MA, Kinnaird JA, Grobler DF, Costin G, Abramova VD, Dunnet T, Barnes S-J (2017) Zonation of Merensky style platinum mineralization in Turfspruit thick reef facies (northern limb of the Bushveld Complex). Econ Geol 112(6):1333–1365

Zeh A, Ovtcharova M, Wilson AH, Schaltegger U (2015) The Bushveld Complex was emplaced and cooled in less than one million years – results of zirconology, and geotectonic implications. Earth Planet Sci Lett 418:103–114

CHAPTER 7 :
DISCUSSION AND CONCLUSIONS

7.1 Summary of key findings

7.1.1. Summary of key findings emanating from Chapter 4

A detailed Sr isotope investigation of the Flatreef inclusive of the Bastard and Merensky reefs, as intersected by borehole UMT-393 on the farm Macalacaskop, was carried out in this study. The results indicate an increase in $^{87}Sr/^{86}Sr$ (Sr_i) from values of about 0.706 to 0.707 in the Footwall Cyclic Unit (FCU) to values > 0.709 near the top of the Merensky Reef, all of which are lower than the Sr_i values reported for the Platreef up-dip (0.710-0.715; Kruger 2005). This isotopic shift matches the isotopic shift described for the eastern and western BC. Variations in the Sr_i and An% of plagioclase, support the contention that the Flatreef is a correlate of the uppermost UCZ as initially proposed by Grobler et al. (2019). The Flatreef appears to be the down-dip extension of the near surface Platreef that has not been significantly affected by footwall interaction. Previous studies (Holwell et al. 2005; Jordaan and Holwell 2006) have shown that intrusion of the MZ in the northern limb significantly post-dated the formation of the Platreef, and for this reason, the MZ cannot be regarded as the source of PGEs within the Flatreef / Platreef, and by extension, the Merensky Reef. Our findings, along with published field observations on the Platreef and MZ relationship elsewhere in the northern limb, support models (McDonald et al. 2005; McDonald and Holwell, 2007; Penniston-Dorland et al., 2008; Sharman et al., 2013; McDonald and Holwell, 2011) that attribute the observed PGE mineralization of the Flatreef/Platreef/Merensky Reef to processes that operated within a sub-Bushveld staging chamber, as opposed to processes that operated within the presently exposed confines of the Rustenburg Layered Suite.

7.1.2. Summary of key findings emanating from Chapter 5

The variation in whole-rock S-isotope composition across the FCU, Main Reef, Middling Unit, Upper Reef and hanging wall units of the Flatreef as exposed in boreholes UMT-393 and UMT-276 shows that the Main Reef has a S isotopic signature comparable to that of the Merensky Reef in the western and eastern limbs of the BC. It is suggested that the consistent near-mantle S isotopic signature and associated metal enrichment of the Main Reef may be due to the large-scale interaction of sulfides trapped in LZ conduits with large volumes of uncontaminated magma. The HW and FCU have $\delta^{34}S$ values that are significantly higher than the mineralized units of the Flatreef, indicating that these units experienced a higher degree of assimilation and contamination by sedimentary S from footwall rocks or dolomitic xenoliths. Contrary to the whole-rock S-isotopic compositions reported for the Merensky Reef in the

western and eastern limbs of the BC, the Merensky Reef at Two Rivers Platinum mine (TRP) display slightly heavier $\delta^{34}S$ values. The $\delta^{34}S$ values at TRP is also more elevated than the values reported for the Merensky Reef in both UMT-393 and UMT-276. This heavier S-isotopic signature is suggested to be the result of assimilation of surrounding 'brown sugar norite' (BSN) as well as the degassing of underlying carbonates.

7.1.3. Summary of key findings emanating from Chapter 6

The Nd-isotopic composition of the Flatreef rocks show significant overlap with the isotopic data of the UCZ-MZ interval of the western and eastern BC, which further supports the correlation of the Flatreef with the uppermost UCZ inclusive of the Merensky Reef and Bastard Reef. The similar ε_{Nd}^{i} values reported for the hanging wall and footwall lithologies of the Flatreef are therefore suggested to indicate that these units may initially have been continuous but were subsequently separated by the intrusion of different pulses of the remainder of the Flatreef, as proposed by Keet et al. (2021) on the basis of S isotopic results. It is evident that the interaction of mantle-derived magma with footwall rocks as local contaminants fails to explain the Nd-isotopic composition observed for the Flatreef. Alternatively, it is suggested that the Flatreef magma(s) attained their contaminated Nd-isotopic signature within a sub-Bushveld staging chamber where mantle-derived melts interacted with lower and upper crustal melts of the Kaapvaal Craton (cf. Roelofse and Ashwal (2012)), prior to their final emplacement into the presently exposed part of the RLS. Interestingly, the Sr-isotopic composition of the Flatreef is more radiogenic than is expected for the mixture of magmas (60:40 B1:B2) that produced the UCZ, which suggests syn- to post-emplacement modification of the isotopic composition of the parental magma through interaction with locally available Transvaal Supergroup dolomitic rocks may have occurred.

7.2 Correlation of Platreef/Flatreef with the UCZ in the remainder of the BC

South of the Thabazimbi-Murchison Lineament (TML), which separates the northern limb from the remainder of the BC, a connection between the eastern and western limbs have been confirmed by geophysical studies (Cawthorn and Webb, 2001; Webb et al., 2004; Cole et al., 2013). However, a connection of these arcuate limbs with the northern limb has not yet been proven. Apart from being seemingly disconnected structurally from the rest of the BC, various authors have also shown that the stratigraphy of the northern limb is different in certain respects compared to the RLS south of the TML. These discrepancies of the northern limb include, 1) a troctolitic unit of approximately 200 m thick present in the MZ that is not documented elsewhere (van der Merwe et al., 1976; Ashwal et al., 2005); 2) a possible hiatus between the formation of the Platreef and the subsequent intrusion of the MZ, evidence for which is observed only in the northern limb (Holwell et al., 2005; Holwell and Jordaan, 2006);

3) the presence of well-developed chromitite layers in the LZ which are absent in the LZ in the remainder of the BC (Hulbert and von Gruenewaldt) and 4) the intrusion of the LZ as discrete satellite bodies and irregular intrusions separated from the mineralized Platreef by Transvaal Supergroup interlayers (Yudovskaya et al., 2013). Notwithstanding these differences, it is broadly accepted that the UZ, MZ, as well as the LZ is present in the northern, as it is in the western and eastern limbs of the BC. The correlation of the Platreef, a Ni-Cu-PGE mineralized unit unique to the northern limb, poses the greatest uncertainty.

Historically, the correlation of the Platreef with the Merensky Reef in the western and eastern BC was first proposed by Wagner (1929), and this interpretation was expanded on in subsequent studies. The Platreef is generally located at a stratigraphic position below the MZ, which in terms of the RLS succession, makes it equivalent to the UCZ in the remainder of the BC. Therefore, in addition to the Platreef being PGE mineralized, the idea of correlation between these two sequences appears plausible. However, reliable scientific evidence in support of this contention has been lacking. Prior to the discovery of the Flatreef about a decade ago, several studies of the Platreef on Turfspruit and Macalacaskop, the current study area, focused on the shallow, complex and highly contaminated Platreef (e.g., Kruger, 2005; Kinnaird, 2005; Kinnaird et al., 2005; Hutchinson and Kinnaird, 2008; Hutchinson and McDonald, 2008; Pronost et al., 2008; Sharman-Harris et al., 2013). Correlation of the Platreef to the UCZ in the remainder of the BC remained challenging due to discrepancies arising from the amount of footwall interaction recorded by these investigations.

Recent isotopic investigations on the newly discovered Flatreef (Beukes et al., 2021; Mayer et al., 2021; Keet et al., 2021; Keet et al., 2022 submitted and Keir-Sage et al., 2021) have proven to be an effective geochemical means of getting a better understanding of the Flatreef / Platreef petrogenesis and how it relates to the remainder of the BC. These isotopic studies provide the first isotopic correlation between the Flatreef/Platreef and the Merensky Reef in the western and eastern BC. The S-Sr-Nd isotopic data of the Flatreef stratigraphy of this study are similar to the isotopic data reported for the uppermost part of the UCZ inclusive of the Bastard Reef and Merensky Reef in the western and eastern limbs of the BC. The relationships between these mineralized units are summarized in sections 7.1.1, 7.1.2 and 7.1.3, above.

7.3 Towards a petrogenetic model for the Flatreef

Due to its economic significance, the Merensky Reef in the RLS of the BC, particularly, has been extensively studied over the last century to determine the source of PGE mineralization as well as its emplacement mechanism (e.g. Campbell et al., 1983; Ballhaus et al., 1988; Boudreau and McCallum, 1992; Mathez et al., 1997; Barnes and Maier, 2002; Cawthorn et

al., 2002; Cawthorn, 2005; Seabrook et al., 2005; Roberts et al., 2007; Naldrett et al., 2009; Maier et al., 2013; Latypov et al., 2015). The contention that the Platreef / Flatreef is a correlate of the Merensky Cyclic Unit and Bastard Cyclic Unit in the remainder of the BC suggests that these units may have formed from similar processes. It was proposed that the Platreef is a marginal extension of the UCZ inclusive of the Merensky Reef and Bastard Reef as recognized in the western and eastern limbs of the BC (Naldrett et al., 2008, 2009; Maier et al., 2008). The Platreef is therefore expected to progressively convert into a layered sequence similar to the upper part of the UCZ towards the center of the limb (Maier et al., 2008; Smith et al., 2014). Based on this implication, Stephenson (2019) suggested that the Flatreef represents a transitional unit between the highly contaminated Platreef up-dip and more magmatic UCZ sequences at depth (Fig. 7.1). Others have also proposed that the Platreef was emplaced with high PGE tenor base metal sulfides that formed from a pre-existing magma chamber prior to emplacement (McDonald et al., 2009; Holwell et al., 2007; McDonald and Holwell, 2007).

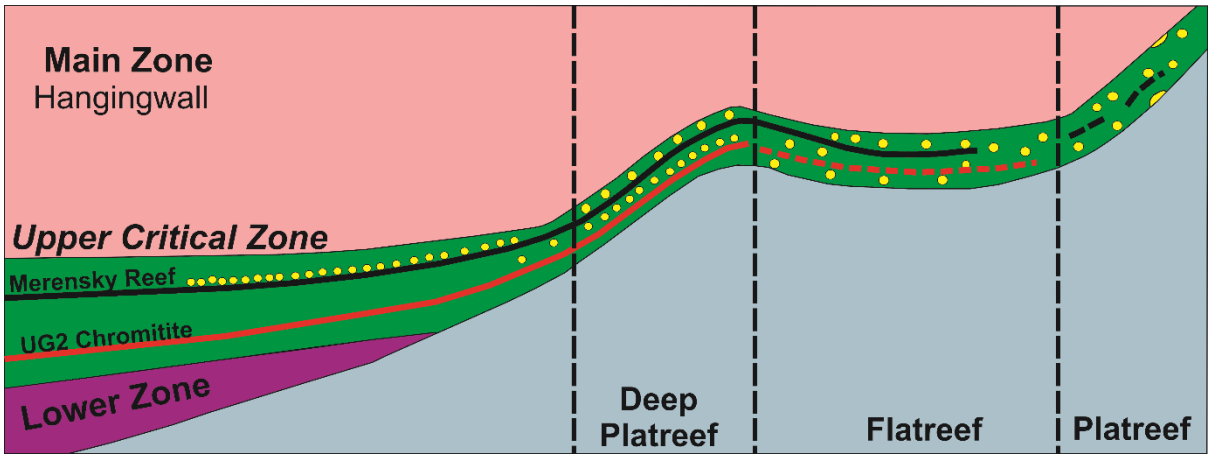

Figure 7.1 An illustration showing the transition from near surface Platreef to the UCZ with depth on the Turfspruit locality. Modified after Stephenson (2019).

Based on detailed U-Pb dating data from the UCZ stratigraphy in the western limb, it was suggested that the UCZ does not display an upward-younging stratigraphy (Mungall et al. 2016), leading to the suggestion that specific layers may have been intruded as sills. Similarly, Scoates et al. (2021) proposed out-of-sequence emplacement for the RLS in the eastern limb (the dated Merensky Reef sample in this study is from the Rustenburg Platinum mine, western limb). Interestingly, these authors reported an age for Bastard pyroxenite (2059.34 ± 0.55 Ma) that is older than their two Merensky reef samples (with ages of 2057.04 ± 0.55 and 2056.88 ± 0.41 Ma). However, Mitchell (2021) argued the impossibility of this as Viljoen and Hieber (1986) has conclusively shown by collective underground observations that the Bastard Reef transgresses and eliminates Merensky Reef at the Rustenburg Section of the

Rustenburg Platinum Mines. The emplacement of the Platreef as multiple sills is supported by well-established geochemical studies by Kinnaird (2005) and Manyeruke (2005). Due to complicated igneous layering of the Platreef Unit at Akanani, an upward-younging stratigraphy is not proposed (Scoon et al., 2020). This interpretation is complemented by a recent geochronological investigation of zircons from the Flatreef stratigraphy and a Merensky Reef sample from Northam mine by Abernethy (2020). The U-Pb data of the Main Reef overlaps with that of the Northam Merensky Reef suggesting that the upper Flatreef can be correlated with the UCZ in the remainder of the BC. Non-sequential layering is also evident from the zircon analysis of the Flatreef stratigraphy as the Upper Reef is younger than overlying Main Zone; and the Main Reef is older than the underlying UG-2 chromitite (Abernethy, 2020). These geochronological findings are, however, inconsistent with the well-documented magmatic unconformity at the base of the MZ in the northern limb (Holwell et al., 2005; Holwell and Jordaan, 2006).

Initially the Platreef was characterised as exclusively comprising of contact style-mineralization due to its significant thickness, its position along the base of the northern limb, the presence of massive to disseminated ores and base metal sulfide enrichment (Maier et al., 2008). This style of mineralization in the northern limb was described as disconnected from specific stratigraphic units or magma types and that it formed by a number of diverse processes (Maier et al., 2008). However, stratiform or reef-style mineralization has been identified in the undisturbed upper part of the Platreef at Turfspruit (Yudovskaya et al., 2017) which is equated with the Flatreef. Isotopic data from our study allows us to constrain the petrogenesis of the down-dip, sub-horizontal extension of the Platreef.

The δ^{34}S values reported for the mineralized Main Reef of the Flatreef (Yudovskaya et al., 2017; Keet et al., 2021; Keir-Sage et al., 2021) overlap with the mantle range (around -2‰ to 0‰; Labidi et al., 2012) and with the Merensky Reef in the remainder of the BC. These findings support the contention by Holwell et al. (2007) that the sulfides and associated mineralization of the Platreef did not form by in-situ contamination. The assimilation of S from country rock is considered as an ore modifying process rather than an initiator of primary mineralization (McDonald and Holwell, 2011), consistent with the findings of Holwell et al. (2007) and Hutchinson and McDonald (2008) who showed that metal tenors of the sulfides are diluted by high proportions of country rock input. Therefore, assimilated S from surrounding country rock had limited influence during the formation of the Flatreef. Yudovskaya et al. (2017), in line with the emplacement mechanism proposed by Cawthorn (2012) for layered intrusions, attributed the consistent mantle-like S isotopic signature of the PGE-rich stratiform reefs of the Platreef to channelized magmatic currents which would provide for unlimited exchange with magmatic S (Ripley and Li, 2003).

The findings from Keet et al. (2021) have shown that the $\delta^{34}S$ values of the Main Reef at UMT-276 are more negative compared to that of UMT-393 as well as UMT-094 (Keir-Sage et al., 2021). This isotopically lighter signature of the Main Reef in borehole UMT-276 indicates a limited degree of contamination with heavy S (Keet et al. 2021). In comparing the S isotopic data of the Main Reef at the different borehole intersections, it is apparent that the Flatreef magma may have experienced differing amounts of crustal contamination, possibly upon ascent from a staging chamber. Although the Nd-isotopic composition of the Flatreef cannot be explained by the influence of local contaminants on mantle-derived magma (Fig. 6.10; Keet et al. 2022 submitted), the variation in Sr_i could be attributed to the interaction of Flatreef magma with country rocks en route to the emplacement site, as well as possibly post-emplacement. In this study it is apparent that the HW and FW stratigraphic units of the Flatreef have distinct Sr, Nd and S isotopic signatures compared to the mineralized remainder of the Flatreef. On this basis, it is suggested that the FW and HW units were initially contiguous, only to be later separated by pulses or sills of the mineralized portions of the Flatreef.

Considering the findings of this study, an emplacement model is proposed where the mineralized portions of the Flatreef were emplaced as sills fed from a deep seated staging chamber as follows (Fig. 7.2):

- LZ and CZ magmas were emplaced into basinal structures present in the floor rocks (Fig 7.2A).
- The mineralized units of the Flatreef, namely, the Upper Reef and Main Reef, were intruded into the upper reaches of the CZ as sills. These mineralized units carried base metal sulfides with high PGE tenors that formed due to the interaction of sulfide melts with large volumes of silicate melts within a sub-Bushveld plumbing system. The magmas of the Flatreef / Platreef likely experienced syn- to post- emplacement modification as a result of interaction with locally available dolomitic country rocks as recorded by Sr-Nd isotopic compositions (Beukes et al., 2021; Keet et al., 2022 (submitted)). Where sills onlapped onto basement rocks, extensive interaction with local country rocks lead to the development of the “erratic” Platreef (Fig 7.2B).
- Extant CZ magma was displaced upwards due to this sill intrusion, forming the lowermost HW units of the Flatreef succession (Fig 7.2B)
- MZ magma was emplaced following a hiatus, leading to the development of finger-like intrusions cross-cutting the Platreef at Sandsloot and Zwartfontein (Holwell et al., 2005 and Holwell and Jordaan, 2006) (Fig 7.2C).

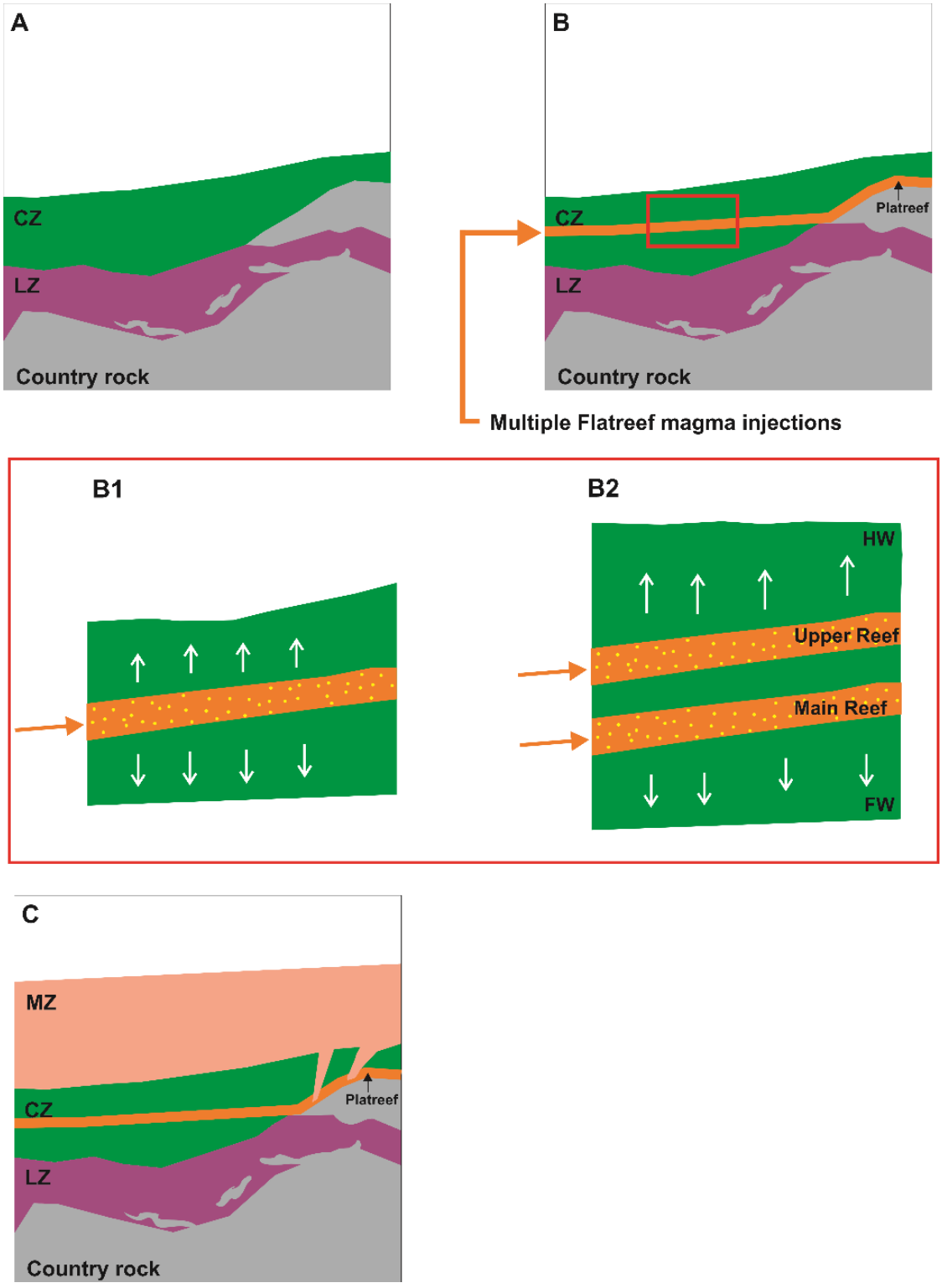

Figure 7.2 A schematic representation showing the sill-like emplacement of the mineralized portions of the Flatreef. **A** Emplacement of LZ and CZ magmas into basinal structures. **B** Sill-like emplacement of the mineralized units of the Flatreef. Where magma is brought into contact with country rocks, the erratic Platreef characterised by disturbed S-, Sr- and Nd-isotopic compositions is developed. Insets **B1** and **B2** show the displacement of extant CZ magma as a result of the sill intrusions. **C** The MZ is emplaced following a hiatus during which the Platreef / Flatreef solidified, leading to cross-cutting relationships between Platreef and MZ as seen at Sandsloot and Zwartfontein.

7.4 Conclusions and Recommendations

The S-Sr-Nd isotopic composition of the Flatreef shows significant overlap with the uppermost UCZ which includes the Merensky Reef and the Bastard Reef in the western and eastern limbs of the BC. The findings in this study provide isotopic evidence in support of the contention that the Flatreef is a correlate of the Merensky and Bastard reefs as initially proposed by Grobler et al. (2019) based on their lithostratigraphic evidence.

The Sr-Nd isotopic composition of the Flatreef cannot be accounted for by the mixing of mantle-derived magmas with locally available country rocks. Instead, the magma(s) that gave rise to the Flatreef likely acquired their Sr-Nd isotopic compositions through interaction with upper and lower crustal rocks of the Kaapvaal craton within a sub-Bushveld staging chamber, possibly with syn- and / or post-emplacement modification of particularly its Sr-isotopic composition through interaction with dolomitic country rocks of the Transvaal Supergroup.

The proposed correlation between the Flatreef / Platreef and the Merensky / Bastard reefs holds important implications for the source of PGEs present in the latter within the context of clear, field-based evidence that shows that intrusion of the Main Zone significantly post-dated solidification of the Platreef. This implies that the Main Zone could not have been the source of PGEs that became incorporated into the Merensky Reef, at least not in the manner envisaged by commonly invoked models.

Underground observations of the Flatreef lithologies and its footwall and hangingwall will be important for the confirmation of cross-cutting relationships in the study area, and should be further assessed as mine development proceeds. Field evidence of the presence of possible “potholes” where the footwall is transgressed by overlying units would further support the correlation between the Flatreef and the Merensky Reef in the remainder of the BC.

REFERENCES

The references listed below are for chapters 1, 2, 3 and 7:

Abernethy, K. (2020). Assimilation of Dolomite by Bushveld Magmas in the Flatreef; Implications for the Origin of Ni-Cu-PGE Mineralization and the Precambrian Atmosphere. PhD thesis, Cardiff University, Cardiff.

Ashwal, L. D., Webb, S. J., and Knoper, M. W. (2005). Magmatic stratigraphy in the Bushveld Northern Lobe: continuous geophysical and mineralogical data from the 2950m Bellevue drill core. South African Journal of Geology, 108, 199–232.

Ballhaus, C. G., Cornelius, M., and Stumpfl, E. F. (1988). The Upper Critical Zone of the Bushveld Complex and the origin of Merensky-type ores; a discussion. Economic Geology, 83, 1082–1085.

Barnes, S.-J., and Maier, W. D. (2002). Platinum-group element distributions in the Rustenburg layered suite of the Bushveld Complex, South Africa. In L. J. Cabri, (Ed.), Geology, geochemistry, mineralogy and mineral beneficiation of platinum group elements, Vol. 54, Canadian Institute of Mining, Metallurgy and Petroleum, Montreal, pp. 431–458.

Bekker, A., Kaufman, A. J., Karhu, J. A., Beukes, N. J., Swart, Q. D., Coetzee, L. L., and Eriksson, K. A. (2001). Chemostratigraphy of the Paleoproterozoic Duitschland Formation, South Africa: Implications for coupled climate change and carbon cycling. American Journal of Science, 30, 261–285.

Beukes, J. J., Roelofse, F., Gauert, C. D. K., Grobler, D. F., and Ueckermann, H. (2021) Strontium isotope variations in the Flatreef on Macalacaskop, northern limb, Bushveld Complex: implications for the source of platinum-group elements in the Merensky Reef. Mineralium Deposita, 56, 45–57.

Boudreau, A. E. (2008). Modeling the Merensky Reef, Bushveld Complex, Republic of South Africa. Contributions to Mineralogy and Petrology, 156, 431–437.

Boudreau, A. E., and McCallum, I. S. (1992). Concentration of Platinum-Group Elements by Magmatic Fluids in Layered Intrusions. Economic Geology and the Bulletin of the Society of Economic Geologists, 87:1830–1848.

Buchanan, D. L., Nolan, J., Suddaby, P., Rouse, J. E., Viljoen, M. J., and Davenport, J. W. J. (1981). The genesis of sulfide mineralization in a portion the Potgietersrus Limb of the Bushveld Complex. Economic Geology, 76, 568–579.

Buchanan, P., Reimold, W., Koeberl, C. and Kruger, F. (2002). Geochemistry of intermediate to siliceous volcanic rocks of the Rooiberg Group, Bushveld Magmatic Province, South Africa. Contributions to Mineralogy and Petrology, 144, 131–143.

Cameron, E.N. (1978). The Lower zone of the eastern Bushveld complex in the Olifants River trough. Journal of Petrology, 19, 437–462.

Cameron, E. N. (1980). Evolution of the Lower Critical Zone, central sector, eastern Bushveld Complex, and its chromite deposits. Economic Geology, 75, 845–871.

Cameron, E. N. (1982). The Upper Critical Zone of the eastern Bushveld Complex; precursor to the Merensky Reef. Economic Geology, 77, 1307–1327.

Campbell, I. H., Naldrett, A. J., and Barnes, S. J. (1983). A model for the origin of the platinum-rich sulfide horizons in the Bushveld and Stillwater complexes. Journal of Petrology, 24, 133–165.

Cawthorn, R. G. (1999). Platinum-group element mineralization in the Bushveld Complex - a critical reassessment of geochemical models. South African Journal of Geology, 102, 268–281.

Cawthorn, R. G. (2005). Pressure fluctuations and the formation of the PGE-rich Merensky and chromitite reefs, Bushveld Complex. Mineralium Deposita, 40, 231–235.

Cawthorn, R. G. (2007). Cr and Sr: Keys to parental magmas and processes in the Bushveld Complex, South Africa. Lithos, 95, 381–398.

Cawthorn, R. G. (2010). The platinum group element deposits of the Bushveld Complex in South Africa. Platinum Metals Review, 54, 205–215.

Cawthorn, R.G. (2012). Multiple sills or a layered intrusion? Time to decide: South African Journal of Geology, 115, 283–290.

Cawthorn, R. G. (2015). The Bushveld Complex, South Africa. In B. Charlier, O. Namur, R. Latypov and C. Tegner (Eds.), Layered Intrusions. Springer Netherlands, pp. 517-587.

Cawthorn, R. G. (2020). Massive pyroxene compositional oscillations on a metre scale in the Pyroxenite Marker, northern limb, Bushveld Complex, South Africa. Lithos, 356-357 105392.

Cawthorn, R. G., Barnes, S.-J., Ballhaus, C., and Malitch, K. N. (2005). Platinum-group element, chromium, and vanadium deposits in mafic and ultramafic rocks. Economic Geology 100th Anniversary Volume, 215–249.

Cawthorn, R. G., and Boerst, K. (2006). Origin of the Pegmatitic Pyroxenite in the Merensky Unit, Bushveld Complex, South Africa. Journal of Petrology, 47, 1509–1530.

Cawthorn, R. G., and Davies, G. (1983). Experimental data on the parental magmas to the Bushveld Complex. Contributions to Mineralogy Petrology, 83, 128–135.

Cawthorn, R. G., Eales, H. V., Walraven, F., Uken, R. and Watkeys, M. K. (2006). The Bushveld Complex. In M. R. Johnson, C. R. Anhaeusser and R. J. Thomas (Eds) The Geology of South Africa, Geological Society of South Africa, Johannesburg, pp. 261-281.

Cawthorn, R. G., Merkle, R. K. and Viljoen, M. J. (2002). Platinum group element deposits in the Bushveld Complex, South Africa. In: Cabri, L. J. (ed.) The Geology, Geochemistry, Mineralogy and Mineral Beneficiation of Platinum-Group Elements. Canadian Institute of Mining and Metallurgy, Special Volume 54, 389–429.

Cawthorn, R. G., Meyer, P. S., and Kruger, F. J. (1991). Major addition of magma at the Pyroxenite Marker in the western Bushveld Complex, South Africa. Journal of Petrology, 32, 739–763.

Cawthorn, R. G., and Molyneux, T. G. (1986). Vanadiferous magnetite deposits of the Bushveld Complex, in C. R. Anhaeusser & S. Maske (eds) Mineral deposits of Southern Africa. Geological Society of South Africa, Johannesburg, pp. 1251–1266.

Cawthorn, G., and Walraven, F. (1998). Emplacement and crystallisation time for the 807 Bushveld Complex. Journal of Petrology, 39, 1669–1687.

Cawthorn, R. G., and Webb, S. J. (2001). Connectivity between the western and eastern limbs of the Bushveld Complex. Tectonophysics, 330, 195–209.

Cheshire, P. (2011). Frontier Resources (Pty) Ltd, Forge Project. Prospecting report: Potential for platinum-group mineral enrichment: Vliegekraal 783LR, Vogelstruisfontein 765LR, Vriesland 781LR farms, Mokopane district. Unpublished exploration report, 67pp.

Cole, J., Finn, C. A. and Webb, S. J. (2013). Overview of the magnetic signatures of the Palaeoproterozoic Rustenburg layered suite, Bushveld complex, South Africa. Precambrian Research, 236, 193–213.

Cowley, A. (2021). Johnson Matthey PGM Market Report May 2021. Accessed from https://matthey.com/documents/161599/162993/JM-Pgm-Market-Report-May-2021.pdf/b954f429-7c60-f31e-9ebd-a47f0c87ea9d?t=1650968145902, on 22 August 2022).

De Villiers, J. S. (1970). The structure and petrology of the mafic rocks of the Bushveld Complex south of Potgietersrus. Geological Society of South Africa (special publication), 1, 23–25.

Davies, G., Cawthorn, R. G., Barton, J. M., Jr., and Morton, M. (1980). Parental magma to the Bushveld Complex. Nature, 287, 33–35.

Eales, H. V., and Cawthorn, R. G. (1996). Bushveld Igneous Complex. In R. G. Cawthorn (Ed.), Layered intrusions, Vol. 15, Elsevier, pp. 181-229.

Eglington, B., and Armstrong, R. (2004). The Kaapvaal Craton and adjacent orogens, southern Africa: a geochronological database and overview of the geological development of the craton. South African Journal of Geology, 107, 13–32.

Finn, C. A., Bedrosian, P. A., Cole, J. C., Khoza, T. D., and Webb, S. J. (2015). Mapping the 3-D extent of the Northern Lobe of the Bushveld layered mafic intrusion from geophysical data. Precambrian Research, 268, 279–294.

Gain, S. B., and Mostert, A. B. (1982). The geological setting of the platinoid and base metal sulfide mineralization in the Platreef of the Bushveld Complex in Drenthe, north of Potgietersrus. Economic Geology, 77, 1395–1404.

Godel, B. (2015). Platinum-Group Element Deposits in Layered Intrusions: Recent Advances in the Understanding of Ore Forming Processes. In B. Charlier, O. Namur, R. Latypov and C. Tegner (Eds.), Layered Intrusions, Springer Netherlands, pp. 379-432.

Grobler, D. F., Brits, J. A. N., Maier, W. D., and Crossingham, A. (2019). Litho- and chemostratigraphy of the Flatreef PGE deposit, northern Bushveld Complex. Mineralium Deposita, 54, 3–28.

Hahn, U.F. and Ovendale, B. (1994). UG2 chromitite layer potholes at Wildebeestfontein North Mine, Impala Platinum Limited. XVth CMMI Congress, Johannesburg. South African Institute Mine Metall, 3, 195–200.

Hall, A. L. (1932). The Bushveld Complex in the central Transvaal. South African Geological Survey Memoir, 28, Pretoria, pp. 544.

Harris, C., and Chaumba, J. B. (2001). Crustal contamination and fluid-rock interaction during the formation of the Platreef, northern limb of the Bushveld Complex, South Africa. Journal of Petrology, 42, 1321–1347.

Harmer, R., and Sharpe, M. R. (1985). Field relations and strontium isotope systematics of the marginal rocks of the eastern Bushveld Complex. Economic Geology, 80, 813–837.

Holwell, D. A., Armitage, P. E. B., and McDonald, I. (2005). Observations on the relationship between the Platreef and its hangingwall. Transactions of the Institutions of Mining and Metallurgy, Section B: Applied Earth Science, 114, 199–208.

Holwell, D. A., Boyce, A. J., and McDonald, I. (2007). Sulfur isotope variations within the Platreef Ni-Cu-PGE deposit: genetic implications for the origin of sulfide mineralization. Economic Geology, 102, 1091–1110.

Holwell, D. A., and Jordaan, A. (2006). Three-dimensional mapping of the Platreef at the Zwartfontein South mine: Implications for the timing of magmatic events in the northern limb of the Bushveld Complex, South Africa. Transactions of the Institutions of Mining and Metallurgy, Section B, Applied Earth Science, 115, 41–48.

Holwell, D. A., and McDonald, I. (2006). Petrology, geochemistry and the mechanisms determining the distribution of platinum-group element and base metal sulphide mineralisation in the Platreef at Overysel, northern Bushveld Complex, South Africa. Mineralium Deposita, 41, 575–598.

Holwell, D. A., McDonald, I., and Armitage, P.E.B. (2006). Platinum-group mineral assemblages in the Platreef at the Sandsloot Mine, northern Bushveld Complex, South Africa. Mineralogical Magazine, 70, 83–101.

Holwell D. A., and McDonald, I. 2007. Distribution of platinum-group elements in the Platreef at Overysel, northern Bushveld Complex: a combined PGM and LA-ICP-MS study. Contributions to Mineralogy and Petrology, 154, 171 – 190.

Holwell, D. A., Jones, A., Smith, J. W., and Boyce, A.J. (2013). New mineralogical and isotopic constraints on Main Zone-hosted PGE mineralisation at Moorddrift, northern Bushveld Complex. Mineralium Deposita, 48, 675–686.

Hulbert, L. J. (1983). A petrographical investigation of the Rustenburg Layered Suite and associated mineralization south of Potgietersrus. Unpublished D.Sc. dissertation, Pretoria, South Africa, The University of Pretoria.

Hulbert, L. J., and von Gruenewaldt, G. (1982). Nickel, copper, and platinum mineralization in the Lower Zone of the Bushveld Complex, south of Potgietersrus. Economic Geology, 77, 1296–1306.

Hulbert, L. J., and von Gruenewaldt, G. (1985). Textural and compositional features of chromite in the Lower and Critical Zones of the Bushveld Complex south of Potgietersrus. Economic Geology, 80, 872–895.

Hutchinson, D., and Kinnaird, J. A. (2005). Complex multistage genesis for the Ni-Cu-PGE mineralisation in the southern region of the Platreef, Bushveld Complex, South Africa. Applied Earth Science (Transactions of the Institute of Mining and Metallurgy B), 114, 209–224.

Hutchinson, D., and McDonald I. (2008). Laser ablation ICP-MS study of platinum-group elements in sulfides from the Platreef at Turfspruit, northern limb of the Bushveld Complex, South Africa. Mineralium Deposita, 43, 695–711.

Huthmann, F. M., Yudovskaya, M. A., Frei, D., and Kinnaird, J. A. (2016). Geochronological evidence for an extension of the Northern lobe of the Bushveld Complex, Limpopo Province, South Africa. Precambrian Research, 280, 61–75.

Huthmann, F. M., Yudovskaya, M. A., Kinnaird, J. A., McCreesh, M. J. G., and McDonald, I. (2018). Geochemistry and PGE of the lower mineralized Zone of the Waterberg Project, South Africa. Ore Geology Reviews, 92, 161–185.

Junge, M., Oberthür, T., Kraemer, D., Melcher, F., Piña, R., Derrey, I. T., Manyeruke, T., and Strauss, H. (2019). Distribution of platinum-group elements in pristine and near-surface oxidized Platreef ore and the variation along strike, northern Bushveld Complex, South Africa. Mineralium Deposita, 54, 885–912.

Keet, J. J., Roelofse, F., Gauert, C. D. K., Grobler, D., and Butler, M. (2021). A comparative study of sulfur isotope variations within the Flatreef and Merensky Reef of the Bushveld Complex, South Africa. The Canadian Mineralogist, 59, 1363–1380.

Keir-Sage, E., Leybourne, M. I., Jugo, P. J., Grobler, D. F., and Mayer, C. C. (2021). Assessing the extent of local assimilation within the Flatreef, northern limb of the Bushveld Igneous Complex, using sulfur isotopes and trace element geochemistry. Mineralium Deposita, 56, 91–102.

Kinnaird, J. A. (2005). Geochemical evidence for multiphase emplacement in the southern Platreef. Applied Earth Science (Transactions of the Institute of Mining and Metallurgy lB), 114, B225–242.

Kinnaird, J. A., Hutchinson, D., Schurmann, L., Nex, P. A. M., and de Lange, R. (2005). Petrology and Mineralisation of the southern Platreef: northern limb of the Bushveld Complex, South Africa. Mineralium Deposita 40,576–597.

Kinnaird, J. A, Kruger, F. J., Nex, P. A. M., Cawthorn, R. G. (2002). Chromitite formation—a key to understanding processes of platinum enrichment. Applied Earth Science (Transactions of the Institute of Mining and Metallurgy B), 111, 23–35.

Kinnaird, J. A., and McDonald, I., (2005). An introduction to mineralisation in the northern limb of the Bushveld Complex. Transactions of the Institution of Mining and Metallurgy, 114, 194–198.

Kinnaird, J. A., and Nex, P. A. M. (2015). An Overview of the Platreef. In: Hammond, N. Q., Hatton, C. (Eds) Platinum-group element (PGE) mineralisation and resources of the Bushveld Complex. Council for Geoscience, Pretoria, South Africa, pp.293–341.

Kinnaird, J. A., Yudovskaya, M. A., McCreesh, M. J. G., Huthmann, F. M., and Botha, T. J. (2017). The Waterberg PGE Deposit – A typical mineralization in mafic-ultramafic rocks of the Bushveld Complex, South Africa. Economic Geology, 112, 1367–1394.

Kinnaird, J. A., Yudovskaya, M., Naldrett, A. J., Botha, M. J., and Chunnett, G. K. (2012). PGE mineralisation in the Main Zone of the northern limb of the Bushveld Complex. In: 12th International Ni–Cu–(PGE) Symposium, Guiyang, China. Abstracts 73–76

Klemd, R., Beinlich, A., Kern, M., Junge, M., Martin, L., Regelous, M., and Schouwstra, R. (2020). Magmatic PGE Sulphide Mineralization in Clinopyroxenite from the Platreef, Bushveld Complex, South Africa. Minerals, 10(6):570.

Kruger, F. J. (1990). The stratigraphy of the Bushveld Complex; a reappraisal and the relocation of the Main Zone boundaries. South African Journal of Geology, 93, 376–381.

Kruger, F. J. (1992). The origin of the Merensky cyclic unit: Sr isotopic and mineralogical evidence for an alternative orthomagmatic model. Australian Journal of Earth Sciences, 39, 255–261.

Kruger, F. J. (1994). The Sr-isotopic stratigraphy of the western Bushveld Complex. South African Journal of Geology, 97, 393–398.

Kruger, F. J. (2005). Filling the Bushveld Complex magma chamber: lateral expansion, roof and floor interaction, magmatic unconformities, and the formation of giant chromitite, PGE and Ti-V-magnetitite deposits. Mineralium Deposita, 40, 451–472.

Labidi, J., Cartigny, P., Birck, J. L., Assayag, N., and Bourrand, J.J. (2012). Determination of multiple sulfur isotopes in glasses: a reappraisal of the MORB d^{34}S. Chemical Geology, 334, 189–198.

Latypov, R., Chistyakova, S., Barnes, S. J. and Hunt, E. J. (2017). Origin of platinum deposits in layered intrusions by in situ crystallization: evidence from undercutting Merensky Reef of the Bushveld Complex. Journal of Petrology, 58, 715–761.

Latypov, R., Chistyakova, S., Page, A. and Hornsey, R. (2015). Field Evidence for the In Situ Crystallization of the Merensky Reef. Journal of Petrology, 56, 2341–2372.

Lee, C. A. (1996). A review of mineralization in the Bushveld Complex and some other layered intrusions. In R. G. Cawthorn (Ed.), Layered intrusions, Vol. 15, Elsevier, pp. 103-145.

Lee, C. A, and Tredoux, M. (1986). Platinum-group element abundances in the lower and the lower critical zones of the eastern Bushveld Complex. Economic Geology, 81, 1087–1095.

Li, C., Maier, W., and de Waal, S.A. (2001). The role of magma mixing in the genesis of PGE mineralization in the Bushveld Complex: Thermodynamic calculations and new interpretations. Economic Geology, 96, 653–662.

Maier, W. D., and Barnes, S-J. (1999). Platinum-Group Elements in Silicate Rocks of the Lower, Critical and Main Zones at Union Section, Western Bushveld Complex. Journal of Petrology, 40, 1646–1671.

Maier, W. D. and Barnes, S. J. (2010). The petrogenesis of platinum-group element reefs in the Upper Main Zone of the Northern Lobe of the Bushveld Complex on the farm Moorddrift, South Africa. Economic Geology, 105, 841–854.

Maier, W. D., Barnes, S. -J. and van der Merwe, M. J. (2001). Platinum-group elements in the Pyroxenite Marker, Bushveld Complex: implications for the formation of the Main Zone. South African Journal of Geology, 104, 301–308.

Maier, W. D., de Klerk, L., Blaine, J., Manyeruke, T., Barnes, S. -J, Stevens, M. V. A., and Mavrogenes, J. A. (2008). Petrogenesis of contact-style PGE mineralization in the northern lobe of the Bushveld Complex: comparison of data from the farms Rooipoort, Townlands, Drenthe and Nonnenwerth. Mineralium Deposita, 43, 255–280.

Maier, W. D., Barnes, S. -J., and Groves, D. I. (2013). The Bushveld Complex, South Africa: formation of platinum–palladium, chrome- and vanadium rich layers via hydrodynamic sorting of a mobilized cumulate slurry in a large, relatively slowly cooling, subsiding magma chamber. Mineralium Deposita, 48, 1–56.

Manyeruke, T. D., Maier, W. D., and Barnes S. -J. (2005). Major and Trace Element Geochemistry of the Platreef on the farm Townlands, northern Bushveld Complex. South African Journal of Geology, 108, 381–396.

Mathez, E. A. (1995). Magmatic metasomatism and formation of the Merensky reef, Bushveld Complex. Contributions to Mineralogy and Petrology, 119, 277-286.

Mathez, E. A., Hunter, R. H. and Kinzler, R. (1997). Petrologic evolution of partially molten cumulate: the Atok section of the Bushveld Complex. Contributions to Mineralogy and Petrology, 129, 20–34.

Mayer, C. C., Jugo, P. J., Leybourne, M. I., Grobler, D. F., and Voinot, A. (2021). Strontium isotope stratigraphy through the Flatreef PGE-Ni-Cu mineralization at Turfspruit, northern limb of the Bushveld Igneous Complex: evidence of correlation with the Merensky Unit of the eastern and western limbs. Mineralium Deposita, 56, 59–72.

McDonald, I., Harmer, R. E., Holwell, D. A., Hughes, H. S. R., and Boyce, A. J. (2017). Cu-Ni-PGE mineralisation at the Aurora Project and potential for a new PGE province in the Northern Bushveld Main Zone. Ore Geology Reviews, 80, 1135–1159.

McDonald, I., and Holwell, D. A. (2007). Did lower zone magma conduits store PGE-rich sulfides that were later supplied to the Platreef? South African Journal of Geology, 110, 611–616.

McDonald, I., and Holwell, D. A. (2011). Geology of the Northern Bushveld Complex and the Setting and Genesis of the Platreef Ni-Cu-PGE Deposit. Society of Economic Geologists. Reviews in Economic Geology, 17, 297–327.

McDonald, I., Holwell, D. A., and Armitage, P. E. B. (2005). Geochemistry and mineralogy of the Platreef and “Critical Zone” cumulates of the Northern limb of the Bushveld Complex, South Africa: implications for Bushveld Stratigraphy and the development of PGE mineralisation. Mineralium Deposita, 40, 526 – 549.

McDonald, I., Holwell, D. A., and Wesley, B. (2009). Assessing the potential involvement of an early magma staging chamber in the generation of the Platreef Ni-Cu-PGE deposit in the northern limb of the Bushveld Complex: a pilot study of the Lower Zone Complex at Zwartfontein. Applied Earth Science (Transactions of the Institute of Mining and Metallurgy B), 118, 5–20.

Mitchell, A. A. (1990). The stratigraphy, petrography and mineralogy of the Main Zone of the Northwestern Bushveld Complex. South African Journal of Geology, 93, 818–831.

Mitchell, A. (2021). Comment on ‘Dating the Bushveld Complex: timing of crystallization, duration of magmatism, and cooling of the world’s largest layered intrusion and related rocks’ by J. S. Scoates, C. J. Wall, R. M. Friedman, D. Weis, E. A. Mathez & J. A. Van Tongeren (2021) Journal of Petrology, doi:10.1093/petrology/egaa107. Journal of Petrology, 62, 1−2.

Molyneux, T.G. (1970). The geology of the area in the vicinity of Magnet Heights, eastern Transvaal, with special reference to the magnetic iron ore. Special Publication Geological Society South Africa, 1, 228–241.

Mudd, G. M., Jowitt, S. M., and Werner, T. (2018). Global platinum group element resources, reserves and mining – A critical assessment. Science of the Total Environment, 622-623, 614–625

Mungall, J. E., Kamo, S. L. and McQuade, S. (2016). U-Pb geochronology documents out-of-sequence emplacement of ultramafic layers in the Bushveld Igneous Complex of South Africa: Nature Communications, 7, p. 13385

Naldrett, A. J. (1989). Stratiform PGE deposits in layered intrusions. Reviews in Economic Geology, 4, 135–166.

Naldrett, A. J., Gasparrini, E. C., Barnes, S. J., von Gruenewaldt, G. and Sharpe, M. R. (1986). The Upper Critical Zone of the Bushveld Complex and the origin of Merensky-type ores. Economic Geology, 81, 1105–1117.

Naldrett, A.J. and von Gruenewaldt, G. (1989). The association of platinum-group elements with chromite in layered intrusions and ophiolite complexes. Economic Geology, 84, 80–187.

Naldrett, A. J., Kinnaird, J., Wilson, A. H. and Chunnett, G. (2008). Concentration of PGE in the Earth's Crust with Special Reference to the Bushveld Complex. Earth Science Frontiers, 15, 264–297.

Naldrett, A. J., Wilson, A., Kinnaird, J. and Chunnett, G. (2009). PGE tenor and metal ratios within and below the Merensky Reef, Bushveld Complex: implications for its genesis. Journal of Petrology, 50, 625–659.

Nex, P. A. M., Cawthorn, R. G. and Kinnaird, J. A. (2002). Geochemical effects of magma addition: compositional reversals and decoupling of trends in the Main Zone of the western Bushveld Complex. Mineralogical Magazine, 66, 833–856.

Osbahr, I., Klemd, R., Oberthür, T., Brätz, H. and Schouwstra R. (2013). Platinum-group element distribution in base-metal sulfides of the Merensky Reef from the eastern and western Bushveld Complex, South Africa. Mineralium Deposita, 48, 211–232.

Osbahr, I., Oberthür, T., and Klemd, R. (2014). Platinum-group element distribution in base-metal sulphides of the UG2 chromitite, Bushveld Complex, South Africa – a reconnaissance study. Mineralium Deposita, 49, 655 – 665.

Penniston-Dorland, S. C., Wing, B. A., Nex, P. A. M., Kinnaird, J. A., Farquhar, J., Brown, M., and Sharman, E. R. (2008). Multiple sulfur isotopes reveal a primary magmatic origin for the Platreef PGE deposit, Bushveld Complex, South Africa. Geology, 36, 979–982.

Pronost, J., Harris, C., and Pin, C. (2008). Relationship between footwall composition, crustal contamination, and fluid-rock interaction in the Platreef, Bushveld Complex, South Africa. Mineralium Deposita, 43, 825–848.

Ripley, E. M., and Li, C., (2003). Sulfur isotope exchange and metal enrichment in the formation of magmatic Cu–Ni–(PGE) deposits. Economic Geology, 98, 635–641.

Roberts, M. D., Reid, D. L., Miller, J. A., Basson, I. J., Roberts, M. and Smith, D. (2007). The Merensky Cyclic Unit and its impact on footwall cumulates below Normal and Regional Pothole reef types in the Western Bushveld Complex. Mineralium Deposita, 42, 271–292.

Roelofse, F., and Ashwal, L. D. (2012). The Lower Main Zone in the Northern Limb of the Bushveld Complex - a > 1.3 km Thick Sequence of Intruded and Variably Contaminated Crystal Mushes. Journal of Petrology, 53, 1449–1476.

Scoates, J. S., Wall, C. J., Friedman, R. M., Weis, D., Mathez, E. A., and Van Tongeren, J. A. (2021). Dating the Bushveld Complex: timing of crystallization, duration of magmatism, and cooling of the world's largest layered intrusion and related rocks. Journal of Petrology, 62, 1-39.

Scoon, R. N., Costin, G., Mitchell, A., and Moine, B. (2020). Non-sequential injection of PGE-rich ultramafic sills in the Platreef unit at Akanani, northern limb of the Bushveld Complex: evidence from Sr and Nd isotopic systematics. Journal of Petrology, 61, egaa032

Seabrook, C. L., Cawthorn, R. G., and Kruger, J. F. (2005). The Merensky reef, Bushveld Complex: Mixing of minerals not mixing of magmas. Economic Geology, 100, 1191–1206.

Sharman-Harris, E. R., Kinnaird, J. A., Harris, C., and Horstmann, U. E. (2005). A new look at sulphide mineralisation of the northern limb, Bushveld Complex: a stable isotope study. Transactions of the Institution of Mining and Metallurgy, 114, B252–263.

Sharman, E. R., Penniston-Dorland, S. C., Kinnaird, J. A., Nex, P. A. M., Brown, M., and Wing, B., A. (2013). Primary Origin of Marginal Ni-Cu-(PGE) Mineralization in Layered Intrusions: $\Delta^{33}S$ evidence from the Platreef, Bushveld, South Africa. Economic Geology, 108, 365–377.

Sharpe, M. (1981). The chronology of magma influxes to the eastern compartment of the Bushveld Complex as exemplified by its marginal border groups. Journal of the Geological Society, 138, 307–326.

Sharpe, M. R. (1985). Strontium isotope evidence for preserved density stratification in the Main Zone of the Bushveld Complex, South Africa. Nature, 316, 119–126.

Sharpe, M. R., and Hulbert, L. J. (1985). Ultramafic Sills beneath the Eastern Bushveld Complex: Mobilized Suspensions of Early Lower Zone Cumulates in a Parental Magma with Boninitic Affinities. Economic Geology, 80, 849–871.

Smith, J. W., Holwell, D. A., McDonald, I. (2014). Precious and base metal geochemistry and mineralogy of the Grasvally Norite–Pyroxenite–Anorthosite (GNPA) member, northern Bushveld Complex, South Africa: implications for a multistage emplacement. Mineralium Deposita, 49, 667–692.

South African Committee for Stratigraphy (SACS). (1980). Stratigraphy of South Africa.Part1. In L. E. Kent, & (Comp) (Eds.), Lithostratigraphy of the Republic of South Africa, South West Africa/Namibia, and the Republics of Bophuthatswana, Transkei and Venda. (8 ed.)

Stephenson, H. (2019). The Platreef magma event at the world-class Turfspruit Ni-Cu-PGE deposit: implications for mineralisation processes and the Bushveld Complex stratigraphy. Ph.D. thesis, Cardiff University, Cardiff.

Tegner, C., Cawthorn, R. G. and Kruger, F. J. (2006). Cyclicity in the Main and Upper Zones of the Bushveld Complex, South Africa: Crystallization from a Zoned Magma Sheet. Journal of Petrology, 47, 2257–2279.

Teigler, B. (1990). Mineralogy, petrology and geochemistry of the Lower and Lower Critical Zones, northwestern Bushveld Complex. Ph.D. thesis, Rhodes University, Grahamstown.

Teigler, B. and Eales, H. V. (1993). Correlation between chromite composition and PGE mineralisation in the Critical Zone of the western Bushveld Complex. Mineralium Deposita, 28, 291–302.

Teigler, B., and Eales, H. V. (1996). The Lower and Critical Zones of the Western Limb of the Bushveld Complex as intersected by the Nooitgedacht Boreholes. Bulletin of the Geological Survey of South Africa, 111, p. 121.

Thormann, L., Buchspies, B., Mbohwa, C., and Kaltscmitt, M. (2017). PGE Production in Southern Africa, Part I: Production and Market Trends. Minerals, 7, 224.

van der Merwe, M. J. (1976). The Layered Sequence of the Potgietersrus Limb of the Bushveld Complex. Economic Geology, 71, 1337–1351.

van der Merwe, M. J. (1978). The geology of the basic and ultramafic rocks of the Potgietersrus limb of the Bushveld Complex: Unpublished dissertation, University of Witwatersrand.

van der Merwe, M. J. (2008). The geology and structure of the Rustenburg Layered Suite in the Potgietersrus/Mokopane area of the Bushveld Complex South Africa. Mineralium Deposita, 43, 405–419.

Vermaak, C. F. (1985). The UG2 layer - South Africa's slumbering chromitite giant. Chromium Review 1(5), 9–22.

Viljoen, M. J. (1999). The nature and origin of the Merensky Reef of the western Bushveld Complex based on geological facies and geophysical data. South African Journal of Geology, 102, 221–239.

Viljoen, M. J. (2016). The Bushveld Complex: Host to the World's Largest Platinum, Chromium and Vanadium Resources. Episodes, 39 (2): 239-268.

Viljoen, M. J. and Hieber, R. (1986). The Rustenburg Section of Rustenburg Platinum Mines Limited, with reference to the Merensky Reef. In: Anhaeusser, C. R. and Maske, S. (eds) Mineral Deposits of southern Africa. Vol. I & II. Johannesburg: Geological Society of South Africa, pp.1107–1134.

Viljoen, M. J., and Schürmann, L. W. (1998). Platinum group metals. In: Wilson, M. G., Anhaeusser, C. R., (eds) The mineral resources of South Africa. Council for Geosciences, Pretoria, pp 532-568.

von Gruenewaldt, G. (1973). The Main and Upper Zones of the Bushveld Complex in the Roossenekal area, Eastern Transvaal. Transactions of the Geological Society of South Africa, 76, 207–227.

von Gruenewaldt, G., Sharpe, M. R., and Hatton, C. J. (1985). A special issue devoted to the Bushveld Complex - The Bushveld Complex - Introduction and Review. Economic Geology, 80, 803–812.

Wagner, P. (1929). The Platinum Deposits and Mines of South Africa, Struick, London.

Webb, S. J., Cawthorn, R. G., Nguuri, T. and James, D. (2004). Gravity modeling of Bushveld Complex connectivity supported by Southern African seismic experiment results. South African Journal of Geology, 107, 207–218.

White, J. A. (1994). The Potgietersrus Prospect – Geology and exploration history XVth CMMI Congress, South Africa. Southern African Institute of Mining and Metallurgy, 3, 173–181.

Wilson, A. H. (2012). A chill sequence to the Bushveld Complex: insight into the first stage of emplacement and implications for the parental magmas. Journal of Petrology, 53, 1123–1168.

Wilson, A. H. (2015). The Earliest Stages of Emplacement of the Eastern Bushveld Complex: Development of the Lower Zone, Marginal Zone and Basal Ultramafic Sequence. Journal of Petrology, 56, 347–388.

Wilson, A., and Chunnett, G. (2006). Trace Element and Platinum Group Element Distributions and the Genesis of the Merensky Reef, Western Bushveld Complex. South African Journal of Petrology, 47, 2369–2403.

Yudovskaya, M. A., Kinnaird, J. A., Grobler, D. F., Costin, G., Abramova, V. D., Dunnet, T., Barnes, S. -J. (2017). Zonation of Merensky style platinum mineralization in Turfspruit thick reef facies (northern limb of the Bushveld Complex). Economic Geology, 112, 1333–1365.

Yudovskaya, M. A., Kinnaird, J. A., Sobolev, A. V., Kuzmin, D. V., McDonald, I. and Wilson, A. H. (2013). Petrogenesis of the Lower Zone olivine-rich cumulates beneath the Platreef and their correlation with recognized occurrences in the Bushveld Complex. Economic Geology, 108, 1923–1952.

Zeh, A., Ovtcharova, M., Wilson, A. H., and Schaltegger, U. (2015). The Bushveld Complex was emplaced and cooled in less than one million years–results of zirconology, and geotectonic implications. Earth and Planetary Science Letters, 418, 103–114.

LIST OF APPENDICES

APPENDIX A

For Chapter 4, Article 1.

Table A1: Online Resource 1. In situ Sr isotopic composition of plagioclase in relation to stratigraphic height, Flatreef, northern limb of the BC. Initial $^{87}Sr/^{86}Sr_i$ is recalculated to 2054.89 Ma (Zeh et al., 2015)

.

Sample	Depth (m)	Litho	Strat	Texture	Position	$^{87}Sr/^{86}Sr$	$^{87}Rb/^{86}Sr$	$^{87}Sr/^{86}Sr$ i	2SE
JDJ053	739.08	GN	MZ	c	core	0.708183	0.010634	0.7079	0.0002
JDJ053	739.08	GN	MZ	c	rim	0.708062	0.004110	0.7079	0.0002
JDJ053	739.08	GN	MZ	c	core	0.708531	0.027039	0.7077	0.0002
JDJ053	739.08	GN	MZ	c	core	0.708060	0.013887	0.7077	0.0002
JDJ053	739.08	GN	MZ	c	core	0.708241	0.011276	0.7079	0.0002
JDJ053	739.08	GN	MZ	c	core	0.708107	0.007469	0.7079	0.0002
JDJ053	739.08	GN	MZ	c	rim	0.707885	0.002568	0.7078	0.0002
JDJ054	742.37	SAN	HW2	c	core	0.708143	0.007173	0.7079	0.0003
JDJ054	742.37	SAN	HW2	c	rim	0.708152	0.009986	0.7079	0.0002
JDJ054	742.37	SAN	HW2	c	core	0.708034	0.008426	0.7078	0.0002
JDJ054	742.37	SAN	HW2	c	rim	0.707918	0.003606	0.7078	0.0002
JDJ054	742.37	SAN	HW2	c	core	0.707849	0.001112	0.7078	0.0002
JDJ054	742.37	SAN	HW2	c	rim	0.707775	0.001483	0.7077	0.0002
JDJ056	748.30	MAN	HW2	c	core	0.707613	0.003509	0.7075	0.0002
JDJ056	748.30	MAN	HW2	c	core	0.708207	0.019442	0.7076	0.0002
JDJ056	748.30	MAN	HW2	c	core	0.707862	0.006837	0.7077	0.0002
JDJ059	760.37	MAN	HW2	c	core	0.708140	0.005381	0.7080	0.0002
JDJ059	760.37	MAN	HW2	c	core	0.708122	0.002331	0.7081	0.0002
JDJ059	760.37	MAN	HW2	c	core	0.708160	0.007193	0.7080	0.0002
JDJ061	765.98	MAN	HW2	c	core	0.708195	0.017049	0.7077	0.0002
JDJ061	765.98	MAN	HW2	c	core	0.707929	0.005871	0.7078	0.0002
JDJ061	765.98	MAN	HW2	c	core	0.707828	0.002652	0.7078	0.0002
JDJ063	772.93	MAN	HW2	c	core	0.707858	0.003639	0.7078	0.0002
JDJ063	772.93	MAN	HW2	c	core	0.707967	0.002512	0.7079	0.0002
JDJ063	772.93	MAN	HW2	c	rim	0.708126	0.007196	0.7079	0.0002
JDJ064	775.52	MAN	HW2	c	core	0.707928	0.005684	0.7078	0.0002
JDJ064	775.52	MAN	HW2	c	core	0.707917	0.001590	0.7079	0.0002
JDJ064	775.52	MAN	HW2	c	core	0.708147	0.008701	0.7079	0.0002
JDJ064	775.52	MAN	HW2	c	core	0.707888	0.002372	0.7078	0.0002
JDJ065	779.37	MAN	HW2	c	core	0.707733	0.001580	0.7077	0.0002
JDJ065	779.37	MAN	HW2	c	core	0.708055	0.012518	0.7077	0.0002
JDJ065	779.37	MAN	HW2	c	rim	0.707994	0.013425	0.7076	0.0002
JDJ065	779.37	MAN	HW2	c	core	0.708031	0.005975	0.7079	0.0002
JDJ065	779.37	MAN	HW2	c	core	0.708233	0.009048	0.7080	0.0002
JDJ065	779.37	MAN	HW2	c	core	0.707677	0.009113	0.7074	0.0002
JDJ069A	787.38	N	HW2	c	core	0.707765	0.016200	0.7073	0.0002
JDJ069A	787.38	N	HW2	c	rim	0.707796	0.010203	0.7075	0.0002
JDJ069A	787.38	N	HW2	c	core	0.708419	0.032834	0.7075	0.0002
JDJ069A	787.38	N	HW2	c	rim	0.709103	0.056498	0.7075	0.0002

Sample	Depth (m)	Litho	Strat	Texture	Position	$^{87}Sr/^{86}Sr$	$^{87}Rb/^{86}Sr$	$^{87}Sr/^{86}Sr$ i	2SE
JDJ069A	787.38	N	HW2	c	core	0.707361	0.005552	0.7072	0.0002
JDJ069B	787.69	MAN	HW2	c	core	0.707793	0.015961	0.7073	0.0002
JDJ069B	787.69	MAN	HW2	c	core	0.707904	0.013519	0.7075	0.0002
JDJ069B	787.69	MAN	HW2	c	rim	0.707492	0.001681	0.7074	0.0002
JDJ069B	787.69	MAN	HW2	c	core	0.707509	0.001897	0.7075	0.0002
JDJ069B	787.69	MAN	HW2	c	rim	0.707480	0.000654	0.7075	0.0002
JDJ069B	787.69	MAN	HW2	c	core	0.707606	0.002141	0.7075	0.0002
JDJ070	787.85	MAN	HW2	c	line	0.707309	0.001332	0.7073	0.0003
JDJ070	787.85	MAN	HW2	c	line	0.707303	0.004645	0.7072	0.0002
JDJ070	787.85	MAN	HW2	c	line	0.707496	0.007538	0.7073	0.0003
JDJ071	789.30	SAN	HW2	c	core	0.708352	0.005182	0.7082	0.0002
JDJ071	789.30	SAN	HW2	c	core	0.707866	0.000775	0.7078	0.0002
JDJ071	789.30	SAN	HW2	c	core	0.707616	0.005255	0.7075	0.0002
JDJ072	789.74	N	HW1	c	core	0.707395	0.000727	0.7074	0.0002
JDJ072	789.74	N	HW1	c	rim	0.707450	0.000739	0.7074	0.0002
JDJ072	789.74	N	HW1	c	core	0.707915	0.004423	0.7078	0.0002
JDJ072	789.74	N	HW1	c	rim	0.707759	0.003529	0.7077	0.0002
JDJ072	789.74	N	HW1	c	core	0.707670	0.002225	0.7076	0.0002
JDJ072	789.74	N	HW1	c	core	0.707470	0.000467	0.7075	0.0002
JDJ072	789.74	N	HW1	c	rim	0.707456	0.001255	0.7074	0.0002
JDJ073	793.45	N	HW1	c	line	0.708073	0.001905	0.7080	0.0003
JDJ073	793.45	N	HW1	c	line	0.708014	0.003154	0.7079	0.0002
JDJ073	793.45	N	HW1	c	line	0.708248	0.004500	0.7081	0.0002
JDJ074	797.00	N	HW1	c	core	0.707532	0.000965	0.7075	0.0002
JDJ074	797.00	N	HW1	c	rim	0.707936	0.004295	0.7078	0.0002
JDJ074	797.00	N	HW1	c	core	0.707334	0.001478	0.7073	0.0002
JDJ074	797.00	N	HW1	c	core	0.707664	0.009161	0.7074	0.0002
JDJ074	797.00	N	HW1	c	core	0.707849	0.005065	0.7077	0.0002
JDJ074	797.00	N	HW1	c	rim	0.707909	0.006017	0.7077	0.0002
JDJ074	797.00	N	HW1	c	core	0.707925	0.012242	0.7076	0.0002
JDJ076	802.43	N	HW1	c	line	0.707970	0.003461	0.7079	0.0002
JDJ076	802.43	N	HW1	c	line	0.707792	0.001133	0.7078	0.0003
JDJ076	802.43	N	HW1	c	line	0.707888	0.000802	0.7079	0.0003
JDJ077	807.60	N	HW1	c	line	0.707687	0.001201	0.7077	0.0002
JDJ077	807.60	N	HW1	c	line	0.707798	0.001659	0.7077	0.0002
JDJ077	807.60	N	HW1	c	line	0.707589	0.009543	0.7073	0.0002
JDJ078	810.60	N	HW1	c	core	0.707597	0.001993	0.7075	0.0002
JDJ078	810.60	N	HW1	c	core	0.707418	0.004565	0.7073	0.0002
JDJ078	810.60	N	HW1	c	core	0.707612	0.004759	0.7075	0.0002
JDJ078	810.60	N	HW1	c	core	0.707593	0.004326	0.7075	0.0002
JDJ079	811.06	N	HW1	c	line	0.707904	0.000926	0.7079	0.0003
JDJ079	811.06	N	HW1	c	line	0.707798	0.002155	0.7077	0.0002
JDJ079	811.06	N	HW1	c	line	0.707388	0.001426	0.7073	0.0003
JDJ080	811.49	N	HW1	c	core	0.707976	0.001896	0.7079	0.0002
JDJ080	811.49	N	HW1	c	core	0.707592	0.004421	0.7075	0.0002
JDJ080	811.49	N	HW1	c	core	0.707912	0.007905	0.7077	0.0002
JDJ082	816.02	N	HW1	c	core	0.707616	0.000597	0.7076	0.0002
JDJ082	816.02	N	HW1	c	core	0.707444	0.001162	0.7074	0.0002
JDJ082	816.02	N	HW1	c	core	0.708266	0.019826	0.7077	0.0002
JDJ082	816.02	N	HW1	c	core	0.707852	0.004146	0.7077	0.0002
JDJ083	819.00	N	HW1	c	core	0.707581	0.001068	0.7075	0.0002

Sample	Depth (m)	Litho	Strat	Texture	Position	$^{87}Sr/^{86}Sr$	$^{87}Rb/^{86}Sr$	$^{87}Sr/^{86}Sr$ i	2SE
JDJ083	819.00	N	HW1	c	core	0.707547	0.001978	0.7075	0.0002
JDJ083	819.00	N	HW1	c	core	0.707388	0.000771	0.7074	0.0002
JDJ085	822.78	N	HW1	c	core	0.707366	0.005837	0.7072	0.0002
JDJ085	822.78	N	HW1	c	core	0.708889	0.054291	0.7073	0.0002
JDJ085	822.78	N	HW1	c	rim	0.707396	0.003806	0.7073	0.0002
JDJ085	822.78	N	HW1	c	core	0.707550	0.003030	0.7075	0.0002
JDJ086	824.42	PX	HW1	i	core	0.707818	0.000252	0.7078	0.0001
JDJ086	824.42	PX	HW1	i	core	0.707436	0.006002	0.7073	0.0001
JDJ086	824.42	PX	HW1	i	core	0.707467	0.000719	0.7074	0.0001
JDJ086	824.42	PX	HW1	i	core	0.707505	0.000582	0.7075	0.0001
JDJ086	824.42	PX	HW1	i	core	0.707691	0.000363	0.7077	0.0001
JDJ086	824.42	PX	HW1	i	core	0.707502	0.000227	0.7075	0.0001
JDJ087	825.17	N	HW1	c	core	0.707701	0.000818	0.7077	0.0002
JDJ087	825.17	N	HW1	c	core	0.707447	0.002124	0.7074	0.0002
JDJ087	825.17	N	HW1	c	core	0.707623	0.000876	0.7076	0.0002
JDJ087	825.17	N	HW1	c	core	0.707887	0.010494	0.7076	0.0002
JDJ092	834.32	FPX	HW1	i	core	0.707921	0.005460	0.7078	0.0001
JDJ092	834.32	FPX	HW1	i	core	0.708074	0.007628	0.7079	0.0001
JDJ092	834.32	FPX	HW1	i	core	0.707818	0.005694	0.7077	0.0001
JDJ092	834.32	FPX	HW1	i	core	0.707927	0.008678	0.7077	0.0001
JDJ097	848.63	FPX	BAR	i	core	0.707788	0.003731	0.7077	0.0002
JDJ097	848.63	FPX	BAR	i	core	0.708202	0.006108	0.7080	0.0002
JDJ097	848.63	FPX	BAR	i	rim	0.708441	0.004724	0.7083	0.0002
JDJ097	848.63	FPX	BAR	i	core	0.708401	0.003583	0.7083	0.0002
JDJ098	849.35	FPX-CR	BAR	i	core	0.709011	0.035972	0.7080	0.0002
JDJ098	849.35	FPX-CR	BAR	i	core	0.708482	0.005361	0.7083	0.0002
JDJ098	849.35	FPX-CR	BAR	i	core	0.708020	0.003145	0.7079	0.0002
JDJ098	849.35	FPX-CR	BAR	i	core	0.707969	0.005720	0.7078	0.0002
JDJ099	851.88	FPX	BAR	i	core	0.708208	0.002261	0.7081	0.0002
JDJ099	851.88	FPX	BAR	i	core	0.708045	0.001271	0.7080	0.0002
JDJ099	851.88	FPX	BAR	i	core	0.708134	0.001857	0.7081	0.0002
JDJ104	868.63	FPX	MD1	i	core	0.708456	0.001389	0.7084	0.0002
JDJ104	868.63	FPX	MD1	i	core	0.707896	0.001996	0.7078	0.0002
JDJ104	868.63	FPX	MD1	i	core	0.708174	0.008082	0.7079	0.0002
JDJ104	868.63	FPX	MD1	i	core	0.710554	0.036093	0.7095	0.0002
JDJ105	871.20	FPX	MD1	i	core	0.707942	0.002130	0.7079	0.0002
JDJ105	871.20	FPX	MD1	i	core	0.708361	0.052223	0.7068	0.0002
JDJ105	871.20	FPX	MD1	i	rim	0.708015	0.005227	0.7079	0.0002
JDJ105	871.20	FPX	MD1	i	core	0.707788	0.001319	0.7077	0.0002
JDJ107	877.07	FPX	MD1	i	core	0.707828	0.013152	0.7074	0.0003
JDJ107	877.07	FPX	MD1	i	core	0.706944	0.002357	0.7069	0.0003
JDJ107	877.07	FPX	MD1	i	core	0.707971	0.003813	0.7079	0.0002
JDJ107	877.07	FPX	MD1	i	core	0.708109	0.002887	0.7080	0.0002
JDJ109	884.50	FPX	MD1	i	core	0.707710	0.002786	0.7076	0.0001
JDJ109	884.50	FPX	MD1	i	core	0.707456	0.002617	0.7074	0.0002
JDJ109	884.50	FPX	MD1	i	core	0.707634	0.001298	0.7076	0.0002
JDJ109	884.50	FPX	MD1	i	core	0.708215	0.017054	0.7077	0.0002
JDJ112A	888.80	FPX	M2	i	core	0.707839	0.001248	0.7078	0.0003
JDJ112A	888.80	FPX	M2	i	core	0.707602	0.002506	0.7075	0.0003
JDJ112A	888.80	FPX	M2	i	core	0.707899	0.002695	0.7078	0.0003
JDJ112B	888.98	FPX	M2	i	core	0.707746	0.010673	0.7074	0.0002

Sample	Depth (m)	Litho	Strat	Texture	Position	$^{87}Sr/^{86}Sr$	$^{87}Rb/^{86}Sr$	$^{87}Sr/^{86}Sr$ i	2SE
JDJ112B	888.98	FPX	M2	i	core	0.707994	0.010381	0.7077	0.0002
JDJ112B	888.98	FPX	M2	i	core	0.707405	0.002687	0.7073	0.0002
JDJ117	906.86	OPX	M2	i	core	0.709376	0.000559	0.7094	0.0003
JDJ117	906.86	OPX	M2	i	core	0.709695	0.002073	0.7096	0.0003
JDJ117	906.86	OPX	M2	i	rim	0.709416	0.000103	0.7094	0.0003
JDJ117	906.86	OPX	M2	i	core	0.710108	0.000190	0.7101	0.0003
JDJ117	906.86	OPX	M2	i	rim	0.709599	0.000078	0.7096	0.0002
JDJ119	912.27	FPX	M2	i	core	0.708608	0.000361	0.7086	0.0001
JDJ119	912.27	FPX	M2	i	core	0.709071	0.014984	0.7086	0.0001
JDJ119	912.27	FPX	M2	i	core	0.708691	0.001093	0.7087	0.0002
JDJ119	912.27	FPX	M2	i	core	0.708894	0.010480	0.7086	0.0001
JDJ120	915.35	FPX	M2	i	core	0.707420	0.000195	0.7074	0.0001
JDJ120	915.35	FPX	M2	i	core	0.707453	0.000454	0.7074	0.0002
JDJ120	915.35	FPX	M2	i	core	0.707341	0.000522	0.7073	0.0001
JDJ120	915.35	FPX	M2	i	core	0.707268	0.000805	0.7072	0.0001
JDJ121	918.12	MPV	M2	i	core	0.707890	0.004169	0.7078	0.0002
JDJ121	918.12	MPV	M2	i	core	0.708078	0.008615	0.7078	0.0002
JDJ121	918.12	MPV	M2	i	core	0.707871	0.002742	0.7078	0.0002
JDJ123	922.84	FPX	M2	i	core	0.707480	0.010739	0.7072	0.0002
JDJ123	922.84	FPX	M2	i	core	0.707387	0.003866	0.7073	0.0002
JDJ123	922.84	FPX	M2	i	core	0.706995	0.001322	0.7070	0.0002
JDJ123	922.84	FPX	M2	i	core	0.707630	0.009922	0.7073	0.0002
JDJ123	922.84	FPX	M2	i	core	0.707663	0.008047	0.7074	0.0002
JDJ125A	926.97	FPX	$M1_U$	i	core	0.707305	0.003860	0.7072	0.0002
JDJ125A	926.97	FPX	$M1_U$	i	core	0.706952	0.001171	0.7069	0.0002
JDJ125A	926.97	FPX	$M1_U$	i	core	0.708391	0.023253	0.7077	0.0002
JDJ125A	926.97	FPX	$M1_U$	i	rim	0.707626	0.012206	0.7073	0.0003
JDJ125A	926.97	FPX	$M1_U$	i	core	0.707241	0.001909	0.7072	0.0002
JDJ125B	927.32	PPXT	$M1_U$	i	core	0.707601	0.004514	0.7075	0.0002
JDJ125B	927.32	PPXT	$M1_U$	i	core	0.707628	0.010468	0.7073	0.0002
JDJ125B	927.32	PPXT	$M1_U$	i	core	0.707254	0.010026	0.7070	0.0002
JDJ125B	927.32	PPXT	$M1_U$	i	core	0.707217	0.003550	0.7071	0.0002
JDJ125B	927.32	PPXT	$M1_U$	i	core	0.707271	0.006457	0.7071	0.0002
JDJ125B	927.32	PPXT	$M1_U$	i	core	0.707727	0.008536	0.7075	0.0002
JDJ126A	928.39	OPX	$M1_U$	i	core	0.707419	0.007656	0.7072	0.0001
JDJ126A	928.39	OPX	$M1_U$	i	core	0.707229	0.003980	0.7071	0.0002
JDJ126A	928.39	OPX	$M1_U$	i	core	0.707267	0.003707	0.7072	0.0001
JDJ126A	928.39	OPX	$M1_U$	i	core	0.707340	0.004233	0.7072	0.0002
JDJ126B	928.47	OPX-CR	$M1_U$	i	core	0.707357	0.001289	0.7073	0.0001
JDJ126B	928.47	OPX-CR	$M1_U$	i	core	0.707141	0.000966	0.7071	0.0001
JDJ126B	928.47	OPX-CR	$M1_U$	i	core	0.707180	0.002454	0.7071	0.0002
JDJ126B	928.47	OPX-CR	$M1_U$	i	core	0.708383	0.025802	0.7076	0.0002
JDJ126B	928.47	OPX-CR	$M1_U$	i	core	0.707329	0.004786	0.7072	0.0001
JDJ126B	928.47	OPX-CR	$M1_U$	i	core	0.707407	0.000454	0.7074	0.0002
JDJ127	930.83	OPX	$M1_U$	i	core	0.707343	0.010659	0.7070	0.0001
JDJ127	930.83	OPX	$M1_U$	i	core	0.707544	0.004169	0.7074	0.0001
JDJ127	930.83	OPX	$M1_U$	i	core	0.707619	0.002628	0.7075	0.0001
JDJ127	930.83	OPX	$M1_U$	i	core	0.707496	0.006761	0.7073	0.0001
JDJ127	930.83	OPX	$M1_U$	i	core	0.707564	0.002946	0.7075	0.0001
JDJ127	930.83	OPX	$M1_U$	i	core	0.707160	0.003857	0.7070	0.0001
JDJ127	930.83	OPX	$M1_U$	i	core	0.707075	0.002086	0.7070	0.0002

Sample	Depth (m)	Litho	Strat	Texture	Position	$^{87}Sr/^{86}Sr$	$^{87}Rb/^{86}Sr$	$^{87}Sr/^{86}Sr$ i	2SE
JDJ127	930.83	OPX	$M1_U$	i	core	0.707383	0.004450	0.7073	0.0001
JDJ128	931.39	HA	$M1_L$	i	core	0.707220	0.014398	0.7068	0.0002
JDJ128	931.39	HA	$M1_L$	i	core	0.706955	0.002058	0.7069	0.0002
JDJ128	931.39	HA	$M1_L$	i	core	0.707197	0.002523	0.7071	0.0002
JDJ128	931.39	HA	$M1_L$	i	core	0.707351	0.009772	0.7071	0.0002
JDJ129	934.20	HA	$M1_L$	i	core	0.707800	0.040476	0.7066	0.0002
JDJ129	934.20	HA	$M1_L$	i	core	0.707273	0.001302	0.7072	0.0002
JDJ129	934.20	HA	$M1_L$	i	core	0.707417	0.016336	0.7069	0.0002
JDJ129	934.20	HA	$M1_L$	i	core	0.707533	0.005128	0.7074	0.0002
JDJ129	934.20	HA	$M1_L$	i	core	0.707419	0.003880	0.7073	0.0002
JDJ129	934.20	HA	$M1_L$	i	core	0.707054	0.001059	0.7070	0.0002
JDJ133	942.27	HA	$M1_L$	i	core	0.707412	0.010553	0.7071	0.0007
JDJ133	942.27	HA	$M1_L$	i	core	0.707855	0.019742	0.7073	0.0003
JDJ133	942.27	HA	$M1_L$	i	core	0.706958	0.001867	0.7069	0.0003
JDJ133	942.27	HA	$M1_L$	i	core	0.707602	0.019987	0.7070	0.0003
JDJ136	945.53	HA	$M1_L$	i	core	0.707213	0.001876	0.7072	0.0002
JDJ136	945.53	HA	$M1_L$	i	core	0.707177	0.005647	0.7070	0.0002
JDJ136	945.53	HA	$M1_L$	i	core	0.707089	0.001695	0.7070	0.0002
JDJ136	945.53	HA	$M1_L$	i	core	0.707162	0.003630	0.7071	0.0002
JDJ136	945.53	HA	$M1_L$	i	core	0.707451	0.006341	0.7073	0.0002
JDJ137	948.08	HA	$M1_L$	i	core	0.707119	0.002519	0.7070	0.0001
JDJ137	948.08	HA	$M1_L$	i	core	0.707693	0.018544	0.7072	0.0001
JDJ137	948.08	HA	$M1_L$	i	core	0.707317	0.004575	0.7072	0.0001
JDJ137	948.08	HA	$M1_L$	i	core	0.707357	0.004276	0.7072	0.0001
JDJ137	948.08	HA	$M1_L$	i	core	0.707174	0.002986	0.7071	0.0001
JDJ139	953.63	HA	$M1_L$	i	core	0.706830	0.000369	0.7068	0.0002
JDJ139	953.63	HA	$M1_L$	i	core	0.707154	0.000481	0.7071	0.0002
JDJ139	953.63	HA	$M1_L$	i	core	0.707097	0.001053	0.7071	0.0002
JDJ139	953.63	HA	$M1_L$	i	core	0.707683	0.027274	0.7069	0.0002
JDJ139	953.63	HA	$M1_L$	i	core	0.706904	0.000824	0.7069	0.0002
JDJ141	960.06	FPX	$M1_L$	i	core	0.707249	0.006422	0.7071	0.0002
JDJ141	960.06	FPX	$M1_L$	i	core	0.707125	0.004748	0.7070	0.0002
JDJ141	960.06	FPX	$M1_L$	i	core	0.707357	0.000325	0.7073	0.0002
JDJ143	962.00	FPX	FCU	i	core	0.706921	0.000485	0.7069	0.0001
JDJ143	962.00	FPX	FCU	i	core	0.707342	0.009182	0.7071	0.0001
JDJ143	962.00	FPX	FCU	i	core	0.707191	0.005867	0.7070	0.0001
JDJ143	962.00	FPX	FCU	i	core	0.707166	0.001971	0.7071	0.0001
JDJ147	975.63	FPX	FCU	i	core	0.707071	0.002337	0.7070	0.0001
JDJ147	975.63	FPX	FCU	i	core	0.706817	0.003525	0.7067	0.0002
JDJ147	975.63	FPX	FCU	i	core	0.707004	0.009609	0.7067	0.0001
JDJ147	975.63	FPX	FCU	i	core	0.706678	0.001120	0.7066	0.0001
JDJ147	975.63	FPX	FCU	i	core	0.706944	0.002950	0.7069	0.0001
JDJ147	975.63	FPX	FCU	i	core	0.706902	0.004411	0.7068	0.0002
JDJ152	981.20	FPX	FCU	i	core	0.706881	0.002260	0.7068	0.0002
JDJ152	981.20	FPX	FCU	i	core	0.706792	0.015263	0.7063	0.0002
JDJ152	981.20	FPX	FCU	i	core	0.706795	0.004130	0.7067	0.0002
JDJ154	983.20	N	FCU	c	core	0.706721	0.001559	0.7067	0.0002
JDJ154	983.20	N	FCU	c	rim	0.706376	0.004650	0.7062	0.0002
JDJ154	983.20	N	FCU	c	core	0.706806	0.004663	0.7067	0.0002
JDJ154	983.20	N	FCU	c	core	0.706529	0.003407	0.7064	0.0002
JDJ157A	989.06	FPX	FCU	c	core	0.706607	0.005712	0.7064	0.0002

Sample	Depth (m)	Litho	Strat	Texture	Position	$^{87}Sr/^{86}Sr$	$^{87}Rb/^{86}Sr$	$^{87}Sr/^{86}Sr$ i	2SE
JDJ157A	989.06	FPX	FCU	c	core	0.706649	0.004951	0.7065	0.0002
JDJ157A	989.06	FPX	FCU	c	core	0.706732	0.011220	0.7064	0.0002
JDJ157A	989.06	FPX	FCU	c	core	0.707292	0.042881	0.7060	0.0002
JDJ157B	989.35	MAN	FCU	c	core	0.706500	0.008456	0.7063	0.0002
JDJ157B	989.35	MAN	FCU	c	core	0.706637	0.003622	0.7065	0.0002
JDJ157B	989.35	MAN	FCU	c	core	0.706429	0.001206	0.7064	0.0002
JDJ158	989.44	N	FCU	c	core	0.706657	0.002634	0.7066	0.0002
JDJ158	989.44	N	FCU	c	core	0.706533	0.003378	0.7064	0.0002
JDJ158	989.44	N	FCU	c	core	0.706321	0.003613	0.7062	0.0003
JDJ163	1003.34	N	FCU	c	core	0.706762	0.010306	0.7065	0.0002
JDJ163	1003.34	N	FCU	c	rim	0.706618	0.009114	0.7064	0.0001
JDJ163	1003.34	N	FCU	c	core	0.706705	0.005666	0.7065	0.0001
JDJ163	1003.34	N	FCU	c	core	0.706759	0.010209	0.7065	0.0001
JDJ163	1003.34	N	FCU	c	rim	0.706668	0.005610	0.7065	0.0001
JDJ170	1028.28	N	FCU	c	core	0.706689	0.009866	0.7064	0.0002
JDJ170	1028.28	N	FCU	c	core	0.706486	0.003863	0.7064	0.0002
JDJ170	1028.28	N	FCU	c	core	0.706764	0.020727	0.7062	0.0002
JDJ170	1028.28	N	FCU	c	core	0.706514	0.002559	0.7064	0.0002
JDJ170	1028.28	N	FCU	c	core	0.706680	0.003650	0.7066	0.0002

SAN, MAN, N, FPX, OPX, PPXT, MPV and HA indicate spotted anorthosite, mottled anorthosite, norite, feldspathic pyroxenite, orthopyroxenite, pegmatoidal pyroxenite, mafic pegmatoidal vein and harzburgite, respectively.
HW1, BAR, MD1, M1U, M1L and FCU indicate hanging wall 1, Bastard reef, Middling unit, M1 Upper, M1 Lower and the Footwall Cyclic Unit, respectively.

Table A2: Online Resource 2. In situ anorthite content of plagioclase in relation to stratigraphic height, Flatreef, northern limb of the BC.

Sample	Depth	Litho	Strat	An
JDJ053	739.08	GN	MZ	68
JDJ053	739.08	GN	MZ	67
JDJ053	739.08	GN	MZ	69
JDJ053	739.08	GN	MZ	76
JDJ053	739.08	GN	MZ	68
JDJ053	739.08	GN	MZ	69
JDJ053	739.08	GN	MZ	69
JDJ053	739.08	GN	MZ	68
JDJ053	739.08	GN	MZ	70
JDJ053	739.08	GN	MZ	73
JDJ058	756.46	MAN	HW2	71
JDJ058	756.46	MAN	HW2	71
JDJ058	756.46	MAN	HW2	71
JDJ058	756.46	MAN	HW2	69
JDJ058	756.46	MAN	HW2	72
JDJ064	775.52	MAN	HW2	69
JDJ064	775.52	MAN	HW2	63
JDJ064	775.52	MAN	HW2	73
JDJ064	775.52	MAN	HW2	67
JDJ064	775.52	MAN	HW2	73
JDJ064	775.52	MAN	HW2	69
JDJ070	787.85	MAN	HW2	72
JDJ070	787.85	MAN	HW2	70
JDJ070	787.85	MAN	HW2	72
JDJ070	787.85	MAN	HW2	76
JDJ070	787.85	MAN	HW2	76
JDJ070	787.85	MAN	HW2	73
JDJ070	787.85	MAN	HW2	76
JDJ078	810.6	N	HW1	71
JDJ078	810.6	N	HW1	70
JDJ078	810.6	N	HW1	69
JDJ078	810.6	N	HW1	72
JDJ086	824.42	FPX	HW1	73
JDJ086	824.42	FPX	HW1	73
JDJ086	824.42	FPX	HW1	71
JDJ088	825.62	FPX	HW1	65
JDJ088	825.62	FPX	HW1	67
JDJ088	825.62	FPX	HW1	60
JDJ088	825.62	FPX	HW1	63
JDJ088	825.62	FPX	HW1	63
JDJ088	825.62	FPX	HW1	69
JDJ092	834.32	FPX	HW1	54
JDJ092	834.32	FPX	HW1	61
JDJ092	834.32	FPX	HW1	62

Sample	Depth	Litho	Strat	An
JDJ092	834.32	FPX	HW1	61
JDJ092	834.32	FPX	HW1	58
JDJ097	848.63	FPX	BAR	63
JDJ097	848.63	FPX	BAR	61
JDJ097	848.63	FPX	BAR	73
JDJ097	848.63	FPX	BAR	67
JDJ097	848.63	FPX	BAR	61
JDJ098	849.35	FPX-CR	BAR	57
JDJ098	849.35	FPX-CR	BAR	56
JDJ098	849.35	FPX-CR	BAR	57
JDJ105	871.2	FPX	MD1	75
JDJ105	871.2	FPX	MD1	63
JDJ105	871.2	FPX	MD1	63
JDJ105	871.2	FPX	MD1	64
JDJ105	871.2	FPX	MD1	64
JDJ109	884.5	FPX	MD1	60
JDJ109	884.5	FPX	MD1	64
JDJ109	884.5	FPX	MD1	75
JDJ109	884.5	FPX	MD1	75
JDJ109	884.5	FPX	MD1	73
JDJ109	884.5	FPX	MD1	60
JDJ109	884.5	FPX	MD1	61
JDJ110	885.22	FPX	M2	75
JDJ110	885.22	FPX	M2	76
JDJ110	885.22	FPX	M2	76
JDJ110	885.22	FPX	M2	76
JDJ110	885.22	FPX	M2	77
JDJ112	888.8	FPX	M2	75
JDJ112	888.8	FPX	M2	76
JDJ112	888.8	FPX	M2	76
JDJ112	888.8	FPX	M2	66
JDJ112	888.8	FPX	M2	67
JDJ119	912.27	FPX	M2	72
JDJ119	912.27	FPX	M2	72
JDJ119	912.27	FPX	M2	71
JDJ119	912.27	FPX	M2	69
JDJ120	915.35	FPX	M2	67
JDJ120	915.35	FPX	M2	71
JDJ120	915.35	FPX	M2	70
JDJ120	915.35	FPX	M2	66
JDJ120	915.35	FPX	M2	65
JDJ121	918.12	MPV	M2	67
JDJ121	918.12	MPV	M2	69
JDJ121	918.12	MPV	M2	65
JDJ124	925.28	FPX	M2	57
JDJ124	925.28	FPX	M2	56
JDJ124	925.28	FPX	M2	56

Sample	Depth	Litho	Strat	An
JDJ124	925.28	FPX	M2	58
JDJ126	928.39	OPX	M1U	60
JDJ126	928.39	OPX	M1U	60
JDJ126	928.39	OPX	M1U	59
JDJ126	928.39	OPX	M1U	61
JDJ126	928.39	OPX	M1U	57
JDJ126	928.39	OPX	M1U	60
JDJ127	930.83	OPX	M1U	66
JDJ127	930.83	OPX	M1U	64
JDJ127	930.83	OPX	M1U	64
JDJ127	930.83	OPX	M1U	58
JDJ127	930.83	OPX	M1U	59
JDJ127	930.83	OPX	M1U	60
JDJ131	935.12	OPX	M1L	62
JDJ131	935.12	OPX	M1L	60
JDJ137	948.08	HA	M1L	61
JDJ137	948.08	HA	M1L	64
JDJ137	948.08	HA	M1L	62
JDJ143	958.5	FPX	FCU	59
JDJ143	958.5	FPX	FCU	60
JDJ143	958.5	FPX	FCU	66
JDJ149	976.54	MAN	FCU	78
JDJ149	976.54	MAN	FCU	80
JDJ149	976.54	MAN	FCU	80
JDJ149	976.54	MAN	FCU	80
JDJ149	976.54	MAN	FCU	79
JDJ149	976.54	MAN	FCU	79
JDJ155	986.22	N	FCU	73
JDJ155	986.22	N	FCU	77
JDJ155	986.22	N	FCU	75
JDJ155	986.22	N	FCU	75
JDJ155	986.22	N	FCU	75
JDJ155	986.22	N	FCU	79
JDJ155	986.22	N	FCU	80
JDJ163	1003.34	N	FCU	74
JDJ163	1003.34	N	FCU	73
JDJ163	1003.34	N	FCU	74
JDJ163	1003.34	N	FCU	76
JDJ163	1003.34	N	FCU	76
JDJ163	1003.34	N	FCU	72
JDJ163	1003.34	N	FCU	69
JDJ163	1003.34	N	FCU	76

MAN, N, FPX, OPX and MPV indicate mottled anorthosite, norite, feldspathic pyroxenite orthopyroxenite and mafic pegmatoidal vein and harzburgite, respectively.
HW1, BAR, MD1, M1U, M1L and FCU indicate hanging wall 1, Bastard Reef, Middling unit, M1 Upper, M1 Lower and the Footwall Cyclic Unit, respectively.

Table A3: Online Resource 3_Measured in situ Sr isotope compositions of reference glass standard BHVO-2G (with 2SE error bars) over the course of the study

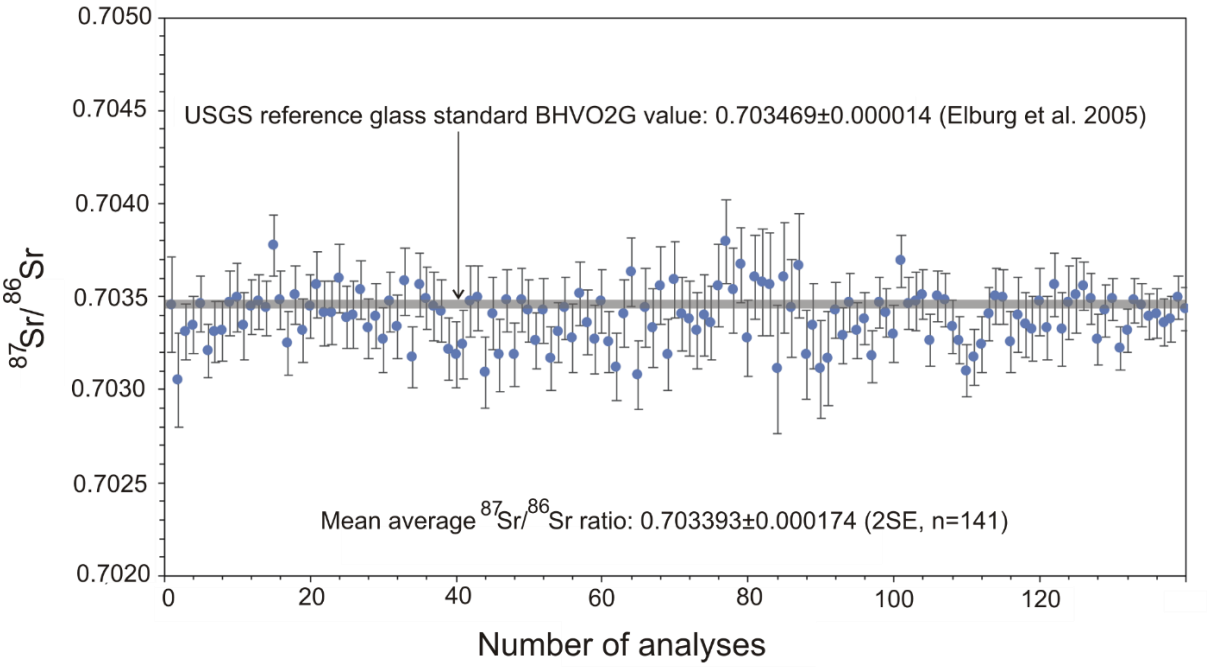

APPENDIX B

For Chapter 5: Article 2

Index:

Table B1: Estimated Modal Mineralogy for UMT393.

Sample	Depth	Lithology	Orthopyroxene	Clinopyroxene	Plagioclase	Biotite + Muscovite	Olivine	Amphibole	Sericite	Serpentine	Chlorite	Chromite	BMS	Magnetite	Other	Alteration
JDJ054B	742,37	AN	16	15	59	2		1	4			2.5	0.5		0	Sericitization of plagioclase.
JDJ056	748,30	AN	11	16	56	8		1	5		1	2			0	Sericitization of plagioclase. Biotite found on the edge of chromite.
JDJ059	760,37	AN	12	15	56	4		2	4			4.5	1		1.5	Sericitization of plagioclase. Biotite interstitial to chromite and minor sulfides.
JDJ061	765,98	AN	13	7	56	8		3	8			4	1		0	Orthopyroxene alters to mica and amphibole at rims. Sericitization of plagioclase core and veins of fine mica observed.
JDJ063	772,93	AN	14	13	54	4		3	5			3	2		2	Sericitization of plagioclase. Mica associated with secondary chromite and minor sulfides.
JDJ065B	779,37	AN	14	9	57	8		1	9			1	1		0	Plagioclase altered to sericite.
JDJ069A	787,38	AN	10	7	40	19		2	6		2	2	2		10	Increased sericitization. Biotite found at orthopyroxene rims
JDJ070	787,85	AN	12	8	56	7		6	5		3	2	1		0	Interstitial orthopyroxene alters to amphibole.
JDJ071	789,30	AN	15	13	54	5		1	3		4	1	2		2	Secondary biotite interstitial to plagioclase.
JDJ072	789,74	N	17	11	51	9		1	2		3	3.5	1		1.5	Biotite present as an alteration phase, associated with orthopyroxene.
JDJ076	802,43	N	17	15	60	3		1	1			1	1		1	Biotite present as an alteration phase, associated with orthopyroxene.
JDJ077	807,60	N	15	12	63.5	3		1	2.5			2	1		0	Minor mica at pyroxene rims.
JDJ078B	810,60	N	20	13	60	3			3			0.5	0.5		0	Slight alteration of plagioclase to sericite.
JDJ079	811,06	N	20	6	62	4			7			0.5	0.5		0	Sericitization of plagioclase. Minor alteration of orthopyroxene to mica at rims
JDJ080	811,49	N	23	8	58	4		1	3.5			1.5	1		0	Chromite found in association with biotite. Plagioclase alter to sericite.
JDJ082	816,02	N	15	5	35	15.5		8	15		3	2	1.5		0	Biotite present as an alteration phase along exsolution lamellae of clinopyroxene in orthopyroxene and at its edges
JDJ083	819,00	N	40	18	29	6.5		2	1			1.5	2		0	Orthopyroxene is replaced by clinopyroxene and amphibole along its edges and cleavage planes

Sample	Depth	Lithology	Orthopyroxene	Clinopyroxene	Plagioclase	Biotite + Muscovite	Olivine	Amphibole	Sericite	Serpentine	Chlorite	Chromite	BMS	Magnetite	Other	Alteration
JDJ085	822,78	N	18	13	61	3		1	2			0.25	1.75		0	Slight alteration of plagioclase to sericite.
JDJ087	825,17	N	20	8	48	3		6	15				0		0	Amphibole, biotite and chlorite observed as discontinuous alteration rims around orthopyroxene. Sericitization of plagioclase.
JDJ093	838,25	FPX	40	14	22	6		2	10			2	4		0	Sericitization of plagioclase.
JDJ097	848,63	FPX	40	18	24	6		1.5	3			5	2.5		0	Sericitization of plagioclase. Mica found adjacent and interstitial to orthopyroxene crystals.
JDJ099	851,88	FPX	49	7	29	5		2	2			2	4		0	Sericitization of plagioclase.
JDJ104	868,63	FPX	45	3	36	6		2	3		1	1.5	2.5		0	Sericitization of plagioclase. Biotite and muscovite present as an alteration phase along cleavage planes and rims of orthopyroxene.
JDJ105	871,20	FPX	42	7	37.5	3		2	2		1	1.5	4		0	Sericitization of plagioclase.
JDJ107	877,07	FPX	37	13	32	5		2	8			1	2		0	Sericitization of plagioclase. Muscovite associated with late phase sulfides.
JDJ112	888,80	FPX	38	7	39	4		2	7				3		0	Sericitization of plagioclase.
JDJ117	906,86	OPX	52	12	7	8		2	4		1	4	8		2	Biotite present as minor alteration phase at the edges of some orthopyroxene. Plagioclase alters to sericite.
JDJ125	926,97	FPX	39	13	30	1			1			10	3		3	Slight alteration of plagioclase to sericite.
JDJ126	928,39	OPX	51	12	19	3.5		2	4			8	0.5		0	Sericitization of plagioclase.
JDJ127	930,83	OPX	54	10	20	5		1	2.5			5.5	2		0	Minor alteration of orthopyroxene to biotite at rims.
JDJ130	934,85	HA	30	6	7	3	14	2	4	16		8	3.5	4.5	2	Serpentinised olivine associated with magnetite, mesh textured. Plagioclase alters to sericite.
JDJ133	942,27	HA	26	5.5	3.5	3	13	3	16	14	1	8	3	2	2	Serpentinised olivine associated, mesh textured. Orthopyroxene alters to amphibole. Plagioclase alters to sericite.
JDJ138	951,18	HA	18	10	5	2	32	2	4	13		3	3	5	3	Serpentinised olivine associated with magnetite, mesh textured. Interstitial plagioclase alters to sericite.
JDJ141B	960,06	FPX	33	12	16	2	21	2	3	3		4	2	2	0	Serpentinised olivine associated with magnetite, mesh textured. Plagioclase alters to sericite.
JDJ143	962,00	FPX	40	12	34	3		5	1				2		3	Orthopyroxene alters to mica and amphibole at rims. Sericitization of plagioclase.

Sample	Depth	Lithology	Orthopyroxene	Clinopyroxene	Plagioclase	Biotite + Muscovite	Olivine	Amphibole	Sericite	Serpentine	Chlorite	Chromite	BMS	Magnetite	Other	Alteration
JDJ149	976,54	AN	9	17	72	0			1.75				0.25		0	Slight sericitization of plagioclase.
JDJ152	981,20	N	45	18	34	1			1.5				0.5		0	Slight sericitization of plagioclase.
JDJ157	989,44	N	35	16	30	3		1	3		5				7	Sericitization of plagioclase.
JDJ170	1028,28	N	36	14	33	6		2	4				1		4	Sericitization of plagioclase.
JDJ174A	1035,43	N	28	12	34	7		3	7		2		7		0	Sericitization of plagioclase.
JDJ182	1059,00	N	26	15	45	5		1	5				1		2	Sericitization of plagioclase.

* AN, N, FPX, OPX, PPXT, MPV and HA indicate anorthosite, norite, feldspathic pyroxenite, orthopyroxenite, pegmatoidal pyroxenite, mafic pegmatoidal vein and harzburgite, respectively.

Table B2: Estimated Modal Mineralogy for UMT276.

Sample	Depth	Lithology	Orthopyroxene	Clinopyroxene	Plagioclase	Biotite + Muscovite	Olivine	Amphibole	Sericite	Serpentine	Chlorite	Chromite	BMS	Magnetite	Other	Alteration
JDJ001	730,09	GN	8	14	65.5	3	0	1	2	0		6	0.5		0	Slight alteration of plagioclase to sericite.
JDJ004	740,60	AN	14	4	70	2			7			2.75	0.25		0	Sericitization of plagioclase.
JDJ007	751,09	AN	16	10	63	2			8			1			0	Sericitization of plagioclase.
JDJ011	764,18	FPX	51	17	23	4			1			1	3		0	Sericitization of plagioclase. Biotite present as an alteration phase along cleavage planes and rims of orthopyroxene. Late phase veins cut through silicate minerals.
JDJ013A	772,62	FPX	48	14	25	5		1	3			2	2		0	Sericitization of plagioclase.
JDJ013B	775,30	FPX	50	13	27	3.5			2			1.5	3		0	Sericitization of plagioclase.
JDJ015	777,40	FPX	49	16	24	0		1	3			4	3		0	Slight sericitization of plagioclase.
JDJ019	784,33	OPX	59	10	8	10		2				7	4		0	Biotite present as alteration phase along rims of orthopyroxene
JDJ020	785,12	OPX	61	5	0	14.5		2	2	3	2	2.5	3		5	Plagioclase alters to sericite. Serpentinization. Biotite and muscovite present as an alteration phase along cleavage planes and rims of orthopyroxene
JDJ022	786,27	HA	49	6	0	2	4	2	10	12	0	2	6		2	Serpentinised olivine associated with magnetite, mesh textured. Sericitization plagioclase.
JDJ026	798,15	HA	20	2	0	3	11	3	12	30	3		5	6 8	3	Serpentinised olivine associated with magnetite and secondary sulfides. Plagioclase alters to sericite.
JDJ032	814,64	FPX	42	12	16	13		1	8	6			1		0	Serpentinized veins cut through orthopyroxene crystals. Plagioclase alters to sericite.
JDJ035	825,36	FPX	39	17	23	4.5		2	3	5		1	3.5	1 2	0	Minor serpentinization. Plagioclase alters to sericite.
JDJ042	842,15	N	30	10	42	8		1	8				1		0	Minor sulfides associated with secondary silicates. Orthopyroxene crystals alter to biotite along rims.
JDJ045	849,08	MPV	35	9	45	5		1					2		3	

Sample	Depth	Lithology	Orthopyroxene	Clinopyroxene	Plagioclase	Biotite + Muscovite	Olivine	Amphibole	Sericite	Serpentine	Chlorite	Chromite	BMS	Magnetite	Other	Alteration
			40	13	27	9		3	4			0.5				Slight alteration of plagioclase to sericite. Biotite and muscovite present as an alteration phase along cleavage planes and rims of orthopyroxene
JDJ047	853,00	FPX											1.5		2	
			30	18	26	6		2	9		1	0				Plagioclase alters to sericite. Late phase carbonate veins cut through minerals
JDJ052	866,69	FPX											3		5	

* GN, AN, N, FPX, OPX, PPXT, MPV and HA indicate gabbronorite, anorthosite, norite, feldspathic pyroxenite, orthopyroxenite, pegmatoidal pyroxenite, mafic pegmatoidal vein and harzburgite, respectively.

Figure B3: Modal mineralogy chart of BSN, a mela-gabbronorite, within the Merensky Reef pyroxenite in the underground exposure profile (not to scale). (Beukes et al. 2016)

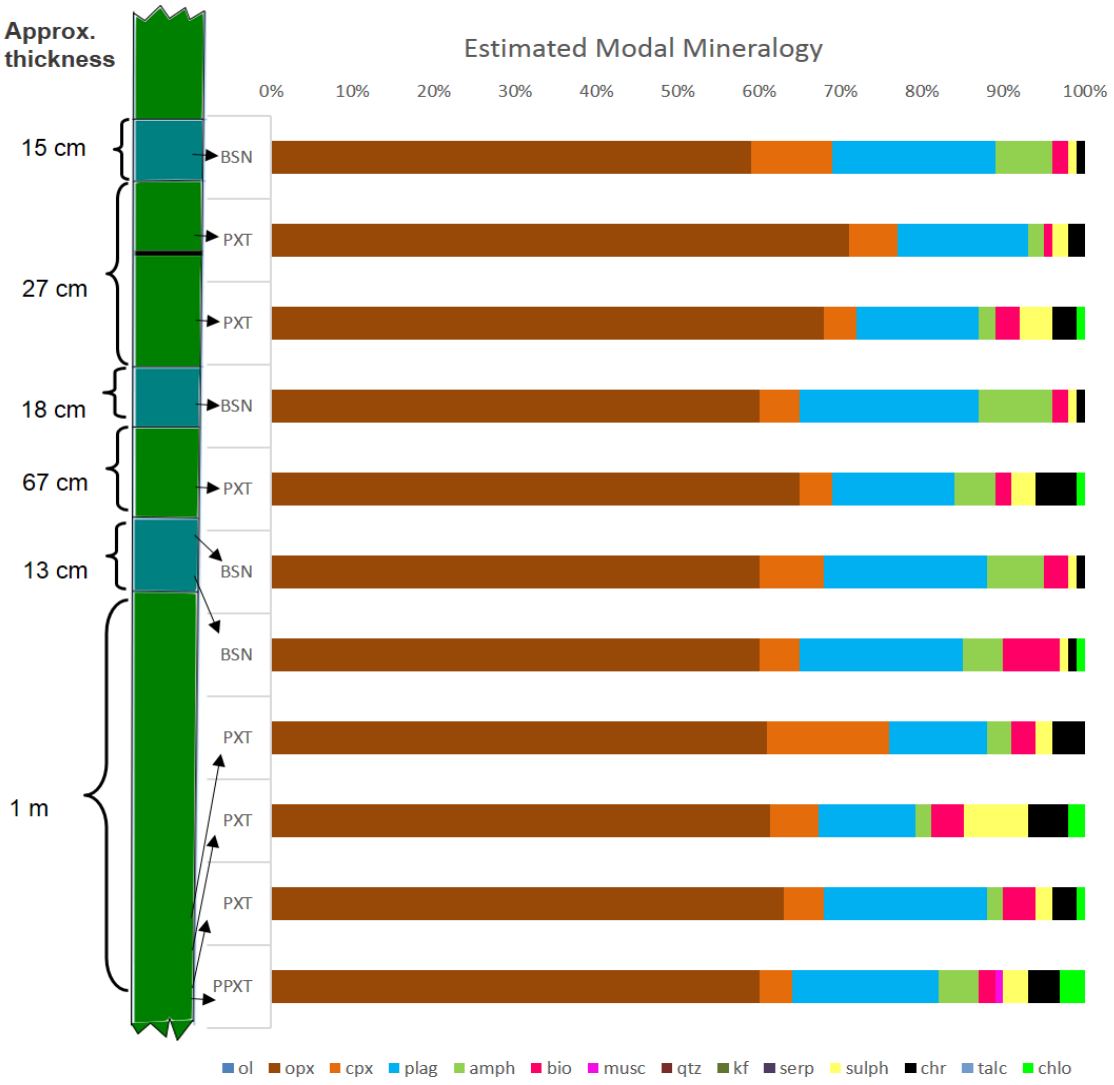

Table B4: OGS CRM data calibrated by the Council for Geoscience by Dr Uwe Horstmann

Run	Standard	Analysis	d 34S/32S	Average	SD	2SD
1	OGS-1	1	20.533	21.292	1.073388	2.146776
	OGS-1	2	22.051			
2	OGS -1	3	26.041	25.5355	0.714885	1.42977
	OGS -1	4	25.03			
3	OGS -1	5	22.602	21.844	1.071974	2.143948
	OGS -1	6	21.086			
4	OGS -1	7	21.805	21.6435	0.228395	0.456791
	OGS -1	8	21.482			
5	OGS -1	9	23.428	22.58	1.199253	2.398506
	OGS -1	10	21.732			
6	OGS -1	11	21.847	21.5815	0.375474	0.750947
	OGS -1	12	21.316			
7	OGS -1	13	19.094	19.1404	0.102958	0.205916
	OGS-1	14	19.029			
	OGS-1	15	19.305			
	OGS -1	16	19.156			
	OGS -1	17	19.118			

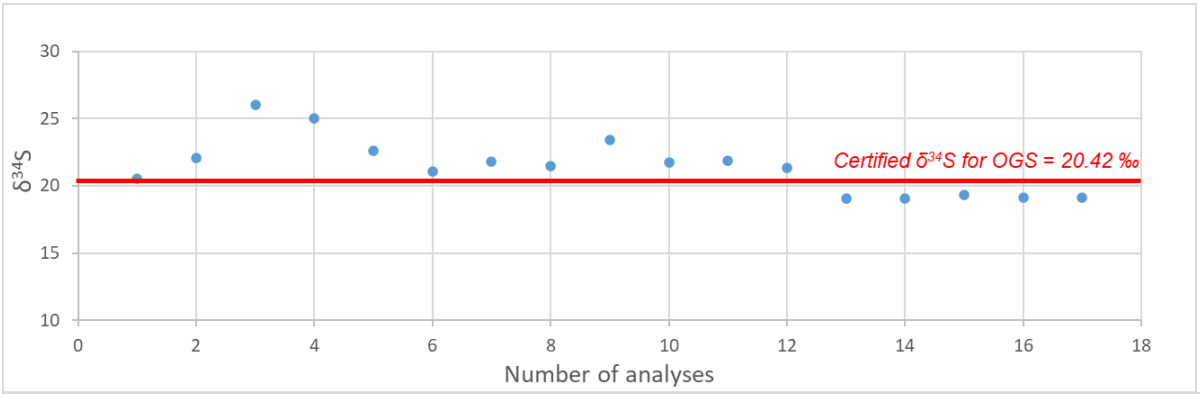

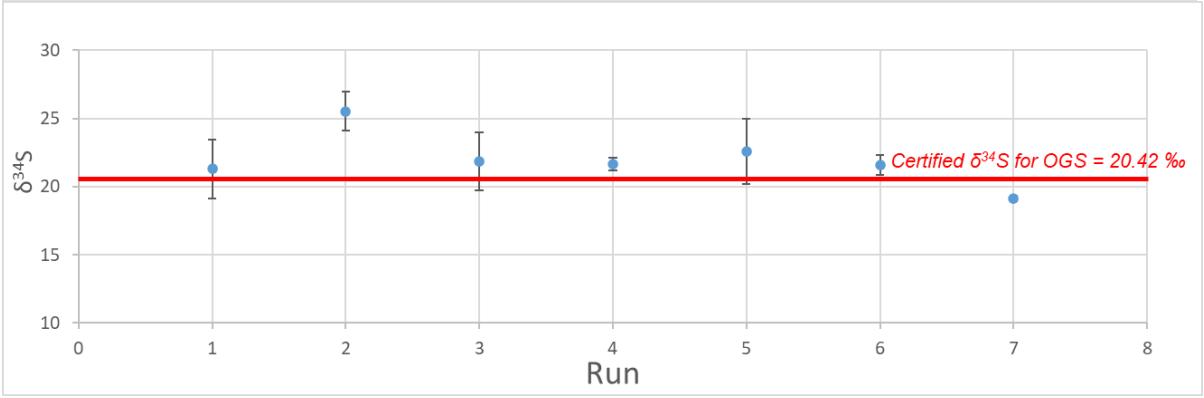

Average, 2SD

Table B5: Major oxide data for UMT393 (XRF)

Sample	Depth	Stratigraphy	SiO_2 (wt. %)	TiO_2 (wt.%)	Al_2O_3 (wt. %)	Fe_2O_3 wt.%)	MgO (wt.%)	MnO (wt. %)	CaO (wt. %)	NaO (wt. %)	K_2O (wt. %)	P_2O5 (wt. %)	LOI (wt. %)	Total	CaO/Al_2O_3
JDJ054B	742.37	HW	54.51	0.13	24.98	3.36	3.17	0.06	13.33	1.95	0.25	0.03	0.22	102.00	0.53
JDJ056	748.30	HW	54.48	0.15	26.35	2.95	2.18	0.05	12.90	2.00	0.35	0.03	0.97	102.41	0.49
JDJ059	760.37	HW	55.43	0.18	24.13	4.00	3.31	0.06	12.90	1.89	0.30	0.05	0.17	102.41	0.53
JDJ061	765.98	HW	55.29	0.68	24.87	3.28	1.85	0.07	13.21	2.24	0.47	0.02	0.59	102.56	0.53
JDJ063	772.93	HW	56.13	0.22	21.74	5.35	4.18	0.09	12.36	2.31	0.34	0.01	-0.13	102.59	0.57
JDJ065B	779.37	HW	54.79	0.19	24.82	3.76	2.72	0.06	12.97	2.02	0.47	0.02	0.72	102.52	0.52
JDJ069A	787.38	HW	54.24	0.13	26.85	2.71	2.52	0.04	12.50	1.78	0.47	0.03	1.34	102.60	0.47
JDJ070	787.85	HW	56.47	0.13	26.27	2.47	2.34	0.04	13.27	1.94	0.59	0.01	0.76	104.30	0.51
JDJ071	789.30	HW	49.20	0.13	24.89	3.58	4.17	0.06	13.04	1.85	0.40	0.23	0.56	98.12	0.52
JDJ072	789.74	HW	57.70	0.27	14.09	8.32	13.55	0.17	8.10	1.16	0.31	0.01	0.67	104.36	0.57
JDJ076	802.43	HW	56.34	0.19	17.32	6.73	11.73	0.13	9.53	1.18	0.23	0.03	0.48	103.88	0.55
JDJ077	807.60	HW	55.88	0.15	19.97	5.53	9.26	0.18	10.71	1.34	0.21	0.02	0.32	103.57	0.54
JDJ078B	810.60	HW	53.20	0.13	20.31	4.85	8.11	0.12	11.19	1.59	0.22	0.02	0.42	100.17	0.55
JDJ079	811.06	HW	55.48	0.13	23.25	4.23	6.37	0.07	12.02	1.58	0.29	0.02	0.37	103.82	0.52
JDJ080	811.49	HW	56.22	0.16	18.26	6.44	11.04	0.12	9.92	1.51	0.17	0.02	0.34	104.20	0.54
JDJ082	816.02	HW	49.33	0.13	21.44	4.88	7.78	0.09	11.64	1.61	0.24	0.01	0.60	97.74	0.54
JDJ083	819.00	HW	48.86	0.11	22.65	4.39	6.97	0.08	11.87	1.55	0.41	0.02	0.40	97.31	0.52
JDJ085	822.78	HW	49.31	0.12	22.22	4.47	7.33	0.08	11.25	1.61	0.43	0.01	0.50	97.34	0.51
JDJ087	825.17	HW	55.21	0.09	22.18	4.33	7.20	0.22	11.70	1.63	0.37	0.02	0.60	103.55	0.53
JDJ093	838.25	HW	58.58	0.24	4.69	12.14	23.53	0.22	4.45	0.40	0.10	0.01	0.37	104.75	0.95
JDJ097	848.63	UR	48.99	0.24	5.75	12.44	21.59	0.21	4.38	0.42	0.09	0.01	0.14	94.26	0.76
JDJ099	851.88	UR	56.44	0.20	5.65	11.17	21.62	0.21	4.78	0.56	0.09	0.01	-0.22	100.51	0.85
JDJ104	868.63	Md	50.95	0.21	4.77	12.04	23.10	0.22	4.54	0.39	0.04	0.01	0.13	96.40	0.95
JDJ105	871.20	Md	55.39	0.20	4.60	12.21	22.97	0.22	4.34	0.35	0.03	0.01	0.17	100.50	0.94
JDJ107	877.07	Md	56.48	0.19	5.18	11.97	22.66	0.22	4.53	0.38	0.03	0.03	0.25	101.91	0.87
JDJ112A	888.80	Md	50.55	0.17	7.52	11.64	20.46	0.20	4.76	0.85	0.10	0.01	-0.07	96.20	0.63

Sample	Depth	Stratigraphy	SiO_2 (wt. %)	TiO_2 (wt.%)	Al_2O_3 (wt. %)	Fe_2O_3 wt.%)	MgO (wt.%)	MnO (wt. %)	CaO (wt. %)	NaO (wt. %)	K_2O (wt. %)	P_2O5 (wt. %)	LOI (wt. %)	Total	CaO/Al_2O_3
JDJ112B	888.98	M2	50.08	0.15	7.87	10.16	20.61	0.18	5.95	0.68	0.12	0.01	0.02	95.85	0.76
JDJ117	906.86	M2	50.77	0.16	5.08	12.47	23.46	0.22	4.86	0.28	0.09	0.01	0.14	97.53	0.96
JDJ125	926.97	M2	51.79	0.24	4.18	12.80	23.88	0.23	4.24	0.42	0.03	0.01	0.08	97.90	1.01
JDJ126	928.39	M1U	51.02	0.22	6.44	11.27	21.12	0.21	6.00	0.68	0.11	0.01	-0.18	96.90	0.93
JDJ127	930.83	M1U	48.90	0.21	5.03	14.31	23.79	0.23	3.40	-0.01	0.01	0.01	2.98	98.86	0.68
JDJ130	934.85	M1L	46.00	0.13	6.09	12.41	25.08	0.23	4.37	0.21	0.04	0.01	3.34	97.91	0.72
JDJ133	942.27	M1L	44.99	0.18	2.67	14.54	27.78	0.26	3.63	0.03	0.06	0.01	3.19	97.34	1.36
JDJ138	951.18	M1L	40.86	0.12	3.24	15.12	28.92	0.25	2.65	0.01	0.06	0.01	5.87	97.12	0.82
JDJ141B	960.06	M1L	53.60	0.13	4.52	12.44	25.70	0.24	4.10	0.31	0.03	0.01	0.44	101.53	0.91
JDJ143	962.00	M1L	53.37	0.17	4.77	13.05	24.68	0.22	4.13	0.21	0.04	0.01	1.47	102.11	0.87
JDJ149	976.54	FCU	48.63	0.06	27.06	2.99	5.01	0.06	15.04	1.63	0.19	0.01	0.70	101.38	0.56
JDJ152	981.20	FCU	52.15	0.13	7.09	10.49	22.86	0.20	5.94	0.49	0.05	0.01	0.13	99.54	0.84
JDJ157	989.06	FCU	52.47	0.06	27.26	3.47	1.83	0.03	14.22	2.02	0.35	0.01	1.14	102.86	0.52
JDJ170	1028.28	FCU	54.63	0.18	9.74	15.08	15.84	0.19	6.29	0.82	0.07	0.01	0.47	103.32	0.65
JDJ174A	1035.43	FCU	54.53	0.11	21.48	6.16	6.51	0.10	11.27	1.85	0.15	0.01	0.65	102.82	0.52
JDJ182	1059.00	FCU	50.07	0.17	13.33	11.71	14.22	0.16	8.39	1.24	0.11	0.01	0.46	99.88	0.63

* MZ, HW, UR, Md, M2, M1U, M1L and FCU indicate Main Zone, Hanging wall, Upper reef, Middling unit, M1 upper, M1 lower and Footwall Cyclic Unit, respectively

Standard

NIM P	SiO_2	TiO_2	Al_2O_3	Fe_2O_3	MgO	MnO	CaO	NaO	K_2O	P_2O5
measured	50.639	0.203	3.907	12.6	25.409	0.226	2.677		0.059	0.019
Certified value	51.1	0.2	4.18	12.7	25.33	0.22	2.66	0.37		

Table B6: Major oxide data for UMT276 (XRF)

Sample	Depth	Stratigraphy	SiO_2 (wt. %)	TiO_2 (wt.%)	Al_2O_3 (wt. %)	Fe_2O_3 wt.%)	MgO (wt.%)	MnO (wt. %)	CaO (wt. %)	NaO (wt. %)	K_2O (wt. %)	P_2O5 (wt. %)	LOI (wt. %)	Total	CaO/Al_2O_3
JDJ001	730.09	MZ	49.71	0.20	21.27	5.72	6.07	0.09	11.67	1.72	0.30	0.03	0.16	96.95	0.55
JDJ004	740.60	HW	54.88	0.09	27.54	2.15	1.65	0.03	13.04	2.10	0.27	0.01	0.37	102.14	0.47
JDJ007	751.09	HW	55.76	0.13	23.54	3.94	4.25	0.07	13.03	2.11	0.24	0.03	0.37	103.46	0.55
JDJ011	764.18	UR	51.00	0.27	5.64	12.56	21.30	0.21	4.49	0.49	0.21	0.02	0.13	96.33	0.80
JDJ013A	772.62	Md	57.38	0.24	4.69	12.08	22.87	0.21	4.20	0.26	0.11	0.02	-0.16	101.91	0.90
JDJ013B	775.30	M2	56.44	0.23	4.77	12.10	22.39	0.21	4.28	0.45	0.14	0.02	0.87	101.91	0.90
JDJ015	777.40	M2	50.90	0.23	4.82	12.74	22.89	0.22	4.43	0.51	0.12	0.02	0.29	97.18	0.92
JDJ019	784.33	M1U	51.13	0.26	2.91	14.76	23.84	0.23	5.49	0.23	0.04	0.01	-0.20	98.70	1.89
JDJ020	785.12	M1U	53.45	0.26	2.03	15.42	21.73	0.24	4.00	0.23	0.19	0.01	-0.09	97.49	1.97
JDJ022	786.27	M1L	43.18	0.13	2.10	15.06	29.18	0.21	1.97	0.02	0.05	0.02	5.21	97.14	0.94
JDJ026	798.15	M1L	37.71	0.08	2.75	17.45	31.10	0.15	1.58	0.04	0.13	0.01	9.37	100.38	0.57
JDJ032	814.64	FCU	56.02	0.15	6.36	10.68	22.43	0.20	4.34	0.49	0.14	0.01	0.15	100.98	0.68
JDJ035	825.36	FCU	55.95	0.13	10.19	8.50	20.64	0.15	6.42	0.42	0.22	0.01	0.64	103.28	0.63
JDJ042	842.15	FCU	57.81	0.17	4.92	11.31	24.73	0.21	3.63	0.26	0.03	0.01	0.55	103.62	0.74
JDJ045	849.08	FCU	55.27	0.33	20.43	4.85	5.48	0.10	9.53	2.38	0.43	0.20	0.51	99.49	0.47
JDJ047	853.00	FCU	57.69	0.20	4.96	11.35	22.21	0.20	6.12	0.38	0.07	0.03	0.07	103.28	1.23
JDJ052	866.69	FCU	51.91	0.11	9.75	7.89	14.90	0.17	14.22	0.13	0.07	0.01	3.22	102.38	1.46

* MZ, HW, UR, Md, M2, M1U, M1L and FCU indicate Main Zone, Hanging wall, Upper reef, Middling unit, M1 upper, M1 lower and Footwall Cyclic Unit, respectively

Table B7: Major oxide data for TRP (XRF) from Beukes et al. 2016

Sample	Depth	Stratigraphy	SiO2 (wt. %)	TiO2 (wt.%)	Al2O3 (wt. %)	Fe2O3 wt.%)	MgO (wt.%)	MnO (wt. %)	CaO (wt. %)	NaO (wt. %)	K2O (wt. %)	P2O5 (wt. %)	Cr_2O_3 (wt. %)	LOI (wt. %)	Total	CaO/Al_2O_3
JJB1		HW	51.42	0.00	22.35	5.63	7.94	0.00	11.06	1.63	0.06	0.00	0.11	0.07	100.26	0.495125
JJB7		HW	51.40	0.19	7.35	11.41	23.53	0.19	4.80	0.58	0.08	0.01	0.37	0.09	100.01	0.653752
JJB9B		MR	54.34	0.04	5.33	12.59	24.17	0.09	4.26	-0.32	0.00	0.00	0.41	-0.22	100.68	0.799661
JJB10		MR	47.94	0.06	4.28	17.34	21.46	0.07	3.68	-0.43	0.00	0.00	0.65	1.26	96.31	0.860771
JJB18.1	980.45	MR	53.20	0.01	6.20	12.60	22.98	0.08	4.38	0.39	0.00	0.00	0.40	0.07	100.32	0.707238
JJB17	980.52	MR	51.90	0.04	6.02	12.55	22.98	0.07	4.11	0.34	0.00	0.00	0.50	0.12	98.63	0.681479
JJB14	980.89	MR	54.34	0.05	3.73	13.21	26.44	0.10	3.10	0.19	0.00	0.00	0.45	-0.23	101.37	0.831274
JJB15	981.39	MR	51.83	0.06	6.82	12.12	22.71	0.06	4.06	0.44	0.00	0.00	1.38	0.16	99.64	0.594555
JJB12	982	MR	55.02	0.21	3.01	14.80	26.24	0.12	2.57	0.24	0.05	0.02	0.42	-0.33	102.37	0.850915
JJB11	982.51	MR	53.13	0.10	5.51	12.58	22.32	0.08	3.91	-0.44	0.07	0.00	0.52	0.09	97.88	0.710269
JJB19.1	982.64	MR	48.70	0.10	4.60	16.45	21.12	0.08	4.02	0.27	0.00	0.00	0.89	1.00	97.22	0.873655
JJB20	982.7	FW	50.53	0.28	5.20	13.32	24.53	0.23	4.56	0.37	0.02	0.01	0.83	0.06	99.94	0.877908
JJB19.2	982.87	FW	47.94	0.03	31.09	0.84	0.34	0.02	15.21	1.87	0.14	0.01	-0.01	0.32	97.79	0.489324

* MZ, HW, UR, Md, M2, M1U, M1L and FCU indicate Main Zone, Hanging wall, Upper reef, Middling unit, M1 upper, M1 lower and Footwall Cyclic Unit, respectively

Table B8: Ivanplats assay data for UMT393

Sample start	Stratigraphy	4PGE (ppb)	Au (ppb)	Pt (ppb)	Pd (ppb)	Cr (ppm)	Cu (ppm)	Ni (ppm)	S (ppm)
821	HW	7.23	1	4	2	320	20	180	250
822	HW	6.12	1	2	3	360	18	204	200
823	HW	6.23	1	4	1	600	18	286	250
824	HW	13.53	1	9	3	750	20	340	250
824.59	HW	4.12	1	2	1	310	16	174	150
825.56	HW	7.18	1	3	3	1360	30	508	350
827	HW	27.76	3	13	11	1600	54	582	450
828	HW	6.12	1	2	3	1490	42	564	350
829	HW	25.64	2	11	12	1580	64	606	450
830	HW	44.05	5	18	20	1630	92	644	750
831	HW	43.59	17	10	16	1640	188	806	950
832	HW	59.64	34	11	14	1540	334	1060	1800
833	HW	37.53	19	9	9	1470	174	772	850
834.09	HW	19.29	9	5	5	1510	122	668	850
835.05	HW	42.53	23	9	10	1490	152	630	850
836.21	HW	4.12	1	2	1	20	22	30	600
836.9	HW	53.17	12	20	20	1490	142	712	1000
838	HW	99.69	18	46	33	1530	136	710	850
839	HW	146.39	40	58	45	1700	278	990	1650
840	HW	99.05	34	35	28	1730	230	898	1250
841	HW	206.67	38	97	66	1620	434	1030	1950
842.23	UR	10.41	1	7	2	100	16	64	550
842.94	UR	50.76	8	30	11	330	66	200	850
843.61	UR	53.88	27	15	11	1470	170	810	1050
845	UR	95	38	34	19	1420	238	878	1450
846	UR	362	97	146	112	1390	578	1350	2850
847	UR	1129	144	611	347	1680	692	1710	3000
848	UR	2987	284	1570	1060	3140	1800	3600	9800
849	UR	3088	374	1470	1160	6470	2340	4510	13100
850	UR	1989	279	924	749	1640	1870	3260	9150
851	UR	1699	192	839	631	1630	1530	2830	7450
852	UR	163	40	75	47	1430	234	834	850
853	Md	653	82	307	238	1480	502	1260	2600
854	Md	283.13	54	139	82	1410	276	876	1300
855	Md	56.46	20	25	10	1480	120	648	500
856	Md	125.33	44	57	21	1510	228	786	1050
857	Md	195.32	64	91	35	1630	300	900	1600
858	Md	147.15	43	71	29	1640	220	824	1200
859	Md	83.52	18	43	20	1430	114	658	1000
860	Md	75.11	17	36	20	1690	114	684	950

Sample start	Stratigraphy	4PGE (ppb)	Au (ppb)	Pt (ppb)	Pd (ppb)	Cr (ppm)	Cu (ppm)	Ni (ppm)	S (ppm)
861	Md	36.88	17	15	4	1580	116	630	650
862	Md	42.05	18	18	5	1620	132	662	650
863	Md	19.35	10	6	3	1520	90	608	500
864	Md	211.03	86	86	34	1620	438	1130	2500
865	Md	134.93	67	50	15	1560	328	1030	1850
866	Md	95.99	51	34	9	1990	272	950	1600
867	Md	123.87	59	49	13	1860	276	932	1550
868	Md	129.45	51	59	16	1870	286	950	1650
869	Md	148.21	58	72	14	1660	272	950	1600
870	Md	147.5	48	77	18	1610	254	886	1450
871	Md	115.16	43	54	15	1560	222	822	1350
872	Md	121.57	37	61	20	1550	222	846	1300
873	Md	119.57	37	61	18	1600	216	840	1300
874	Md	145.39	46	75	20	1720	218	840	1300
875	Md	144.33	48	74	18	1700	220	814	1300
876	Md	103.98	35	51	15	1550	202	782	1350
877	Md	116.57	37	61	15	1690	192	778	1200
878	Md	119.63	38	62	16	1540	202	794	1200
879	Md	123.8	40	65	15	1450	194	760	1150
880	Md	134.33	39	74	17	1620	222	828	1700
881	Md	175.56	42	95	33	1630	256	890	1750
882	Md	159.21	44	89	21	1650	282	938	1550
883	Md	254	65	131	48	1570	348	1020	1850
884	Md	3186	391	1780	937	1620	1170	2150	6100
885	MR	2453	172	1050	1130	3160	1140	2290	6650
886	MR	1002	74	425	465	2180	510	1370	2700
887	MR	646	75	275	266	1700	448	1140	2250
888	MR	1058	113	439	471	1710	748	1490	3400
889	MR	720	127	349	223	2210	522	1240	3000
890	MR	1125	159	586	350	2400	688	1490	3100
891	MR	1269	180	628	424	2210	892	2120	5850
892	MR	467	118	208	133	1930	390	1130	2300
893	MR	338	118	119	94	2010	412	1200	2500
894	MR	306	122	110	70	1740	418	1150	2050
895	MR	420	72	194	150	1320	184	744	1600
896	MR	531	96	258	165	1940	320	1070	1900
897	MR	478	201	163	108	1890	510	1340	2500
898	MR	1119	305	534	269	1980	672	1600	3150
899	MR	862	139	506	203	1960	316	1080	1200
900	MR	1997	138	1210	623	2310	398	1180	1750
901	MR	3216	211	2040	900	2940	692	1640	2500
902	MR	1730	172	1060	472	2620	510	1310	1700

Sample start	Stratigraphy	4PGE (ppb)	Au (ppb)	Pt (ppb)	Pd (ppb)	Cr (ppm)	Cu (ppm)	Ni (ppm)	S (ppm)
903	MR	1737	133	1090	483	2820	460	1330	2000
904	MR	5064	397	2880	1740	2890	1640	2350	5800
905	MR	1822	99	1260	431	1960	344	970	1200
906	MR	3534	248	1920	1300	3690	1190	1860	3800
907	MR	5316	247	3150	1730	3500	1400	2630	7550
908	MR	1379	64	680	563	3550	786	1720	4000
909	MR	315	20	178	108	3070	192	782	800
910	MR	1361	170	619	549	3480	690	1550	3450
911	MR	1660	103	609	887	3070	992	2260	5400
912	MR	976	73	482	380	3930	834	1920	5100
913	MR	536.8	39	270	212	2880	530	1300	2800
914	MR	731.78	54	321	338	2880	822	1820	4550
915	MR	921.92	73	426	398	3620	1070	2390	6600
916	MR	927.39	61	434	407	3640	778	1780	4500
917.2	MR	386.77	40	167	170	680	430	694	1900
918.11	MR	1206.02	105	479	594	710	806	1050	2700
919.11	MR	372.77	29	167	167	3040	376	1200	2200
920.11	MR	736.72	54	320	344	4180	630	1660	3200
921	MR	1633.72	94	867	622	5560	1110	2020	4400
921.75	MR	14.35	3	6	5	20	28	34	350
922.6	MR	1370.26	61	637	635	4580	832	2010	5450
924	MR	1652.2	56	841	706	4960	1140	2490	7600
925	MR	1722.22	109	585	994	3700	1300	2630	6700
926	MR	914.95	65	324	507	3790	670	1520	3200
927	MR	200.86	20	93	82	3010	242	838	1200
928	MR	52.57	8	25	18	3800	166	734	600
928.66	MR	1417.4	71	608	697	7120	722	1780	3600
929.94	MR	2289.14	153	839	1240	4330	1350	3750	6850
931.28	MR	1430.39	49	740	591	4450	488	2390	2700
932	MR	723.97	56	308	339	3950	508	2560	2600
933	MR	1181.85	75	497	576	4230	1280	2990	4600
934	MR	1549.1	101	677	725	4630	1580	3050	7100
935	MR	1016.53	51	419	518	5060	990	2030	3950
936	MR	1002.48	64	521	382	4460	966	1910	2550
937	MR	2024.21	101	752	1120	5580	848	2390	6250
938	MR	1916.81	124	658	1090	4940	838	2660	5050
939	MR	847.38	55	358	410	4280	548	1930	2800
940	MR	1206.42	37	432	708	3630	654	1980	3350
941	MR	2137.87	97	703	1290	7740	1500	3490	6800
942	MR	1974.93	93	601	1240	5930	1310	3200	5550
943	MR	1305.37	85	446	744	4770	1010	2390	4900
944	MR	1009.01	80	382	521	4850	980	1990	4100

Sample start	Stratigraphy	4PGE (ppb)	Au (ppb)	Pt (ppb)	Pd (ppb)	Cr (ppm)	Cu (ppm)	Ni (ppm)	S (ppm)
945	MR	1270.51	65	492	680	5150	1210	2400	5100
946	MR	1423.26	65	459	868	3790	988	2460	5300
947	MR	667.51	51	262	338	3360	698	1690	3400
948	MR	885.3	42	354	467	5710	574	1720	3550
949	MR	770.32	70	275	408	4840	712	1690	3100
950	MR	775.21	39	305	412	4330	618	1770	2950
951	MR	753.16	82	320	331	4240	630	1820	2950
952	MR	1030.66	70	439	494	3740	972	2290	5450
953	MR	892.27	59	290	525	2480	1220	2490	7000
954	MR	563.87	38	236	275	2710	704	1680	3300
955	MR	1008.25	67	369	549	2760	1500	2280	6650
956.25	MR	55.26	3	20	31	90	62	128	500
956.8	MR	1176.24	58	480	608	2700	830	2000	4200
958	MR	1969.83	86	775	1060	2890	1100	2360	6350
959	MR	1097.96	53	428	590	2900	876	2010	4750
960	FCU	705.9	35	300	352	3090	528	1420	2450
961	FCU	696.96	54	285	340	4200	748	1730	3600
962	FCU	1351.29	91	449	783	2740	1330	2720	6850
963	FCU	1241.3	76	465	671	2180	1030	2230	5800
964	FCU	690.32	34	259	381	2270	612	1610	3500
965	FCU	798.04	51	334	392	2420	570	1320	3100
966	FCU	631.96	21	285	308	2710	288	1090	1600
967	FCU	446.41	23	197	214	3930	254	1120	1400
968.26	FCU	13.38	1	6	6	70	22	72	150
969.69	FCU	717.27	28	290	381	3200	404	1450	2300
971	FCU	1012.08	58	414	514	2660	578	1770	4200
972	FCU	1165.08	80	414	645	1920	1070	1990	5250
973	FCU	857.07	47	271	522	1530	1170	2250	6350
974	FCU	551.39	51	165	325	1240	622	1240	2650
975	FCU	775.25	87	258	414	1170	630	1540	3150
976	FCU	2112.7	154	535	1390	950	1530	3720	9900
976.6	FCU	371.08	28	160	173	160	390	606	2050
977.45	FCU	82.78	4	60	15	300	104	260	250
978.35	FCU	344.69	40	138	158	1260	428	1050	1600
979	FCU	933.75	85	377	448	1300	1000	2040	6450
980	FCU	737.48	49	325	343	1410	712	1670	3700
981	FCU	304.69	19	122	156	1420	306	988	1650
982	FCU	454.96	42	174	228	1270	552	1370	2600
983	FCU	206.98	15	79	108	1310	194	736	800
984	FCU	772.34	53	307	393	880	510	1060	2650
985	FCU	563.23	49	210	291	780	670	1090	3450
986	FCU	446.45	38	150	249	770	604	1110	3450

Sample start	Stratigraphy	4PGE (ppb)	Au (ppb)	Pt (ppb)	Pd (ppb)	Cr (ppm)	Cu (ppm)	Ni (ppm)	S (ppm)
987	FCU	625.37	57	244	309	760	656	1210	3600
988	FCU	639.37	56	244	324	800	778	1310	4600
989	FCU	386.82	29	140	209	500	626	966	3850
990	FCU	121.9	12	46	61	250	380	658	2600
991	FCU	183.16	27	66	86	420	874	1420	6200
992	FCU	262.62	36	105	115	250	856	1170	6100
993	FCU	167.22	30	67	66	230	946	1190	6550
994	FCU	213.61	45	89	74	380	1130	1440	7500
995	FCU	176.16	35	66	71	350	826	1020	4850
996	FCU	120.52	18	40	60	350	544	744	3850
997	FCU	43.88	6	14	23	330	238	358	1700
998	FCU	174.41	23	70	77	290	596	788	4500
999	FCU	114.9	21	46	45	250	646	830	5750
1000	FCU	70.51	10	24	35	340	358	574	4150
1001	FCU	72.83	11	29	31	310	290	424	2950
1002	FCU	88.02	14	32	40	340	506	568	4950
1003	FCU	95.71	11	43	39	360	366	492	3100
1004	FCU	127.21	13	51	60	340	398	488	2900
1005	FCU	43.26	4	20	18	120	62	126	550

Table B9: Ivanplats assay data for UMT276

Sample start	Stratigraphy	4PGE (ppb)	Au (ppb)	Pt (ppb)	Pd (ppb)	Cr (ppm)	Cu (ppm)	Ni (ppm)	S (ppm)
752	HW	10.41	1	7	2	60	18	76	50
753	HW	12.47	1	8	3	60	22	78	50
754	HW	8.23	1	4	3	70	36	78	50
755	HW	25.64	4	11	10	70	28	78	100
756	HW	13.53	2	9	2	60	34	94	300
757	HW	22.76	2	13	7	60	36	86	200
758	HW	18.82	1	14	3	70	14	84	100
759	HW	2053.94	80	922	998	30	528	412	2650
759.54	HW	957.91	47	272	623	890	950	1250	8250
759.96	HW	407.35	10	23	373	140	580	432	3400
760.42	HW	374	56	165	144	1340	814	1890	2650
761	UR	353	166	98	79	1380	984	1910	4350
762	UR	2878	613	1430	790	1650	2120	3760	10100
763	UR	4928	590	2160	2080	1930	1980	4370	10600
764	UR	1368	211	672	456	1720	764	1750	3550
765	UR	586	124	269	174	1590	542	1260	2800
766	UR	2080	270	942	824	1670	936	2160	4900
767	UR	5208	540	2500	2070	1730	1520	4000	8650
767.46	Md	2400	304	1160	889	1600	3550	2620	7200
768	Md	3459	440	1700	1260	1790	1190	2790	6800
769	Md	408	113	193	91	1900	396	916	1850
770	Md	352	89	174	79	1550	280	868	1350
771	Md	893.63	178	421	270	1630	514	1100	2800
772	Md	831.05	154	394	260	1240	416	1070	2350
773	M2	2049	285	1040	694	1580	686	1840	4200
774	M2	422.93	84	221	105	1600	266	886	1450
775	M2	399.99	80	222	85	1680	244	912	1450
776	M2	672.59	174	369	108	1880	432	1170	2400
777	M2	4245	376	2280	1460	2330	1030	2080	4750
778	M2	9735	421	5590	3440	1810	1400	2950	7050
779	M2	8824	457	4850	3230	1860	1140	2580	5500
780	M2	1779	55	1110	574	1860	190	838	950
781	M2	1339.14	99	795	391	2760	294	918	1050
782	M2	811	26	518	223	2230	140	600	350
783	M2	924	12	581	291	2680	92	654	450
784	M2	5265	97	3030	1880	6240	544	1480	3050
784.31	$M1_U$	5278	219	2370	2510	4290	1380	2880	7650
785.13	$M1_U$	3486	124	1250	1980	1180	1800	2980	8200
786	$M1_L$	7573	234	2290	4730	1400	2460	7260	21500
786.32	$M1_L$	6364	290	2020	3830	1390	3270	6850	17300

Sample start	Stratigraphy	4PGE (ppb)	Au (ppb)	Pt (ppb)	Pd (ppb)	Cr (ppm)	Cu (ppm)	Ni (ppm)	S (ppm)
787	$M1_L$	4805	218	1540	2890	1000	2560	5910	13900
788	$M1_L$	2645.79	121	922	1540	2460	1050	2910	4850
789	$M1_L$	1663.09	102	574	948	1260	1750	3010	5400
790	$M1_L$	2135.99	109	690	1290	2180	1220	2970	6050
791	$M1_L$	1296.17	124	399	746	2470	840	2560	4700
792	$M1_L$	807.52	58	316	412	910	856	2570	4100
793	$M1_L$	1205.16	81	487	604	710	1230	2600	4850
794	$M1_L$	1003.06	53	412	510	750	818	2240	3200
795	$M1_L$	816.11	61	266	471	1510	1180	2450	4300
796	$M1_L$	444.69	28	201	202	950	448	1690	1850
797	$M1_L$	1744.24	222	635	844	1300	1720	2500	6250
798	$M1_L$	1635.72	139	642	811	2500	1590	2870	6950
799	$M1_L$	1189.92	78	454	627	2010	980	2170	4400
800	$M1_L$	660.14	47	193	407	1230	416	1740	2300
801	$M1_L$	856.66	41	274	523	1990	412	1800	2200
802	$M1_L$	1650.04	78	676	850	2110	1200	3140	8000
803	$M1_L$	1715.81	118	702	848	2530	900	2420	6800
804	$M1_L$	226.99	11	95	115	2660	136	990	2000
804.83	FCU	47.7	8	27	11	1610	238	686	950
805.6	FCU	111.72	10	59	39	2170	168	610	250
806.4	FCU	50.33	6	37	5	1980	138	578	300
807	FCU	143.04	6	80	52	1940	186	632	600
808	FCU	70.9	3	46	19	2260	112	550	400
809	FCU	200.43	9	102	83	2420	174	634	500
810	FCU	259.5	25	119	108	1680	458	972	2400
811	FCU	188.17	20	82	81	1330	344	860	3000
812	FCU	127.65	21	58	45	1550	294	764	2450
813	FCU	166.48	10	87	64	2270	152	630	800
814	FCU	266.51	7	135	116	2450	290	876	1050
815	FCU	225.62	9	121	88	2130	370	1070	3000
816	FCU	133.54	9	72	48	1920	206	688	850
817	FCU	106.84	6	61	36	2110	224	662	1000
818	FCU	275.95	8	142	117	1800	176	718	1200
819	FCU	493.86	26	220	234	1770	240	920	1800
820.05	FCU	944.29	52	338	533	1650	782	1860	5050
821	FCU	987.06	47	366	551	1720	722	1880	4050
822	FCU	184.87	6	109	63	2380	86	670	500
823	FCU	268.26	10	147	102	2580	212	1020	1050
824	FCU	162.93	3	110	43	2230	86	658	450
825	FCU	408.59	26	184	187	1650	428	1050	1750
826	FCU	921.38	89	387	421	1920	1240	1780	4400
827	FCU	1277.41	70	562	610	1670	1850	2640	8050

Sample start	Stratigraphy	4PGE (ppb)	Au (ppb)	Pt (ppb)	Pd (ppb)	Cr (ppm)	Cu (ppm)	Ni (ppm)	S (ppm)
828	FCU	1402.86	125	474	774	2670	2330	3110	10100
829	FCU	1763.79	133	695	892	2770	2600	3430	11400
829.54	FCU	501.51	32	278	174	2350	558	1050	2000
830	FCU	401.29	14	211	163	1990	288	762	1500
831	FCU	320.83	14	156	141	1760	132	712	600
832	FCU	207.06	6	128	65	1450	64	500	200
833	FCU	246.63	10	137	91	730	64	426	250
833.59	FCU	807.94	90	380	314	1960	356	1260	2850
834	FCU	557.26	22	274	244	2470	92	678	550
835	FCU	718.28	26	306	367	2590	126	786	700
836	FCU	346.32	20	148	169	2430	86	670	500
837	FCU	181.43	10	102	63	2450	50	612	200
838	FCU	248.13	14	129	97	2260	94	682	500
839	FCU	154.61	7	89	53	1920	66	602	450

Table B10: $\delta^{34}S$ for UMT393

Sample	Depth	Sample Origin	Lithology	$\delta^{34}S$ (‰)	S (wt. %)
JDJ054B	742.37	HW	AN	12.47	
JDJ056	748.3	HW	AN	14.32	
JDJ059	760.37	HW	AN	15.47	
JDJ061	765.98	HW	AN	14.99	
JDJ063	772.93	HW	AN	14.19	
JDJ065B	779.37	HW	AN	13.62	
JDJ069A	787.38	HW	AN	15.66	
JDJ070	787.85	HW	AN	15.61	
JDJ071	789.3	HW	AN	11.66	
JDJ072	789.74	HW	N	12.13	
JDJ076	802.43	HW	N	16.11	
JDJ077	807.6	HW	N	15.82	
JDJ078B	810.6	HW	N	15.31	
JDJ079	811.06	HW	N	16.85	
JDJ080	811.49	HW	N	14.25	
JDJ082	816.02	HW	N	15.74	
JDJ083	819	HW	N	16.28	
JDJ085	822.78	HW	N	16.67	0.02
JDJ087	825.17	HW	N	15.2	0.015
JDJ093	838.25	HW	FPX	8.05	0.085
JDJ097	848.63	UR	FPX	-0.52	0.98
JDJ099	851.88	UR	FPX	11.26	0.745
JDJ104	868.63	Md	FPX	4.55	0.165
JDJ105	871.2	Md	FPX	4.64	0.135
JDJ107	877.07	Md	FPX	5.92	0.12
JDJ112A	888.8	M2	FPX	1.53	0.34
JDJ112B	888.8	M2	FPX	4.97	0.34
JDJ117	906.86	M2	OPX	-0.22	0.38
JDJ125	926.97	M2	FPX	9.73	0.32
JDJ126	928.39	$M1_U$	OPX	11.1	0.06
JDJ127	930.83	$M1_U$	OPX	1.36	0.685
JDJ130	934.85	$M1_L$	HA	0.9	0.71
JDJ133	942.27	$M1_L$	HA	0.2	0.555
JDJ138	951.18	$M1_L$	HA	-0.07	0.295
JDJ141B	960.06	$M1_L$	FPX	7.85	0.245
JDJ143	962	$M1_L$	FPX	0.85	0.685
JDJ149	976.54	FCU	AN	15.6	0.205
JDJ152	981.2	FCU	N	18.62	0.165
JDJ157	989.06	FCU	N	17.37	0.385
JDJ170	1028.28	FCU	N	2.67	

Sample	Depth	Sample Origin	Lithology	$\delta^{34}S$ (‰)	S (wt. %)
JDJ174A	1035.43	FCU	N	2.03	
JDJ182	1059	FCU	N	8.39	

* S (wt. %) is from assay data
* MZ, HW, UR, Md, M2, $M1_U$, $M1_L$ and FCU indicate Main Zone, Hanging wall, Upper reef, Middling unit, M1 upper, M1 lower and Footwall Cyclic Unit, respectively.
* AN, N, FPX, OPX, PPXT, MPV and HA indicate anorthosite, norite, feldspathic pyroxenite, orthopyroxenite, pegmatoidal pyroxenite, mafic pegmatoidal vein and harzburgite, respectively.

Table B11: $\delta^{34}S$ for UMT276

Sample	Depth	Sample Origin	Lithology	$\delta^{34}S$ (‰)	S (wt. %)
JDJ001	730,09	MZ	GN	7.4	
JDJ004	740,60	HW	AN	10.83	
JDJ007	751,09	HW	AN	5.96	
JDJ011	764,18	UR	FPX	3.19	0.355
JDJ013A	772,62	Md	FPX	4.64	0.235
JDJ013B	775,30	M2	FPX	-0.96	0.145
JDJ015	777,40	M2	FPX	2.24	0.475
JDJ019	784,33	$M1_U$	OPX	-0.61	0.765
JDJ020	785,12	$M1_U$	OPX	-1.01	0.82
JDJ022	786,27	$M1_L$	HA	-1.05	1.73
JDJ026	798,15	$M1_L$	HA	-0.94	0.695
JDJ032	814,64	FCU	FPX	6.6	0.105
JDJ035	825,36	FCU	FPX	4.26	0.175
JDJ042	842,15	FCU	N	13.65	
JDJ045	849,08	FCU	MPV	8.49	
JDJ047	853,00	FCU	FPX	0.69	
JDJ052	866,69	FCU	FPX	4.18	

* S (wt. %) is from assay data
* MZ, HW, UR, Md, M2, $M1_U$, $M1_L$ and FCU indicate Main Zone, Hanging wall, Upper reef, Middling unit, M1 upper, M1 lower and Footwall Cyclic Unit, respectively.
* AN, N, FPX, OPX, PPXT, MPV and HA indicate anorthosite, norite, feldspathic pyroxenite, orthopyroxenite, pegmatoidal pyroxenite, mafic pegmatoidal vein and harzburgite, respectively.

Table B12: $\delta^{34}S$ for TRP MR

Sample	Depth	Sample Origin	Lithology	$\delta^{34}S$ (‰)
JJB9B		HW	BSN	3,73
JJB1		HW	AN	2,89
JJB7		MR	FPX	2,82
JJB10		MR	FPX	1,24
JJB18A	980,45	MR	FPX	3,29
JJB17	980,52	MR	FPX	3,35
JJB14	980,89	MR	BSN	2,94
JJB15	981,39	MR	FPX	3,68
JJB12	982,00	MR	BSN	5,23
JJB11	982,51	MR	FPX	4,83
JJB19A	982,64	MR	FPX	1,46
JJB20	982,70	FW	FPX	3,27
JJB19B	982,87	FW	AN	5,70

* MZ, HW, UR, Md, M2, $M1_U$, $M1_L$ and FCU indicate Main Zone, Hanging wall, Upper reef, Middling unit, M1 upper, M1 lower and Footwall Cyclic Unit, respectively.
* AN, N, FPX, OPX, PPXT, MPV and HA indicate anorthosite, norite, feldspathic pyroxenite, orthopyroxenite, pegmatoidal pyroxenite, mafic pegmatoidal vein and harzburgite, respectively.

APPENDIX C

For Chapter 6: Article 3

Table C1: Whole-rock trace elements across Flatreef stratigraphy (ppm)

Sample	JDJ076	JDJ086	JDJ097	JDJ107	JDJ109A	JDJ112B	JDJ119	JDJ120	JDJ126	JDJ133	JDJ141A	JDJ152	JDJ154A	JDJ163
ppm														
Li	8.159	4.709	5.041	5.333	3.452	4.314	7.775	5.041	4.73	5.232	4.145	3.846	3.39	3.228
P	104.085	100.218	18.105	139.298	18.898	52.498	20.657	29.181	22.712	24.205	16.499	44.989	28.612	39.829
Sc	12.872	19.678	19.395	26.046	20.844	15.385	30.359	15.622	17.488	17.869	20.829	18.033	18.398	14.456
Ti	1035.992	1227.925	1021.152	975.545	911.223	746.16	1482.203	726.08	1021.117	738.026	867.236	657.508	599.488	729.085
V	84.367	134.086	127.075	124.177	113.785	103.106	187.534	109.176	121.914	95.046	97.902	112.389	114.563	106.529
Cr	966.55	1956.295	4181.521	2090.689	2000.979	2309.898	3633.124	3676.153	3039.273	3610.833	3611.308	2239.123	2271.178	853.923
Co	44.505	83.212	103.69	87.419	131.209	82.668	112.923	102.775	75.968	135.721	96.655	76.221	81.108	41.609
Ni	227.167	447.227	1904.534	701.869	2843.394	1048.654	1160.354	1629.145	585.034	2303.633	767.08	490.061	474.634	132.575
Cu	24.696	29.238	1225.593	223.906	1558.549	529.544	382.826	867.759	187.055	1016.03	175.55	117.548	158.501	59.570
Zn	51.171	90.587	104.459	100.339	110.379	86.688	140.763	99.881	104.088	119.163	140.289	102.293	97.865	43.340
Ga	11.078	5.496	6.058	5.411	5.143	5.981	4.665	5.53	6.219	3.579	4.431	5.181	4.764	11.916
Rb	6.475	5.627	3.317	1.958	6.825	5.895	2.174	4.661	3.679	4.693	2.074	2.412	1.726	2.716
Sr	196.344	53.163	58.954	57.876	56.118	90.276	24.384	78.066	84.873	26.144	45.847	82.625	73.209	248.037
Y	4.132	5.886	3.784	4.503	3.663	2.913	6.433	2.789	4.914	3.646	3.493	2.525	2.335	2.791
Zr	16.873	18.084	6.234	5.111	5.187	8.378	6.132	4.208	7.461	6.75	4.571	5.926	4.939	8.806
Nb	0.703	0.572	0.157	0.086	0.088	0.296	0.103	0.096	0.201	0.361	0.065	0.282	0.177	0.343
Sn	0.348	0.303	0.457	0.148	0.282	0.234	0.419	0.228	0.165	0.223	0.186	0.132	0.18	0.217
Sb	0.05	0.025	0.024	0.024	0.03	0.027	0.169	-0.005	-0.008	0.013	-0.011	0.01	-0.002	0.000
Cs	0.351	0.412	0.607	0.296	0.317	0.46	0.556	0.643	0.416	1.101	0.555	0.331	0.298	0.141
Ba	82.336	31.792	44.203	28.459	32.786	47.446	14.884	35.356	63.766	20.55	23.376	30.934	22.719	71.115
La	4.421	2.777	2.117	2.14	1.511	1.809	1.171	1.287	2.334	1.268	1.082	1.444	1.23	2.578
Ce	8.456	5.635	3.657	4.121	2.536	3.443	2.649	2.422	4.396	2.717	1.843	2.672	1.998	4.637
Pr	0.923	0.681	0.398	0.488	0.271	0.391	0.382	0.258	0.526	0.358	0.229	0.305	0.223	0.519

Sample	JDJ076	JDJ086	JDJ097	JDJ107	JDJ109A	JDJ112B	JDJ119	JDJ120	JDJ126	JDJ133	JDJ141A	JDJ152	JDJ154A	JDJ163
Nd	3.706	2.991	1.703	2.216	1.22	1.718	2.044	1.166	2.435	1.718	1.149	1.339	1.012	2.221
Sm	0.78	0.756	0.414	0.549	0.313	0.393	0.665	0.295	0.621	0.456	0.335	0.321	0.244	0.487
Eu	0.366	0.173	0.185	0.21	0.164	0.183	0.155	0.143	0.269	0.125	0.125	0.134	0.118	0.435
Gd	0.791	0.888	0.51	0.667	0.422	0.447	0.859	0.359	0.752	0.552	0.437	0.374	0.3	0.511
Tb	0.115	0.144	0.079	0.106	0.07	0.064	0.146	0.054	0.121	0.084	0.071	0.054	0.043	0.070
Dy	0.779	1.066	0.649	0.801	0.597	0.518	1.14	0.474	0.912	0.666	0.601	0.449	0.393	0.518
Ho	0.158	0.227	0.141	0.178	0.135	0.106	0.25	0.101	0.193	0.139	0.131	0.093	0.082	0.099
Er	0.459	0.689	0.445	0.544	0.442	0.337	0.773	0.335	0.575	0.428	0.426	0.302	0.274	0.295
Tm	0.075	0.115	0.074	0.092	0.075	0.055	0.131	0.057	0.095	0.07	0.071	0.049	0.047	0.046
Yb	0.498	0.807	0.547	0.663	0.573	0.397	0.983	0.425	0.682	0.501	0.541	0.358	0.343	0.314
Lu	0.069	0.12	0.079	0.097	0.084	0.055	0.148	0.061	0.098	0.071	0.078	0.049	0.048	0.039
Hf	0.478	0.496	0.205	0.182	0.162	0.251	0.253	0.136	0.255	0.234	0.163	0.183	0.148	0.255
Ta	0.075	0.062	0.017	0.018	0.011	0.021	0.019	0.013	0.025	0.107	0.015	0.027	0.019	0.045
W	0.852	1.032	0.389	0.418	0.515	0.286	0.721	0.626	0.595	0.58	0.785	0.764	0.707	1.018
Tl	0.038	0.044	0.078	0.015	0.038	0.035	0.043	0.055	0.027	0.058	0.019	0.014	0.008	0.014
Pb	2.076	0.821	9.457	3.01	13.402	6.809	2.592	15.423	6.085	13.464	5.244	2.062	4.2	1.261
Th	0.783	0.72	0.158	0.098	0.077	0.32	0.055	0.079	0.095	0.136	0.048	0.204	0.121	0.249
U	0.229	0.22	0.056	0.022	0.014	0.085	0.012	0.017	0.026	0.044	0.004	0.052	0.029	0.065

Controls

ppm	Meas BCR2	Meas BHVO2	Recom BCR2	Recom BHVO2
Li	9.479	5.245	9.9	5
P	1511.325	1226.427	1571	1178
Sc	31.755	31.243	32	31
Ti	12479.47	16308.14	13005	15621
V	417.083	326.626	414	329
Cr	15.136	286.44	17	285
Co	36.83	45.722	35.8	47
Ni	10.938	110.459	12.7	112
Cu	19.396	142.033	19.4	142
Zn	141.866	111.018	147	107
Ga	22.144	21.541	22.7	21
Rb	49.161	10.067	49	10.1
Sr	317.138	386.712	321	382
Y	31.086	22.937	31	23
Zr	181.938	171.361	194	160
Nb	11.48	18.531	12.8	16.4
Sn	2.867	2.13	2.1	2.7
Sb	0.735	0.138	0.62	0.16
Cs	1.268	0.102	1.17	0.11
Ba	641.529	128.598	641	128.7
La	24.965	15.316	24.5	15.6
Ce	51.373	36.383	50.5	37
Pr	6.382	4.937	6.3	5
Nd	27.637	23.46	27	24
Sm	6.333	5.77	6.3	5.8
Eu	1.936	1.974	1.91	2
Gd	6.527	5.876	6.5	5.9
Tb	0.976	0.838	0.95	0.86
Dy	6.036	4.871	6	4.9
Ho	1.215	0.899	1.2	0.91
Er	3.362	2.258	3.3	2.3
Tm	0.476	0.29	0.46	0.3
Yb	3.35	1.934	3.2	2.02
Lu	0.476	0.257	0.47	0.26
Hf	4.826	4.254	5	4.1
Ta	0.694	1.073	0.78	0.94
W	0.359	0.349	0.44	0.27
Tl	0.292	0.022	0.3	0.021
Pb	10.901	1.4	10.9	1.4
Th	5.747	1.131	5.5	1.18
U	1.784	0.427	1.73	0.44

*Meas = Measured *Recom = Recommended